First Contact Imaging of nanoparticular siRNA – From synthesis to application of a prodye concept

Dissertation

Zur Erlangung des Grades "Doktor der Naturwissenschaften"

im Promotionsfach Pharmazie

am Fachbereich Chemie, Pharmazie und Geowissenschaften

der Johannes Gutenberg-Universität

in Mainz

vorgelegt von

Herrn Apotheker Okan Osman Oglou

geboren am 20.03.1986 in Xanthi, Griechenland

Mainz, Mai 2015

Vom Fachbereich Chemie, Pharmazie und Geowissenschaften der Johannes Gutenberg-Universität Mainz als Dissertation angenommen.

Die vorliegende Arbeit entstand in der Zeit von Juli 2011 bis Mai 2015 am Institut für Pharmazie und Biochemie – Therapeutische Lebenswissenschaften der Johannes Gutenberg-Universität Mainz unter Anleitung von Herrn Prof. Dr.

Dekan:

1. Gutachter:

2. Gutachter:

Datum der mündlichen Prüfung: 30.06.2015

Hiermit versichere ich eidesstattlich, dass ich die vorliegende Arbeit selbständig und unter Verwendung der angegebenen Quellen und Hilfsmittel angefertigt habe, sowie wörtliche oder inhaltliche Zitate als solche gekennzeichnet habe.

Ich habe keinen anderen Promotionsversuch unternommen.

Mainz, Mai 2015

Okan Osman Oglou

Zusammenfassung

Der gezielte Wirkstofftransport und die Freisetzung von therapeutischen Nukleinsäuren ist weiterhin eine große Herausforderung in den therapeutischen Lebenswissenschaften. Um dieses Problem zu lösen, ist eine präzise Untersuchungsmethode der RNA-Interferenz-Wege nötig. Diese Doktorarbeit beschreibt die Entwicklung eines neuen Ansatzes zur Untersuchung potentiell therapeutischer Nukleinsäuren am Beispiel profluoreszenter Farbstoff-Nukleinsäure Konstrukte. Um das Konzept zu verwirklichen wurden einige neuartige profluoreszente, farblose und asymmetrische Fluoreszeine organisch-präparativ synthetisiert und ihre spektroskopischen Eigenschaften untersucht. Click-Konjugationschemie auf Basis von organischen Aziden und Alkinen wurde im schwach Sauren angewandt, um intakte Prodye-Nukleinsäure-Konstrukte zu bilden. Gel-permeationschromatographische Untersuchungen und Küvettenexperimente zeigten bemerkenswerte hyperchromische Effekte dieser neuen Konstrukte unter physiologischen Bedingungen. Nach salzfreier Aufreinigung, anschließender Hybridisierung zu doppelsträngigen Ribonukleinsäuren und Formulierung zu Lipoplexen wurden die Prodye-siRNA Konstrukte *in vitro* auf den Erst-Kontakt mittels CLSM untersucht. In Küvettenexperimenten konnte nach erfolgter Hydrolyse der esteraseempfindlichen Schutzgruppen starke Fluoreszenz gezeigt werden, jedoch nicht eindeutig in zellulären Aufnahmeexperimenten. Als mögliche Optimierung des Ansatzes wurden neue profluoreszente Fluoreszeine modelliert und synthetisiert, welche an 6‘-Position eine biolabile Carbonatfunktion und an 3‘-Position eine wasserlösliche „clickbare Azid Funktion“ an der aliphatischen Linker besitzen. Diese neuen, nicht-fluoreszierenden, aber farbigen Moleküle haben 12 – 320-fache hyperchromische AUS-zu-AN-Quoten. Dieser neue Ansatz mit 3‘ und 6‘ Funktionen des Fluoreszeins ist noch nicht in der Literatur berichtet.

Abstract

Delivery of therapeutic nucleic acid based drugs is still very demanding and difficult to manage and monitor. For this reason, a precise method for the monitoring of RNAi pathways is necessary. This thesis explores a new approach for sensing of potentially therapeutic nucleic acids, using the interaction of so called prodyes with intracellular enzymes in a prodrug manner. To realize this concept, some non-fluorescent, fluorescein based asymmetric dyes were synthesized and their spectroscopic characteristics were studied. Azide-alkyne Click chemistry was applied for conjugation purposes, using a new protocol at weak acidic pH to get intact prodye constructs. Both, an electrophoretic mobility shift assay with polyacrylamide gels and in-cuvette experiments showed remarkable OFF-to-ON behavior of these new siRNA constructs under physiological conditions. After salt-free purification, subsequent hybridization to double-stranded ribonucleic acids and nanoformulation to lipoplexes, the prodye conjugated siRNA was examined in cellular uptake studies for First Contact Imaging. The investigated siRNA-prodye conjugates showed strong sensitivity to esterases, being hydrolyzed at the biolabile function and developing a strong fluorescence which was verified in bulk. As an optimization, a new profluorescent molecule system was designed and synthesized, which has a carbonate as biolabile 6' protecting group and a highly water soluble 3' clickable linker. This new non-fluorescent but colored prodye showed 12 - 320 times increased fluorescence intensities between OFF- and ON- states, depending to the deprotection method. This is the first reported molecule model of an asymmetric profluorescent fluorescein, having the very favorable 3' & 6' functions.

Table of Contents

List of Figures

List of Tables

List of Schemes

1 Introduction

1.1 Concept of color, fluorescence & phosphorescence

Color is an individual perception caused by light. Humans can perceive color stimuli approximately from 380 nm to 700 nm in the electromagnetic radiation spectrum. Big contributions in the field of color science and optics were made by James Clerk Maxwell[1] in the 19th century, resulting in the formula describing the wavelength $\nu = \frac{c}{\lambda}$. Interestingly he brought Louis-Victor de Broglie's[2] theory about matter and wave–particle duality with the Planck's Law, Einstein's relativity theory and his theory in relation, resulting in the formula: $E = h\nu = mc^2 = \frac{hc}{\lambda}$, where *E* is the energy, *h* is Planck's constant, *ν* and *λ* are the frequency and wavelength of the incoming photon respectively, *m* is the mass and *c* is the speed of light.
Light matter interactions result in scattering, ionization and absorbance, which is alongside electromagnetic radiation the second reason reaching exited electronstages, causing photoluminescence.[3]
The emission of light was first described by N. Monardes 1565, after he observed that an infusion of the wood *Lignum nepheriticum*, which he typically used for treating kidney and urinary diseases, was emitting peculiar blue light.[3] In 1852, G.G. Stokes first reported the emission of light by quinine sulfate solution upon excitation with UV light and introduced the term of "fluorescence".[4]
The photoluminescence can be divided in two types of emission. First one is the emission of electrons from electronically excited singlet state to ground state, which does not require change in spin orientation and is the most common relaxation type, called fluorescence. The second one is the relaxation of electrons from an excited triplet state to a ground state, which requires a spin orientation change and is called phosphorescence. Thus one electron transfer causes one photon emission.
Fluorescence is a three-step process, described 1935 by Aleksander Jablonski with his famous Jablonski diagram (**Figure 1).**[5,6]
At room temperature the process starts out at lower vibrational energy levels of the ground state. Ilumination with light at a resonance frequency causes absorption of light and results chromophore excitation to the higher energy level of S_1 and S_2 (Step 1). The absorption

process takes place on a time scale 10^{-15} sec, which is much faster than that of molecular vibration described by the Franck-Codon-principle.[7,8,9]

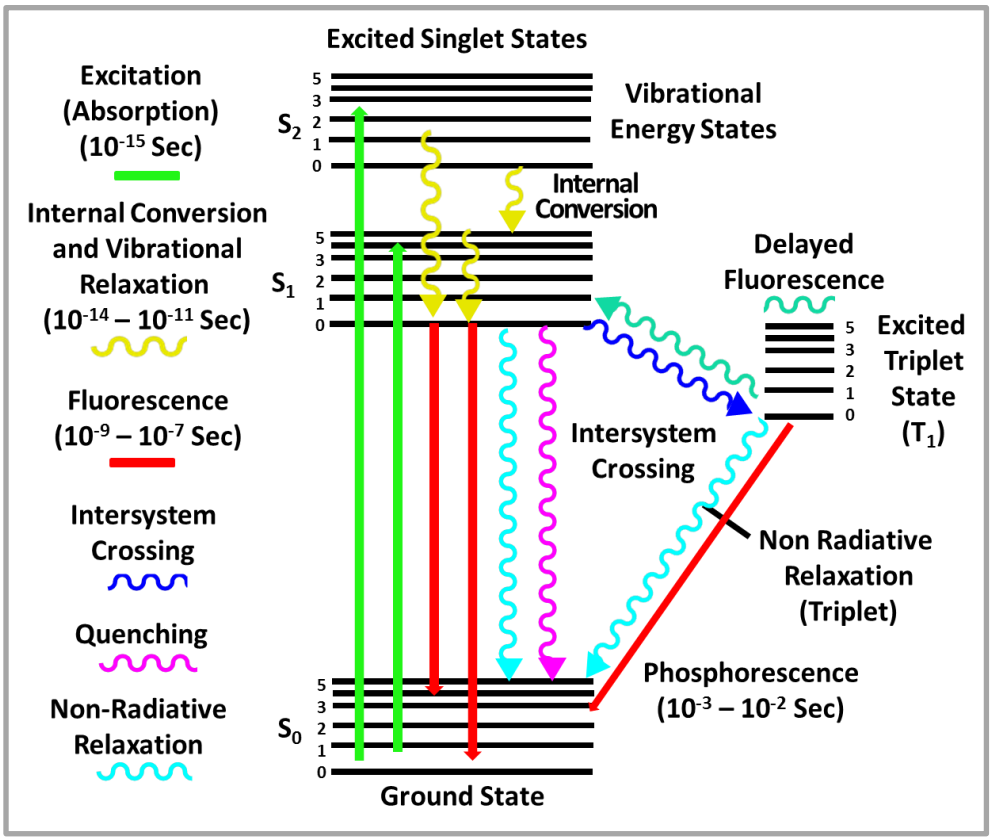

Figure 1. Jablonski energy diagram, adapted from literature[6]

In the excited state, the electron is promoted to an anti-bonding orbital and atoms in the bond are less tightly held. Shifting to the right for S_1 potential, the energy curve and electron is promoted to higher vibrational level in S_1 state than the vibrational level in ground state. This process is known as internal conversion or vibrational relaxation (loss of energy in the absence of light emission) and takes place through *e.g.* intermolecular collisions at a time scale of 10^{-12} sec, which is faster than that of fluorescence process (Step 2).

The electron relaxation from the lowest vibrational energy level of the excited state to a vibrational energy level of the ground state S_0 results in the phenomenon of fluorescence (Step 3) by emitting photons at a certain wavelength with lower energy of these photons than that of the incident photons.

Except of photon emission, the decay of the excited state can occur in a non-radiative (NR) relaxation. This NR quenching of a fluorophore excited state can happen through variety of processes, like bond rotation or vibration, molecular collision and photoinduced electron transfer (PeT)[10]. The excited state can also undergo spin-forbidden intersystem crossing (ITC)

to the triplet excited state (T_1) and subsequent relaxation by either photon emission, widely known as phosphorescence or again NR decay (**Figure 1**). Another important pathway for a decay of excited state is FRET (Förster resonance energy transfer)[11] to an acceptor molecule. This process is distance-dependent and can be used as a measure of proximity of labeled entities.[12]

The emitted light is red-shifted to a higher wavelength than the absorbed light (excitation wavelength) and the energy difference between the excited and emitted photons is named Stokes shift (**Figure 2**). Internal conversion, solvent effects and excited state reactions can affect the magnitude of the Stokes shift. In particular the vibrational relaxation in exited state is always faster than the fluorescence emission, where the difference is a part of Stokes shift.[11, 13]

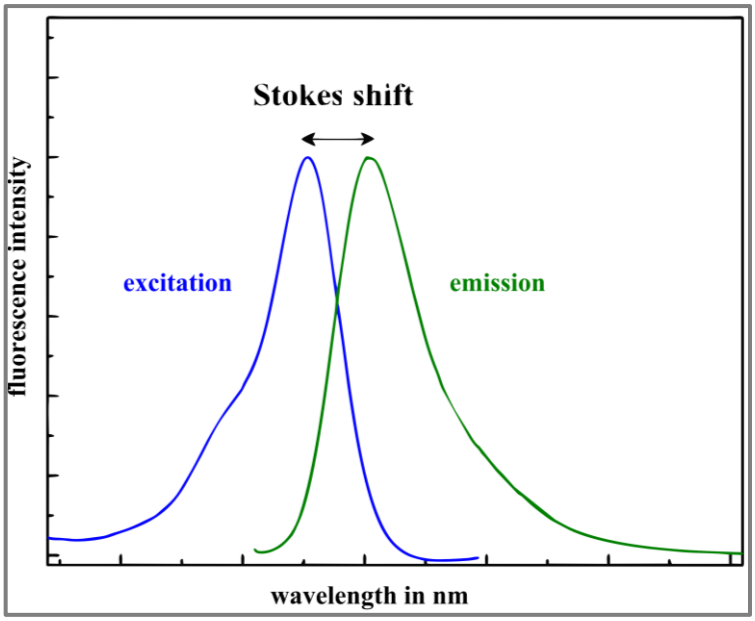

Figure 2. Excitation and emission of a fluorophore with Stokes shift[11]

Fluorophores have specific absorption maxima (abs $\lambda_{max)}$, excitation maxima (ex λ_{max}), emission maxima (em λ_{max}), extinction coefficients and quantum yields.

The molar extinction coefficient (ε given in M^{-1} cm^{-1}, also known as molar absorption coefficient) can be determined by using the Lambert-Beer-Law ($A = \varepsilon * c * l$; *A = absorbance, l = pathlength, c = concentration)* and defines the absorption of a given molecule in dependence on the wavelength.

The quantum yield is defined as the ratio of photons emitted to those absorbed (Φ). In practice it is measured by comparing to a reference compound (e.g. fluorescein or rhodamines), for which Φ has been determined before with a high degree of accuracy. This means ideally, that

the reference compound should have the same absorbance as the compound of interest at a given excitation wavelength, similar ex-em spectra should be dissolved in the same solvent and should yield similar fluorescence intensities. In other words, the quantum yield reflects the probability of the excited state being deactivated by fluorescence rather than by another, non-radiative mechanism such as internal conversion, vibrational relaxation or intersystem crossing (**Figure 1**).[13]

1.2 Topology of chromophores

Organic dyes are chromophores with conjugated π-systems that share electrons responsible for color by absorbing certain wavelengths of visible light. Chromophores usually appear in conjugated π-systems and metal complexes whereas fluorescent dyes occur in heteroaromatic molecules, named fluorophores. Larger systems appear always in absorption and emission spectra shifted to longer (bathochromic) wavelengths, especially in presence of anti-auxochrome groups (electron withdrawing) like nitro (-NO_2), aldehyde (-CHO), imine (-C=N-R) and auxochrome (electron donating) groups like hydroxyl –OH, amine –NH_2, carboxyl –COOH.

Many naturally occurring chromophores exhibit measurable fluorescence, but only some of them produce strong fluorescence suitable for analytical methods. These include aromatic amino acids, nicotinamide cofactors, flavins, porphyrins, pyridoxal derivatives, nucleosides. These endogenous fluorophores are responsible for autofluorescence of biological structures such as mitochondria or lysosomes (**Figure 4**).[14,15]

The "classics" of organic fluorescent dyes are coumarin, fluorescein and rhodamine.

Coumarins (**Figure 3**) exhibit a wide range of fluorescence emission properties with extremely sensitive fluorescence to the local environment of the molecules, especially to the local polarity and microviscosity. Coumarins naturally exist in *e.g.* sweet woodruff and *tonka coumarou* beans. The first total synthesis of coumarin was developed by William Henry Perkin in 1868, Hans Pechmann described in the end of the 19th century the mechanism of action.[16] Present synthesis routes with high yields using modern condensation conditions are described in reference.[17,18,19] Coumarin derivatives have excitation maxima between 350 – 390 nm and emit light between 430 – 470 nm, comparable to the commercial coumarin dye Alexa Fluor 350® (Life technologies). Coumarins are applied as Ca^{2+} ion indicator,[20] profluorescent enzyme substrates[21] and RNA labeling reagents[22].

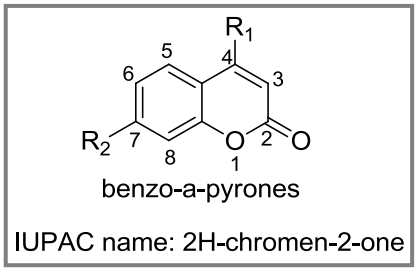

Figure 3. Structure of coumarins, mostly substituted on pos. 3 and 7

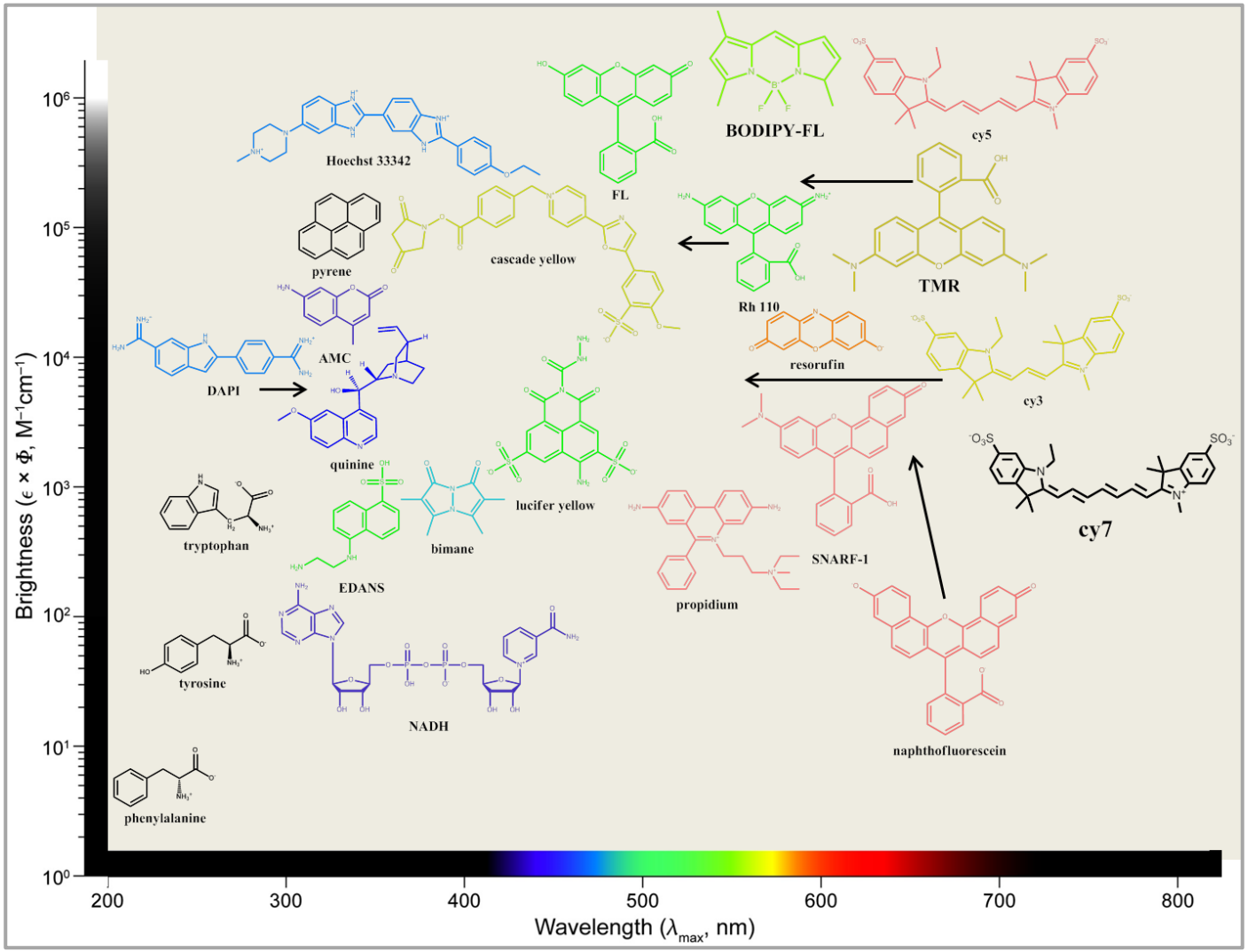

Figure 4. Fluorophore brightness plotted versus the absorption maximum wavelength for the major fluorescent dyes. The emission maximum is indicated in corresponding color of structure. For clarity, only the fluorescent moiety of some molecules is shown. The arrows indicate the exact position of some dyes. Adapted from lit.[15]

Fluorescein and Rhodamine are described in section "1.3 Xanthene dyes" (page 9) in detail. Benzophenoxazin based fluorescent dyes like Meldola's Blue, Nile Red and Blue are known representatives with sophisticated solvatochromie effects but weak fluorescent properties. Benzophenoxazin derivatives can be synthesized *via* different condensation reactions and are particularly applied in rare range as biomolecule labeling agents.[23, 24]

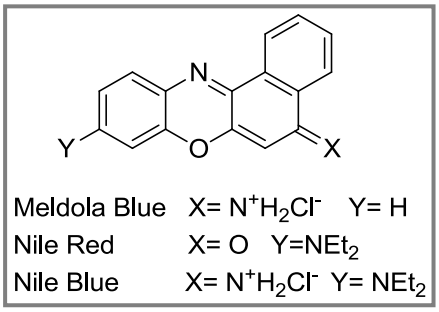

Figure 5. Benzophenoxazin based fluorescent dyes

Another important class with high quantum yields and less reported biological but more technical application (*e.g.* in car industry) are the rylene dyes (**Figure 6**). In 1978, one of the first engineered rylenes is Lucifer Yellow (**Figure 4**) with similar ex-em profiles to fluorescein, which is used as effective polar tracer.[25] Other reported perylenes for site-specific protein labeling and higher molecular weight were developed by the group of Prof. Klaus Müllen.[26] In general adding naphtyl units to a rylene dye decreases the water solubility and limits aqueous application of a labeling candidate, whereas the substitution with water soluble groups improves the labeling application in molecular biology (e.g. protein and DNA labeling).[26, 27, 28]

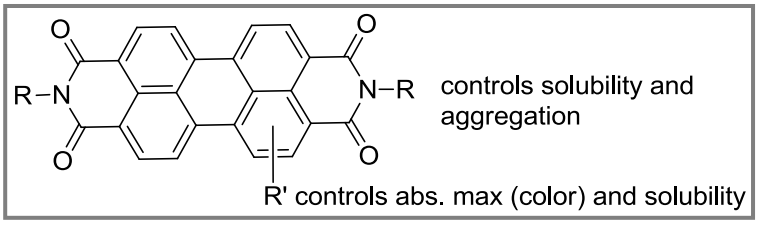

Figure 6. Rylene dyes

The boron difluoro dipyrromethene, better known as BODIPY (**Figure 7**) dye was discovered by Treibs and Kreuzer in 1968.[29] Through appropriate substitution BODIPYs can be used for fluorescent labeling.[30] This nature of BODIPY dyes allows their utilization as surrogates for traditional dyes such as fluorescein and rhodamines in membrane probing. [31]

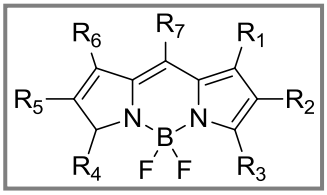

Figure 7. BODIPY dyes with possible substitution positions

Further prominent types of chromophores are the cyanine dyes (**Figure 8**). Cyanines consist of cationic molecules, in which two terminal nitrogen heterocyclic subunits are linked by a polymethine bridge.[15] Cyanine (Cy) dyes in modern bioresearch, also pronounced as the CyDye fluorophores, are those bearing a sulfoindocyanine structure and are named according to the number of carbon atoms between the dihydroindole units, for example, Cy3, Cy5, Cy7.[32] Cyanine dyes are widely used in labeling proteins,[32] antibodies,[33] peptides[34] and nucleic acid probes[35] for various fluorescence detection techniques.

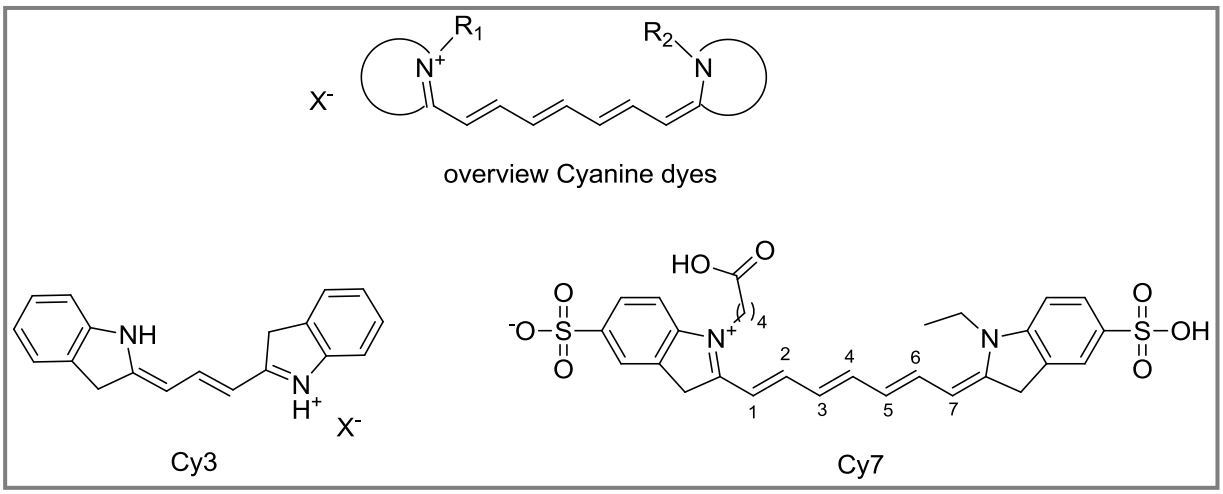

Figure 8. Cyanine dyes

1.3 Xanthene dyes

The three-membered ring structure better known as 9*H*-xanthene or 10*H*-9-oxaanthracene (**Figure 9**) represents the central core of most widely used fluorescent dyes, which includes fluorescein, eosins, and rhodamines. They tend to be fluorescent, yellow to pink to bluish red, brilliant dyes. General synthesis routes are performed by condensation of phthalic anhydride derivatives with resorcinol or 3-aminophenol containing compounds.[15, 36]

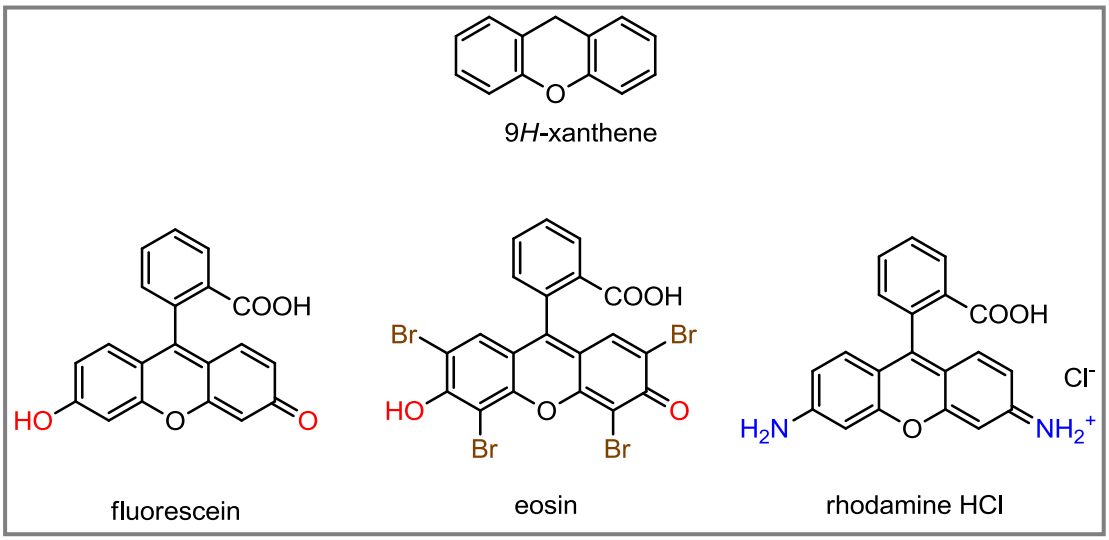

Figure 9. Relationship between xanthene nucleus and corresponding fluorophores

Fluorescein, as the ubiquitous small-molecule fluorophore was first synthesized by Adolf von Beyer in 1871.[37] Despite its antiquity, fluorescein remains one of the most widely utilized fluorophores in modern biochemical, biological, and medicinal research. A key feature of fluorescein is an equilibrium between an "open," fluorescent chinoic form and a "closed," nonfluorescent lactone (**Scheme 1**). Attaching blocking groups on the phenolic oxygens through ester or ether bonds can modulate this equilibrium. This strategy has been used to prepare fluorogenic substrates for many enzymes.[36] Because of its green emission (~ 532 nm) fluorescein is called "green fluorophore" or "green dye".

Depending on the pH, fluorescein predominantly exists in different species in aqueous solution (**Figure 10**). At pH 0 – 2 in the cationic form, from pH 2 – 4 in the non-fluorescent

lactoic and fluorescent chinoic form, at pH 5 – 6 in the monoanionic and from pH 7 – 9 in the strong fluorescent dianionic form.

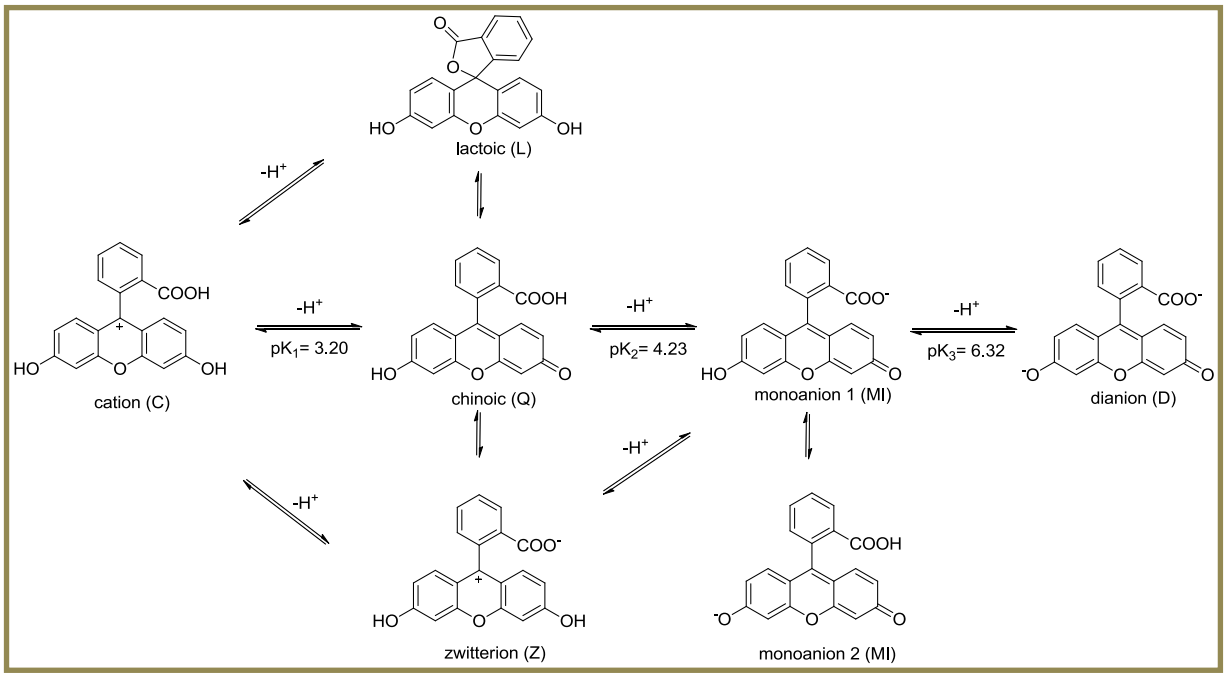

Scheme 1. Prototropic forms of fluorescein, adapted from lit.[38]

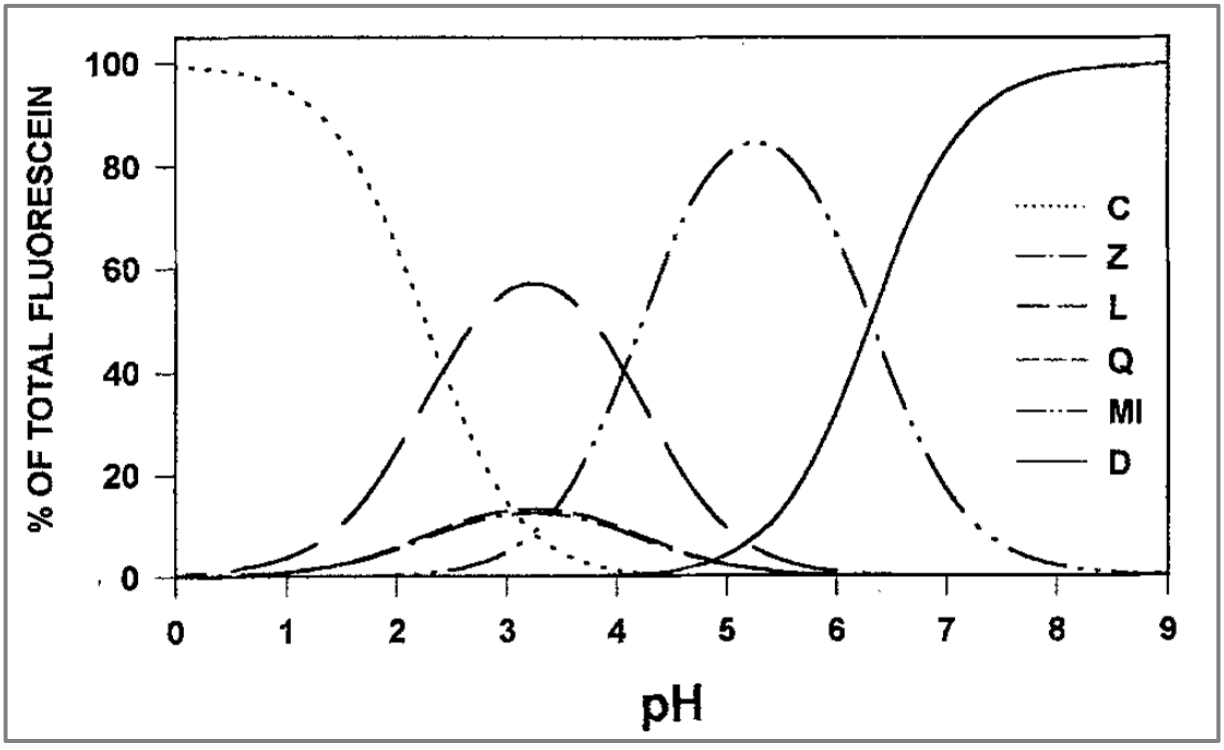

Figure 10. pH dependent structure of fluorescein[38]

Different absorption spectra in relation to the pH values are reported, depending on the present structure of the fluorescein molecule (**Figure 11**). In general, pH increase causes bathochromic absorption shifts of fluoresceins.[38]

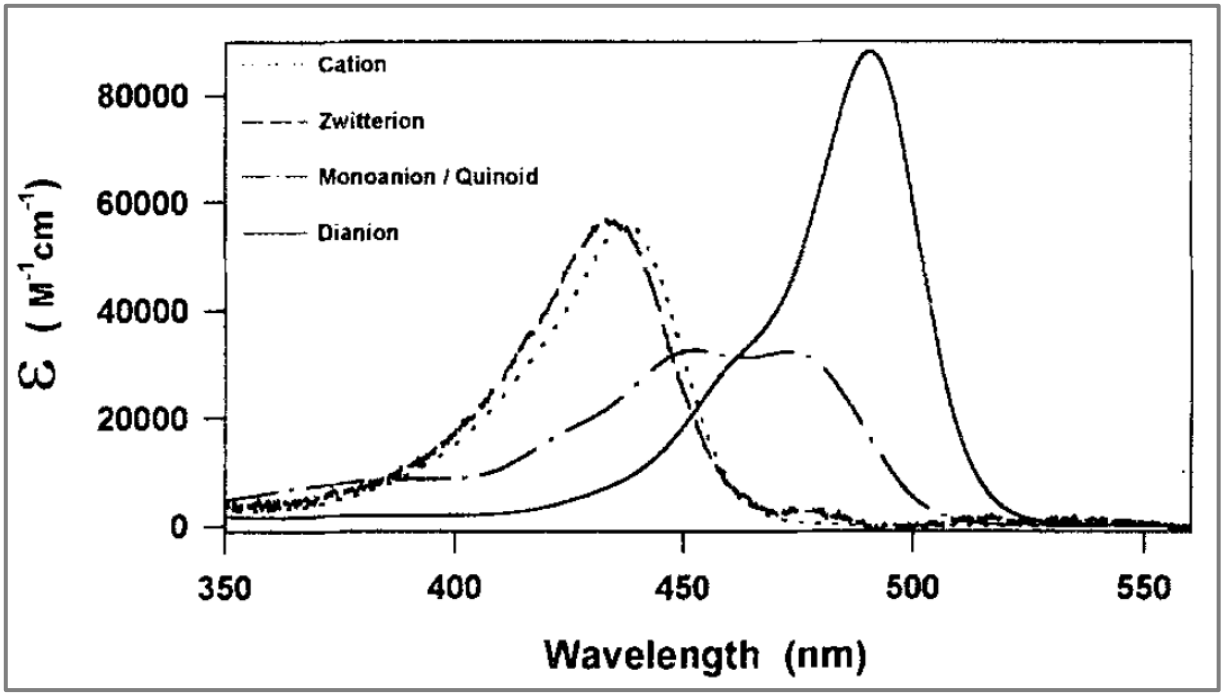

Figure 11. pH dependent absorption spectra of fluorescein[38]

The quantum yields and fluorescence lifetimes in aqueous solution are reported in **Table 1.**[38]

Species	Quantum yield	Lifetime (ns)
Dianion (pH 12)	0.93	4.06 ±0.02
Monoanion (pH 4.5)	0.36	3.37 ±0.02
Chinoic (pH 1.6)	0.29	2.97 ±0.02
Cation[39]	0.9 – 1.0	3.5 – 4.4

Table 1. Quantum yields and fluorescence lifetime of the fluorescein species

Notable is the high quantum yield (Φ = 0.88) of the dianionic structure in physiological pH of 7.4. As most common biological label reagent, fluorescein is used as isothiocyanate (FITC) derivative[40,41] and carboxy (CFL) derivative[42] for amine-selective protein labeling. The biarsenical fluorescein (FlAsH) developed by Roger Tsien exhibits low fluorescence in solution, in parts due to rotation around the C−As bonds. Upon binding to a tetracysteine-

containing helix in an engineered protein, FlAsH is rigidified and exhibits a large increase in quantum yield with spectral properties similar to fluorescein.[43]

A sophisticated example of a FRET system (direct energy transfer from the excited state to an acceptor molecule) is compound FCD (**Figure 12**), which contains a fluorescein donor and azopyridine acceptor dye linked by a cephalosporin moiety. Only after the cleavage by β-lactamase the azopyridine is cleaved, resulting in the cleavage of the quencher and increase in fluorescence.[44]

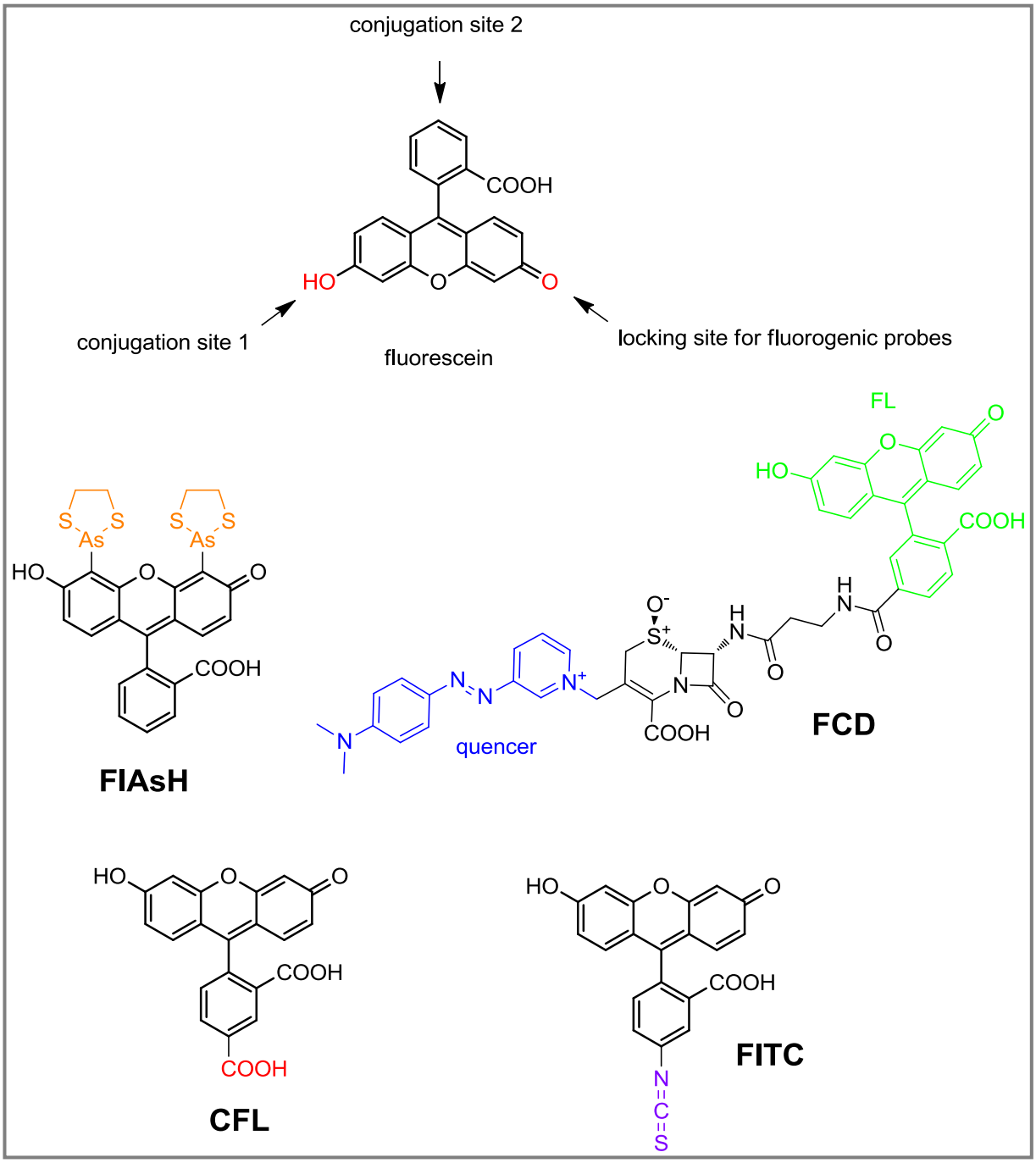

Figure 12. Selected fluorescein derivatives with reactive groups

The so called “red fluorophore” or “red dye” xanthene is rhodamine. As amino counterparts of fluorescein, the rhodamines were first described in 1887.[45] They have several advantages over fluoresceins, including lower pH-sensitivity, higher photostability and tunable spectral properties.[36] The absorption and emission properties are strongly influenced by substituents in the xanthene nucleus.[46] The prototypical rhodamine is the tetraalkylated variant sulforhodamine B (**Figure 13**, SB), which absorbs in the green and emits in the yellow (λ_{max} / λ_{em} = 565 / 586 nm, ε = 8.4 × 10^4 M^{-1} cm^{-1}). Carboxylated sulforhodamine B (**Figure 13**, CSB) is used as common laser dye for amine containing biomacromolecules labeling.[47] Another known laser dye is Texas Red (TR) with remarkable robustness against quenching caused by robustness against acidic MALDI matrixes.[48] Useful rhodamine probes for biological imaging are carbon- and silicium–substituted xanthene derivatives, *e.g.* compound SiRh (**Figure 13**). Introduction of carbon results in 55 nm red-shifted (bathochromic) dyes compared to isologous xanthens.[49]

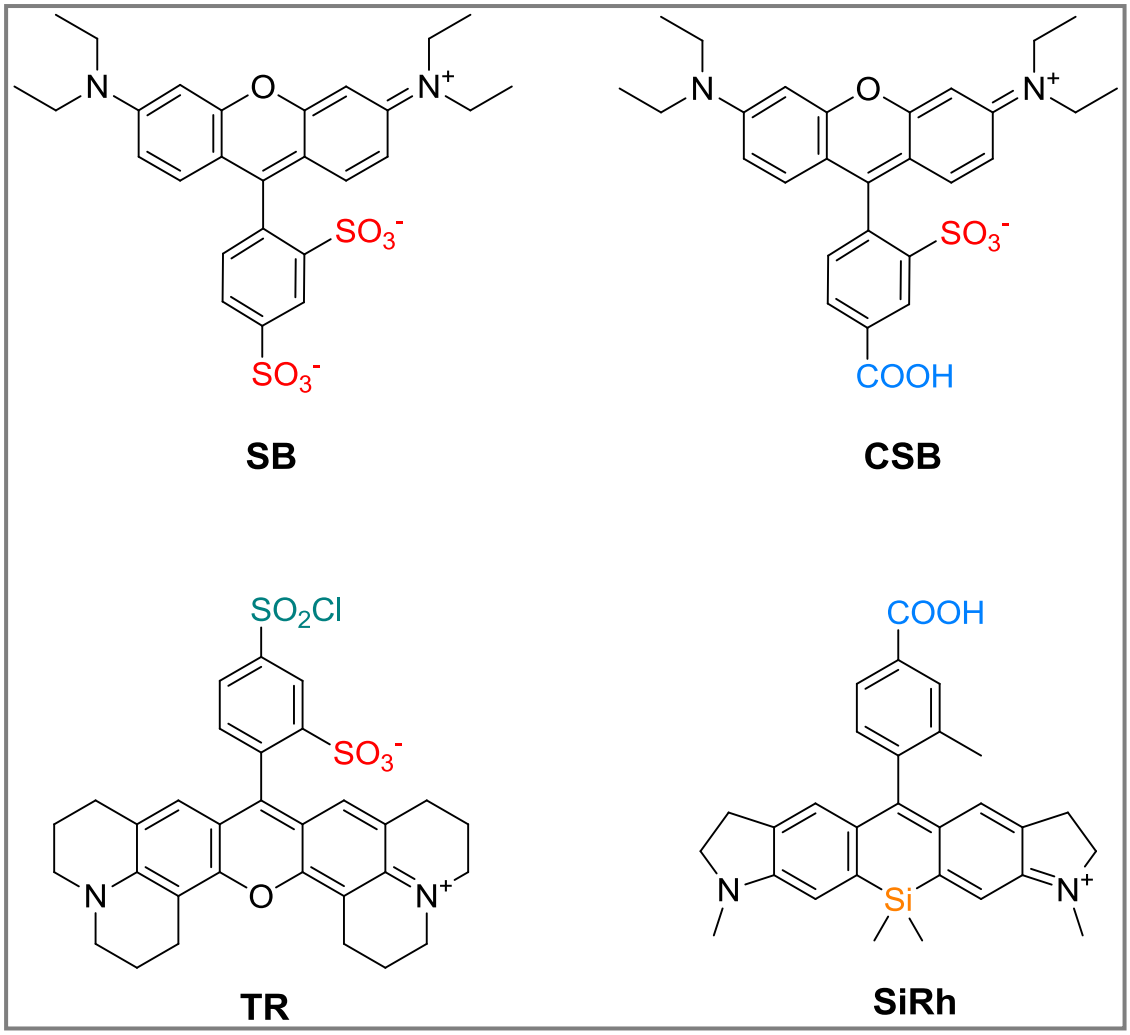

Figure 13. Selected rhodamine derivatives with reactive groups

1.4 Chromogenic & fluorogenic dyes

Chromogenic and fluorogenic probes may be described as reagents that can interact with targets (analytes) accompanied by the changes of their spectroscopic (chromogenic, or luminescent including chemiluminescent properties. On the basis of such changes, the analytes can thus be detectable.[50] Four known, major reaction mechanism play a role in activation: (I) protonation-deprotonation, (II) complexation (including direct and competitive displacement), (III) covalent bond formation or cleavage and (IV) redox reaction.[50]
In the past, a large number of pH sensitive probes has been reported in literature,[25] the most important of these being xanthenes, BODIPYs and cyanines. One major example is a rhodamine based pH probe. The response mechanism is based on the structural change between the colorless & non-fluorescent spirolactam and pink colored & fluorescent chinoic form, caused by protonation (**Scheme 2**), e.g. in acidic organelles such as lysosomes.[51]

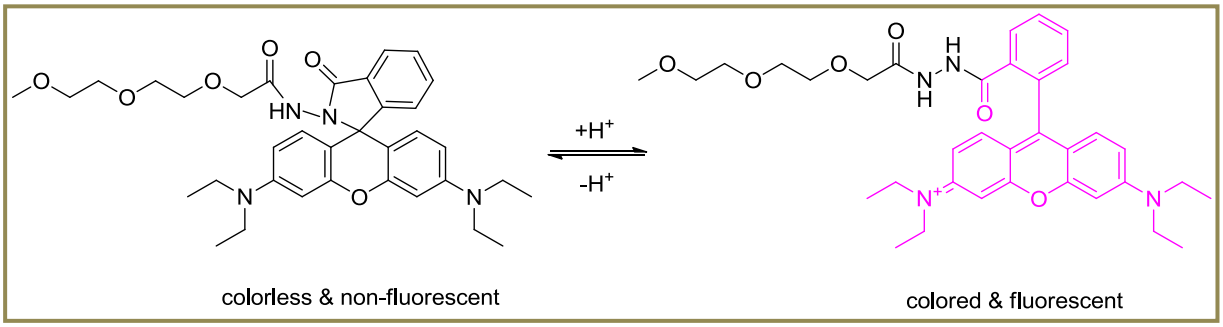

Scheme 2. (I) Protonation-sensitive rhodamine prodye

In complexation-based mechanism the key issue for designing fluorogenic probes is how to construct a specific receptor for an analyte. One interesting probe for Zn^{2+} ions is shown in **Scheme 3**. This FRET system does not emit red light if excited with 485 nm blue light. After Complexation with Zn^{2+}, the molecule results in opening of spirolactame and generating a 560 nm absorption system, which now can be exited with blue light and emits in red light. A major advantage of such a system is the reversibility.[52]

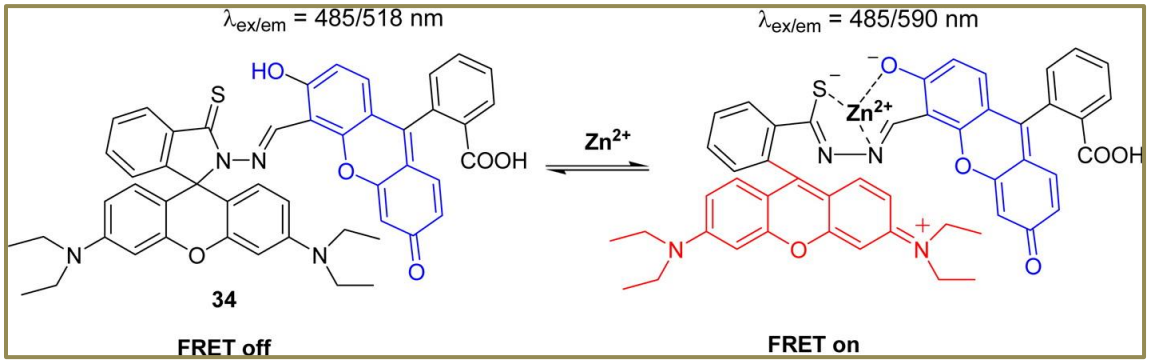

Scheme 3. (II) Zn^{2+} sensitive profluorescent FRET system

In the past decade, many systems with profluorescent dyes with enzymatically cleavable protecting groups have been reported. In most cases these prodyes can be activated by intracellular enzymes such as esterases- or *via* photochemical treatment.

Figure 14 represents some known systems from literature.[53, 54]

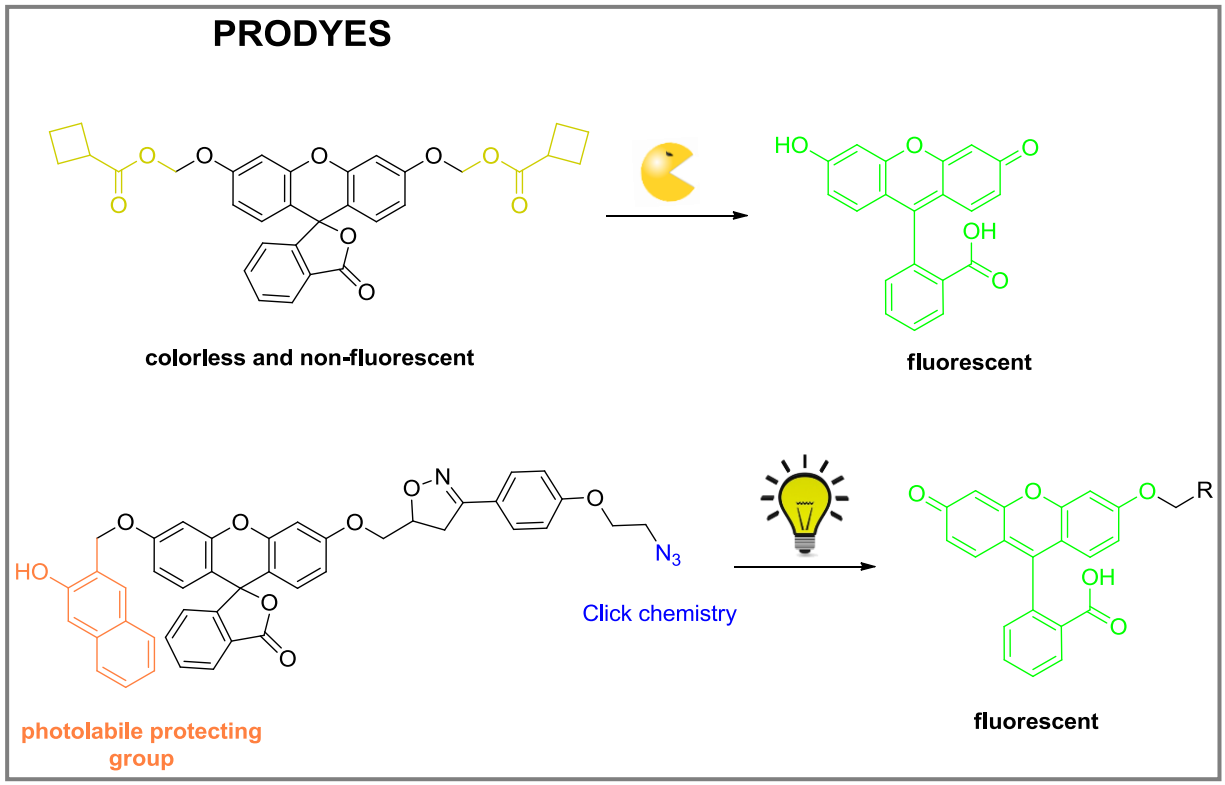

Figure 14. (III) Selected prodyes and activation after bond cleavage[53, 54]

Typical redox reactions are caused by oxygen species, like H_2O_2. A reversible profluorescent dye was developed by Miller et al.[55], in this probe, the fluorescent thiol derivative is formed by oxidation and can be reduced in the cellular environment (HEK 293 cells) back to the nonfluorescent prodye (**Scheme 4**).[55]

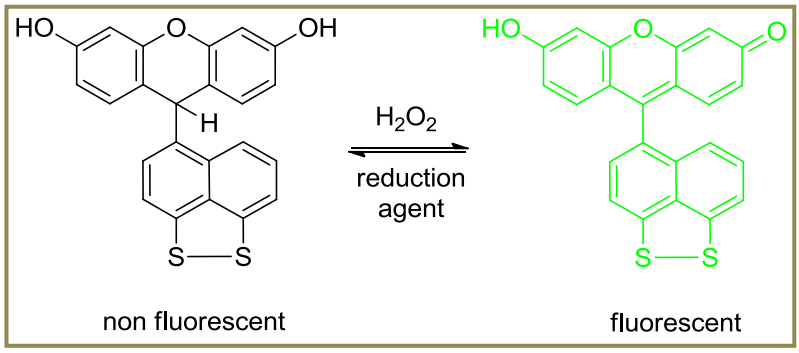

Scheme 4. (IV) Reactive oxygen species sensitive profluorescent redox system

1.5 Fluorophore application in biology

The goal in biomolecule labeling via fluorophores is the development of simple and efficient methods for chemical bonding of biomolecules, in this case with dyes. Functional modification of biological molecules with high degree of selectivity or specifity is needed. Up to now, such a universal coupling method has not been developed.

The easiest way to explain a labeling mechanism is that a reactive group (e.g. -NH_2 , -SH) of a biomolecule forms covalent bond(s) with the other reactive group(s) (COOH , Maleiimide) of a fluorophore with unique spectral properties for analytical purposes. Great attention is devoted to biorthogonal reactions, in which the reaction of compounds A and B bearing bioorthogonal functional groups proceeds in the presence of different functionalities found within living systems (**Figure 15**).[56] For bioorthogonality selectivity, biological & chemical inertness between the reactive partners must be given. The reaction kinetics have to be fast enough and the reactants have to be biocompatible with accessible reporter properties.[56]

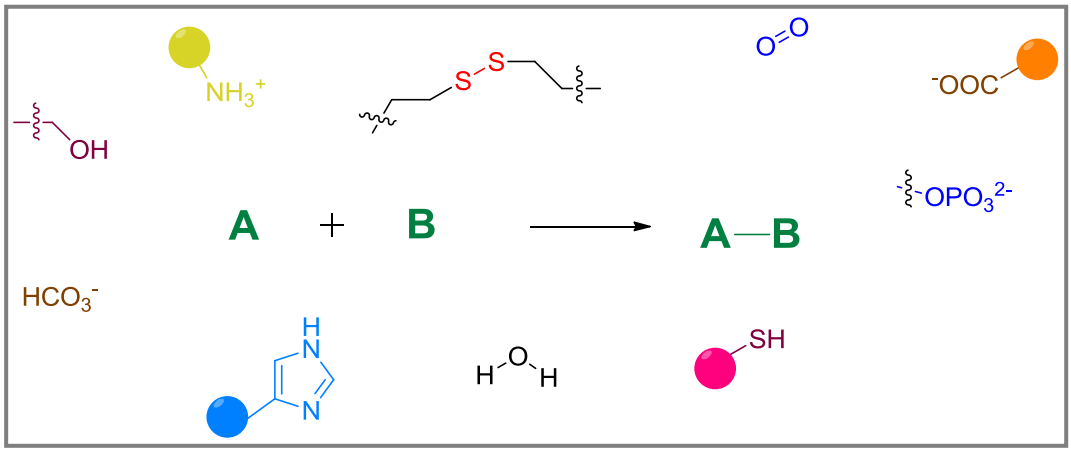

Figure 15. Orthogonal reaction between compound A and B in a biological system, without any other biomolecule interaction

Typical regioselective and biorthogonal reactions are the Staudinger Ligation of azides with triarylphospines and Azide-alkyne Huisgen-like 1,3-dipolar cycloaddtion. In the first above mentioned reaction, triarylphospine attacks the non-natural modified azido biomolecule. Thereby, it releases nitrogen from a four-coordinate transition state to yield an aza-ylide, which undergoes intramolecular attack on the ester, extruding methylalcohol and resulting in a bicycle. Upon hydrolysis, oxidation of the phosphine and formation of an amide bond occur to give the ligated product (**Figure 16** A).[56]

In the second mentioned reaction, terminal alkynes (or strained cyclooctynes) are activated by Cu^{I} to undergo [3+2] cycloaddtion with azides under physiological conditions (**Figure 16** B).[56]

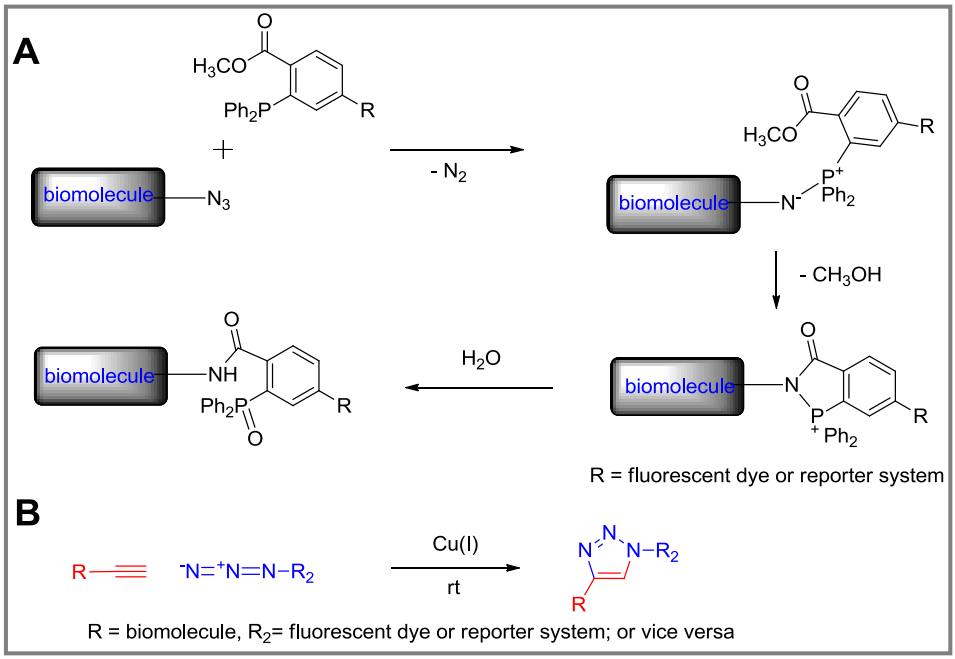

Figure 16. Staudinger Ligation (A) and 1,3 dipolar "Huisgen" cycloaddition (B)

1.6 Fluorophores in context of DNA & RNA

Nucleic acid polymers are characterized by the types of base residues present and the structure of their sugar backbone. The bases are nitrogen containing ring compounds, consisting of either purine or pyrimidine derivatives. A purine is a fused-ring compound containing one 6-membered ring attached to a 5-membered ring, whereas a pyrimidine consists of a single 6-membered ring structure (**Figure 17**).

Nucleic acids can contain any of three kinds of pyrimidine ring systems (uracil, cytosine, or thymine) or two types of purine derivatives (adenine or guanine). Adenine, guanine, thymine, and cytosine are the four main base constituents found in DNA. In RNA molecules, three of these four bases are present, but with thymine replaced by uracil to make up the fourth (**Figure 17**). Some additional unexplored modifications are found in messenger RNA (mRNA), transfer RNA (tRNA), and ribosomal RNA (rRNA) and are listed in the MODOMICS database.[57]

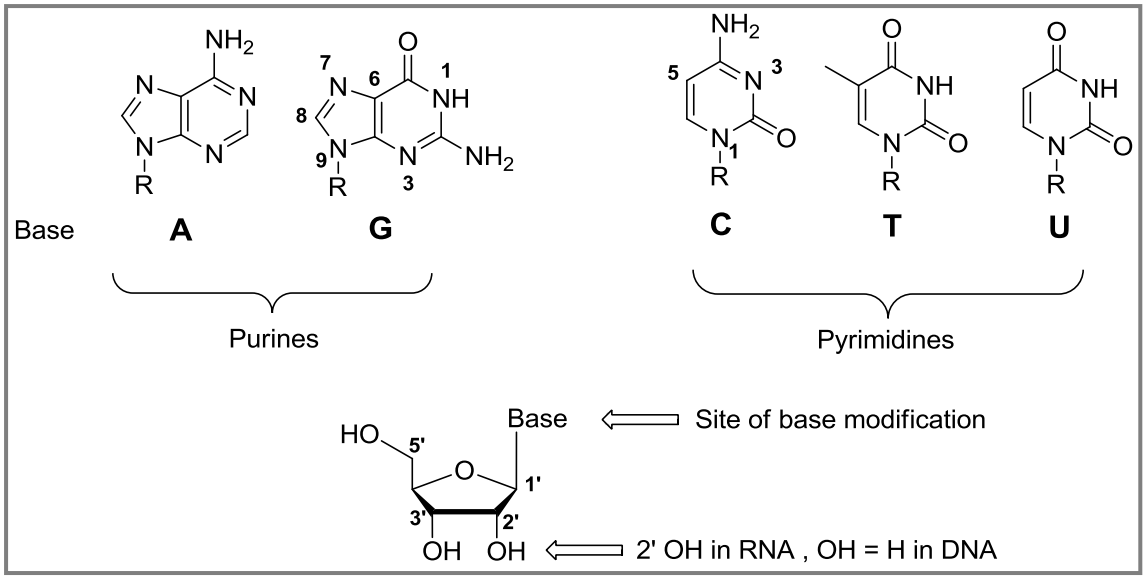

Figure 17. Structures of the 5 major nucleic acids present in nature

Base-pairing in nucleic acids do follow Watson-Crick rule[58], where the bases form H-bonds between cytosines pairing guanines and between adenines pairing thymines/uracils. Furthermore there is the case of the wobble H-bonding between guanine and uracil, which mainly occurs in RNA (**Figure 18**). It is known that for equivalent complementary sequences, the RNA duplex is more stable than the DNA duplex under most physiological and laboratory

conditions.[59] This phenomenon has been explained by a variety of factors, including differential stacking, sugar puckering and solvation.[60, 61, 62]

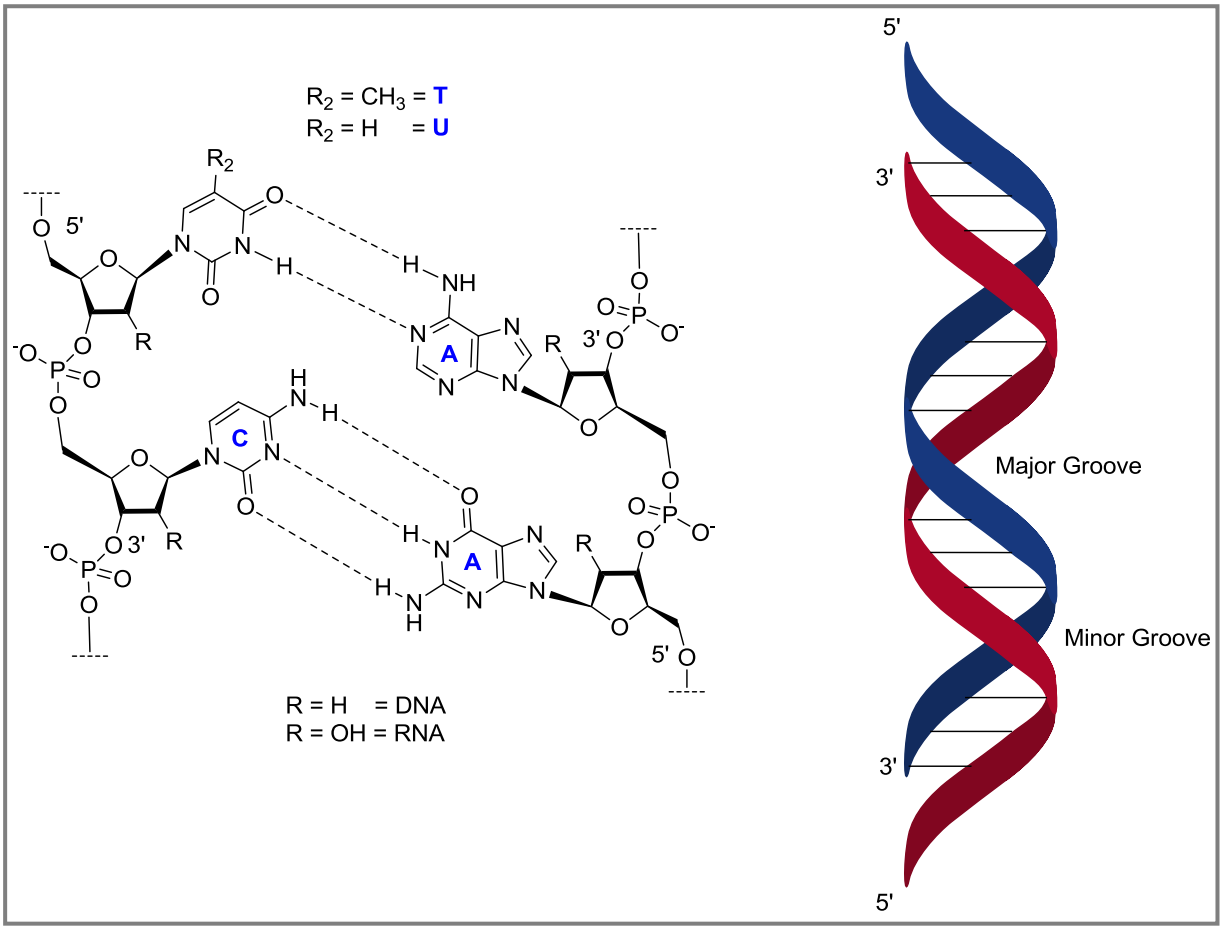

Figure 18. Watson-Crick Model for a double helix between two antiparallel strands

From a non-radioactive labeling point of view, there are several staining and labeling methods of nucleic acids, *e.g.* with either direct or indirect luminescent outcome (fluorescence, chemiluminescence or bioluminescence reporters etc.).[63] Nowadays, the state-of-the-art labeling methods are based on "Click" chemistry, either using copper-catalyzed azide alkyne cycloadditions (CuAAC) for oligonucleotide labeling[64, 65, 66] (see section 1.5) or copper-free cycloadditions for the labeling of biomolecules to circumvent undesired effects of copper ions (**Figure 19**).[65, 56, 67]

Copper-catalyzed Click reactions with azides and terminal alkynes, yielding good amounts of triazol products (**Figure 19 A)** are very common and easy to applicate.[68]

Big contributions in the field of copper-free Click chemistry with oligonucleotides were done by Prof. Jaeschke and coworkers (**Figure 19 B**).[69, 70] The chemistry behind this topic is based on inverse-electron demand Diels – Alder cycloadditions (DAinv), where a strained dienophile reacts with an electron-deficient diazine,[71] triazine[72] or a tetrazine.[73] Furthermore,

biorthogonal proflourescent labeling based on the same conjugation mechanism was reported by Dr. Kath-Schorr (**Figure 19 C)**, with biorthogonal *in vivo* labeling of RNA.[74]

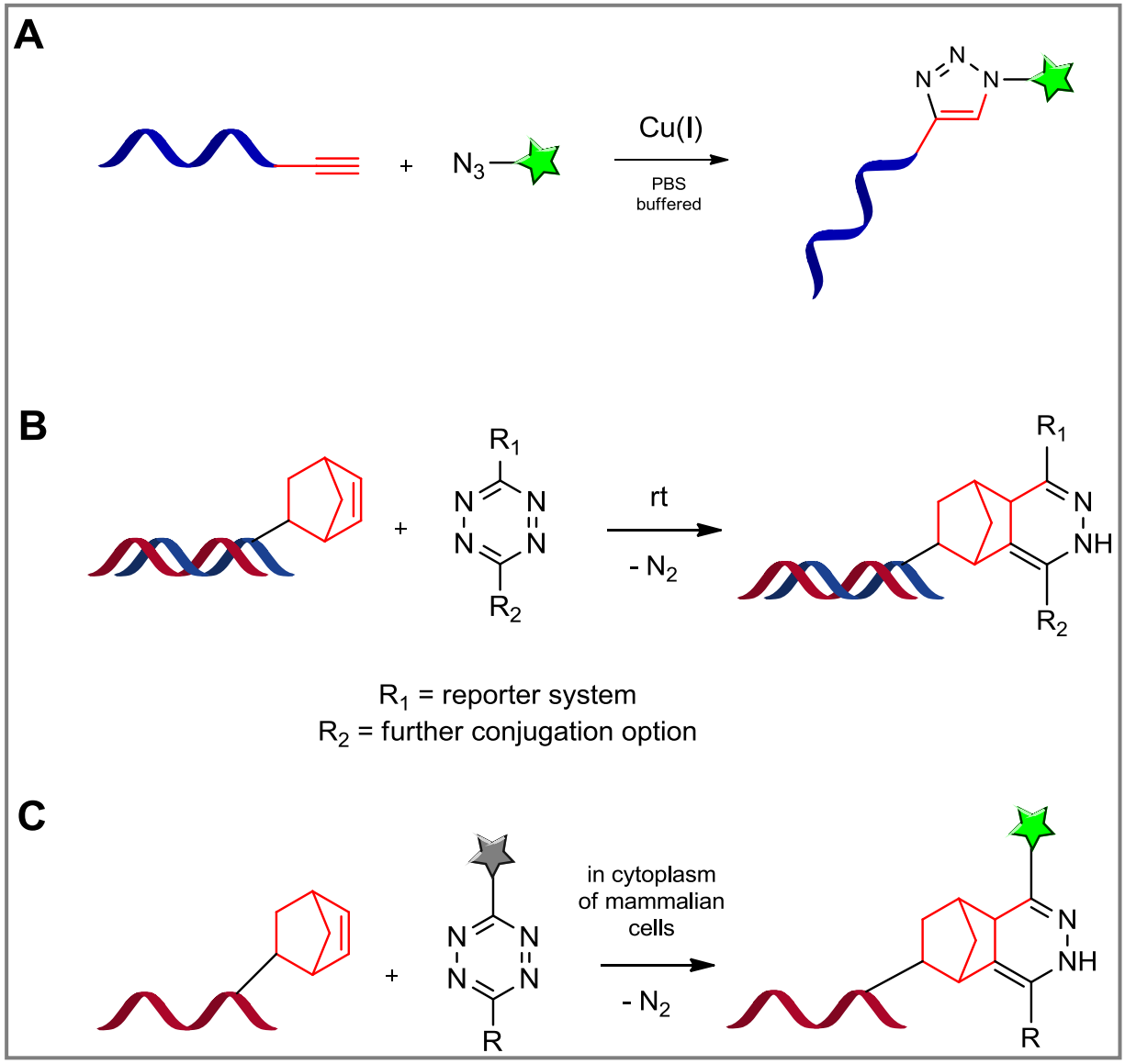

Figure 19. Labeling methods of oligonucleotides by Click chemistry; grey star = non-fluorescent, green star = fluorescent dye

2 Goal of the work

Delivery of therapeutic nucleic acid based drugs is still very demanding and difficult to manage and monitor. For this reason, a precise method for the monitoring of RNAi pathways is necessary. This work pushes the development of a model system for monitoring intracellular release of potentially therapeutic nucleic acids, with siRNA as model payload from nanoparticular formulations and the so called “First Contact” of a prodye-siRNA. According to this major goal, the syntheses of some non-fluorescent and colorless leukodye-azides, based on fluorescein synthons and mainly protected by ester functions were performed. In a second attempt, new asymmetric fluorescent and profluorescent molecules with sophisticated functionalities were developed. Furthermore, these prodyes were conjugated to nucleic acids bearing a terminal alkyne *via* a Cu(I)-catalyzed azide-alkyne cycloaddition (CuAAC). The sensitivity of prodye-siRNA to cellular esterases caused by an esterase labile acetyl function was evaluated. Thus, the approach for the visualization of a release event is based on the action of lytic enzymes in the cell, which will hydrolytically cleave capping groups from the colorless leukodye, converting it to a fluorophore in the process. The conversion of a prodye to a fluorescent dye was analyzed by both, enzymatic and chemical methods, elucidating the mechanism of action. In PAGE experiments the prodye-siRNA was checked for identity and profluorescent character. Furthermore, a major challenge was the adaptation of a purification method, which should be as mild as possible for fully protected prodye-siRNA constructs. *In vitro* cell culture experiments using lipoplexes as standard transfection particles were set in order to investigate the uptake and “First Contact” imaging of nanoparticular siRNA.

3 Results and Discussion

3.1 Prodye synthesis, modification and fluorescent properties of recently synthesized dyes

This section describes the organic synthesis of all designed and developed fluorescent dyes and profluorescent derivatives so called prodyes. The synthesized compounds **1** and **2** were used for conjugation and "First Contact" investigations. The new dyes have following structure-function relationships:

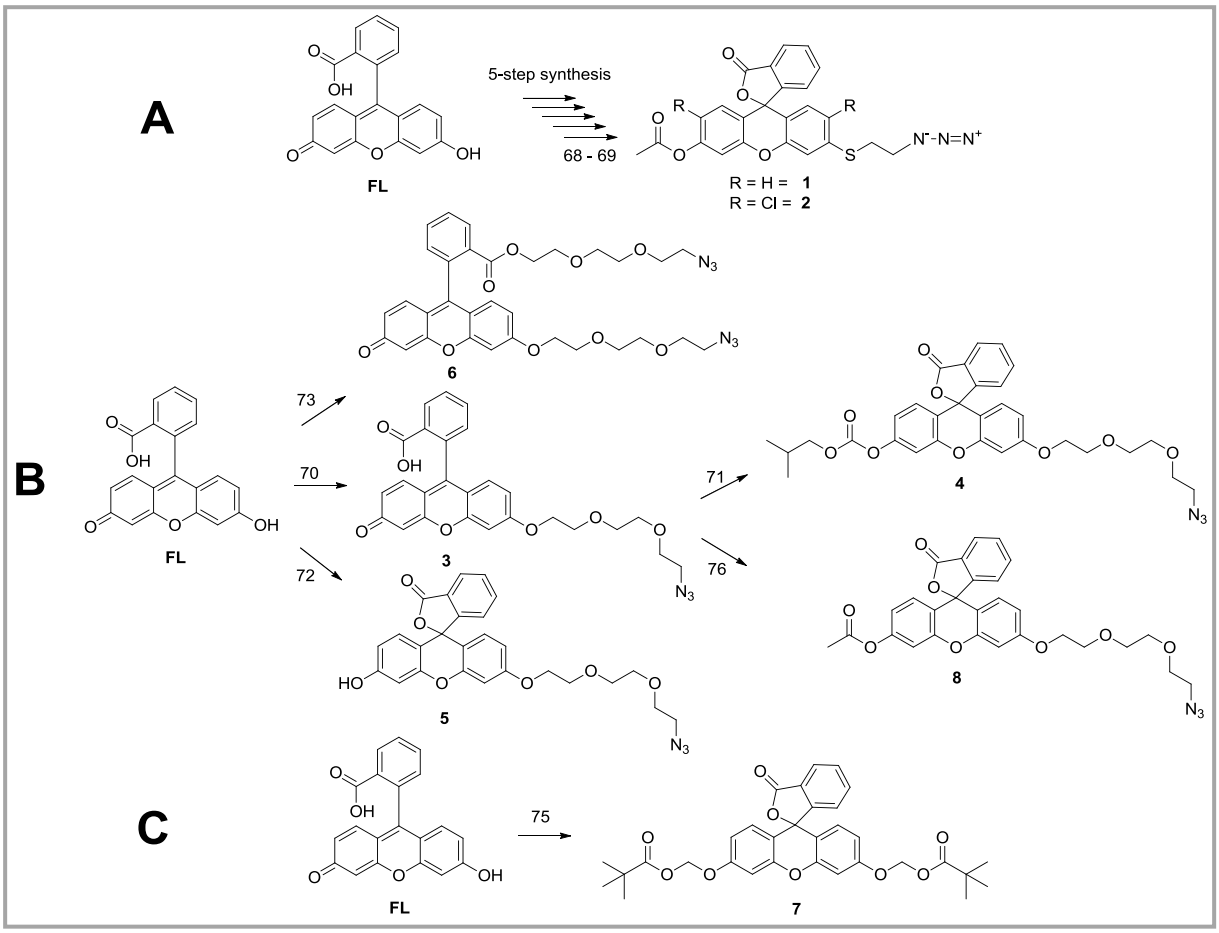

Figure 20. Call-out synthesis route of prodyes and new type of fluorescent dyes; A: route to compound **1** & **2**, B: route to compound **3-6** & **8,** C: route to compound **7** from lit.[53] The numbers on the arrows refer to the pages in the experimental section.

I) “Clickable” azide moiety connected over an aliphatic chain to the fluorescein synthon, allowing high photostability in molecule **1** - **2** and improved water solubility in molecule **3** - **6** and **8**.

II) Biolabile protection group for the 6’ of xanthene core and for locking the non-fluorescent lactoic structure. The protecting groups are either acetyl or carbonate functions that can be cleaved by esterases.

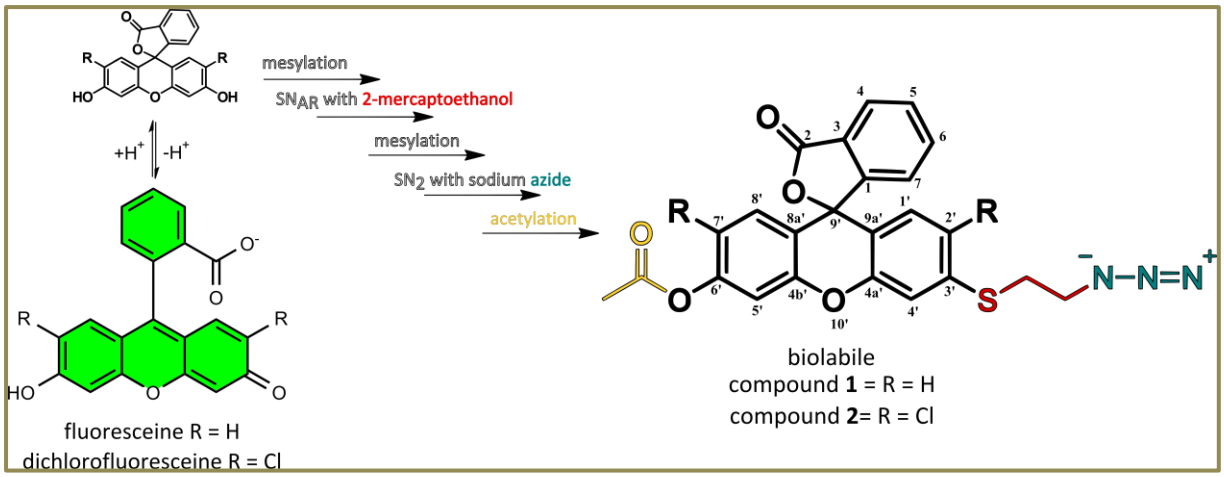

Scheme 5. Synthesis overview of prodye **1** & **2**. The initial four steps were developed by Dr. Michaela Kotaskova.[75]

The five step synthesis of prodye **1** & **2** started with the bisulfonation at the 3’ & 6’ positions of xanthene core leading to colorless pro-fluorophores, termed prodye in this thesis. 2-mercaptoethanolate (provided with DBU) attacked as S-nucleophile the electron rich aromatic ring and formed *via* a nucleophilic aromatic substitution (SN_{Ar}) the orange colored 3’thioether-xanthene, providing access to a new class of asymmetric dyes. The monitored yields were around 40%. Remarkably, the product formation was achieved without a metal catalyst, which is unusual for SN_{Ar}-type reactions and is a major advantage.[76] Yet, substitution is still restricted to N and O nucleophiles and no xanthenes with sulfur atoms at the 3’ or 6’ position have been reported. Further mesylation at 6’ and aliphatic hydroxyl group formed again a colorless prodye, with easily removable leaving groups. Sodium azide was used for deprotection of the 6’ and as azidation reagent on the aliphatic linker. The key analysis to detect either the lactoic structure with corresponding sp^3 hybridized carbon or the chinoic structure featuring a sp^2 carbon was done by using the C^{13}-NMR spectroscopy. With this spectroscopic method, the specific signal for the quarternary 9’ carbon was discovered

around 80 ppm, displaying the mainly existing form of the prodye or fluorophore. **Figure 21** depicts the structures after the inspection of C-NMR signals around 80 ppm. After the fourth synthesis step, investigations showed strong resistance of the new asymmetric dyes to photobleaching. With using equiabsorbing concentration of dye and standard in pH 7.3 buffered aqueous solutions, it was shown that thioether derivatives maintain about 70 % or more of their initial fluorescence, although quantum yields and extinction coefficients were less compared to standard fluorescein and dichlorofluorescein. Nevertheless the improved photostability of the sulfur substituted dyes prompted to use the new dyes for further modification and biomacromolecule labeling. Reaction mixtures were analyzed by denaturating polyacrylamide gel electrophoresis (PAGE) and the isolated click product by an LC-MS analysis. For further information, the reader can refer to the publication "Synthesis of new asymmetric xanthene dyes ***via*** catalyst-free S_NAr with sulfur nucleophiles", Michaela Kotaskova, Okan Osman Oglou & Mark Helm in Org. Biomol. Chem.**,** 2014, 12, 3816-3820.[68]

Acetylation, the key step for biolabile functionalization was performed by the use of acetic anhydride. This reaction is discussed in detail on the coming pages.

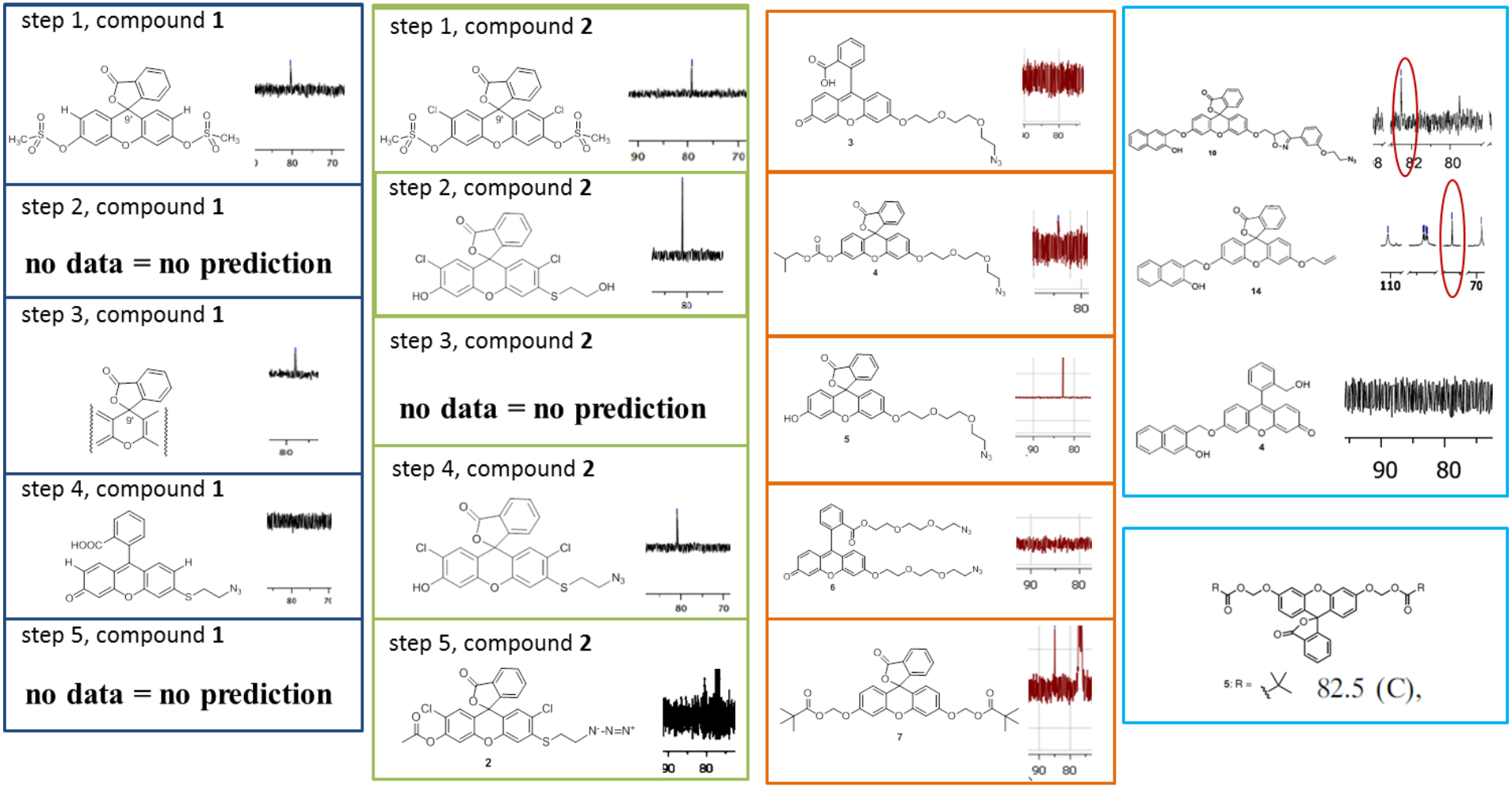

Figure 21. C-NMR analysis of product formation predicting the spiro or lactoic structure, blue rectangles: synthesis route to compound **1**, green rectangles: synthesis route to compound **2**, orange rectangles: synthesis route of **3 - 7**; references: upper cyan rectangle: C-NMR data from Nekongo et al., 2014[54], lower cyan rectangle: C-NMR data from Tian et al., 2012[53]

3.1.1 Acetylation of asymmetric xanthene dyes with profluorescent properties

With the knowledge of the biolability of acetyl esters towards intracellular esterases[36] the question was addressed how to get an ester-locked, clickable fluorescein with tetrahedral structure of 9’ carbon (**Figure 22)**. The easiest way of introducing an acetyl group was performed with acetic anhydride as acetylation reagent, dissolved in pyridine.[77] Using 8 equivalents of acetic anhydride instead of 4 equivalents[77] under refluxing yielded between 70 – 98 % products. TLC Monitoring of product formation was done by the use of UV lamps by (observation of the colorlessness and absorption with 254 nm wavelength). Colorless and non-fluorescent products were obtained and stored under argon atmosphere in – 20°C.

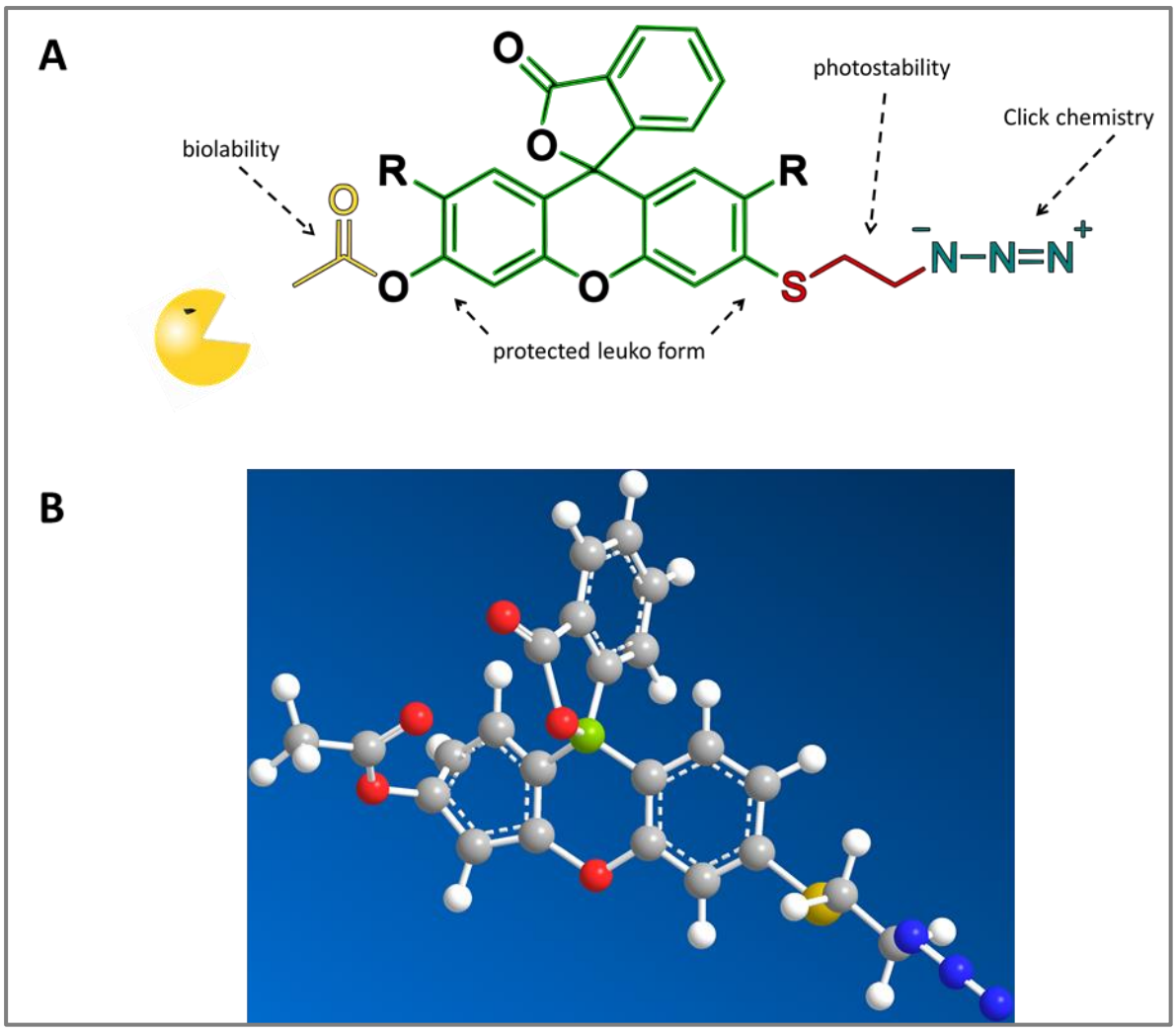

Figure 22. Structure of the first synthesized prodye **1** ; **A)** Chemical structure of compound **1**, in yellow the esterase labile acetyl function, in green the profluorescent core, in the red thio ethyl linker and in dark-blue the clickable azide; **B)** 3D model of compound **1** with the sp^3 hybridized carbon on 9' (in green) xanthene core and the corresponding tetrahedral structure of the ring

Possible acetylation routes are *via* I) isomerization and subsequent acetylation of the phenolic function on the 6', II) intramolecular acetyl transfer or III) intermolecular acetyl transfer over the anhydric structure (**Scheme 6**). The purification can be performed during Gramm scale synthesis by the help of normal phased silica column or during microgram scale by using preparative silica plates (2mm) applying methanol and dichloromethane as eluents in recommended ratios (see experimental section).

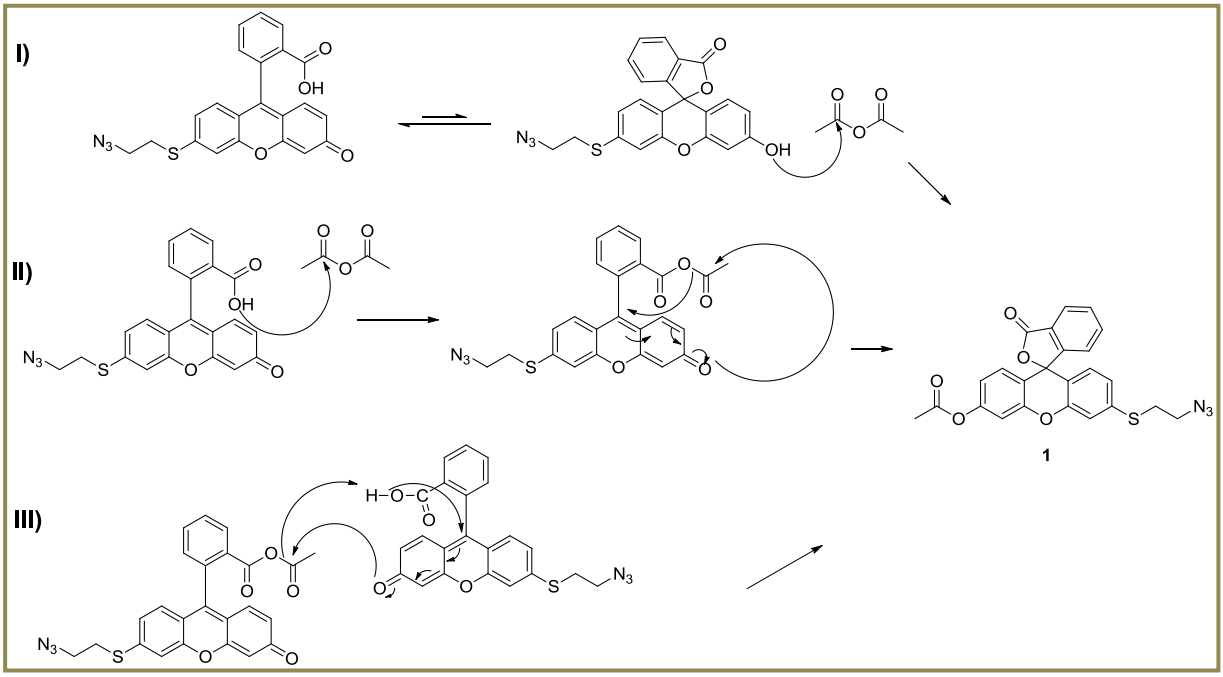

Scheme 6. Possible acetylation mechanism of fluorescein precursors in pyridine after:

I) Isomerization to the lactoic structure

II) Intramolecular acetylation

III) Intermolecular acetylation

3.1.2 Synthesis of new asymmetric xanthenes with carbonate as biolabile function

Observations and results of less molecule stability at a narrow pH window of 6.3 – 7.2, moderate Click yields of conjugation reactions (explained in section 3.2) and difficulties during cell uptake experiments of prodye **1** conjugated siRNA lipolexes (section 3.7) prompted the development of new prodye **4.**

This profluorescent dye (**Scheme 9**) has a water soluble PEG linker with a clickable azide group on the 6’ and an esterase sensitive isobutyl carbonate function on the 3’ of fluorescein, aiming at an improved pH window, due to the steric hindrance and protection characteristics of the isobutyl group compared to a methyl one in compound **1**.[76]

Pegylation of the 3’ fluorescein with 1.05 equivalents of mesylated PEG-azide catalyzed by 2.2 equivalents potassium carbonate delivered 3 different products with an overall yield of 35 % after preparative TLC purification. The highly fluorescent compound **3** was obtained as major product with 27% yield, compound **5** and **6** with 4 % yield, respectively (**Scheme 7**).

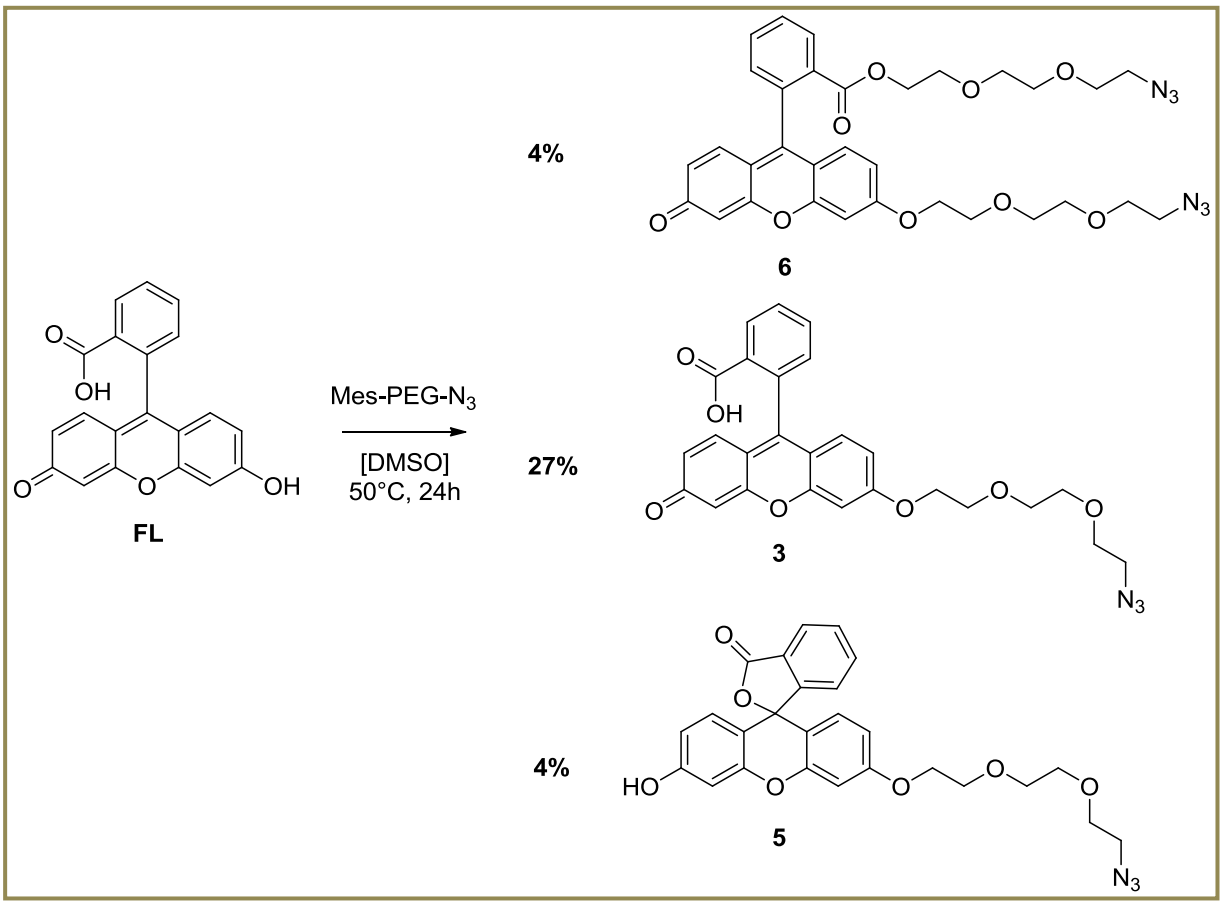

Scheme 7. Pegylation of fluorescein and synthesis of compounds **3, 5** and **6**

The reaction process and monitored by H-NMR, investigating the methylene protons in alpha position to the azide (4.03 & 4.05 ppm, page 70). 24 hours were set as maximum reaction time according to the reaction kinetics. Mesylated PEG was chosen for a nucleophilic substitution reaction because of good leaving character due to good mesylate anion resonance stability. As base potassium carbonate instead of triethylamine[77] was chosen for easier work up conditions.

Noteworthy is the formation of the non-expected two byproducts **5** and **6** under weak basic conditions. According to data in the paper of Clonis et al [38], describing studies of fluorescein among other things in basic environment, the formation of **5** is very unlikely and very surprising, whereas compound **6** formation can be explained by twice substitution of the mainly existing dianionic structure in ~ pH 9.[38] Further impurities in the crude product were not detected, excluding the non-reacted fluorescein. Different biolability strategies were considered. First, acetalization of 6' was tested, because of reported biolability of these groups against esterases.[53] Two synthesis attempts using a Iodoaliphate formed by a

Finkelstein reaction[53] (**Scheme 8 A**) and refluxing with propargylalcoholate in propargylalcohol[75] (**Scheme 8 B**), aiming at the development of asymmetric xanthene prodyes, failed.

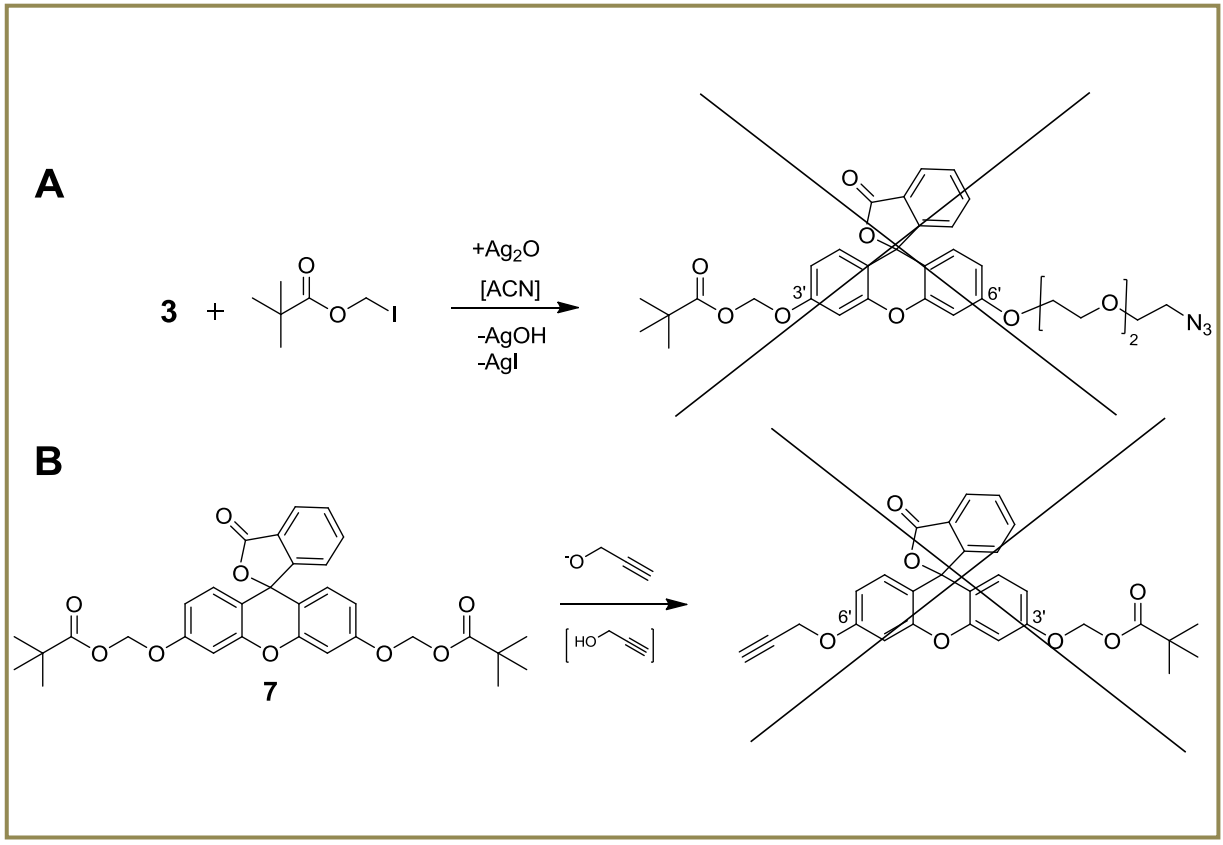

Scheme 8. Failed synthesis attempts of new asymmetric xanthene prodyes

Preceding attempts with acetic anhydride for acetylation of compound **3** produced **8** (experimental section, page 74 fw.), which is non-fluorescent and yellow. Consequently the idea was to develop a carbonate protected 6' (Note: according to the IUPAC criteria, the carbonate substituted 6' is rated higher than the alkoxy substituted 3', thus the synthesized molecules are illustrated in vice versa numbering) by applying isobutyl chloro formate (IBCF) as carboxylation reagent (**Scheme 9**).[78]

Carbonates are well known prodrug groups, having sensitivity to intracellular esterases. Usage in the field of HIV-[79] and cancer-therapy[80] was reported.

Initial carboxylation was performed with pyridine as solvent, after 4 hours the synthesis showed the formation of a lemon yellow compound **4**, but the reaction could not be reproduced due to the reaction reversibility forming the starting material **3**. Synthesis with neat fluid IBCF at 37° C for 6 hours yielded after preparative TLC purification 45 % of **4**.

Preparative TLC with 2 mm silica phase is exerted if the desired compound cannot be precipitated by recrystallization over n-pentane or other apolar solvents.

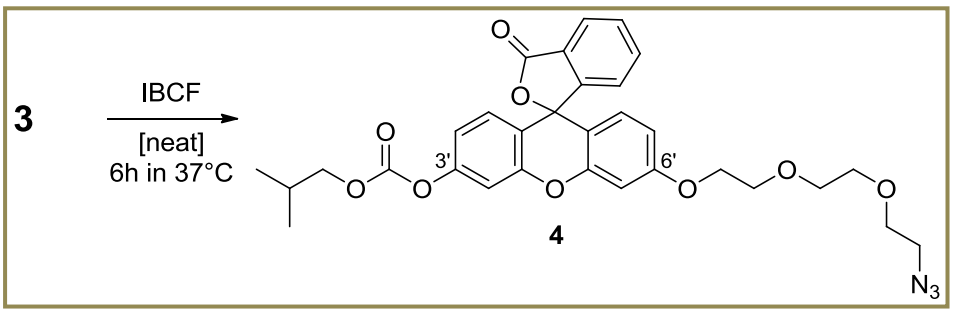

Scheme 9. Carboxylation of the phenolic OH at 3' of the xanthene core

Besides of H-NMR and C-NMR measurements, the LC-MS analysis was performed for structure elucidation. As a significant outcome, the fragmentation pattern of compound 4 is given in **figure 23**, measured with the positive fragmentation mode. The new asymmetric prodye is stored under argon atmosphere in -20 °C. With extended length of the azide linker, the prodye should have improved Click yields.[81] PEGylation is supposed to improve water solubility. Furthermore, the isopropyl carbonate functionalization is supposed to affect the

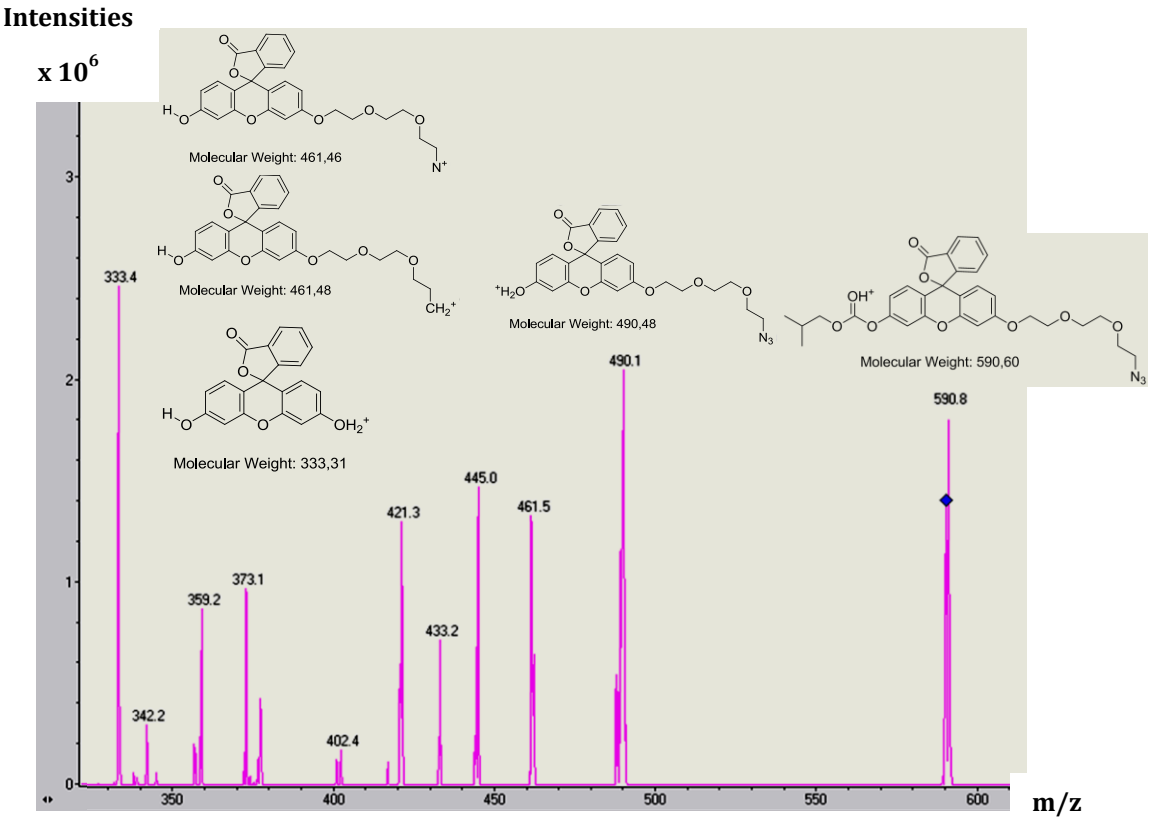

Figure 23. Fragmentation pattern of compound **4** and predicted ion structures, measured on an Agilent LC-MS/MS ion trap (positive mode)

stability against Tris buffered media (PAGE)[82] and increase the stability between pH 5.0 – 7.4.[83]

3.1.3 Fourier transform infrared spectroscopic (FT-IR) analysis of compound 3 – 5 & 7

Using the FT-IR, it was possible to get important structure information about the newly synthesized compounds **3** – **8**. The benefit of this method was the application of a few µg substance for analysis and the significant outcome about the structure. For instance, investigating the absorption between 1600 – 1800 cm^{-1} delivered key results about the lactoic or chinoic of a each compound (**Figure 24**). Here one can see that the lactoic carbonyl group emission was shifted to the higher wavelengths (> 1750 cm^{-1}) than the chinoic- or keto-groups (< 1750 cm^{-1}), as described in literature.[84] Furthermore the presence of the azide function was found by checking the absorption between 2200 – 2300 cm^{-1}.[84]

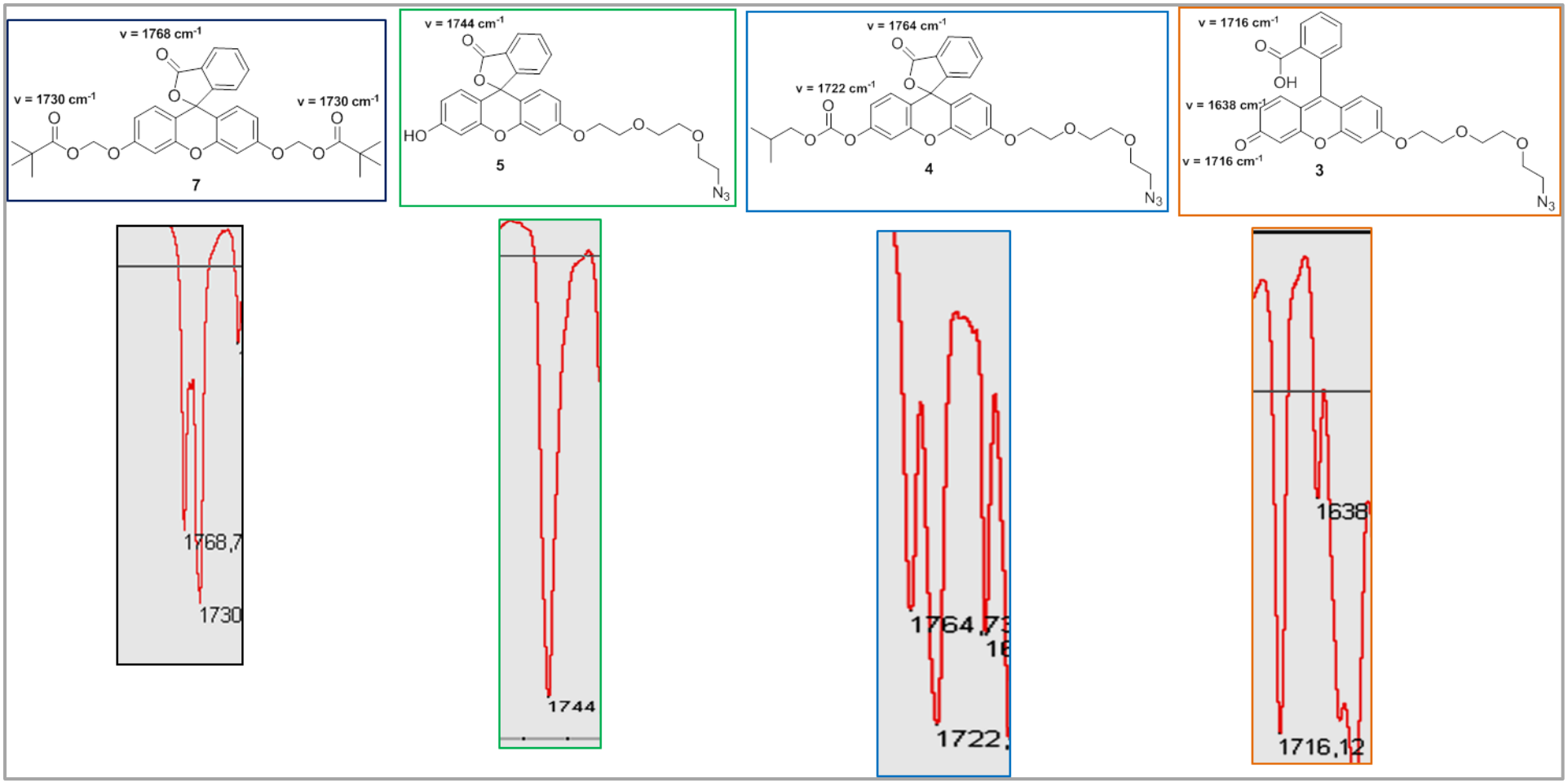

Figure 24. Fourier transform infrared spectroscopy analysis of standard compound **7**[53] and new compounds **3 – 5** with predicted structures resulting from key signals of carbonyl functions.

3.1.4 Spectroscopic data of recently synthesized compounds 3 – 6

Recently synthesized prodyes **3 – 6** were investigated under pH 3, 7.4 and 11 conditions on a JASCO fluorimeter. Detailed spectroscopic data can be found in the experimental section, page 79 - 101. Depending on the pH value and consequent activation of the dyes by their chemical environment, the following abbreviated data was found (**Table 2**).

Remarkable fluorescent turn ON of newly synthesized prodye **4** was registered in the cuvette, showing an 12 x increase at pH 7.4 and 320 x increase at pH 11 of fluorescence. Furthermore, the already fluorescent precursor **3** and byproduct **6** did not show any impressive decrease of fluorescence, verifying the mainly presence of chinoic structures during the respective measurements. Byproduct **5,** isolated as the lactoic isomer of compound **3**, developed 38 x increase at pH 7.4, but did not develop higher fluorescent intensities at pH 11, making clear that the major part of the molecules were already present as fluorescent lactoic molecules at pH 7.4. This observation supported the protecting of the 6' OH with the carboxylate and signified the assumption that prodye **4** mainly exists in the non-fluorescent form in physiological pH and environment. Thus, the activation by esterases can be investigated and the First Contact of interest is supposed to be visible.

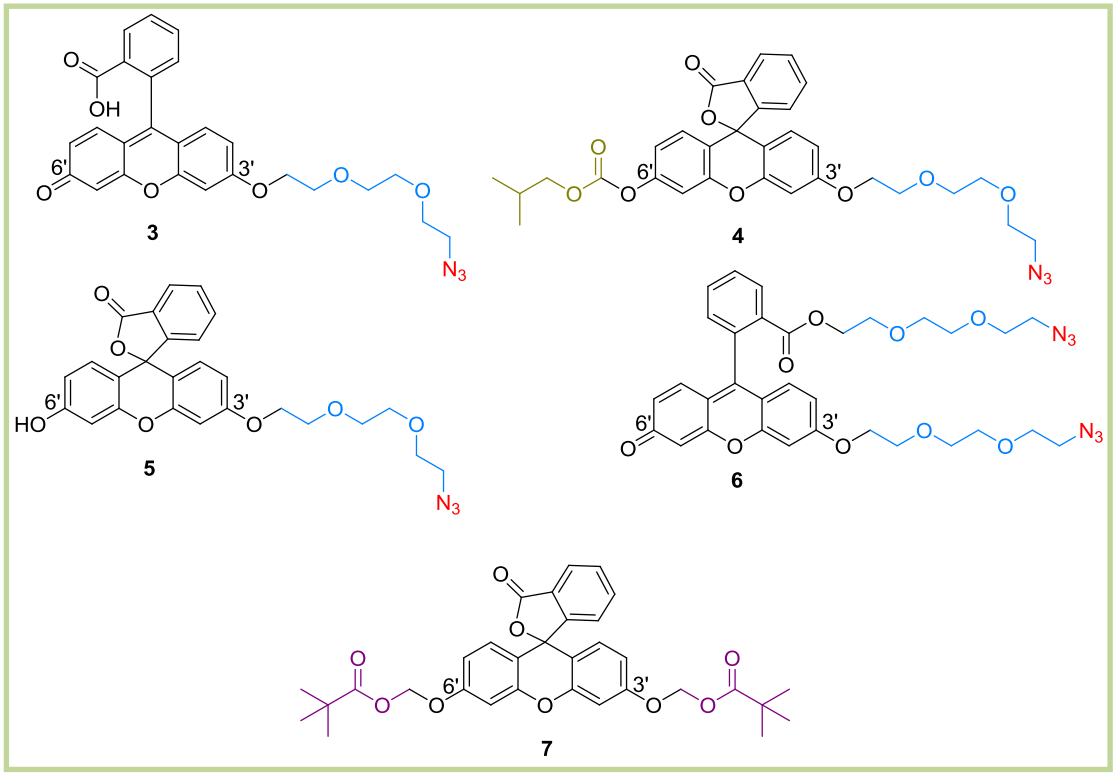

Compound No.	λ_{Ex} pH 7.4 in nm	λ_{Em} pH 7.4 in nm	Φ pH 7.4[a]	Fluorescence increase pH 7.4 / 3	Fluorescence increase pH 11 / 3
No. 3	497	522	0.60	3.4x	3.0x
No. 4	478	518	No ems.	12x	320x
No. 5	479	514	0.51	38x	37x
No. 6	480	514	0.77	1.4x	1.5x
No. 7	n.d	n.d	---	---	---

Table 2. Spectroscopic data of recently synthesized dyes & prodyes, [a]) in pH 7.4 PBS buffered medium, calculated with data from literature, Φ_{FL} = 0.88 in PBS pH 7.4[38, 85]

Surprisingly observations were made after the development of prodye **4**, **8** (page 77 fw.) and **7**. The newly synthesized asymmetric prodyes **4** & **8** were yellow colored but non-fluorescent compared to the colorless compound **1**, **2** and reported, synthesized symmetric prodye **7**[Tian et al], which was also colorless and non-fluorescent, like reported[Tian et al]. Furthermore prodye **7** could not be activated by any cleavage method. Several synthesis attempts aiming the substitution to the asymmetric molecule did not work. Thus, there must be a relation between the molecule symmetry and inertness of the compound **7**. The new compounds **3** and **6** have strong fluorescence and can be used for additional labeling experiments of terminal alkyne containing targets, e.g. ODN, siRNA, proteins, nanoparticle etc. Good yields are also here expected, because of longer click linker and better water solubility due to the PEG-groups. Notable is the bi azide function of compound **6**, opening the perspective for dual click chemistry.[86]

3.2 Conjugation of prodyes to oligonucleotides

This section describes the conjugation methodology of prodyes No. **1** and **2** to different DNA and RNA oligonucleotides (oligo) with alternating terminal alkyne positions and modifications. The overview in **figure 25** depicts a graphical abstract about the Click reaction. Dyes are illustrated as stars, oligonucleotides as saw teeth and magnification is highlighted with a glass. As example dye, compound **1** is presented, which was mainly tested in the coming conjugation reactions.

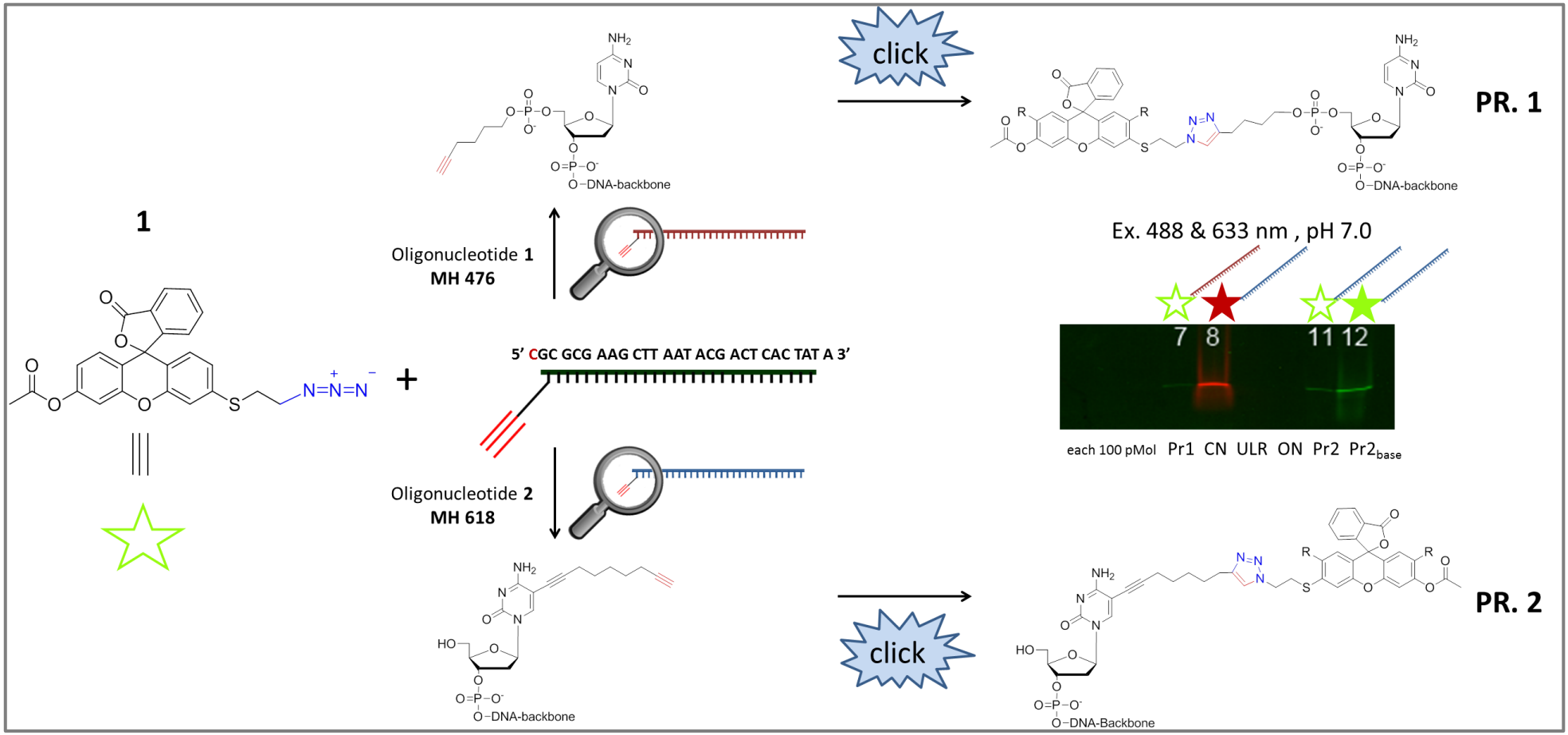

Figure 25. Graphical abstract of the Click reaction, note: filled star = activated or fluorescent dye, not filled star: prodye, native PAGE 20% , the substituents shown as '**R**' are supposed to discriminate the protonated compound **1** from the chlorinated compound **2**.

3.2.1 Conjugation to 27mer DNA oligo with terminal alkyne on 5' phosphate (MH 476)

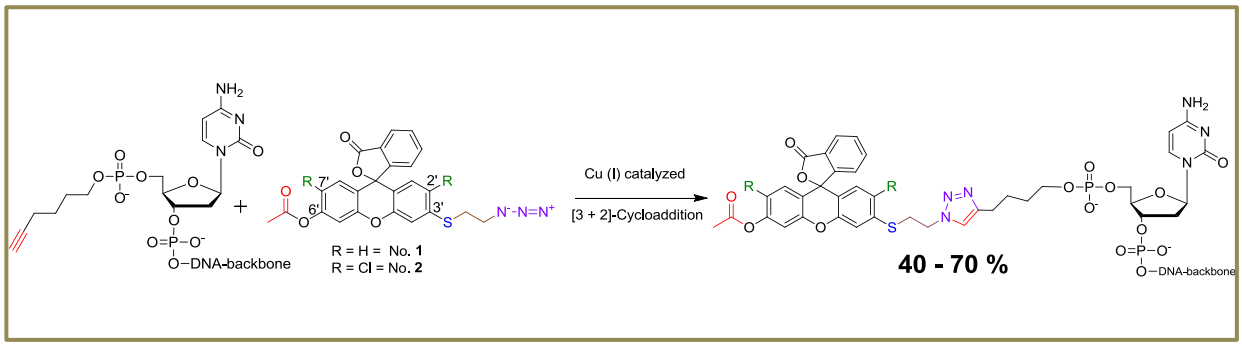

Scheme 10. Click reaction of prodyes with DNA oligo MH 476

The clickability of new synthesized prodyes **1** and **2** was tested using a modified Click chemistry scheme of Dr. Stefanie Kellner[87] and Dr. Olwen Domingo[88] (**Table 3**). As oligodeoxynucleotide (ODN) an external modified ODN with a hexenyl alkyne from commercial supplier IBA was chosen (MH 476, **Scheme 10**). The reaction sample was prepared according to the following pipetting order: MilliQ water – TPTA – NaAsc – $CuSO_4$ • 5 H_2O – oligo – prodye / control dye. The reaction time was 2 hours at 20° C on a thermocycler with 550 rpm. Next, the reaction mixture was precipitated with a $LiClO_4$-solution 2% adapted from Dr. Stefanie Kellner[87], here 10x volume of sample was suspended with the solution described above, centrifuged for 30 minutes at 16000 g, followed by washing of the precipitate with 1x volume of acetone and drying in SpeedVac or room at room temperature (pipetting scheme see table S14, page 103). The dried pellet was dissolved with 1x volume water. In an initial attempt for purification, the material was submitted to conventional denaturating PAGE after the Click reaction. As it can be seen in **figure 25**, some fluorescence is detected, indicating that the acetyl group is removed during electrophoresis. Noteworthy, in the control sample of a addiotinal denat. PAGE analysis (**Figure 26**, CN2, lane 4) incubated with pH 9 – 9.5 TRIS buffer solution nearly all acetyl groups are cleaved off. Denaturating standard PAGE analysis verified the first successful conjugation of prodye **1**, whereas the same reaction of prodye **2** (lane 5, **Figure 26**) failed. Probably this is caused by the electron rich chlorines of prodye **2**, previously investigated on the fluorescent precursor.[68] Yield analysis using a gel scanner by investigating the loading control signals and additional photometric analysis of ODN-conjugate solutions showed 40 – 70 % yield outcome of the Click products.

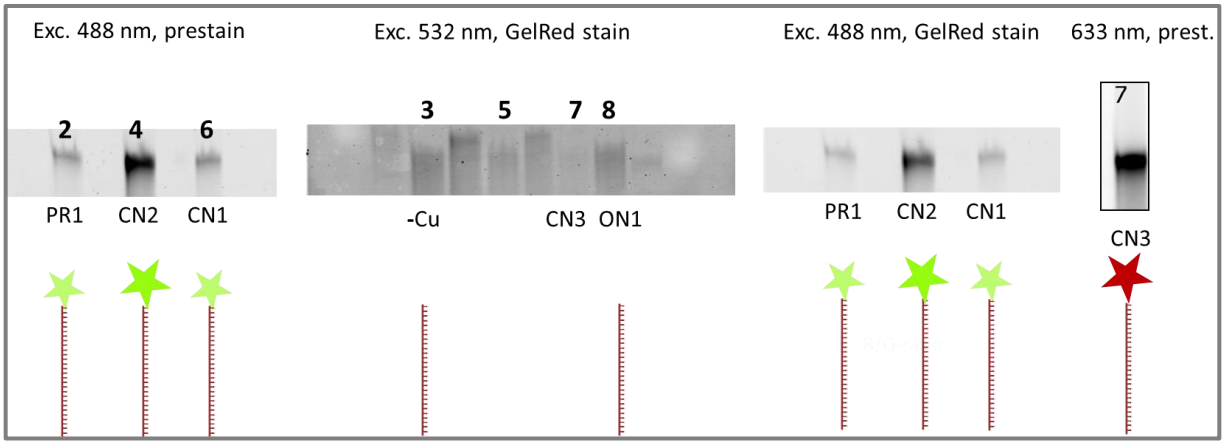

Figure 26. Denaturating PAGE 20 % pH 8.5 - analysis of first Click products (100 pmol); PR1: **1** conjugated to MH 476, CN2: pH 9.1 Tris buffer treated PR1, CN1: fluorescent dye precursor (MK 61) conjugated to MH 476, CN3: control product of Atto 647 N-azide and MH 476, -Cu: copper free MOCK, ON1: MH 476, lane 5: MH 476 and prodye 2 product

In conventional native PAGEs (which are weak basic, verified on a pH-meter) the biolabile and base sensitive, protecting acetyl group will be cleaved off, too. These standard native gel experiments at pH 8.5 explained these undesirable expectations as it is viewed in **figure 27**, lanes 3 + 5 + 7.

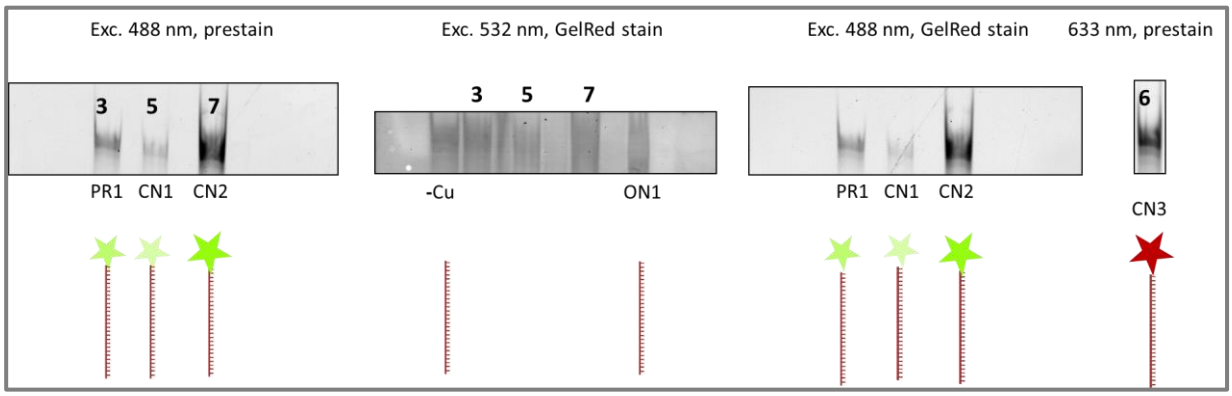

Figure 27. Native PAGE 20 % pH 8.5 – analysis of Click products (100 pmol); PR1: **1** conjugated to MH 476, CN2: pH 9.1 buffer treated PR1, CN1: fluorescent precursor (MK 61) conjugated MH 476, CN3: control product of Atto 647 N-azide and MH 476, -Cu: copper free MOCK, ON1: MH 476

In literature, it is shown that within 45 minutes at pH 8.5 all acetylated hydroxyl functions of a known prodrug (acetyl-propranolol) were cleaved off.[89] These results prompted to develop a new gel detection technique for the biolabile dye conjugated single strands. In agreement with the reported stability of the acetyl groups at < pH 7.4,[89] a pH 7.1 protocol, with native and

"neutral" buffered polyacryl amide gels was developed (see section **5.5 EMSA**). Under pH 7.1 conditions (verified on a pH-meter), the new developed gel protocol indicated that the acetyl groups of leukodye **1** conjugated with ODNs were not cleaved off (lane 7) and were still intact (**Figure 28**).

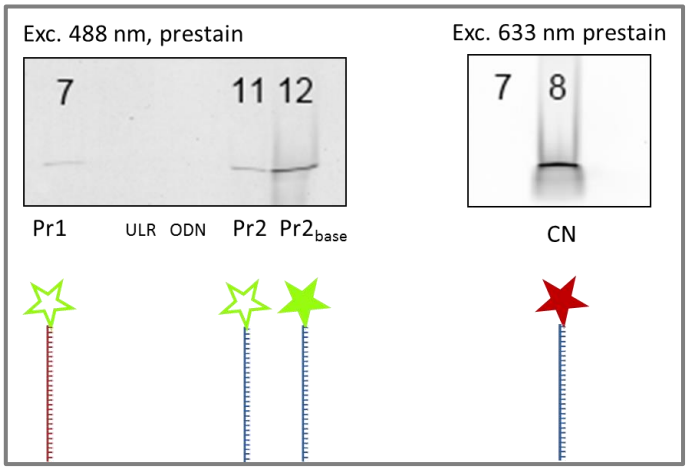

Figure 28. Neutral native PAGE 20 % pH 7.1 analysis of Click products (100 pmol); Pr 1 = CN1, ULR = ultra-low range ladder, Pr2 = **1** conjugated to MH 618, $Pr2_{base}$: pH 9.1 buffer treated Pr2, CN: control product of Atto 647 N-azide and MH 618

3.2.2 Conjugation to 27mer DNA oligo with terminal alkyne on 5' external cytosine (MH 618)

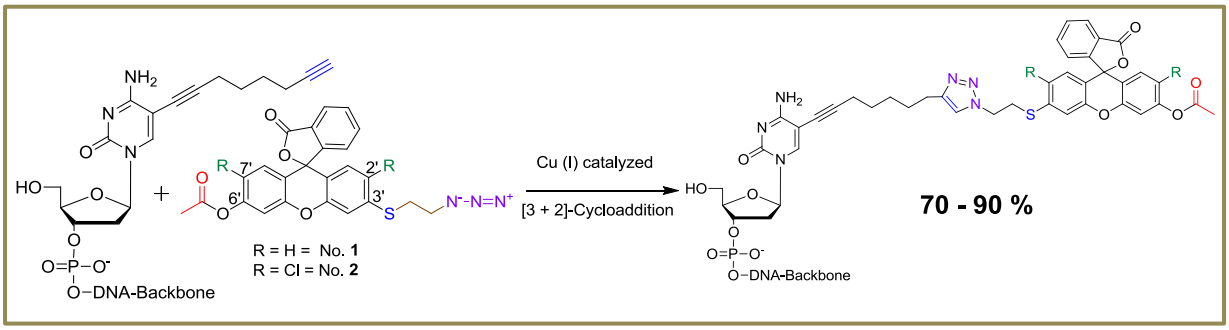

Scheme 11. Click reaction of prodyes with DNA oligo MH 618

Next addressed question was, if altering of the terminal alkyne position from an externally modified (MH 476) to internally modified ODN (MH 618) improves the clickability and reaction yields. In addition to that, the conjugation reaction was optimized by applying a phosphate buffer with pH 6.0 for better protecting conditions of prodye **1** (pipetting scheme

see table S15, page 105).[89] Further improvement of analysis conditions were made by changing the loading buffer from foramide (95 %) to only glycerol (85%) containing, without any nucleophilic reactant. The acetyl functions (initiated by the dissociation of ammonium ions to ammonia and protons in aqueous solution) did not cleave, because of the absence of the basic ammonia. Yield analysis using a gel scanner and additional photometric analysis of ODN-conjugate solutions showed a yield of 70 to 90 % of the Click products.

Successful conjugation of prodye **1** was proven by native PAGE pH 7.1 (**Figure 29**). Remarkably, the fluorescence of intact leukodye connected to MH 618 was very low as expected, whereas in 0.1 M NaOH treated (0.5 h) sample the fluorescent increased. This chemical hydrolysis method aimed and mimicked the enzymatic hydrolysis of an acetyl ester.[90] Moreover, a clear shift induced by size differences between the dye conjugated (lane 1, 2, 4 & 6) and non-conjugated oligonucleotides (lane 3) was visible, verifying the product formation. Gel washing with 0.1 M NaOH for 0.5 h increased the signal of product (**Figure 29**, lane 1 & 2) and considering the diffusion of conjugates plus free dye (micellar spot, lane 4) by signal decrease of previously detected signals. Control reaction was done with the red Atto 647-n-azide dye (lane 6).

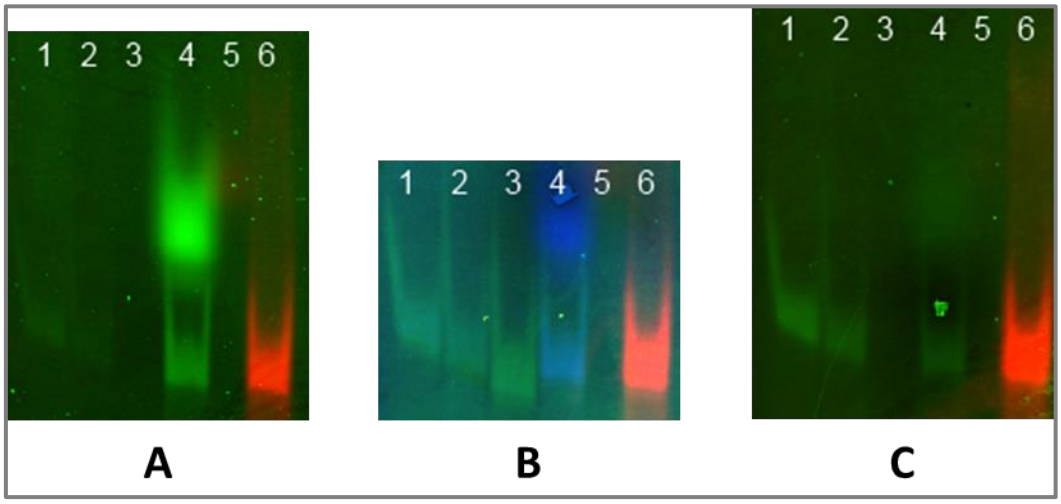

Figure 29. Native PAGE 15% pH 7.1 analysis of Click products (each 50 pmol); 1) reaction mixture MH 618-prodye 1, 2) $LiClO_4$ precipitated reaction mix, 3) – copper control, 4) 0.1 M NaOH treated (0.5 h) reaction mix, 5) LD, 6) MH 618-Atto 647 N-azide control, $LiClO_4$ precipitated; **A**. Prestain emission scan, green = 520 nm BP, red = 670 nm BP, **B**. GelRed® stained gel (loading control), emission scan, blue = 520 nm BP scan, green = 580 nm BP scan, red = 670 nm BP scan, **C**. 0.5 h 0.1 M NaOH treatment of gel, green = 580 nm BP, red = 670 nm BP; overlay of different channels

3.2.3 Conjugation to 22mer sense strand RNA oligo with terminal alkyne on internal cytosine (MH 662)

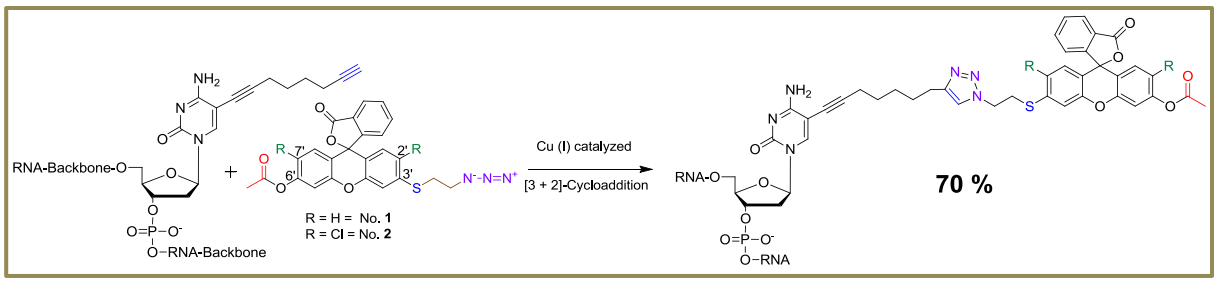

Scheme 12. Click reaction of prodye 1 with RNA oligo MH 662

For cell uptake studies, it was aimed to construct RNA-analogues of ODN. Therefore, the sense strand of anti-GFP siRNA (MH 662) was taken, because of comparable length to the DNA 27-mers and reported application in the field.[91,92,88]

Click reaction conditions were adapted form previously developed and tested conditions on ODN oligos MH 476 and 618 (pipetting scheme see table S16, page 105). Fluorescence analysis on the gel scanner showed a yield of 70 % of precipitated Click products. Similar reaction outcome was registered on native neutral PAGE (**Figure 30**). Notable Fluorescent OFF to ON signals with significant shifts could be detected. Although RNA is more sensitive to OH^- hydrolysis than DNA[93] and consequently able to migrate from the gel by diffusion easily, usage of 70% isopropyl alcohol solution for band fixation prevented these side effects and signals of deprotected prodye RNA were made visible. Each conjugate could be detected clearly (**Figure 30**, panel C).

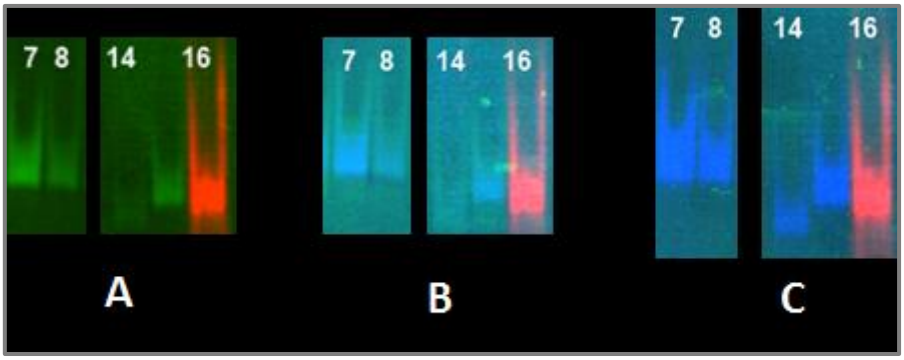

Figure 30. Native PAGE 15% pH 7.1 analysis of Click products (25 - 50 pmol); 7) reaction mixture MH 662-prodye 1, cartridge purified (50 pmol), 8) $LiClO_4$ precipitated reaction mix (25 pmol), 14) MH 618 – prodye 1 , $LiClO_4$ precipitated (25 pMol), 15) MH 618 –prodye 1, $LiClO_4$ precipitated (50 pmol), 16) MH 618 – Atto 647 N-azide control, $LiClO_4$ precipitated (50 pmol); **A**. Prestain emission scan, green = 520 nm BP, red = 670 nm BP, **B**. GelRed® stained gel (loading control), emission scan, blue = 520 nm BP scan, green = 580 nm BP scan, red = 670 nm BP scan **C**. 0.5 h 0.1 M NaOH treatment of gel, blue = 520 nm BP, red = 670 nm BP, overlay of different channels

This PAGE results confirmed the idea of protected, non-fluorescent and with molecular caps synthesized prodye-ODNs. Thus a major hurdle was overcome for "First Contact Imaging" application. Furthermore, these gel experiments gave very first indications about the possible behaviour of leukodye conjugated oligonucleotides for controlled release in physiological environment of pH 6.6 – 9.1.[94] Significant fluorescent OFF-to-ON shifts encouraged to move to purification and siRNA formation experiments for cell uptake purposes, keeping in mind that the new constructs are very sensitive against non-physiological pH, e.g. pH value > 8.5.

3.3 Purification of prodye conjugated oligonucleotides

The conjugated oligonucleotides were purified via lithiumperchlorate ($LiClO_4$-) precipitation, ethanol precipitation, gel extraction, size exclusion or RP-retention chromatography. HPLC purification was not successful. Noted problem was continuous elution of impurities in the system, causing ghost peaks in chromatograms. Purging of HPLC capillaries with different acetonitrile/TEAA buffer variations or changing the injection methods did not solve the problems. Gel-extraction of signal bands yielded less than 10% pure product and was not applied as a further work up procedure. Similar yields were obtained from ethanol precipitation and corresponding work-up was not continued. $LiClO_4$-precipitation with high product yields (> 90 %) was the gold standard for precipitating and cleaning the Click products out of organic impurities, with the disadvantage of water soluble salt content. The purification method of choice either for deoxyoligonucleotides or ribonucleotides was the newly established reversed-phase cartridge purification over SepPak columns (Waters Corporation, **Figure 32 D**). As eluents, mixtures of acetonitrile and milliQ water were checked, with designed and applied gradient in **figure 31**.

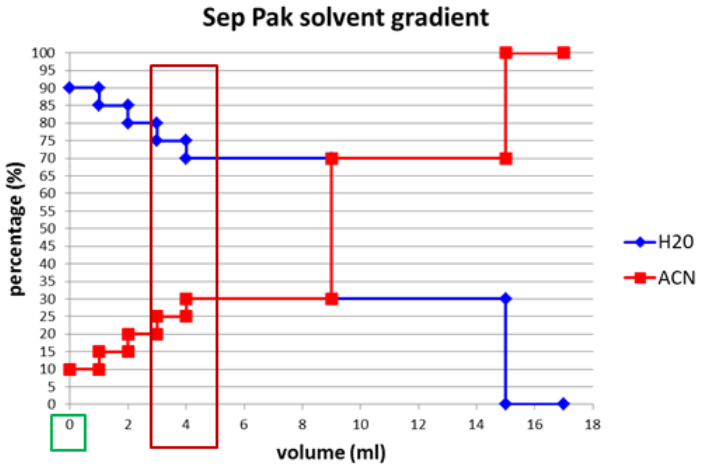

Figure 31. SepPak elution gradient with acetonitrile and milliQ water, for rectangle explanation see thesis

As collector device a 96-well plate was placed and 6 -7 drops in each well were caught, resulting in 300 -320 µl volume. In **figure 31**, one can see the developed and applied gradient. The used protocol is described in section "5.6.4 Reversed phase cartridge purification". The green rectangle highlights the starting point and the red rectangle the elution window for oligonucleotides, either for RNA or DNA. The elution sequence started with strong hydrophilic ions from the conjugation procedure, e.g. copper or ascorbate ions detected by

Nanodrop (absorption measurement) within the first 2 wells. Next like above mentioned, the oligonucleotides eluted, interestingly first the non-conjugated starting oligonucleotides and then the conjugated ones (**Figure 32**) were catched. In all tested purification procedures, the dye did not elute until the gradient was finished and arrested on the column. Therefore it can be concluded, that the elution process can be stopped after 10 ml instead of 18 ml for saving solvent and costs. The overall duration for one purification step took around 30 minutes, which is very comfortable compared to highly time consuming methods like Gel-extraction or HPLC. The major advantage of this method is the pH independency of the purification, by using only water and acetonitrile. This affects less deprotection of prodyes and delivers saltfree pure conjugates of interest. A disadvantage compared to the HPLC purification is the loss of product due to the elution with unclicked starting material (**Figure 32**, B, loading control). Hybridization experiments of intact prodye-sense RNA conjugates showed yields of approximately 62 % of pure, conjugated sense strands. Further information about hybridization is given in section 3.4 “Hybridization of siRNA”.

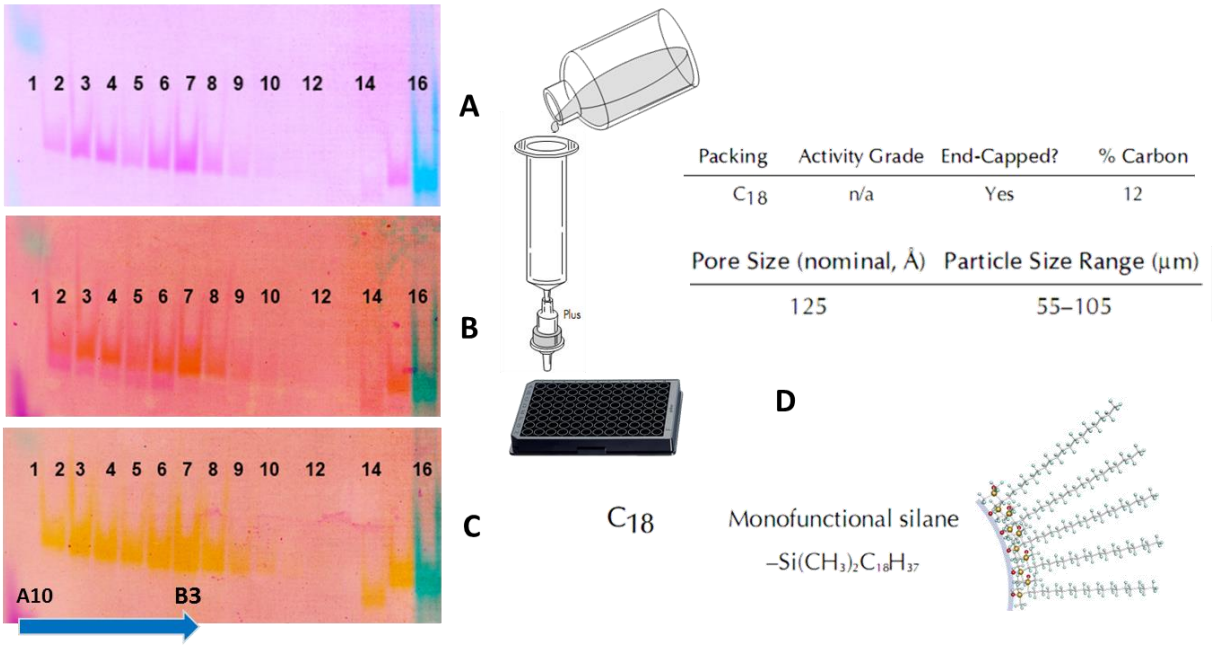

Figure 32. Native PAGE 20% pH 7.1 analysis of SepPak products, here from MH 662–prodye 1 conjugation reaction. 10 µl aliquots from A10 (lane 1) – B9 (lane 13) were checked. The blue arrow indicates wells of the impure product fractions, composed of starting oligo and prodye conjugated. For clarity the colors were inverted, **A)** Prestain emission scan, magenta = 520 nm BP, cyan = 670 nm BP, **B**. Loading control with GelRed® stained gel, emission scan, orange = 520 nm BP scan, magenta = 580 nm BP scan, green = 670 nm BP scan **C**. 0.5 h 0.1 M NaOH treatment of gel, yellow = 520 nm BP, green = 670 nm BP, overlay of different channels

3.4 Hybridization of siRNA

Seeking for an appropriate model for cellular uptake studies of prodye labeled single oligonucleotide strands, the initial route was to prepare double stranded siRNA constructs for siRNA pathway investigation.

siRNA single strands were obtained from commercial suppliers, comprising a range of sense and antisense strands for targeting the enhanced green fluorescent protein (eGFP).

Though all sense and antisense strands, respectively, share the same sequence, the differences between them exist in the position and the kind of fluorescent dye labels.

For this reason, labeled or unlabeled antisense strands were hybridized to the prodye labeled sense strands. Remarkable fluorescence resonance energy transfer (FRET) opportunities were given for testing the integrity of double stranded constructs. Dye pairs for FRET labeled siRNA have been developed prior by Dr. Markus Hirsch.[95,91] Thus the question about the First Contact Imaging in cellular environment is supposed to be accessed using this siRNA-dye construct as declared target from nanoparticular formulations, e.g. lipolexes.

Figure 33 illustrates an overview of utilized RNA oligonucleotides with previously (see section 3.2.3) described deoxycytidine modification, conjugated with prodye **1**.

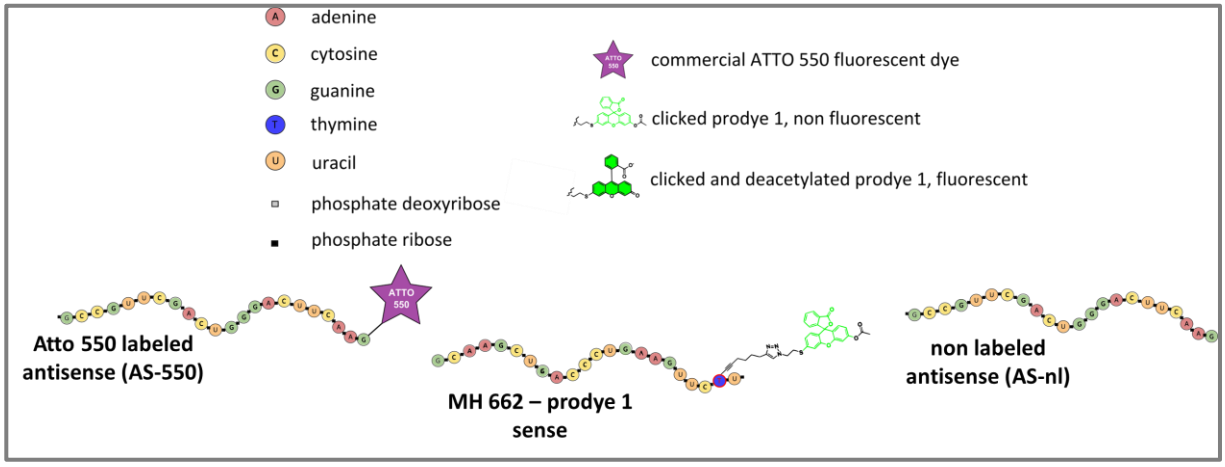

Figure 33. Overview of utilized single strand RNA in hybridization experiments

Hybridizations were carried out in phosphate buffered saline (PBS) starting from single stranded (ss) RNA stock solutions. The concentrations of these stocks were determined by the supplier via UV absorption. In most cases, however, these declarations were obviously not accurate enough, as an equimolar hybridization on the basis of the declared concentrations led to an excess of ss RNA. In analogy, the concentrations of SepPak purified oligonucleotides

measured by the Nanodrop were inaccurate, too. Therefore, a titration was necessary. For this purpose, the volume of sense strand was kept constant and different antisense/sense (vAS/vSE) ratios were tested by varying the volume of antisense strand, in order to obtain the vAS/vSE, which yielded hybridization without ss RNA excess, signifying the input of equimolar amounts of both strands.

Figure 34 shows the PAGE analysis of the hybridization, providing a siRNA construct with labels on both strands. MH 662-prodye **1** ss RNA was applied as sense strand matching the Atto 550 n-azide tagged or non-labeled antisense RNA, giving a FRET labeled in the first case or single labeled double stranded (ds) RNA in the latter one. In both cases, the optimal vAS/vSE ratio was 0.5/1 for equimolar matching amounts, verifying the concentration of prodye labeled sense strand solution. Remarkable signal overlay was observed after activating treatment (**Figure 34**, panel B). Furthermore, the 0.1 M sodium hydroxide treated prodye **1**-siRNA revealed an 18 x increase of green fluorescence intensity in cuvette. Detailed results and discussion can be found in section 3.5 “Fluorescence off and on studies”.

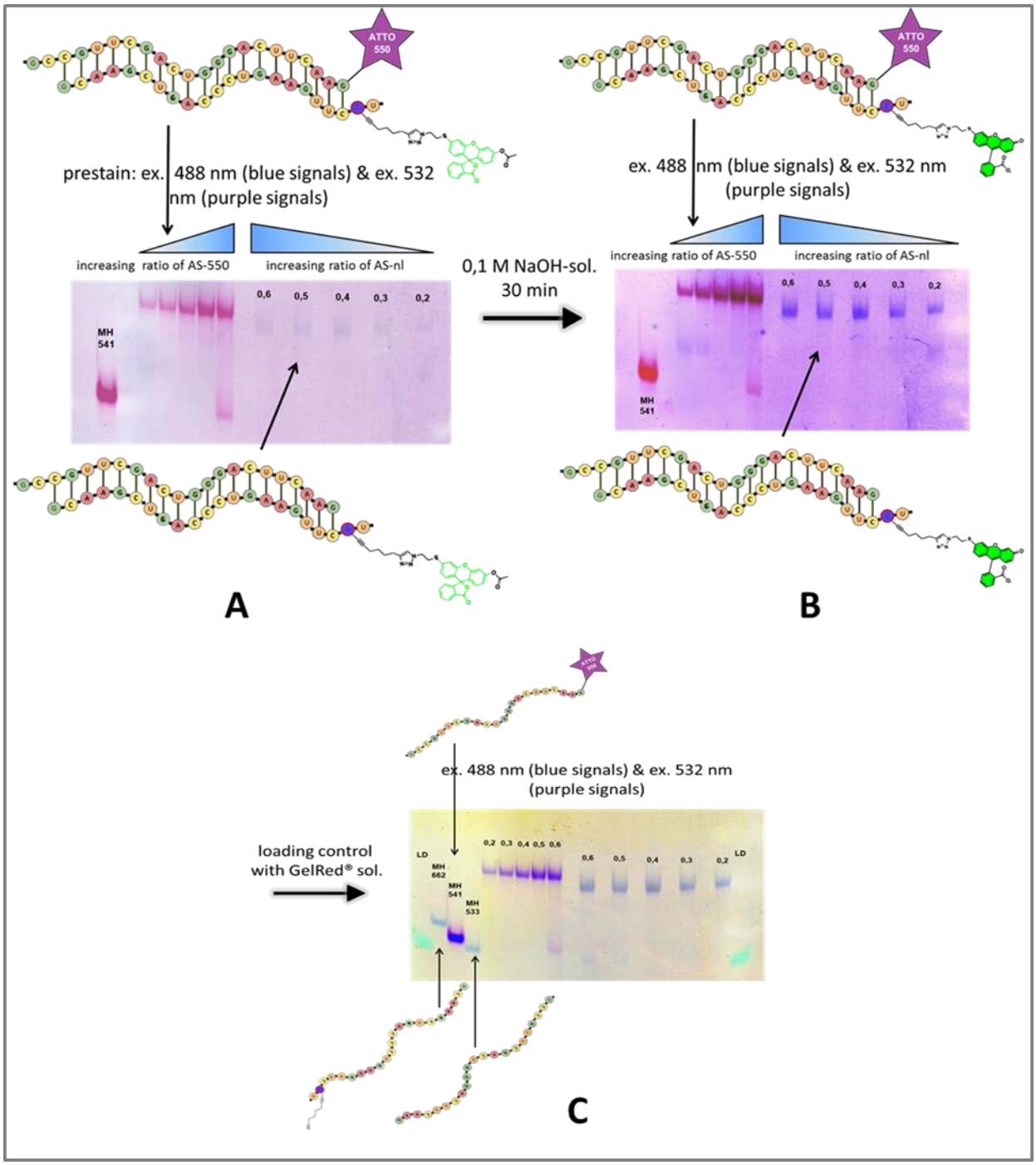

Figure 34. A) Native PAGE 15% analysis pH 7.1; hybridization of a construct with labels on both strands, resulting in a FRET labeled double stranded (ds) RNA or mono prodye labeled RNA, B) after 0.5 h 0.1 M NaOH treatment, emission scans: blue = 520 nm BP , purple = 670 nm BP

3.5 Fluorescence off and on studies

To evaluate the First Contact ability of profluorescent dye modified oligonucleotides, each construct was investigated on a fluorimeter in OFF and ON state, forced by the 0.1 M NaOH treatment. Time dependent emission behavior was also investigated. The mechanism of action reflecting the lactone function opening by deacetylation is illustrated in **figure 35**. Here, the colorless and non-fluorescent prodye **1** – oligonucleotide conjugate (-R) can be activated by esterases or sodium hydroxide treatment (described in section 1.4). Next, the fluorophore can be excited with blue laser light at 488 nm and green emission can be recorded on a fluorimeter. In this work, recorded 'turn ON' ratios in cuvette experiments were between 18 – 81x, comparable or more pronounced, related to other profluorescent systems shown in literature.[54,74,96,97, 98]

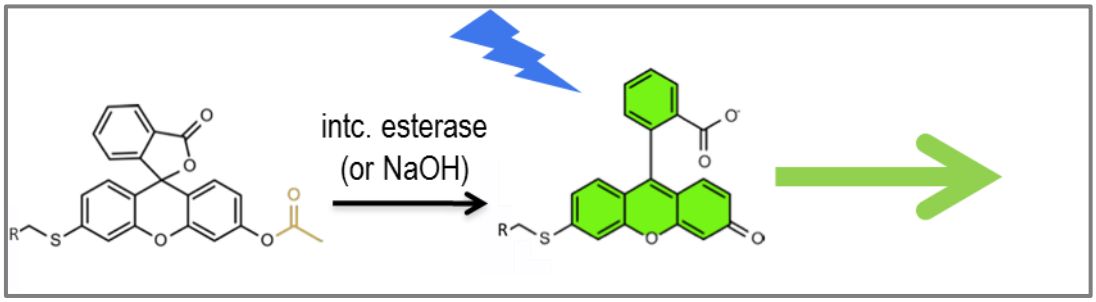

Figure 35. Mechanism of deacetylation by esterases or NaOH and formation of fluorophore, blue lightning: 488 nm excitation, green arrow: 520 nm emission

3.5.1 0.1 M NaOH treatment of MH 618-prodye 1 DNA oligomer

First evaluation of profluorescent activation was performed with the 27mer DNA oligo (MH 618) on neutral native PAGE (**Figure 29**), correlating cuvette experiments under unmasking conditions with 0.1 M NaOH showed 81x increase of fluorescence (529 nm) in non-buffered probes, and 68 x increase in phosphate (pH 6) buffered probes after 24h incubation time at RT (**Figure 36**). Native neutral PAGE experiments confirmed the prior observed results, investigating the green fluorescence. Prior, fixation of oligonucleotide samples with 70% isopropyl alcohol solution was performed.

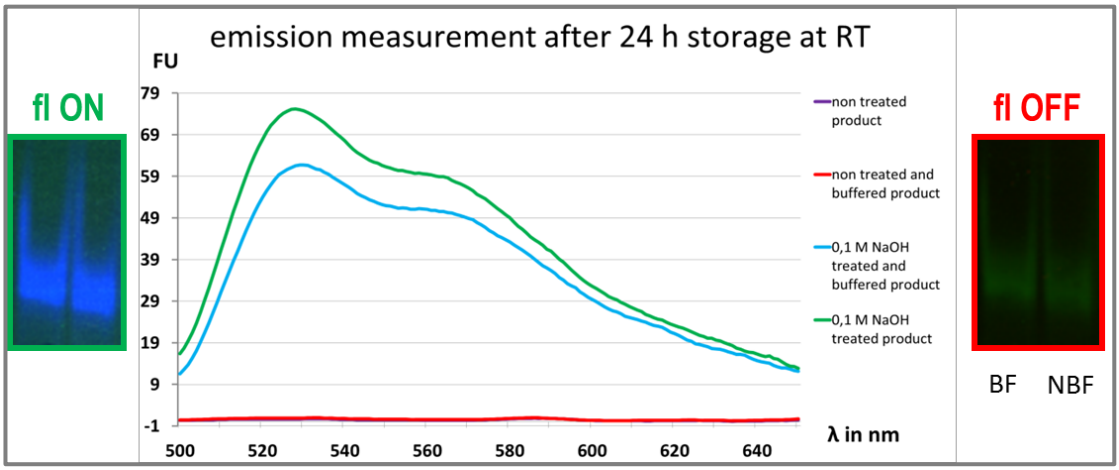

Figure 36. Emission spectra of MH 618 – prodye 1 (DNA) conjugates (each 3 µM) after 488 nm excitation, BF: phosphate pH6 buffered, NBF: non buffered aqueous solution, fl OFF: none treated sample, fl ON: 0.5 h 0.1 M NaOH treatment, native neutral PAGE of MH 618 – prodye 1 immediately after SepPak purification, 520 nm BP emission scan

3.5.2 0.1 M NaOH treatment of MH 662-prodye 1 RNA oligomer

Unmasking with 0.1 M NaOH of prodyes on sense RNA strand MH 662 carried out 64x increase after a few minutes, 62x increase after 1 hour, 60x increase after 2 hours and 57x increase of green fluorescence (529 nm) after 24 hours incubation time at RT (**Figure 37**).
Native neutral PAGE experiments confirmed the observed results with turning the green fluorescent ON. Prior, fixation of oligonucleotide positions on the gel with 70% isopropyl alcohol solution was performed.

In both cases (MH 618 & MH 662 oligo), the reaction mixtures were purified over a SepPak column, using the previously described gradient (Section 3.3). For fluorescence measurements 3 µM solutions of each oligo prodye conjugate was set in a 15 µl quartz cuvette on the photometer.

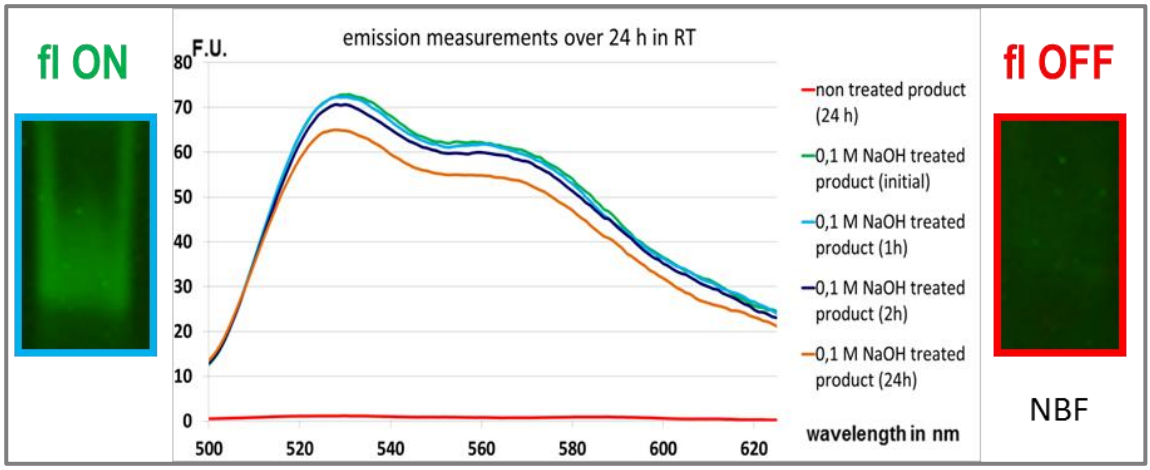

Figure 37. Emission spectra of MH 662 – prodye 1 (RNA) conjugates (each 3 µM) after 488 nm excitation, NBF: non buffered aqueous solution, fl OFF: none treated sample, fl ON: 0.5 h 0.1 M NaOH treatment, native neutral PAGE of sense strand MH 662 – prodye 1 immediately after SepPak purification, 520 nm BP emission scan

3.5.3 0.1 M NaOH treatment of prodye labeled siRNA

Green fluorescence (529 nm) investigations of intact (non treated) and deprotected (treated) prodye **1** of siRNA (**Figure 38**) showed 18x OFF to ON change (ratio) after 24 hours. After this, observed results the question of First Contact Imaging of nanoparticular siRNA in cellular environment was addressed. To access such an environment, the prodye labeled siRNA had to be loaded on an appropriate vehicle in nanometer range.

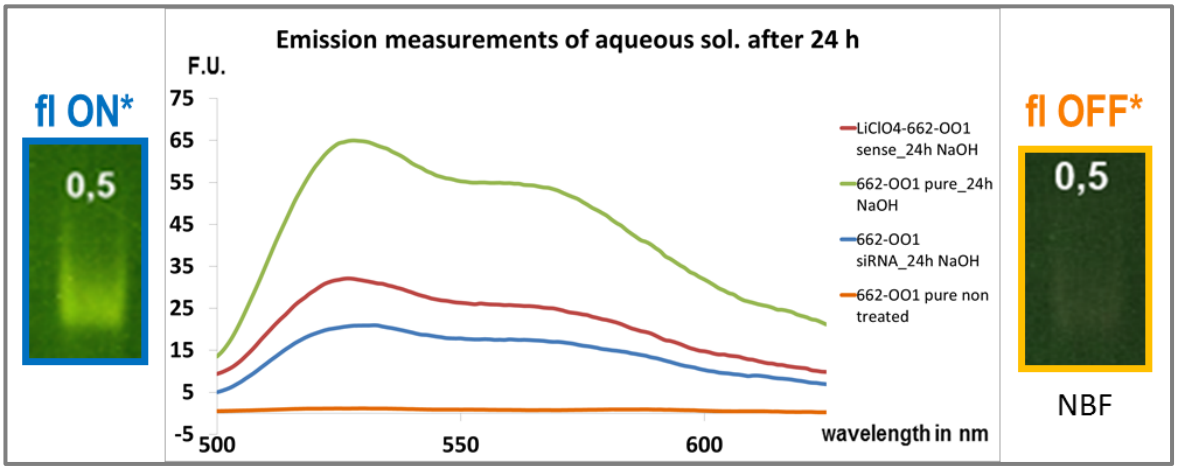

Figure 38. Emission spectra of MH 662 – prodye 1 single strand and siRNA conjugates (each 3 µM) after 488 nm excitation, NBF: non buffered aqueous solution, fl OFF: none treated sample, fl ON: 0.5 h 0.1 M NaOH treatment, *native neutral PAGE of siRNA MH 662 – prodye 1 immediately after SepPak purification, 520 nm BP emission scan

3.5.4 Pig liver esterase treatment of prodye 1 or FL labeled siRNA

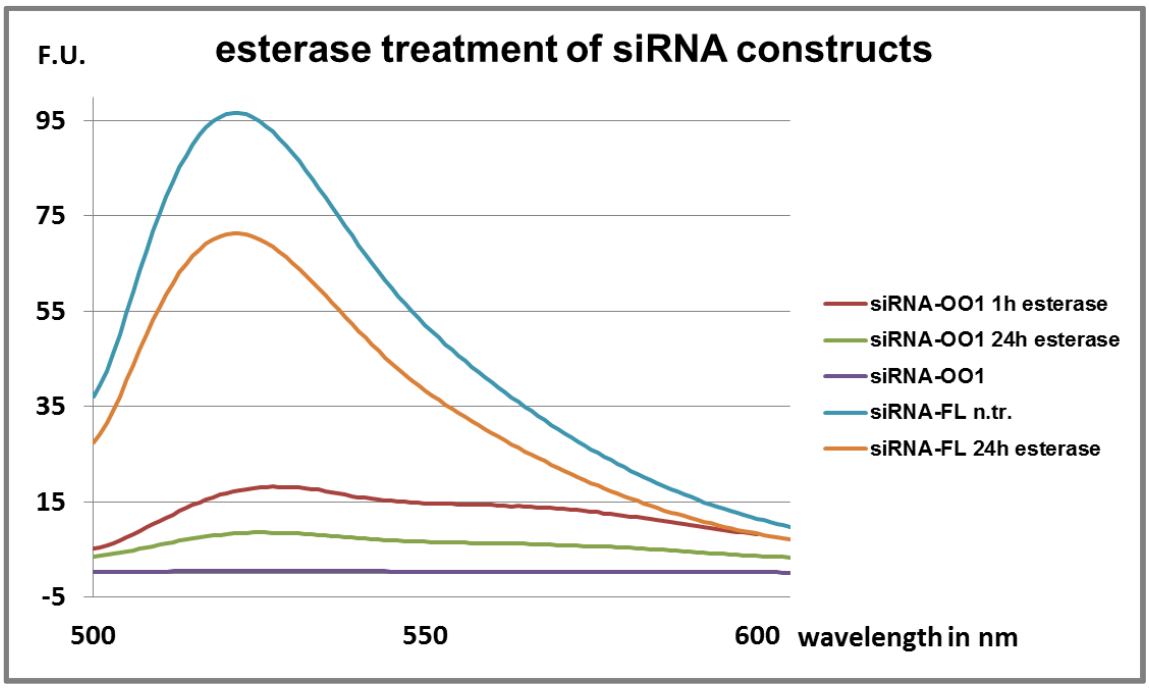

Figure. 39 Emission spectra of siRNA dye conjugates (each 3 µM) after 488 nm excitation, siRNA-OO1: prodye **1** labeled anti-GFP siRNA, siRNA-FL: fluorescein labeled anti-GFP siRNA

Enzymatic activation of prodye **1** was checked using commercial pig liver esterase (PLE, Sigma Aldrich) solution, buffered with PBS on pH 7.4.[99] In pretests the optimal ratio for the catalysis of esterase cleavage was evaluated. According to the information of manufacturer, the enzyme concentration was set to 1 µU/µl, which catalyzes the hydrolysis of 15 pmol ester within one minute. To achieve quantitative ester hydrolysis in prodye **1,** the reaction time was set to one hour, followed by excitation-emission measurements (**Figure 39**).

Here, one can see that the ON-OFF ratio of prodye **1** labeled siRNA was 37x after 1 hour, compared to the untreated probe. After 24 hours it decreased to 17x, showing comparable shifts to sodium hydroxide treated probes. This motivated to start with cell uptake studies on an appropriate nanocontainer, keeping the fact in mind, that the emission after activation was not expressive enough like control fluorescein-siRNA constructs, which showed 5x more fluorescence (**Figure 39**).

During his internship with the topic “Examination of fluorescence & energy-transfer manner of prodye-Atto590 conjugated siRNA-constructs on the JASCO-fluorimeter”, Stefan Hammerschmidt verified by PAGE analysis, that esterase incubated siRNA constructs were still intact and not degraded in a venom phosphodiesterase manner.

3.6 Nanoparticle formulation

For the nanometer ranged particles standard Oligofectamine® was set as transfection agent. The commercially available Oligofectamine® contains cationic lipids, which mask the negative charge of the nucleic acids, DNA or RNA, by positively charged molecules or build a fusogenic particle that is then easily taken up by eukaryotic cells via endocytosis.[100,101] As a standard transfection reagent, oligofectamine has good protection ability against RNases. The cationic lipid is used as gold standard in many transfection experiments.[102]

Figure 40 outlines the complexation of the polyanionic labeled siRNA with the cationic oligofectamine lipids. The resulting lipoplex carries a positive net charge. The complexes sediment onto cell and adhere to the negatively charged cell membrane. After endocytosis the complex is located in endosomes and during the maturation process to lysosomes the complex or cargo gets released into the cytoplasm.[103, 104, 105] Important to mention is that lipoplexes do not represent liposomes with well-defined lamellar structures, lipoplexes have undefined, mixed structure with a cationic charge.[106]

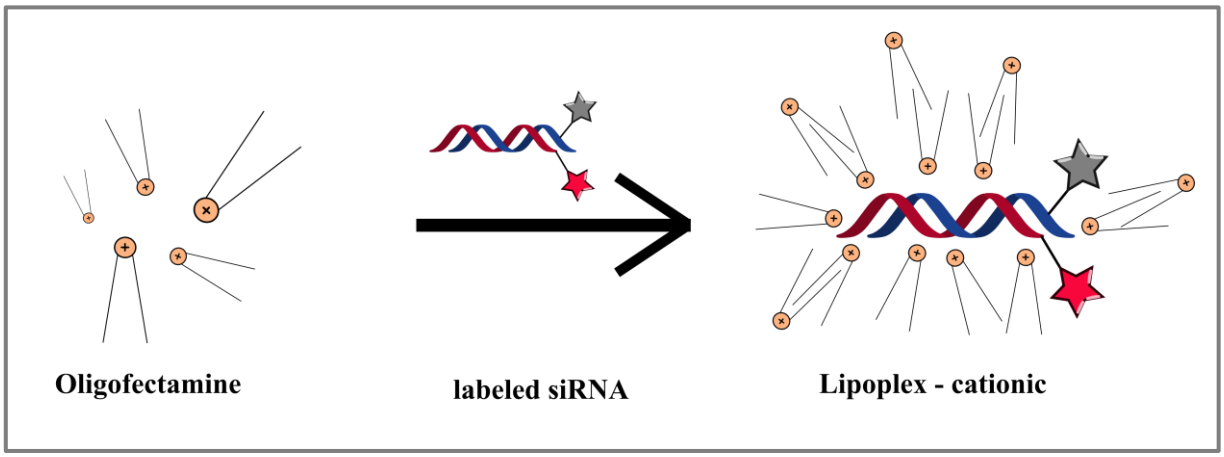

Figure 40. Oligofectamine complexation

The siRNA-to-particle ratio was taken from Dr. Markus Hirsch thesis with 1:14 dilution recipe, which is described in detail in the literature.[91]

3.7 Cell uptake experiments and microscopy

This part reflects the transfection results of RBE4 cells obtained by confocal microscopy. The experiments were performed by Dr. Markus Hirsch at the IMB (Mainz) core facility for microscopy. The *in vivo* imaging of prodye labeled siRNA is necessary to investigate the expected intracellular First Contact of these constructs for further understanding of the releasing mechanism from a nanoparticle of choice and RNAi pathway.

3.7.1 Transfection of RBE4 cells

RBE4 cells are an immortalized cell line obtained from rat brain endothelial cells.[107]
This cells express high levels of p-glycoprotein, which can be found in the blood brain barrier. The cell line has a clearly visible nucleus surrounded by a large volume of cytoplasm. The cells were provided by Dr. Markus Hirsch at passage 32.
In this section RBE4 cells were transfected with previously described lipoplexes, subsequently the cells were fixed by formaldehyde treatment (see experimental section) to prevent diffusion of released siRNA from cytoplasm. Formaldehyde penetrate cells due to its small size very fast and cross-links free amino groups by methylene formation.[108]
Figure 41 depicts the used dyes in siRNA. Four different confocal microscopy experiments were done: (I) fixation, (II) 30 min PBS buffered washing at pH 12, (III) 0.1 M NaOH treatment (pH 13) and (IV) neutralization with equivalent volume of 0.1 M HCl solution.

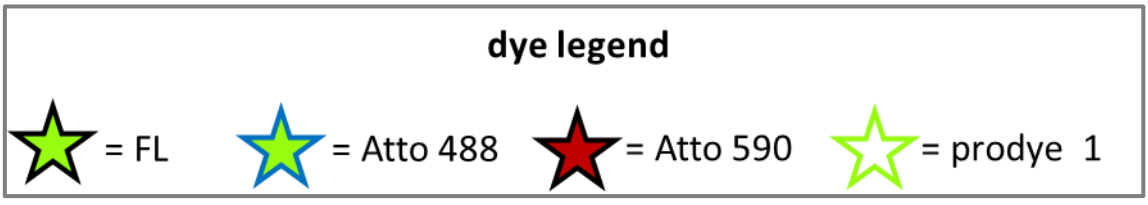

Figure 41. Legend of used fluorescent and profluorescent dyes in related siRNA constructs

3.7.2 Confocal microscopy after fixation

Transfection success of lipolplexes was tested by emission recording during confocal microscopy. Only FL, Atto 488-, Atto 590-n azide labeled siRNA and Atto 488/590 FRET siRNA were used as control with respective signals (**Figure 41**). Prodye **1** and Atto 590 n-azide conjugated siRNA was the main construct for proving the expected First Contact. Control scan of acceptor channel (**Figure 42, D**) confirmed the uptake and release of

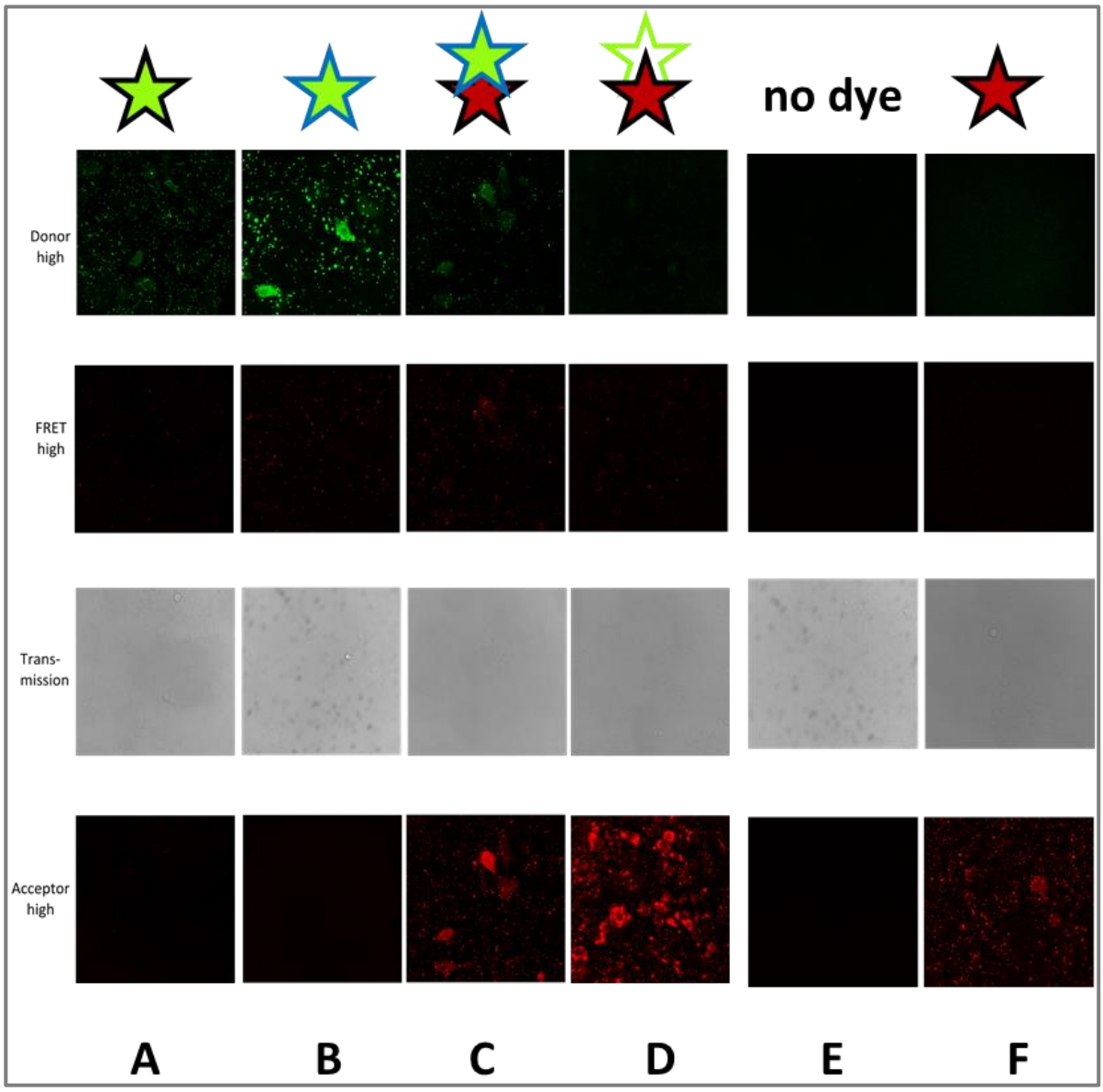

Figure 42. Cell imaging after fixation of transfected RBE4 cells. The cells were excited at 488 nm and emission was recorded for donor signal at 510-540 nm (1st row) and FRET signal at 605-635 nm (2nd row). 3rd row depicts the transmission channel. The last row represents the acceptor signal at 561 nm excitation and emission at 605-635 nm. Column description: A) FL labeled siRNA, B) Atto 488 labeled siRNA, C) Atto 488-Atto 590 labeled FRET siRNA, D) prodye 1-Atto 590 labeled siRNA, E) only siRNA, F) Atto 590 siRNA

respective siRNA. Any expected First Contact could not be detected at this stage. Furthermore, the difficulty was finding a corresponding event, because after fixation the dynamics inside of the cell were not available anymore, compared to real-time living cell experiments with long duration. Furthermore, the catalysis of esterases was stopped by crosslinking their amino functions, also nucleotides and other cellular macromolecules were cross-linked.[109]

3.7.3 Confocal microscopy after pH 12 treatment

For inducing the non-registered First Contact, the fixed cells were incubated 0.5 hour at pH 12 in buffering PBS. In control samples the fluorescence strongly decreased, because of washing the detached siRNA constructs from respective compartments. Furthermore, chromophore destruction (caused by basic hydrolysis of sulfonate groups in Atto 488) decreased the expected intracellular signals (**Figure 43**). In prodye conjugated siRNA (**Figure 40**, D) no significant First Contact could be obtained, the control channel verified again the intracellular uptake and distribution of constructs. One single event of activated siRNA in lipoplexes is depicted in **Figure 44.** Here, one can see the activated prodye inside of the nanoparticle, which was not released from it and existed as lipoplex inside of the RBE4 cell. The signal intensity was comparable to the commercial and proved siRNA control constructs, investigated by Dr. Markus Hirsch[91] (**Figure 44**, panel C). This was the first observation of an induced First Contact in a eukaryotic cell.

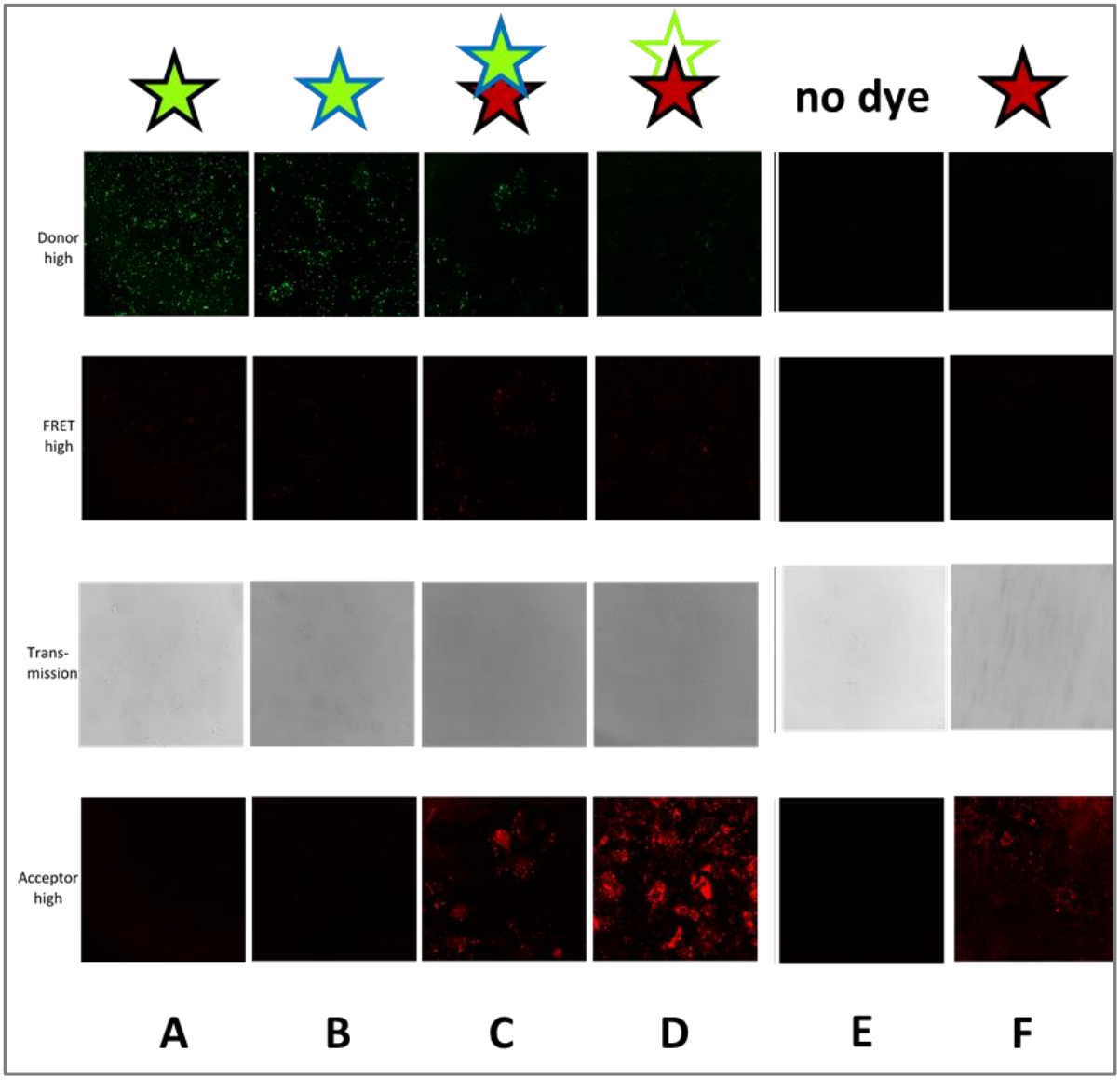

Figure 43. Cell imaging after pH 12 PBS treatment of transfected RBE4 cells, prior to fixation by formaldehyde treatment. The cells were excited at 488 nm and emission was recorded for donor signal at 510-540 nm (1st row) and FRET signal at 605-635 nm (2nd row). 3rd row depicts the transmission channel. The last row represents the acceptor signal at 561 nm excitation and emission at 605-635 nm. Column description: A) FL labeled siRNA, B) Atto 488 labeled siRNA, C) Atto 488-Atto 590 labeled FRET siRNA, D) prodye 1-Atto 590 labeled siRNA, E) only siRNA, F) Atto 590 siRNA

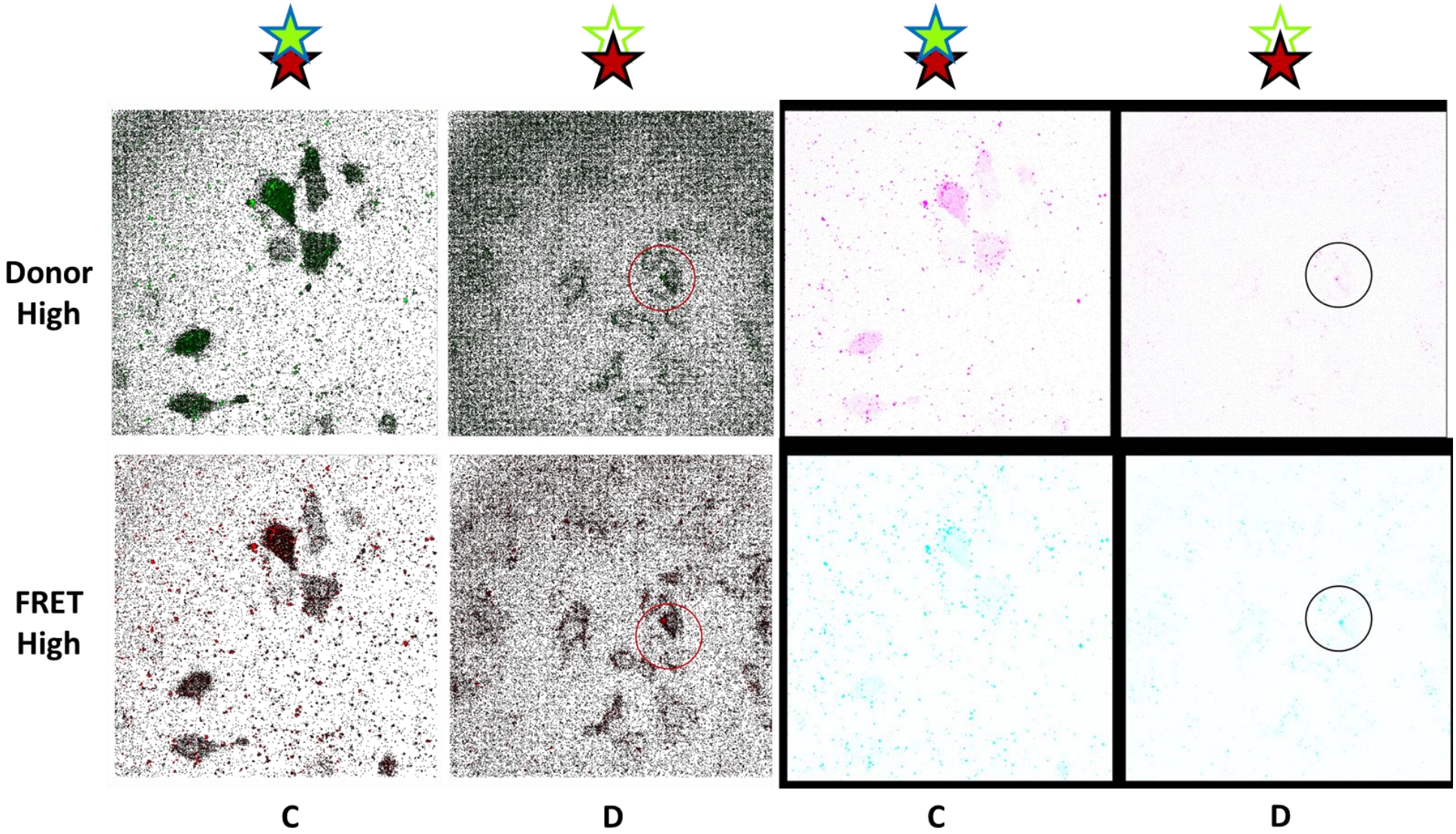

Figure 44. Magnification of panel C&D after pH 12 PBS treatment. For better signal depiction, the background in black or white (inverted pictures on the right) is extracted.

3.7.4 Confocal microscopy after 0.1 M NaOH treatment (pH 13)

Low green emission of prodye 1 conjugated siRNA prompted to move in stronger basic milieu by 0.1 M NaOH treatment for maximizing further deprotection of incompletely cleaved acetyl functions. Expected increase of signals failed. The previously registered signal

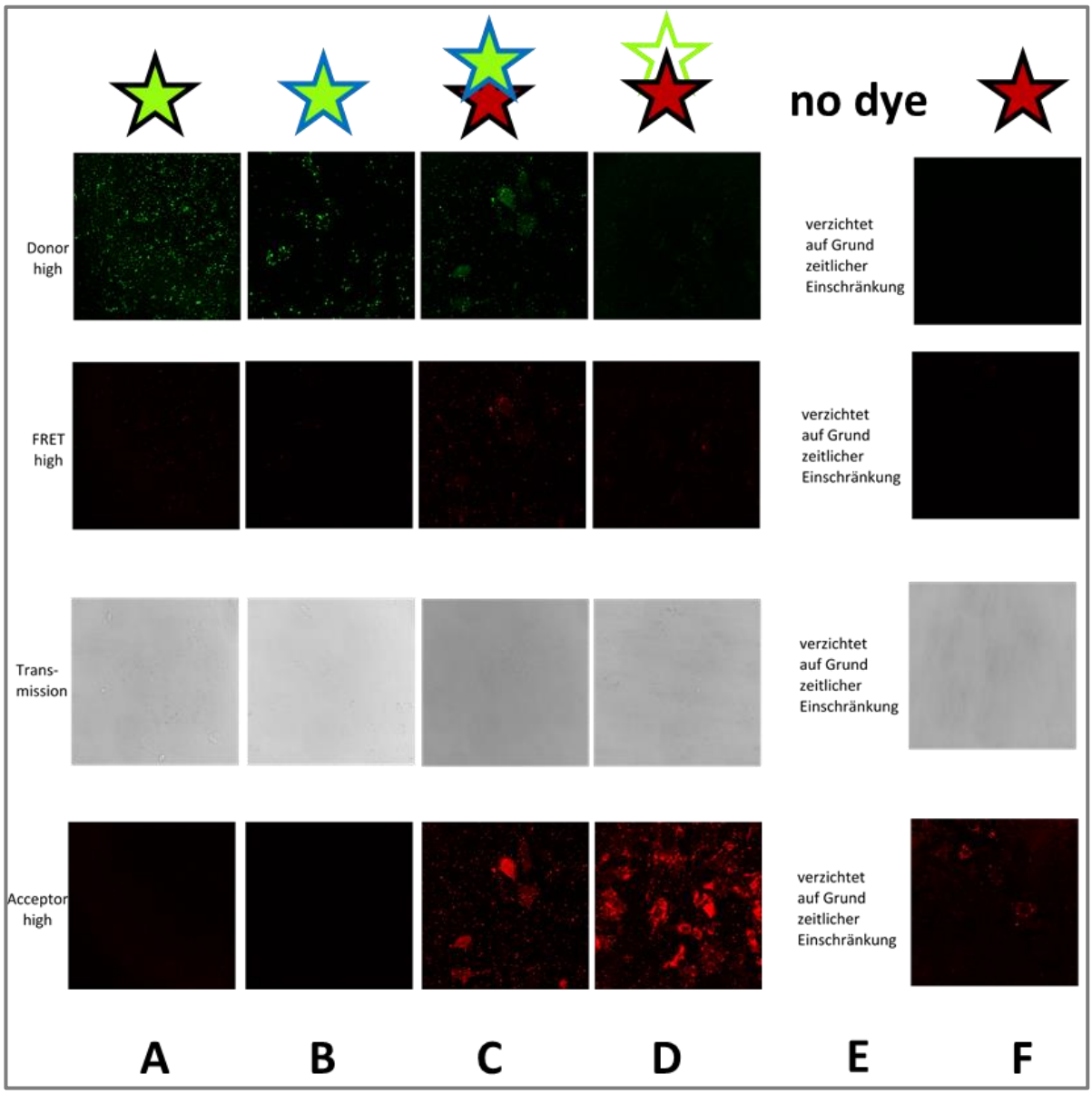

Figure 45. Cell imaging after 0.1 M NaOH treatment (pH 13) of transfected RBE4 cells, prior to fixation by formaldehyde treatment and washed with PBS buffer pH 12. The cells were excited at 488 nm and emission was recorded for donor signal at 510-540 nm (1st row) and FRET signal at 605-635 nm (2nd row). 3rd row depicts the transmission channel. Fourth row represents the acceptor signal at 561 nm excitation and emission at 605-635 nm. Column description: A) FL labeled siRNA, B) Atto 488 labeled siRNA, C) Atto 488-Atto 590 labeled FRET siRNA, D) prodye 1-Atto 590 labeled siRNA, E) only siRNA, F) Atto 590 siRNA

of induced First Contact (**Figure 43 & 44**) in the Donor and FRET channel could be obtained again and verified previously noted results, described in section 3.7.3. Additional magnification was not applied.

3.7.5 Confocal microscopy after neutralization

To check reversibility of fluorescence and effects of neutralization, the fixed cells were incubated for 0.5 hour with equivalent volume of 0.1 M HCl solution. In general, the green signals disappeared, whereas the red emission of Atto 590 n-azide conjugated constructs was present (**Figure 46**). The activated prodye containing compartment was still fluorescent in the acceptor and FRET channel.

In general expected First Contact Imaging could not be obtained significantly. Only one notable intracellular First Contact of the prodye **1** – Atto 590 labeled FRET siRNA was detected. Possible reasons for this negative result were probable hydrolysis of prodye **1** or degradation of dye, because of missing signals in the donor channel. Furthermore the deprotection of prodye **1** in RBE 4 cells could not be fulfilled sufficiently. An appropriate cell line for such an experiment would be a PLE overexpressing cell line of HELA or HEK cells, reported e.g. by Tian et al.[53]. The release from the nanoparticles could be verified by only scanning the acceptor channel, indicating the uptake and distribution of siRNA constructs containing Atto 590 as acceptor dye. Another option was also the interaction possibility of oligofectamine with prodye **1** causing quenching or decreasing of fluorescence. But the major hurdle in such an experiment is finding the needle in a haystack, symbolically describing the localization of a First Contact in live cell experiments by confocal microscopy.

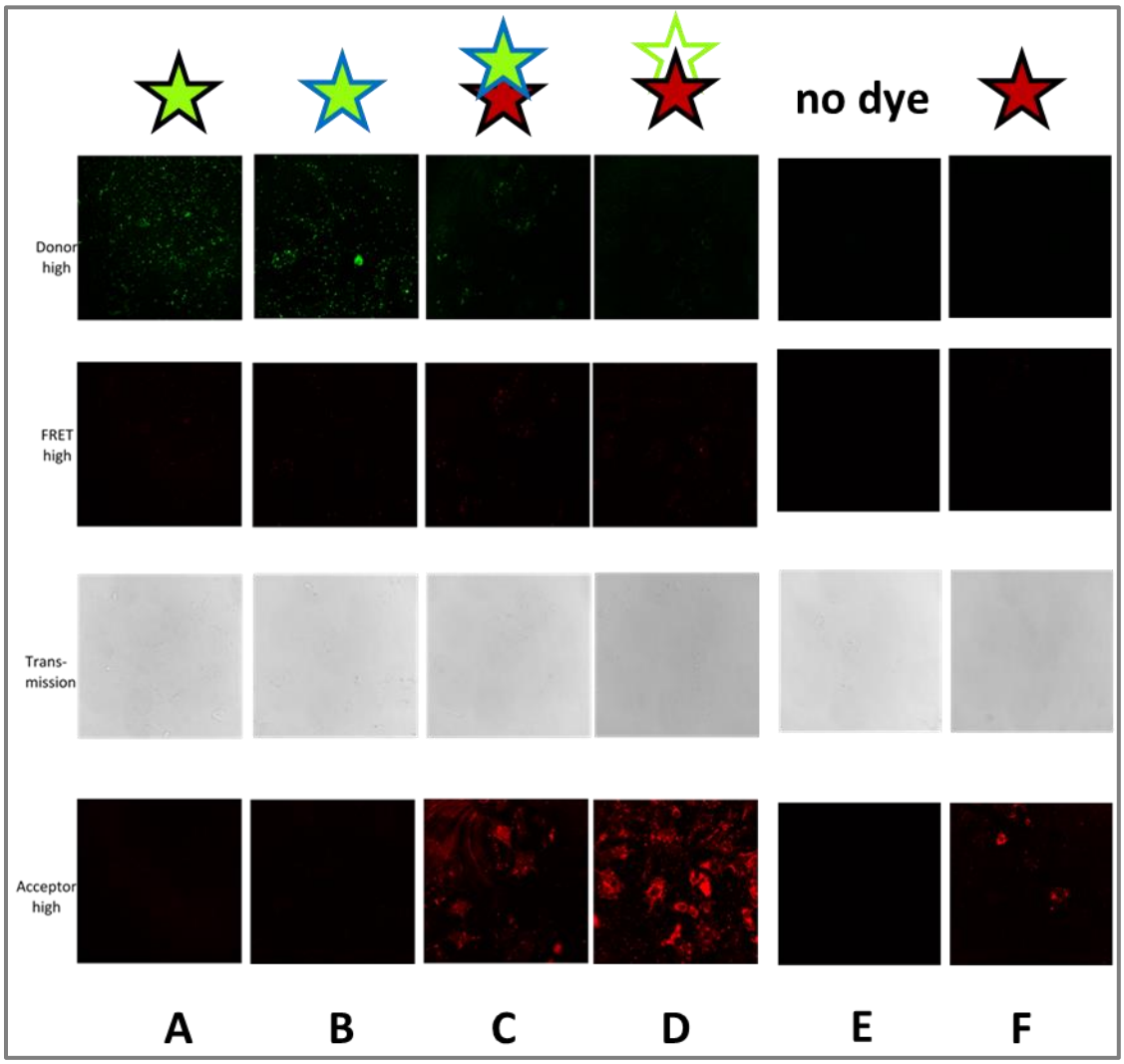

Figure 46. Cell imaging after neutralization with 0.1 M HCl. The cells were excited at 488 nm and emission was recorded for donor signal at 510-540 nm (1st row) and FRET signal at 605-635 nm (2nd row). 3rd row depicts the transmission channel. Fourth row represents the acceptor signal at 561 nm excitation and emission at 605-635 nm. Column description: A) FL labeled siRNA, B) Atto 488 labeled siRNA, C) Atto 488-Atto 590 labeled FRET siRNA, D) prodye 1-Atto 590 labeled siRNA, E) only siRNA, F) Atto 590 siRNA

4 Conclusion and Outlook

In order to investigate a method for First Contact Imaging of nanoparticular siRNA, new types of profluorescent dyes were designed, synthesized and applied. These asymmetric and non-fluorescent fluorescein molecules were successfully synthesized over a 5 step- (prodye **1 & 2)** or over a 3 step reaction (prodye **4**). The compound structures were successfully proven by different instrumental analysis methods like H-NMR, C-NMR, IR spectroscopy and LC-MS/MS. The electromobility shift assay using different PAGE types verified successful conjugation of compound **1** with high yields for DNA- (up to 90%) and RNA-oligonucleotides (up to 70%). No conjugation was obtained for compound **2**. Fluorescent OFF-to-ON studies of prodyes, using 0.1 M NaOH solution showed remarkable increases either on gel or in cuvette experiments. For instance prodye **1** conjugated DNA oligonucleotide MH 618 showed 81x increase, RNA oligonucleotide MH 662 showed 57x increase and the intact siRNA showed 18x increase after 24 hours. Biochemical cleavage with pig liver esterase developed 37x initial increase and still 17x higher fluorescence of intact siRNA after 24 hours. Uptake and release experiments with RBE4 cell line did not show any significant First Contact Imaging. A single event of induced First Contact was made visible, uptake and release control was done scanning the red channel for Atto 590 conjugated antisense strand. Future work should include the conjugation and investigation on the very promising prodye **4** for RNA or a suitable system. This asymmetric xanthene prodye is surprisingly lemon yellow colored and non-fluorescent. Another task for optimizing the prodye concept is the synthesis and conjugation of thiol labile compounds (**Figure 47, A**), which can be activated by intracellular thiols[110,111] (e.g. glutathione), or the development of a "BI-biolabile" concept with presumably improved stability of profluorescent derivatives (**Figure 47, B**). The "BI-biolabile" system concerns the idea, that double deprotection of the non-fluorescent molecule is needed for making a First Contact of interest possible. In this model, *e.g.* the alpha-isomer of peracetylted glucose is initially deprotected by an esterase, which cleaves the acetyl functions, then a mammalian alpha-glucosidase activates the prodye (**Figure 47, B**) and it gets colored, following real-time fluorescence analysis of the cell can be performed.[112, 113]

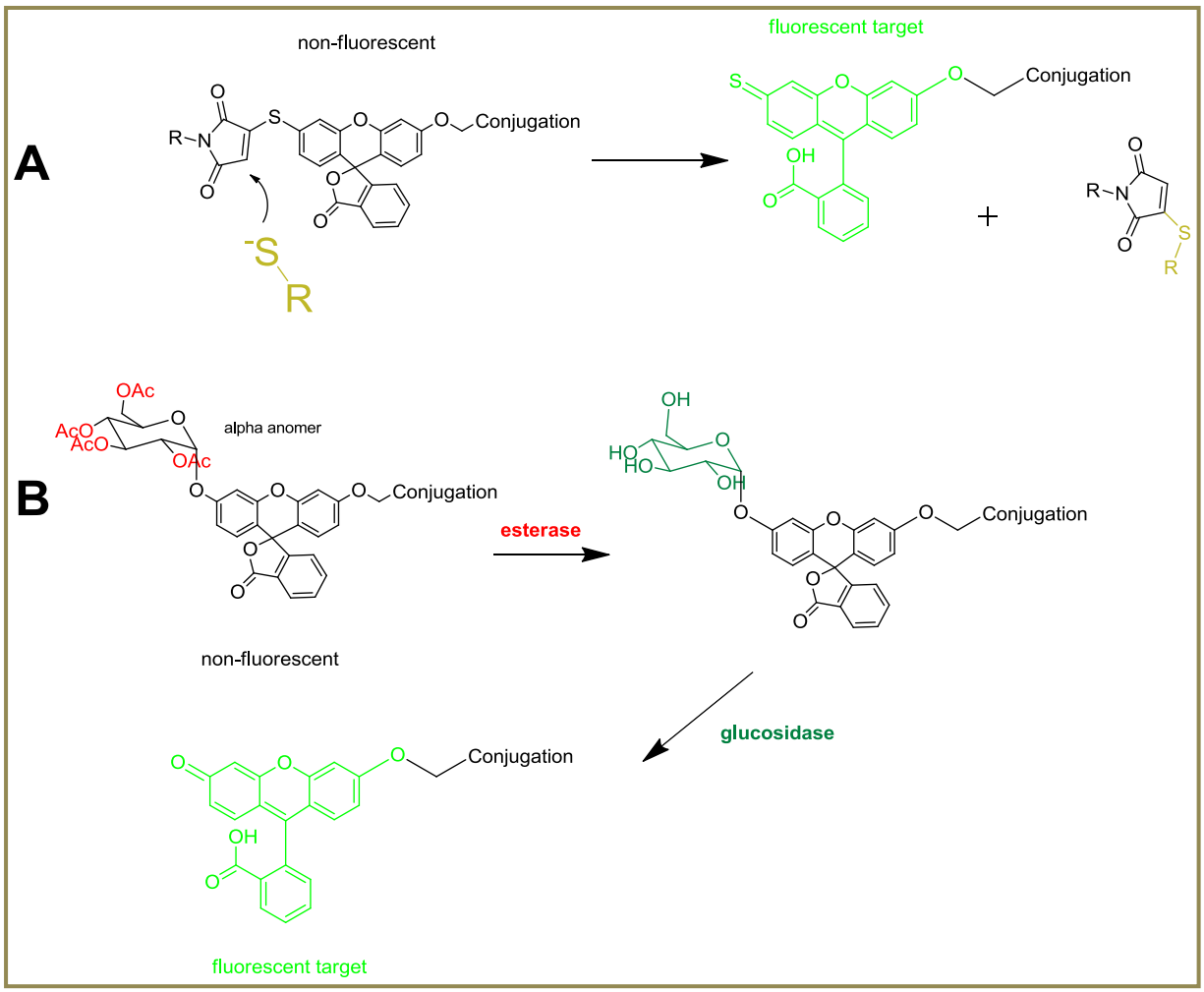

Figure 47. Future perspective of prodyes; A) intracellular thiols (in gold) sensitive prodye concept; B) "BI-biolabile" prodye concept; the fluorescent dye is displayed is green.

5 Experimental Section

5.1 General procedures, materials, instruments and methods

Chemical reagents were purchased from various commercial suppliers, in most cases from from Sigma Aldrich Chemie (Germany), Acros Organics (Steinheim, Germany), Merck KgaA (Darmstadt, Germany), Carl-Roth (Karlsruhe, Germany) and used without further purification. Deuterized solvents were used from Deutero (Kastellaun, Germany).

Thin layer chromatography (TLC): Pre-coated silica gel plates Polygram Sil G/UV$_{254}$ (40 x 80 mm) from Macherey-Nagel, Düren. In general either by iodination (I_2-chamber) or by using UV light at $\lambda = 254$ nm and/or $\lambda = 365$ nm the compounds were made visible.

Preparative thin layer chromatography (pTLC): Pre-coated silica gel glass plates, Silica gel 60 F_{254} (layer thickness 2 mm), from Macherey-Nagel, Düren. Used eluent mixtures can be found in corresponding TLC information of the compounds.

Column chromatography (CC): Silica gel 60 (230-400 mesh) from Fluka, Silica gel 60 (230-400 mesh), Merck KGaA, Darmstadt (Germany)

NMR-spectroscopy: Bruker Fourier 300 MHz (^{1}H: 300 MHz, ^{13}C: 75 MHz), Institute of Pharmacy and Biochemistry (IPB), University of Mainz.

^{1}H and ^{13}C NMR spectra were calibrated to Me_4-Si on the basis of the relative chemical shift of the solvent as an internal standard. Chemical shifts are in ppm and abbreviations used are as follows: s = singlet, d = doublet, pd = pseudodoublet, t = triplet, q = quartet, m= multiplet. Proton signals on xanthene moiety or on the benzene ring of fluorescein are often signed as doublets, because of the lower frequency of the NMR measurements. In reality, they should be split into a doublet of doublets or doublet of triplets. Therefore (if necessary) the signal characterization is done as “pd” in respective sections.

Mass spectrometry: EI mass spectra were recorded on an Agilent 6220 MSD Ion trap.

LC-MS: Agilent 1100, Merck-Hitachi coupled with Agilent MSD Trap 2440 was used

IR spectroscopy: FIT-IR measurements were performed on a Nicolet Avatar 330 FT-IR, Thermo electron corporation, Institute of Pharmacy and Biochemistry, University Mainz.

Melting point temperature: temperature < 200 °C, Apparatur nach Dr. Tottoli, Buchi, Flawil; temperature > 200 °C, Electrothermal IA 9200, Institute of Pharmacy and Biochemistry, University of Mainz.

Microscopy: Living or fixed cells were acquired on the Leica TCS SP5 confocal microscope. The TCS SP5 was equipped with 4 laser lines (405/488/561/633nm), a 63x oil immersion objective (N.A. 1.4), a fast resonance scanner and the Leica filter free detection system (Acousto Opticla tunable excitation filter (AOTF), Acousto-Optical Beam Splitter (AOBS) and spectrophotometer detection system). Image inspection and procession were done using the Leica free LAS AF lite software. The TCS SP5 was provided by the Microscopy Core Facility of the IMB.

Analytical Balance No. 1	Sartorius (Germany)
Analytical Balance No. 2	Mettler Toledo PM460 (Gießen, Germany)
Atto 488 azide	Atto-Tec Siegen (Germany)
Atto 590 azide	Atto-Tec Siegen (Germany)
bFGF, human recombinant	Invitrogen (Karlsruhe, Germany)
Centrifuge 1-15 PK	Sigma (Osterode am Harz, Germany)
Centrifuge Eppendorf 5810 R	Eppendorf (Hamburg, Germany)
Chloramphenicol (35µg/ml in 90%EtOH)	Carl-Roth (Karlsruhe, Germany)
Collagen, Type I from rat tail	Sigma Aldrich (St. Louis, USA)
DAPI	Sigma Aldrich (Munich, Germany)
DMEM	Gibco (Invitrogen, Germany)
DyeEx 2.0 Spin Kit 250	Qiagen, Hilden (Germany)
Electrophoresis Chamber	CBS Scientific
Fast AP thermosensitive AP	Thermo-Fischer, Fermentas Freezer (Darmstadt,Germany)
Eppendorf tubes (silanized)	Carl-Roth (Karlsruhe, Germany)
Filter Tips 10-1000 µl	Greiner Bio One (Vilvoorde, Belgium)
Fluorescent mounting medium	DAKO Cytomation (Hamburg, Germany)
Formamide > 99.5 %	Carl-Roth (Karlsruhe, Germany)
Freeze dryer	Alpha 2-4 LD plus, Christ (Germany)
GelRed	Biotium (Hayward, CA, USA)
HAM’s F-10 culture medium	Invitrogen (Darmstadt, Germany)
HEPES	Sigma Aldrich (Munich, Germany)

HPLC	Agilent 1100 Series, Merck-Hitachi
Inverted Confocal Micoscopy	TCS SP5, Leica (Wetzlar, Germany)
IR (FIT-IR) Spectrometer	AVATAR 330FT-IR (Thermo nicolet)
Jasco FP-6500 fluorimeter	Jasco (Groß-Umstadt, Germany)
Jasco V-6500 spectrophotometer	Jasco (Groß-Umstadt, Germany)
Lipofectamine 2000	Invitrogen (Darmstadt, Germany)
$LiClO_4$ for precipitation	2% (m/m) in acetone
Mass Spectrometer	ESI-MS MSD Trap Agilent 2440
MicroSpin G-25 columns	GE Healthcare (Munich, Germany)
NanoDrop ND-2000	Peqlab (Erlangen, Germany)
NAP columns, Sephadex G-25	GE Healthcare (Amersham Biosciences)
NMR spectrometer	Bruker Fourier 300
NMR Tubes Norell	Norell (USA)
NMR Tubes Deutero	Deutero (Kastellaun, Germany)
Oligofectamine	Invitrogen (Darmstadt, Germany)
OptiMem	Invitrogen (Darmstadt, Germany)
PAGE loading buffer, colorless	1x TBE, 90% (v/v) formamide
PAGE loading buffer	1x TBE, 90% (v/v) formamide, 0.1% bromophenol blue, 0.1% xylene cyanol
pEGFP-N1	Invitrogen (Darmstadt, Germany)
pH-Meter	Mettler Toledo FE20/EL20
Pipettes P2, P10, P20, P100, P200, P1000	Abimed (Langenfeld, Germany)
Pipettes P2, P10, P20, P100, P200, P1000	Eppendorf (Hamburg, Germany)
Rotiphorese sequencing gel buffer concentrate	Carl-Roth (Karlsruhe, Germany)
Rotiphorese sequencing gel concentrate	Carl-Roth (Karlsruhe, Germany)
Rotiphorese sequencing gel diluents	Carl-Roth (Karlsruhe, Germany)
Rotiphorese 10x TBE buffer	Carl-Roth (Karlsruhe, Germany)
IKA - Rotary evaporator	RV 06-ML (Staufen, Germany)
Sep-Pak C18 RP columns	Waters (Eschborn, Germany)
Silica gel 60, (0.063-0.200 nm)	Macherey-Nagel (Germany)

Silica gel plates Polygram® Sil G/UV_{254}	Macherey-Nagel (Germany)
SpeedVac Concentrator plus	Eppendorf (Hamburg, Germany)
Spin filters Nanosep®	Carl-Roth (Karlsruhe, Germany)
StainsAll	Sigma Aldrich (Germany)
TBE buffer	100 mM Tris (pH 8.3), 90 mM boric acid, 1 mM EDTA
Thermomixer comfort	Eppendorf (Hamburg, Germany)
Typhoon 9400 variable mode imager	GE Healthcare (München, Germany)
Ultrapure Water Purification System	Milli-Q, Millipore (Schwalbach, Germany)
UV cuvettes, SUPRASIL quartz glass cuvettes, 10 mm and 3 mm pathlength	Hellma (Müllheim, Germany)
UV-Lamp 254 nm	Herolab Molekulare Trenntechnik (Germany)
ZipTip	Millipore (Schwalbach, Germany)

All other solvents, salts and chemical reagents not included in the list were obtained from the in-house chemical store of the IPB-Mainz, Mainz University.

5.2 Organic synthesis of fluorescent and profluorescent xanthene derivatives

5.2.1 Synthesis of 3'-((2-azidoethyl)thio)-3-oxo-3*H*-spiro[isobenzofuran-1,9'-xanthen]-6'-yl acetate (1)

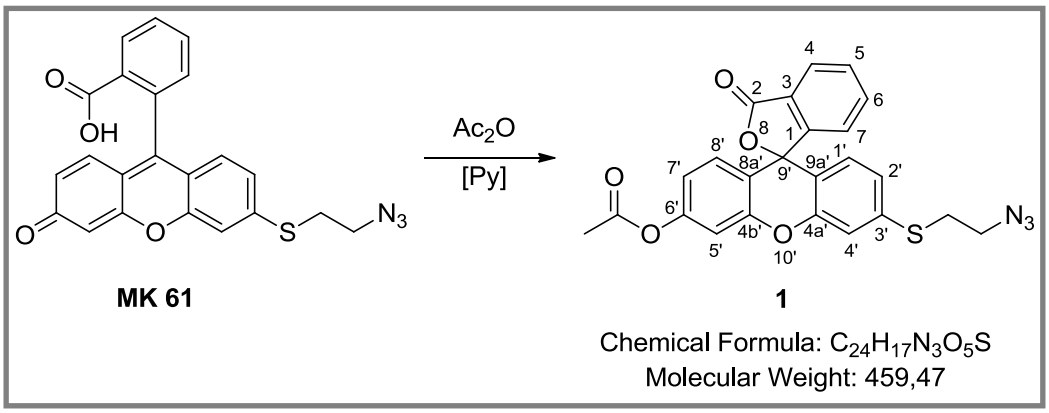

12 mg of MK 61 (0.029 mmol, synthesized by Dr. Kotaskova)[68] was dissolved in 500 µl Pyridine. After cooling to 0°C, 8 equivalents of acetic anhydride (10.3 µl) were added drop wise to the orange colored reaction mixture. Vigorously stirring under light protecting resulted after 12 hours reaction time a white colored crude product. TLC monitoring showed clearly the formation from the orange colored & fluorescent MK 61[75] in to the colorless & nonfluorescent compound **1**. Subsequent preparative TLC (silica, 2mm) purification and lyophilisation overnight yielded 8 mg (0.02 mmol, 70 %) colorless powder **1**.

MP: 120- 121°C (decomposition)

TLC (silica gel, CH_2Cl_2/CH_3OH, 99:1) $R_f = 0.44$

^{1}H-NMR (300 MHz, $CDCl_3$) δ = 8.04 (1H, d, ^{3}J = 7.7 Hz, H-4), 7.67 (2H, m, H-5&6), 7.26 (1H, s, H-5'), 7.17 (1H, d, ^{3}J = 7.4 Hz, H-8'), 7.09 (1H, s, H-4'), 7.01 (1H, dd, ^{3}J = 8.3 Hz, H-7), 6.82 (2H, m, H-1' & H-2'), 6.74 (1H, d, ^{3}J = 8.3 Hz, H-2'), 3.52 (2H, t, ^{3}J = 2.8 ,2H-CN_3), 3.15 (2H, t, ^{3}J = 2.8 , 2H - CS), 2.32 (3H, s, CH_3)

FT-IR $\tilde{V}$ (cm^{-1}): 3076 (w) ν (C-H arom.), 2905 (w) ν (C-H alip.), 2099 (s) ν (N_3), 1757 (s) ν (C=O), 1601 (m) ν (C=C arm.)

5.2.2 Synthesis of 3'-((2-azidoethyl)thio)-2',7'-dichloro-3-oxo-3H-spiro[isobenzofuran-1,9'-xanthen]-6'-yl acetate (2)

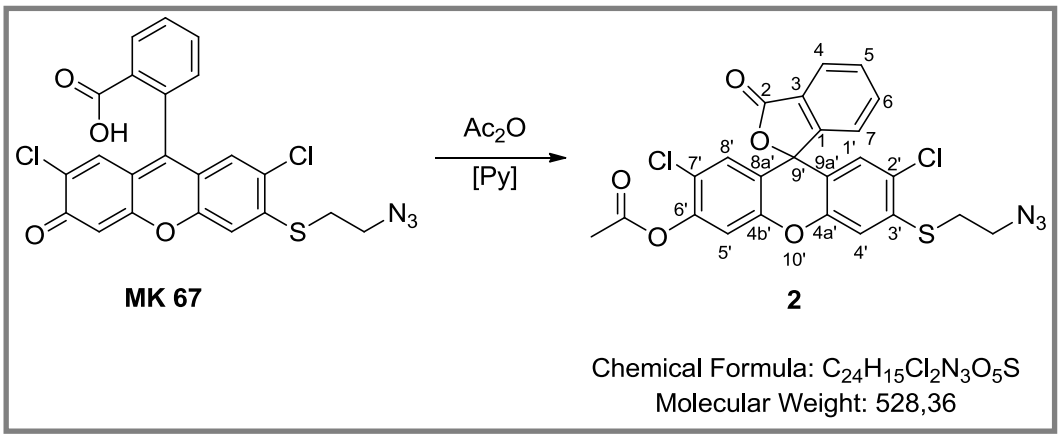

11 mg of MK 67[75] (0.023 mmol, synthesized by Dr. Kotaskova) was dissolved in 500 µl pyridine. After cooling to 0°C, 8 equivalents of acetic anhydride (10.3 µl) were added drop wise to the orange colored reaction mixture. Vigorously stirring under light protecting conditions resulted after 14 hours reaction time a white colored crude product. TLC monitoring showed clearly the formation from the orange colored & fluorescent MK 61 in to the colorless & nonfluorescent compound **2**. Subsequent preparative TLC purification (silica, 2mm) and lyophilisation overnight yielded 12 mg (0.0227 mmol, 98%) of pure and colorless powder **2**.

MP: 131°C (decomposition)

TLC (silica gel, CH_2Cl_2/CH_3OH, 98:2) $R_f = 0.59$

^{1}H-NMR (300 MHz, $CDCl_3$): δ 8.08 (1H, d, ^3J = 7.3 Hz, H-4), 7.72 (2H, m, H5&H6), 7.17 (3H, m, H7, H1' & H8'), 6.86 (1H, s, H5'), 6.79 (1H, s, H4'), 3.73 (2H, t, ^3J = 8,1 Hz, 2H-CN_3), 3.36 (2H, t, ^3J = 8,1 Hz, 2H - CS), 2.38 (3H, s, CH_3)

^{13}C-NMR (75 MHz, $CDCl_3$): δ 168.55 (C=O lac), 167.99 (C=O acetyl), 151.8, 149.8, 149.7, 148.5, 138.6, 135.8, 130.9, 128.9, 128.5, 128.4, 125.8, 123.9, 122.7, 117.7, 117.3, 115.6, 113.3, 112.7, 80.5 (C9'), 41.3 (C-N_3), 34.2 (C-S), 20.7 (C-H_3)

FT-IR $\tilde{V}$ (cm^{-1}): 2924 (w) ν (C-H alip.), 2118 (w) ν (N_3), 1771 (s) ν (C=O), 1600 (w) ν (C=C arm.), 1195 (m)

5.2.3 Synthesis of 2-(6-(2-(2-(2-azidoethoxy)ethoxy)ethoxy)-3-oxo-3*H*-xanthen-9-yl)benzoic acid (3)

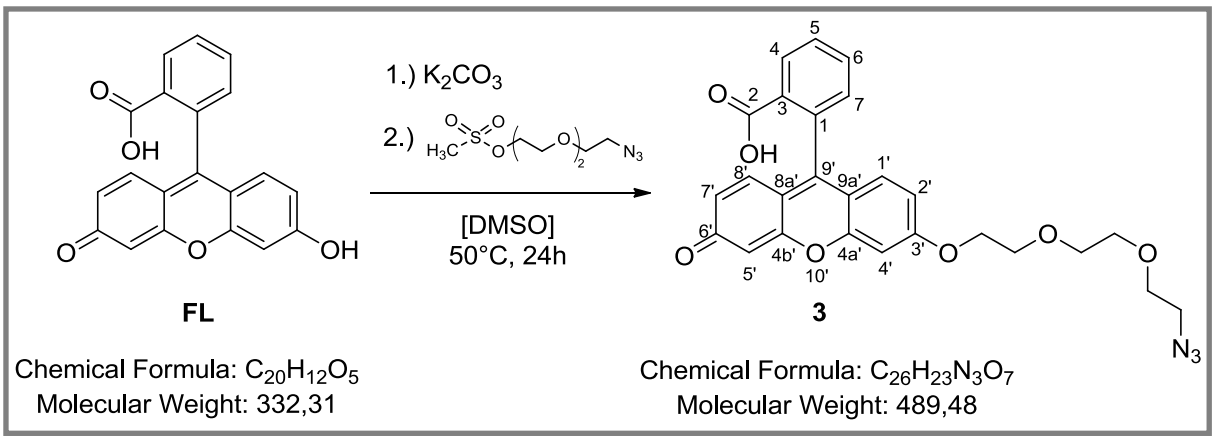

167 mg FL (0,50 mmol) were suspended in 330 µl DMSO and formed a dark red dispersion. 2.2 equivalents of potassium carbonate (1.1 mmol, 152 mg) were added and the mixture was heated to 50°C, which became clear and red after 1 hour. Drop wise adding of 1,05 equivalents Mesyl-PEG-azide (0.525 mmol, 139 mg, kindly provided by Dr. Sven Aldenkortt) formed an orange solution. 24 hours later the absence of MES-PEG-azide was verified by TLC & ^{1}H-NMR, consequently the reaction was finished. Then 50 ml extraction solution (3:1 DCM:$CHCl_3$) was added, the aqueous phase neutralized with 0.01 M H_2SO_4 and 3x extracted with extraction solution. The organic phases were united and evaporation of organic solvents yielded 222 mg gold-orange colored crude product of **3**. Following preparative TLC purification (silica, 2mm) and lyophilisation over 24 hours resulted 60 mg (0.12 mmol, 27%) red-orange colored and pure powder of **3**, with a strong fluorescence in neutral organic solvents.

MP: 211 – 212 °C

TLC (silica gel, CH_2Cl_2/CH_3OH, 95:5) R_f = 0.36 / (ethyl acetate/cyclohexane 7:3) R_f = 0.11

^{1}H-NMR (300 MHz, DMSO-d6): δ 10.17 (1H, s, H-O), 8.00 (1H, pd, ^{3}J = 7.4 Hz, H3), 7.75 (2H, dd, ^{4}J = 16.1, 7.4 Hz, H5 & H6), 7.26 (1H, pd, ^{3}J = 7.4 Hz, H7), 6.94 (1H, pd, ^{3}J = 8.8 Hz, H7'), 6.71 (2H, m, H1' & H2'), 6.64 (1H, pd, ^{3}J = 8.8 Hz, H8'), 6.58 (2H, m, H4'&H5'), 4.16 (2H, t, ^{3}J = 3.0 Hz, 2H-CN_3), 3.76 (2H, t, ^{3}J = 3.0 Hz, 2H-CO-), 3.57 (8H, dd, ^{4}J = 13.0, 3.0 Hz, H-PEG).

^{13}C-NMR (75 MHz, DMSO-d6): δ 165.0 (C2, C=O, acid), 156.3 (C3'), 152.0 (C4b'), 151.3 (C4a'), 133.8, 133.2, 130.9, 130.7, 130.6, 130.3, 130.1, 130.0, 129.7, 128.9, 125.2, 114.8 (C7'), 105.2, 103.3, 99.6 (C4'), 96.3 (C5'), 69.7, 69.6, 69.3, 68.0, 64.4 (PEG), 50.0 (C-N_3)

ESI-MS: (+) Mode: calc. 490.15, found. 490.28 (100%), fragments: 445.3, 333.2

(-) Mode: calc. 488.15, found. 488.00 (100%), fragments: 460.4, 344.4

FT-IR $\tilde{V}$ (cm^{-1}): 3063 (w) ν (CH-arm.), 2918 (w), 2499 (m, b) ν (OH), 2097 (m) ν (N_3), 1716 (m) ν (C=O), 1638 (m) ν (C=C), 1247 (s)

5.2.4 Synthesis of 3'-(2-(2-(2-azidoethoxy)ethoxy)ethoxy)-3-oxo-3*H*-spiro[isobenzofuran-1,9'-xanthen]-6'-yl isobutyl carbonate (4)

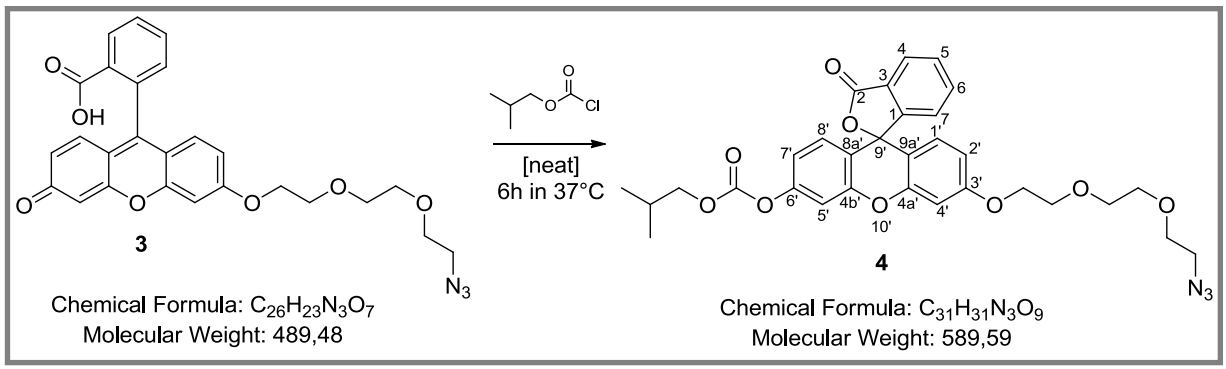

20 mg (0.04 mmol) **3** was suspended in 1 ml isobutyl chloro formiate (IBCF). Slightly heating to 37°C and stirring under argon atmosphere for 6 hours developed a color change from orange to lemon yellow of the suspension. The endpoint of the reaction was monitored with TLC (silica), in which the starting compound **3** fully transformed to **4**. In the next step the mixture was taken in an organic solvent mix of 3:1 DCM:$CHCl_3$ (15 ml) and washed 3x with water (10 ml). Drying over Na_2SO_4 and subsequent evaporation of the solvents delivered dark yellow oil. Following preparative TLC purification (2mm, silica) & lyophilisation over 24 hours yielded 11 mg (0.018 mmol, 45 %) of lemon yellow colored solid **4,** which is non-fluorescent in neutral organic solvents.

MP: 160 - 161 °C

TLC (silica gel, CH_2Cl_2/CH_3OH, 95:5) R_f = 0.59

^{1}H-NMR (300 MHz, DMSO-d6): δ 8.24 (1H, pd, ^{3}J = 7.7 Hz, H4), 7.85 (2H, m, H5&H6), 7.63 (1H, pd, ^{3}J = 8.0 Hz, H7), 7.54 (1H, pd, ^{3}J = 8.3 Hz, H8'), 7.19 (1H, s, H5'), 6.97 (1H, pd, ^{3}J = 8.3 Hz, H7'), 6.85 (1H, pd, ^{3}J = 9.8 Hz, H1'), 6.44 (1H, pd, J = 9.8 Hz, H2'), 6.28 (1H, s, H4'), 4.05 (2H, d, 3J= 2.9 Hz, H_2C), 4.03 (2H, t, ^{3}J= 2.1 Hz, H_2CN_3), 3.52 (5H, m, PEG), 3.44 (2H, t, ^{3}J= 2.1 Hz, PEG), 3.37 (3H, t, ^{3}J = 2.1 Hz, PEG), 1.99 (1H, hept, ^{3}J= 2.9 Hz, HC), 0.95 (3H, s, H_3C), 0.93 (3H, s, H_3C)

^{13}C-NMR (75 MHz, DMSO-d6): δ 184.7, 165.3 (C=O, lacton), 158.6 (C=O, carboxyl), 157.7 (C3'), 154.2 (C4b'), 152.7 (C4a'), 152.4 (C1), 133.8, 131.4, 131.3, 131.0, 130.7, 130.6, 130.0, 129.9, 129.3, 125.3, 119.5, 119.4, 105.5, 83.4 (C9'), 75.1 (C methylene O), 70.0, 69.9, 69.7, 68.4, 67.6 (PEG) 50.4 (C-N_3), 27.7, 19.0 (2 x C ! methyl overlay)

ESI-MS: (+) Mode: calc. 590.21**,** found. 589.5 (100%), fragments: 490.1, 461.5, 445.0, 333.4

FT-IR $\tilde{V}$ (cm^{-1}): 3360 ν (CH-arm.), 2955 (w) ν (C-H aliph.), 2919 (m) ν (C-H aliph.), 2850 (w) ν (C-H alip.), 2101 (m) ν (N_3), 1764 (m) ν (C=O, lactone), 1722 (m) ν (C=O, carbonate), 1225 (s)

5.2.5 Synthesis of 3'-(2-(2-(2-azidoethoxy)ethoxy)ethoxy)-6'-hydroxy-3*H*-spiro[isobenzofuran-1,9'-xanthen]-3-one (5)

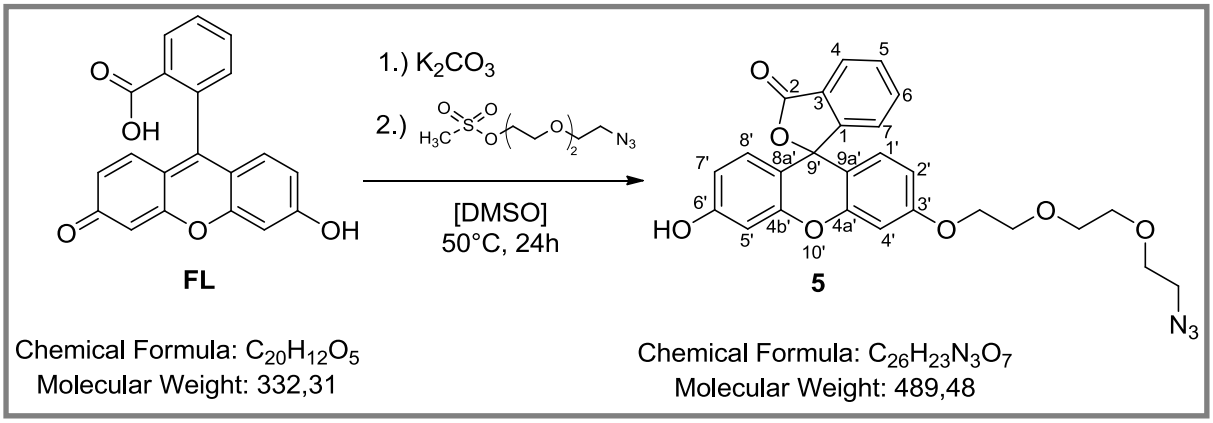

167 mg FL (0,50 mmol) were suspended in 330 µl DMSO and it resulted a dark red dispersion. 2.2 equivalents of potassium carbonate (1.1 mmol, 152 mg) were added and the mixture was heated to 50°C, which became clear and red after 1 hour. Drop wise adding of 1,05 equivalents mesyl-PEG-azide (0.525 mmol, 139 mg) formed an orange solution. After 24 hours the absence of MES-PEG-azide was verified by TLC & H-NMR, consequently the

reaction was stopped. Then, 50 ml extraction solution (3:1 DCM:$CHCl_3$) was added, the aqueous phase neutralized with 0,01 M H_2SO_4 and 3x extracted with extraction solution. The organic phases were united and evaporation of organic solvents yielded 222 mg gold-orange colored crude product of **5**. Following preparative TLC purification (silica, 2mm) and lyophilisation over 24 hours yielded 11 mg (0.021 mmol, 4.1 %) lemon yellow colored and pure solid of **5** as byproduct, which is non-fluorescent in neutral organic solvents.

MP: 140 – 142 °C

TLC (silica gel, CH_2Cl_2/CH_3OH, 95:5) R_f = 0,75 / (ethyl acetate/cyclohexane 7:3) R_f = 0,68

^{1}H-NMR (300 MHz, DMSO-d6): δ 10.17 (1H, s, HO), 8.00 (1H, pd, ^{3}J = 7.5 Hz, H4), 7.76 (2H, m, H5&H6), 7.26 (1H , pd, ^{3}J = 7.5 Hz, H7), 6.94 (1H, s, H4'), 6.72 (2H, pd, ^{3}J = 7.6 Hz, H7'&H8'), 6.63 (1H, s, H5'), 6.58 (2H, pd, J = 8.8 Hz, H1'&H2',), 4.16 (2H, t, ^{3}J = 3.5 Hz, H_2-CN_3), 3.76 (2H,t, ^{3}J = 3.5 Hz, H_2-CO), 3.58 (8H, m, H-PEG)

^{13}C-NMR (75 MHz, DMSO-d6): δ 168.67 (C=O), 160.23 (C6'), 159.56 (C3'), 152.48, 151.85, 151.79, 135.65, 130.14, 128.94, 126.07, 124.67, 123.98, 112.80, 112.29, 111.08, 109.45, 102.24, 101.33, 82.73 (C9'), 72.39, 69.95, 69.71, 69.30, 67.68, 60.24 (C-PEG) 50.00 (C-N_3)

ESI-MS: (+) Mode: calc. 490.15, found. 490.3 (100%), fragments: 445.1, 333.4

(-) Mode: calc. 488.15, found. 488.1 (100%), fragments: 460.6, 344.5

FT-IR $\tilde{V}$ (cm^{-1}): 3376 ν (CH-arm.), 2918 (w) ν (C-H aliph.), 2871 (m) ν (C-H aliph.), 2097 (m) ν (N_3), 1745 (s) ν (C=O, lacton), 1609 (m), 1173 (m)

5.2.6 Synthesis of 2-(2-(2-azidoethoxy)ethoxy)ethyl 2-(6-(2-(2-(2-azidoethoxy)ethoxy)ethoxy)-3-oxo-3*H*-xanthen-9-yl)benzoate (6)

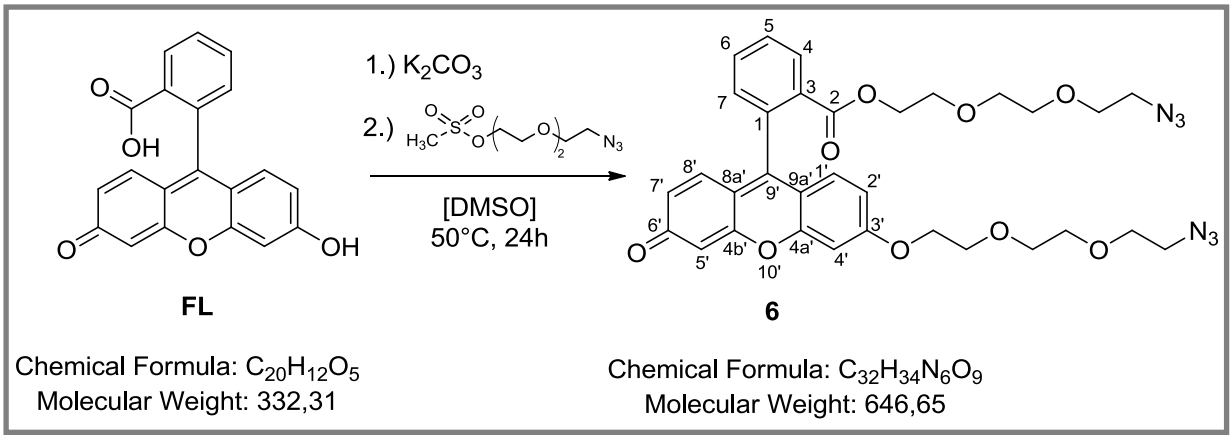

167 mg FL (0,50 mmol) were suspended in 330 µl DMSO and it resulted in a dark red dispersion. 2.2 equivalents of potassium carbonate (1.1 mmol, 152 mg) were added and the mixture was heated to 50°C, which became clear and red after 1 hour. Drop wise adding of 1.05 equivalents Mesyl-PEG-azide (0.525 mmol, 139 mg) formed an orange solution. After 24 hours the absence of MES-PEG-azide was verified by TLC & H-NMR, consequently the reaction was finished. Then 50 ml extraction solution (3:1 DCM:$CHCl_3$) was added, the aqueous phase neutralized with 0,01 M H_2SO_4 and 3x extracted with extraction solution (3:1 DCM:$CHCl_3$) . The organic phases were united and evaporation of organic solvents yielded 222 mg gold-orange colored crude product of **6**. Following preparative TLC purification (silica, 2mm) and lyophilisation over 24 hours resulted 12 mg (0.018 mmol, 3.6 %) orange colored and pure semi-solid of **6** as byproduct, which is weak fluorescent in neutral organic solvents.

TLC (silica gel, CH_2Cl_2/CH_3OH, 95:5) R_f = 0,48 / (ethyl acetate/cyclohexane 7:3) R_f = 0,39

^{1}H-NMR (300 MHz, DMSO-d6): δ 8.21 (1H, pd, ^{3}J = 7.7 Hz, H4), 7.82 (2H, m, H5&H6), 7.49 (1H, pd, ^{3}J = 8.5 Hz, H7), 7.24 (1H, pd, ^{3}J = 2.3 Hz, H1'), 6.86 (3H,m, H2', H7', H8'), 6.39 (1H, s, H4'), 6.23 (1H, s, H5'), 4.26 (2H, t, ^{3}J = 4.3 Hz, H_2-CN_3), 4.05 (2H, t, ^{3}J = 4.3 Hz, H_2-CO), 3.79 (2H, t, ^{3}J = 4.1 Hz, H_2-CN_3), 3.60 (8H, m, PEG), 3.54 (2H, t, ^{3}J = 4.1 Hz, H_2-CO), 3.54 (8H, m, PEG)

^{13}C-NMR (75 MHz, DMSO-d6): δ 183.88, 164.93, 163.10, 158.43, 153.59, 149.91, 133.65, 133.21, 130.83, 130.69, 130.43, 130.00, 129.68, 129.35, 128.93, 116.79, 114.42, 113.90, 104.55, 100.97, 69.95, 69.68, 69.63, 69.49, 69.28, 69.27, 68.65, 68.32, 67.97, 64.34, 49.99, 49.95

ESI-MS: (+) Mode: calc. 646.5, found. 647.7 (100%), fragments: 490.3, 333.3

FT-IR $\tilde{V}$ (cm^{-1}): 3585 (w), 3364 ν (w) (CH-arm.), 3058 (w) ν (C-H alip.), 2869 (m) ν (C-H alip.), 2105 (s) ν (N_3), 1721 (m) ν (C=O, ester), 1642 (m) ν (C=O), 1592 (s) ν (C=C), chinon), 1255 (s)

5.2.7 Synthesis of ((3-oxo-3*H*-spiro[isobenzofuran-1,9'-xanthene]-3',6'-diyl)bis(oxy))bis(methylene) bis(2,2-dimethylpropanoate) (7)

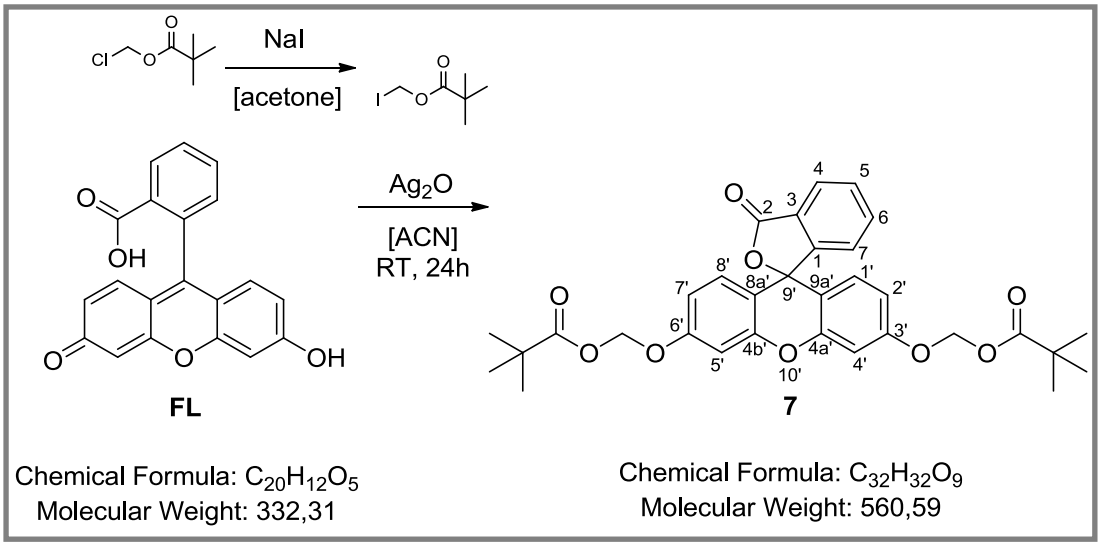

8.8 g NaI (20 Eq., 60 mmol) was suspended in 10 ml acetone. Drop wise adding of 2.25 ml (1 Eq., 3 mmol) chloromethylpivalate caused a color change from white over yellow to brown during an overnight reaction under RT, inert and light protecting conditions. Then 20 ml DCM were added and unreacted salt was washed with 20 ml aqueous solution (NaCl saturated water : water, 9:1), followed by 3 x DCM extraction of the aqueous phase. The organic phases were combined, dried over $MgSO_4$ and evaporation of solvents delivered 2ml brown oil (n_D^{20}: 1.4950), identified as iodomethylpivalate by ^{1}H-NMR. The oil was stored over argon atmosphere at -20°C. 137 mg FL (0.41 mmol), 927 mg Ag_2O (4.1 mmol) and 100 mg was suspended in 2.5 ml ACN (dried) for 1 hours at RT. Adding 400 mg (1,6 mmol) of iodomethylpivalate in a drop wise manner produced over 48 hours under argon atmosphere a grey suspension. The monitoring was proceeded by TLC. Then diluting with 10 ml DCM and filtering through a syringe filter (0.22 µm pore diameter) gave a yellow colored solution, followed by evaporation. The purification with preparative TLC (silica, 2mm, 95:5 DCM:MeOH) and lyophilisation over 24 hours resulted in 90 mg (42,5%, 24 %[53]) of compound **7**, which is colorless and non-florescent in organic solvents.

MP: 108 - 110 °C

TLC (silica gel, CH_2Cl_2/CH_3OH, 95:5) R_f = 0.80

^{1}H-NMR (300 MHz, $CDCl_3$): δ 8.02 (1H, d, ^{3}J = 7.1 Hz, H4), 7.65 (2H, m, H5&6), 7.17 (1H, d, ^{3}J = 8.1 Hz, H7), 6.95 (2H, s, H4'&5'), 6.73 (4H, s, H1',H2',H7',H8'), 5.78 (4H, s, 2x H_2C), 1.21 (18H, s, 6 x H_3C)

^{13}C-NMR (75 MHz, $CDCl_3$) δ 209.1 (2 x C ester), 176.9 (C2), 168.9 (C3'&6'), 158.3 (C4a'&4b'), 151.9 (C1), 134.82, 134.8, 129.1, 124.8, 123.6, 112.9, 112.4, 103.3, 84.9 (C9'), 38.7 (2 x C methylene, 26.68 (6 x C methyl), cave: symmetry!

ESI-MS: (+) Mode: calc. 561.59, found. 561.0 (100%), fragments: 531.1, 501.3

FT-IR $\tilde{V}$ (cm^{-1}): 2978 (w) ν (C-H aliph.), 1768 (m) ν (C=O, lactone), 1730 (m) ν (C=O, ester), 1099 (s)

5.2.8 Synthesis of 3'-(2-(2-(2-azidoethoxy)ethoxy)ethoxy)-3-oxo-3*H*-spiro[isobenzofuran-1,9'-xanthen]-6'-yl acetate (8)

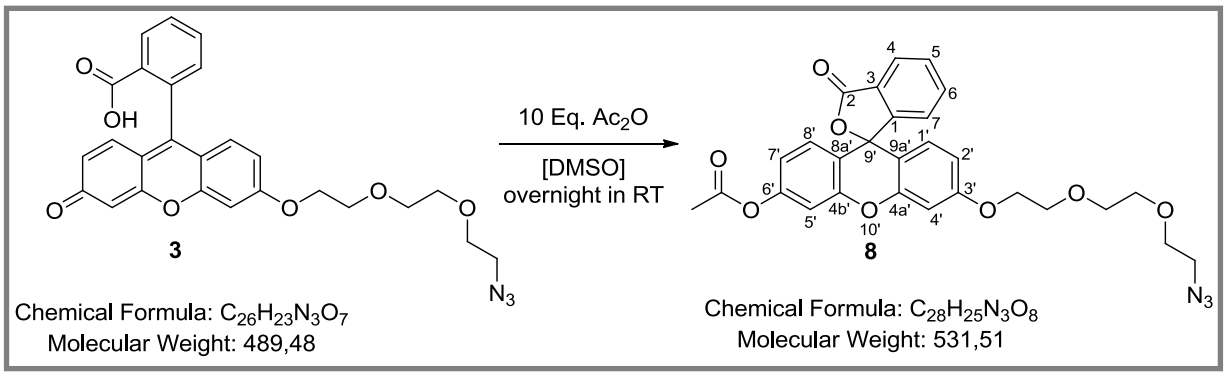

12 mg (0,024 mmol, 1Eq.) of compound **3** was dissolved in 0.5 ml DMSO. After drop wise adding of 23.17 µl acetic anhydride (0.24 mmol, 10 Eq) the solution started getting over orange to lemon yellow. The endpoint of the reaction was verified by TLC. In the next step the reaction mixture was diluted with 10 ml water and 3x extracted with 10 ml DCM. The combined organic phases were dried over $NaSO_4$, evaporated to a yellow oil and purified by preparative TLC (silica, 2mm). Lyophilisation overnight yielded the 10 mg of the lemon yellow solid **8** (0,018 mmol, 78%), which is non-fluorescent in organic solvents.

TLC (silica gel, CH_2Cl_2/CH_3OH, 95:5) R_f = 0,64

ESI-MS: (+) Mode: calc. 531.51, found. 531.5 (100%), fragments: 490.1, 280.1

FT-IR $\tilde{V}$ (cm^{-1}): 3399 ν (CH-arm.), 3065 (w) ν (C-H alip.), 2923 (m) ν (C-H alip.), 2102 (m) ν (N_3), 1764 (w) ν (C=O, lacton), 1719 (m) ν (C=O, ester), 1176 (s) ν (C-O-C), 1104 (s) ν (C-O-C)

5.2.9 Synthesis of 3-bromo-1-methyl-1*H*-pyrrole-2,5-dione (9)

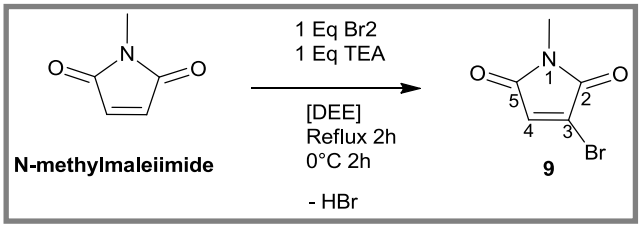

2g (18 mmol) of N-methylmaleiimide was dissolved in 25 ml dried diethyl ether. Then 0,92 ml bromine (18 mmol, 3g) was added drop wise, refluxed for 2 hours and finally under cooling (0°C) 2.8 ml TEA (18 mmol) was set to the reaction mixture. After 2 hours stirring at °C, the mixture was diluted with 40 ml ethyl acetate and washed with water. In the next step, extraction of the aqueous phase with DCM and combination of the organic phases delivered a gold-yellow organic solution, which was dried over $MgSO_4$, filtered and concentrated to gold colored oil. Overnight storage at -20°C yielded 2.1 g white precipitate of **9** (11,9 mmol, 66,7%).

MP: 89°C (88-89[114])

TLC (silica gel, EA: PE, 3:1) R_f = 0.44

^{1}H-NMR (300 MHz, $CDCl_3$): δ 6.88 (1H,s), 3.10 (3H,s)

^{13}C-NMR (75 MHz, $CDCl_3$) δ 168.5 (C=O), 165.3 (C=O), 131.8, 131.3, 24.5 (CH_3)

FT-IR $\tilde{V}$ (cm^{-1}): 1698 (s) ν (C=O), 1228 (s), 704 (s)

5.2.10 Synthesis of (2R,3R,4S,5R,6R)-2-(acetoxymethyl)-6-bromotetrahydro-2*H*-pyran-3,4,5-triyl triacetate (10)

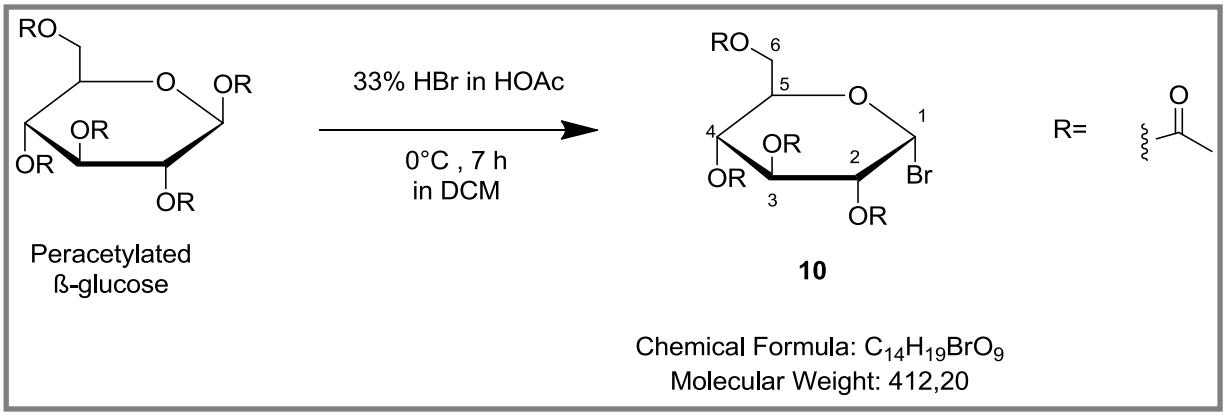

To a stirring DCM solution of 1,2,3,4,6-penta-O-acetyl-β-D-glucopyranose (2.4 g, 6.1 mmol) 10 ml of HBr/HOAc (33%) was added and cooled to °0 C. The resulting solution was stirred for 7 h until 1,2,3,4,6-penta-O-acetyl-β-D-glucopyranose completely disappeared.

The solution was neutralized with saturated $NaHCO_3$ solution, then dried over $MgSO_4$, filtered through a celite pad and evaporated under vacuum to give the crude alpha-glycosylbromide as yellow oil. Recrystallization from ethanol yielded the compound **10** as a white solid (2.5 g, 5.85 mmol, 96%).

MP: 128°C

TLC (silica gel, ACN/H_2O, I_2.chamber) R_f = 0.82

^{1}H-NMR (300 MHz, DMSO-d6): δ 5.96 (1H, d, J = 8.3 H, H-C1), 5.44 (1H, t, J = 9.6 Hz), 4.94 (2H, q, H-C5), 4.18 (1H, t, J = 11.1 Hz), 3.99 (2H, d, J = 10.7 Hz), 2.07 (3H, s,), 2.00 (3H, s,), 1.99 (3H, s), 1.94 (3H, s)

^{13}C-NMR (75 MHz, DMSO-d6): δ 170.02, 169.52, 169.28, 169.13, 168.77, 90.80 (C1), 71.73, 71.36, 70.04, 67.64, 61.44, 20.50, 20.40, 20.30

ESI-MS: (+) Mode: calc. 413.2, found. 412.9 (100%), fragments: 352.9, 293.1, 251.0

FT-IR $\tilde{V}$ (cm^{-1}): 2969 (w) ν (C-H alip.), 1736 (s) ν (C=O, ester), 703 (m)

5.3 Photometry and fluorimetry

For the photophysical characterization of new fluorescent and profluorescent xanthene dye, parameters such as absorption, extinction coefficient at the maximum absorption wavelength (λmax), excitation (λex), emission (λem) were determined with the JASCO photo- and fluorimeter.

Stock solutions were prepared by precise weighing and dissolving of 5-10 mg of pure fluorophore in DMSO (extra pure & dried, > 99.8%) to get 5 mM stocks. **Figure 44** depicts the synthesized, tested profluorescent and fluorescent dyes.

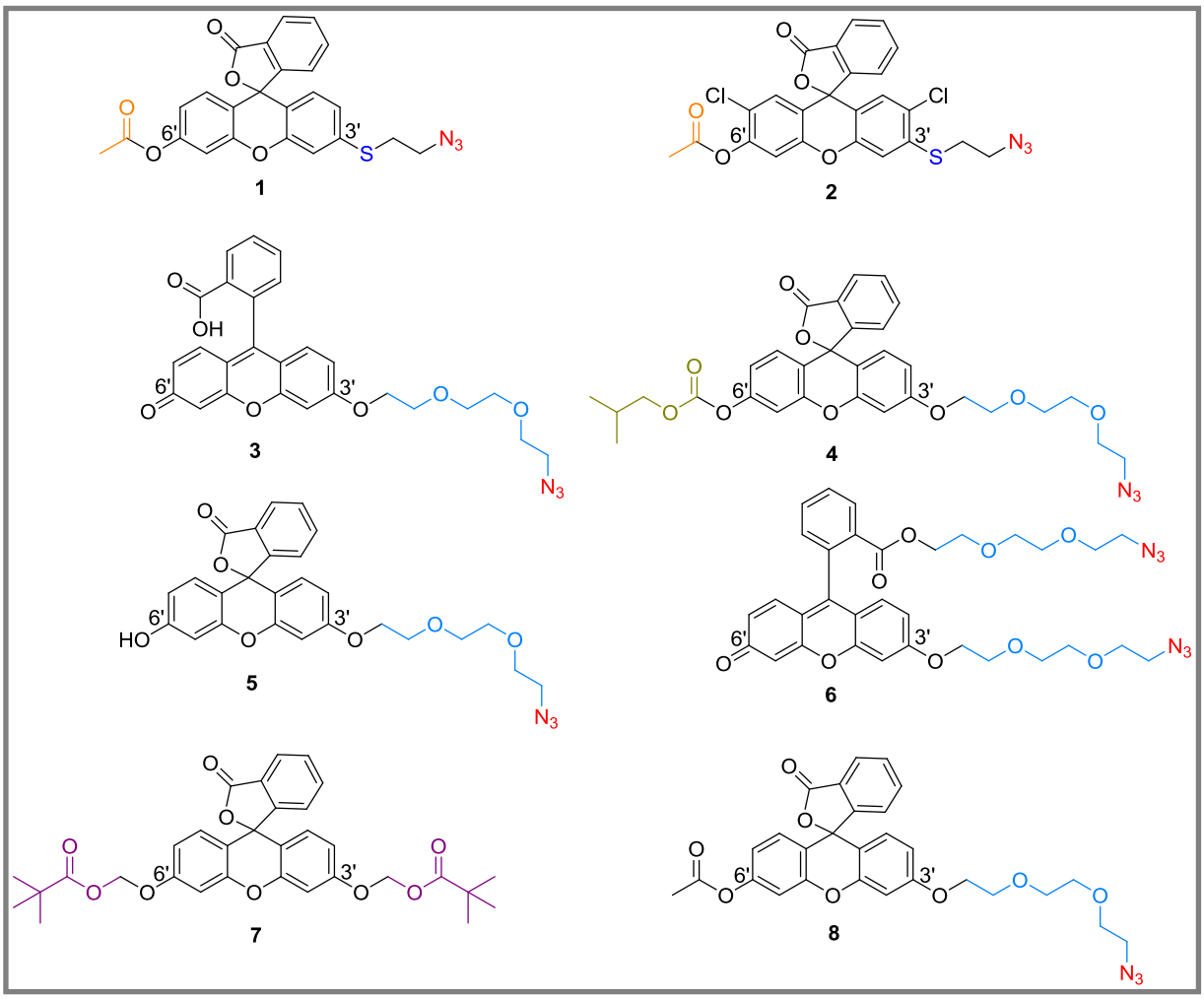

Figure 48. Structures of synthesized asymmetric xanthene dyes

5.3.1 Absorption measurements in acidic, neutral and basic conditions

The spectra were recorded in Suprasil quartz glass cuvettes (Hellma, Müllheim, Germany) with 0.1 cm path length in acidic medium pH = 3 (0.001 M HCl), in neutral medium pH 7.4 (10 x PBS buffered) and in basic medium (0.001 M NaOH) at 25°C. DMSO content did not exceed 1% v/v in the measurements due to the 50 µM final concentrations. As reference dye, fluorescein[85,38] was used. Absorption spectra were recorded on a Jasco V-650 spectrophotometer equipped with a Jasco ETC-505T Peltier temperature programmer (Jasco, Groß-Umstadt, Germany) to observe the impact of pH on the absorption of new dyes and to determine the maximum absorption wavelength (λ_{max}) in respective media. Absorption spectra were recorded from 300 to 600 nm. The impact of pH on absorption at given concentration of xanthene dyes is illustrated in the corresponding graphs from page 81 - 89.

In table S1 – S3 one can see the absorption maxima in nm with corresponding absorption intensity, respectively. Table S4 shows the calculated extinction coefficients of selected dyes by using the Lambert-Beer-law ($E = \varepsilon * c * l$)[13], where E is the extinction in described experiment settings, c is the concentration in mol/l, l is the length of the path in cm and ε is the extinction coefficient in $M^{-1}\,cm^{-1}$.

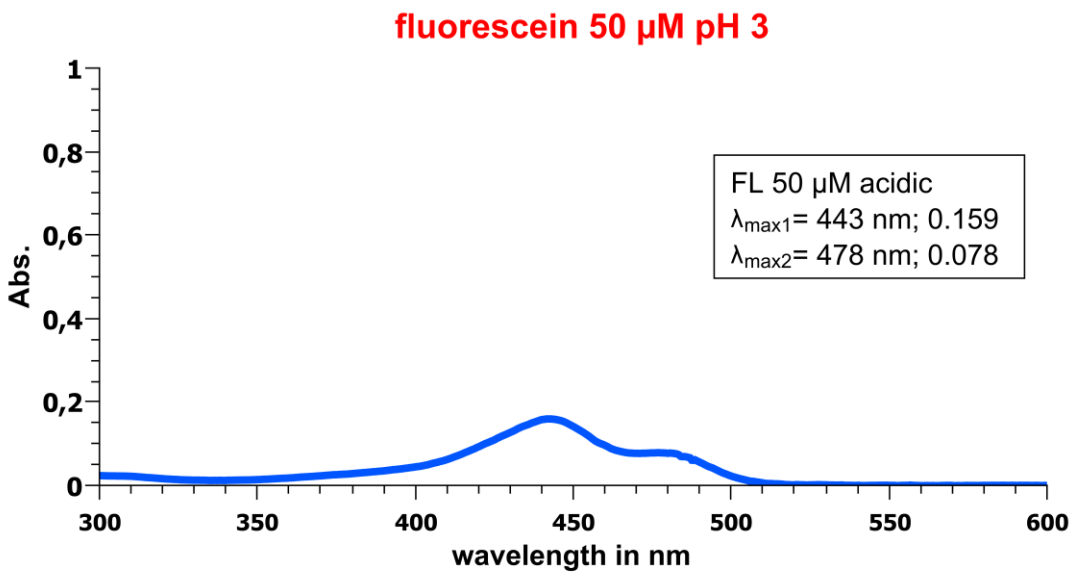
fluorescein 50 µM pH 3
FL 50 µM acidic
λmax1= 443 nm; 0.159
λmax2= 478 nm; 0.078
Abs.
wavelength in nm

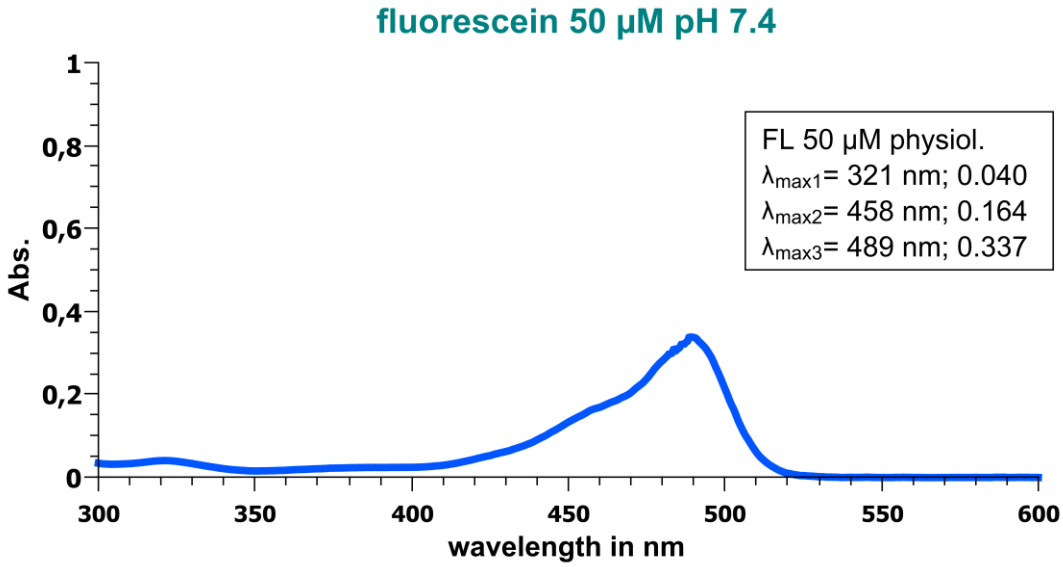
fluorescein 50 µM pH 7.4
FL 50 µM physiol.
λmax1= 321 nm; 0.040
λmax2= 458 nm; 0.164
λmax3= 489 nm; 0.337
Abs.
wavelength in nm

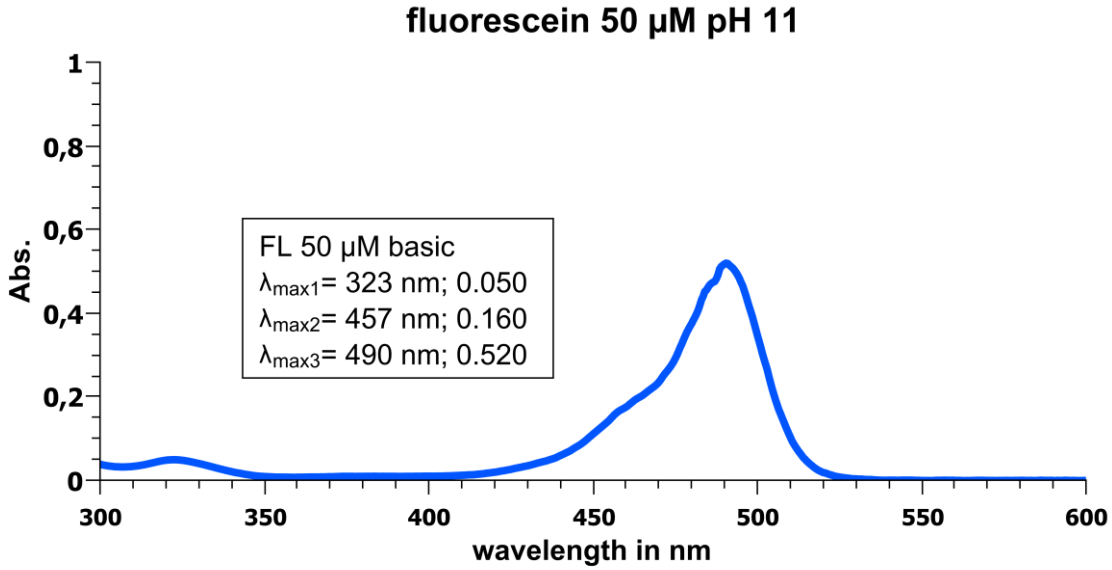
fluorescein 50 µM pH 11
FL 50 µM basic
λmax1= 323 nm; 0.050
λmax2= 457 nm; 0.160
λmax3= 490 nm; 0.520
Abs.
wavelength in nm

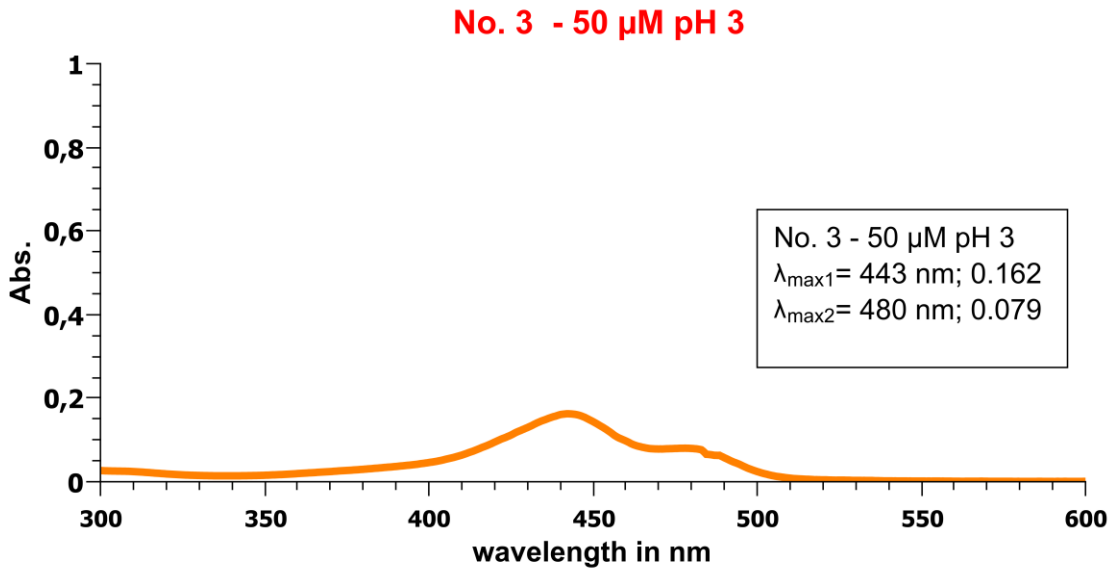
No. 3 - 50 µM pH 3
λmax1= 443 nm; 0.162
λmax2= 480 nm; 0.079
Abs.
wavelength in nm

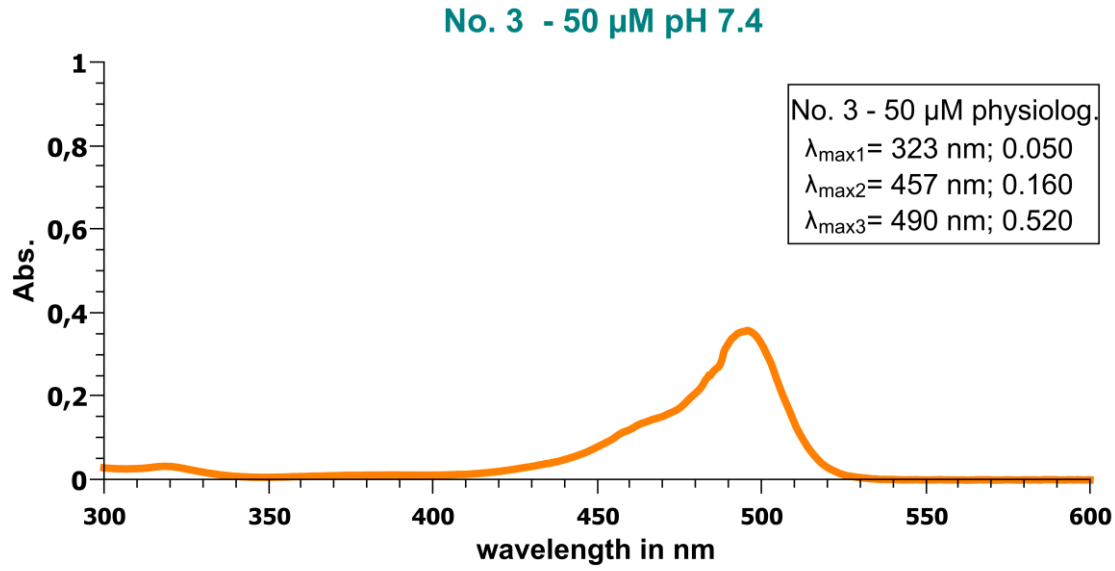
No. 3 - 50 µM pH 7.4
No. 3 - 50 µM physiolog.
λmax1= 323 nm; 0.050
λmax2= 457 nm; 0.160
λmax3= 490 nm; 0.520
Abs.
wavelength in nm

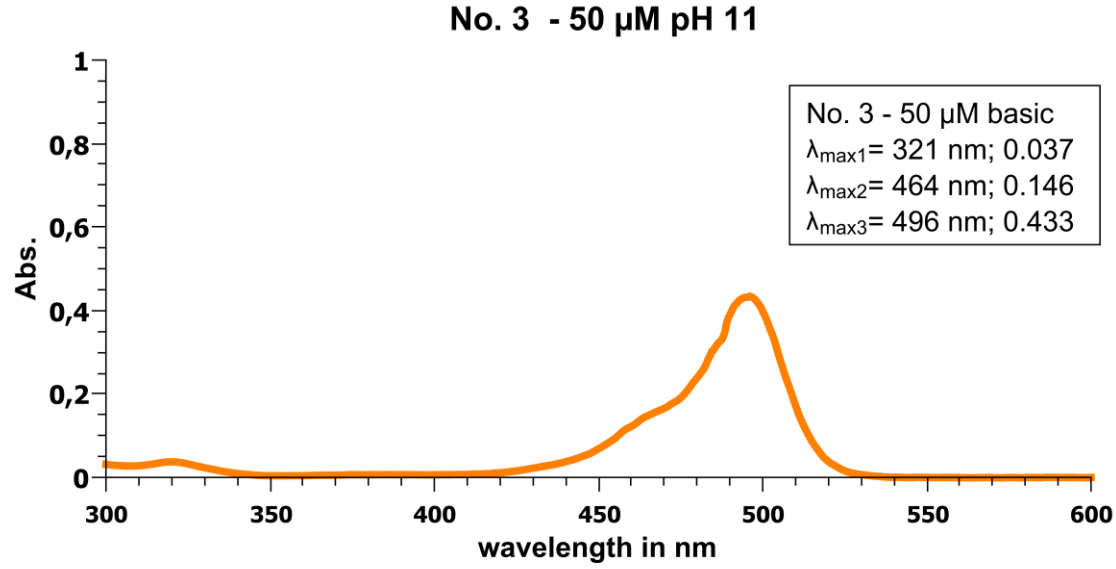
No. 3 - 50 µM pH 11
No. 3 - 50 µM basic
λmax1= 321 nm; 0.037
λmax2= 464 nm; 0.146
λmax3= 496 nm; 0.433
Abs.
wavelength in nm

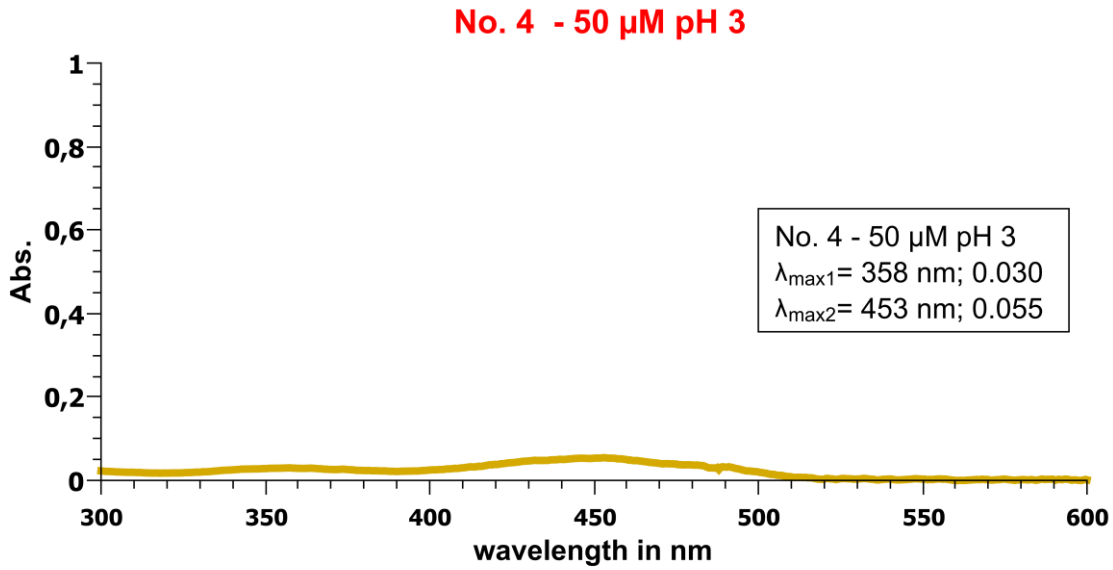
No. 4 - 50 µM pH 3
Abs.
wavelength in nm
No. 4 - 50 µM pH 3
λmax1= 358 nm; 0.030
λmax2= 453 nm; 0.055

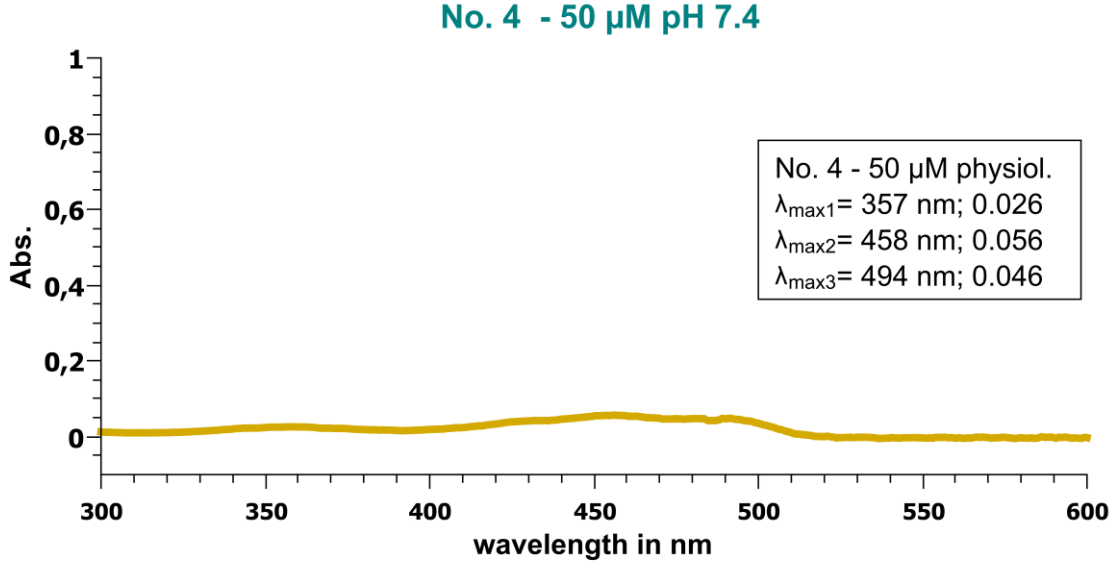
No. 4 - 50 µM pH 7.4
Abs.
wavelength in nm
No. 4 - 50 µM physiol.
λmax1= 357 nm; 0.026
λmax2= 458 nm; 0.056
λmax3= 494 nm; 0.046

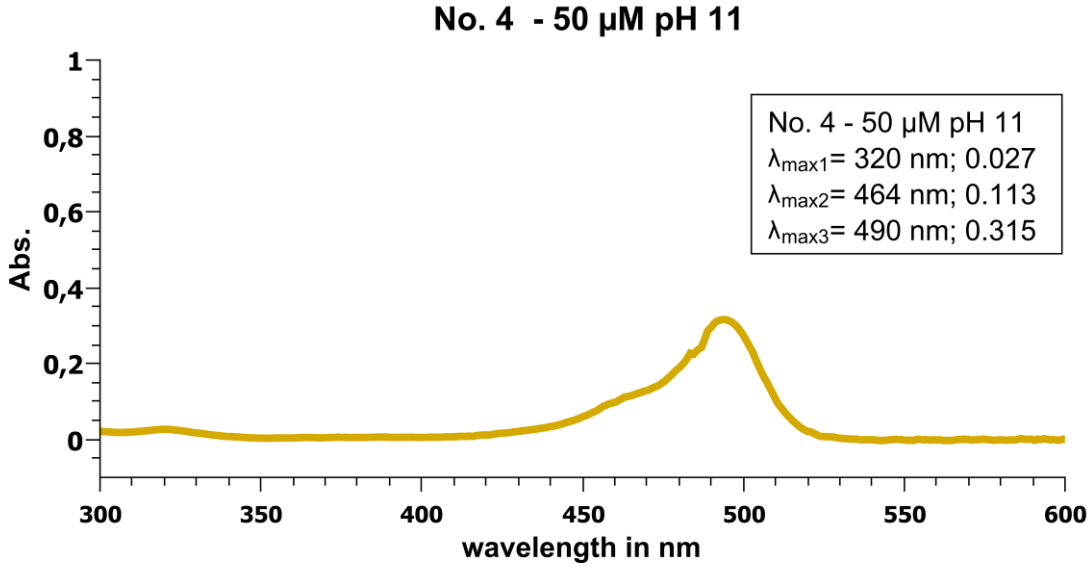
No. 4 - 50 µM pH 11
Abs.
wavelength in nm
No. 4 - 50 µM pH 11
λmax1= 320 nm; 0.027
λmax2= 464 nm; 0.113
λmax3= 490 nm; 0.315

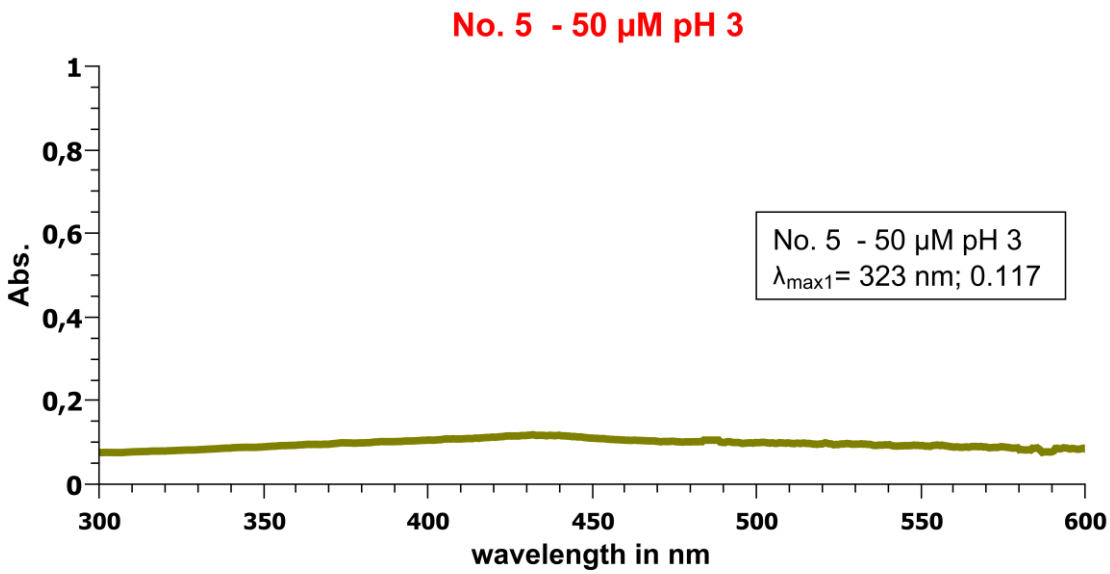
No. 5 - 50 µM pH 3
Abs.
wavelength in nm
No. 5 - 50 µM pH 3
λmax1= 323 nm; 0.117

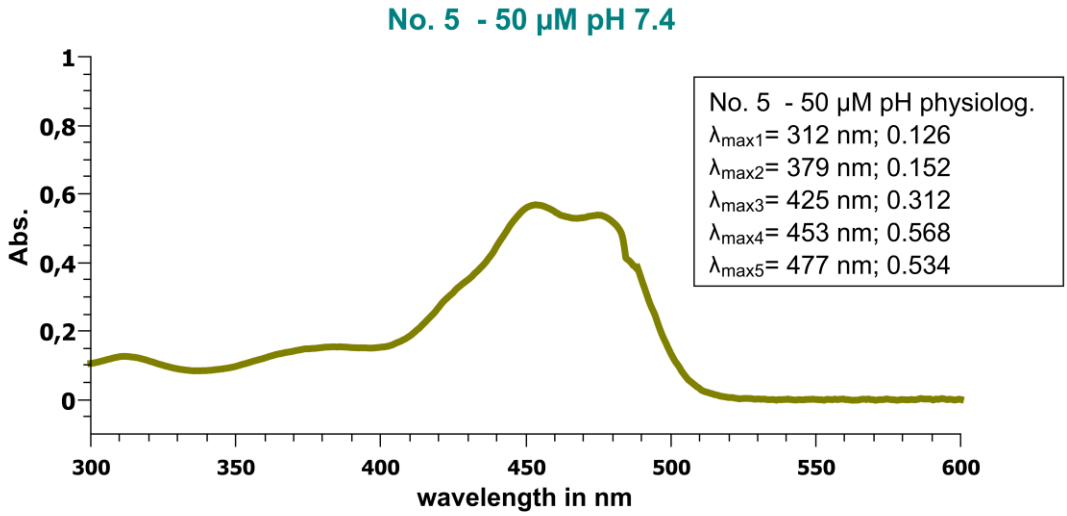
No. 5 - 50 µM pH 7.4
Abs.
wavelength in nm
No. 5 - 50 µM pH physiolog.
λmax1= 312 nm; 0.126
λmax2= 379 nm; 0.152
λmax3= 425 nm; 0.312
λmax4= 453 nm; 0.568
λmax5= 477 nm; 0.534

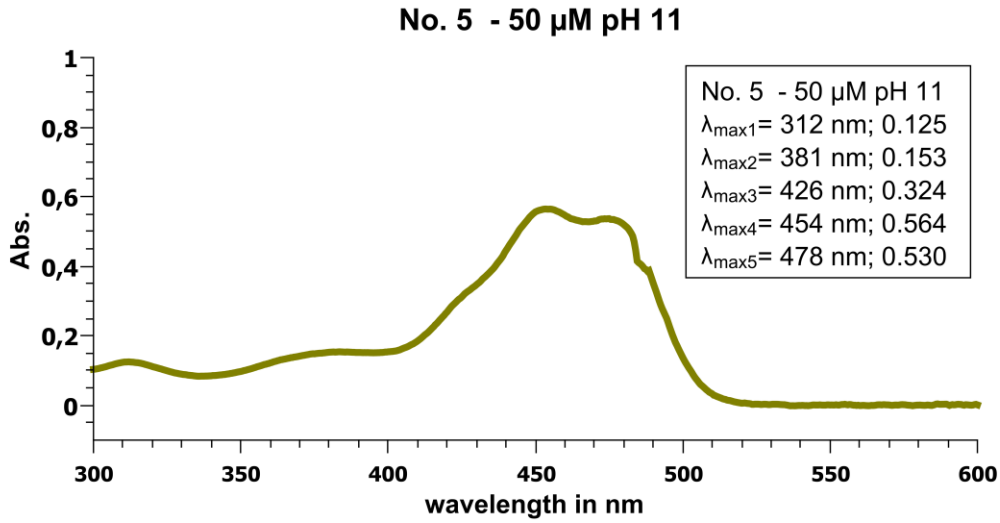
No. 5 - 50 µM pH 11
Abs.
wavelength in nm
No. 5 - 50 µM pH 11
λmax1= 312 nm; 0.125
λmax2= 381 nm; 0.153
λmax3= 426 nm; 0.324
λmax4= 454 nm; 0.564
λmax5= 478 nm; 0.530

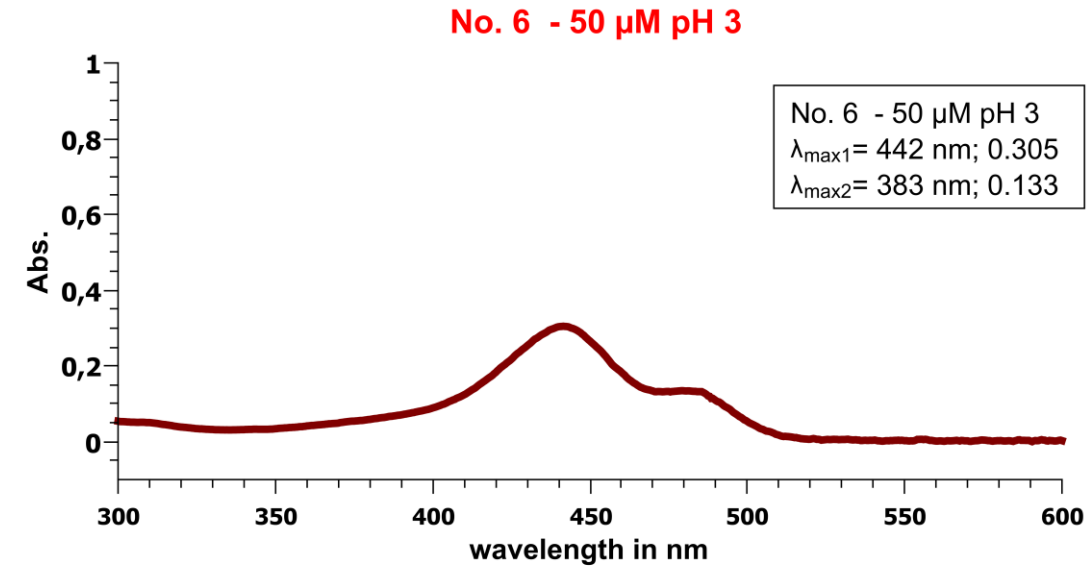
No. 6 - 50 µM pH 3
No. 6 - 50 µM pH 3
λmax1= 442 nm; 0.305
λmax2= 383 nm; 0.133
Abs.
wavelength in nm

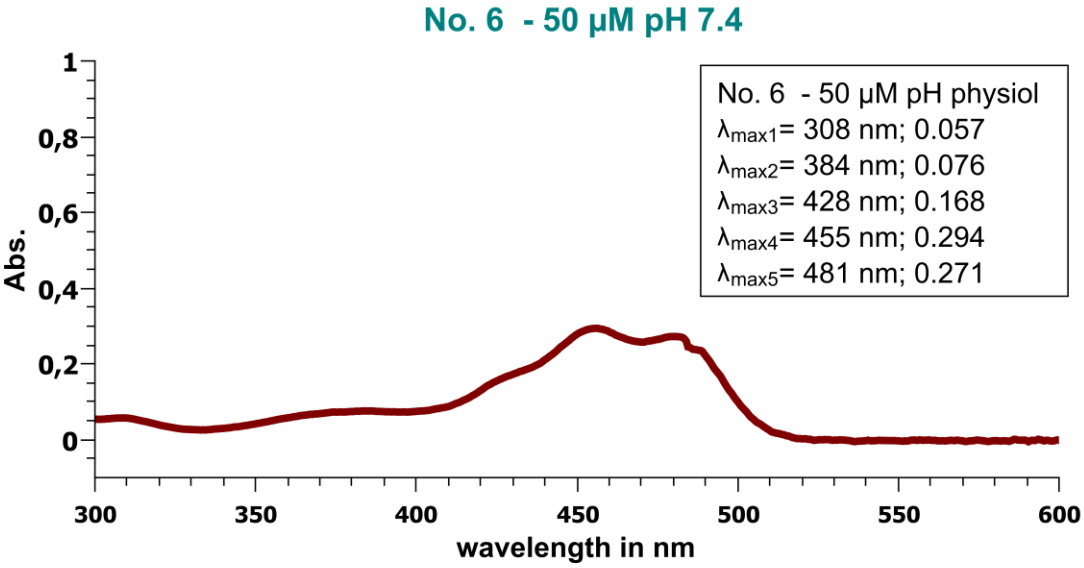
No. 6 - 50 µM pH 7.4
No. 6 - 50 µM pH physiol
λmax1= 308 nm; 0.057
λmax2= 384 nm; 0.076
λmax3= 428 nm; 0.168
λmax4= 455 nm; 0.294
λmax5= 481 nm; 0.271
Abs.
wavelength in nm

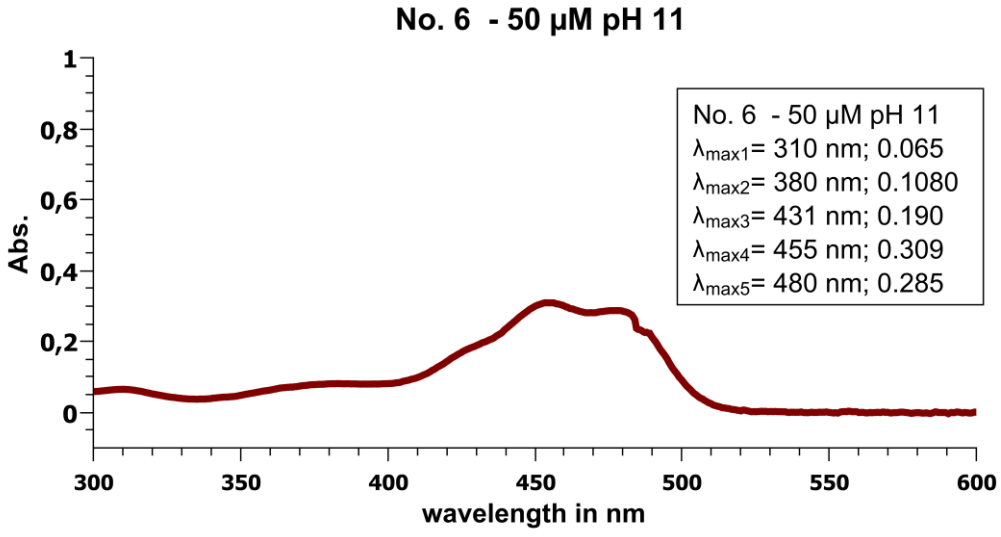
No. 6 - 50 µM pH 11
No. 6 - 50 µM pH 11
λmax1= 310 nm; 0.065
λmax2= 380 nm; 0.1080
λmax3= 431 nm; 0.190
λmax4= 455 nm; 0.309
λmax5= 480 nm; 0.285
Abs.
wavelength in nm

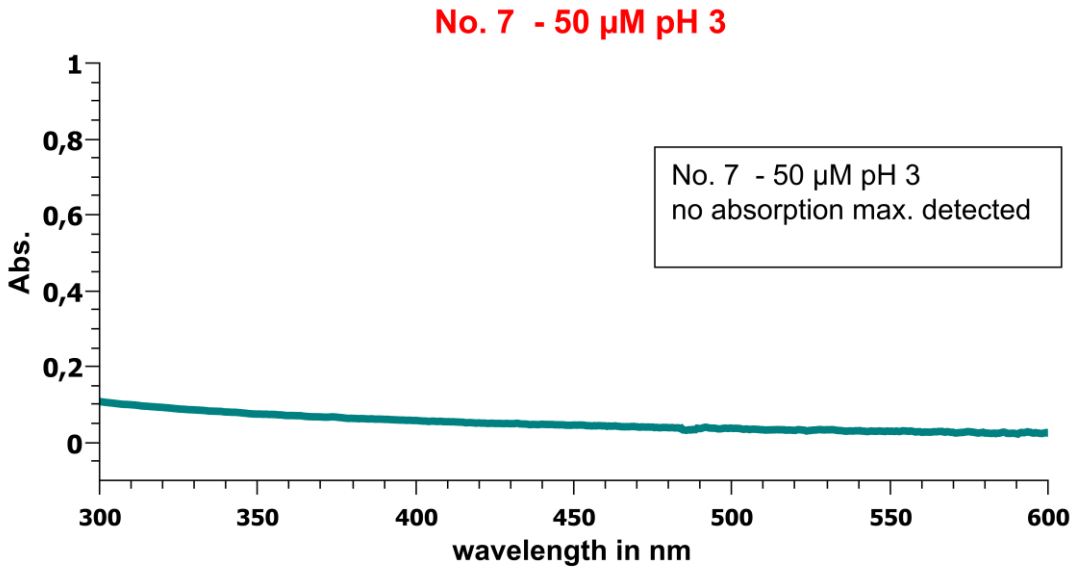
No. 7 - 50 µM pH 3
Abs.
1
0,8
0,6
0,4
0,2
0
300
350
400
450
500
550
600
wavelength in nm
No. 7 - 50 µM pH 3
no absorption max. detected

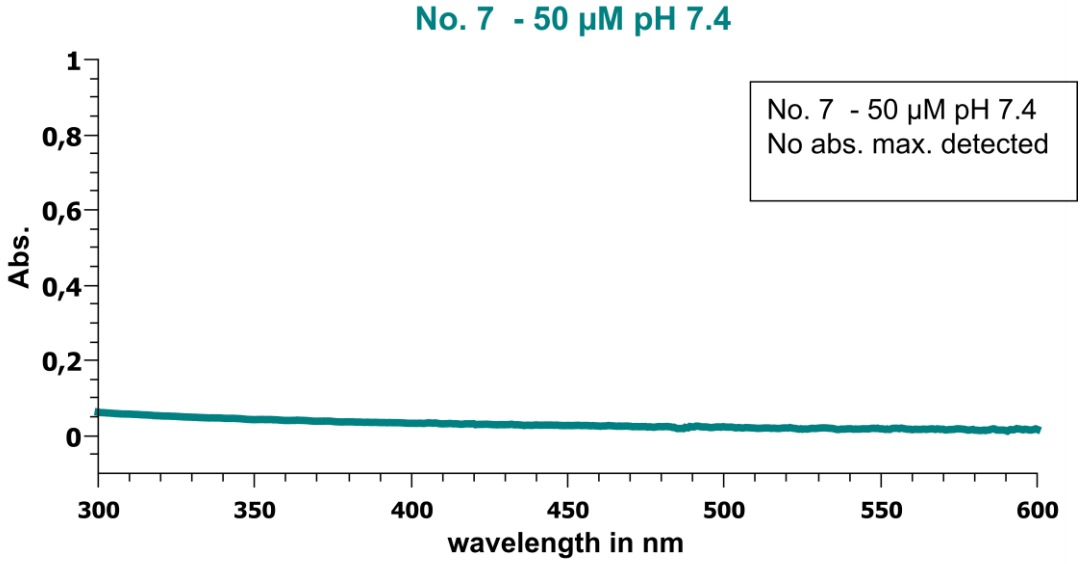
No. 7 - 50 µM pH 7.4
Abs.
1
0,8
0,6
0,4
0,2
0
300
350
400
450
500
550
600
wavelength in nm
No. 7 - 50 µM pH 7.4
No abs. max. detected

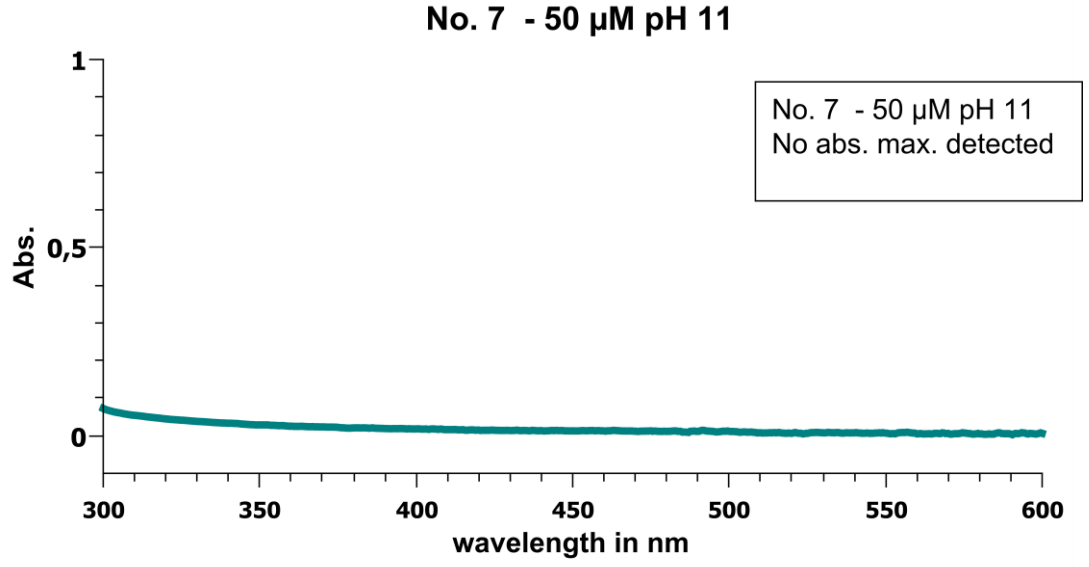
No. 7 - 50 µM pH 11
Abs.
1
0,5
0
300
350
400
450
500
550
600
wavelength in nm
No. 7 - 50 µM pH 11
No abs. max. detected

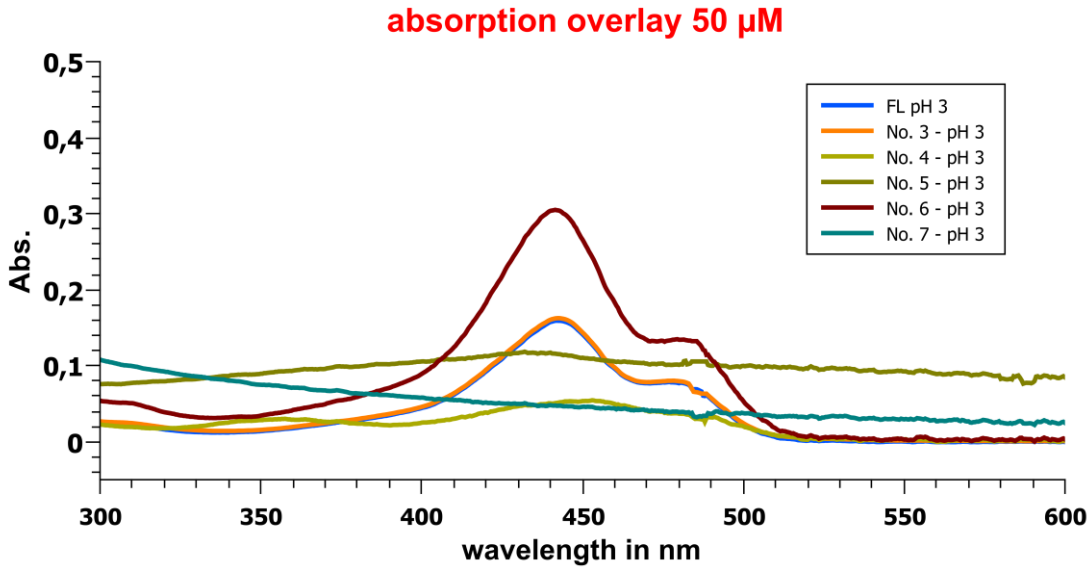
absorption overlay 50 µM
Abs.
wavelength in nm
FL pH 3
No. 3 - pH 3
No. 4 - pH 3
No. 5 - pH 3
No. 6 - pH 3
No. 7 - pH 3

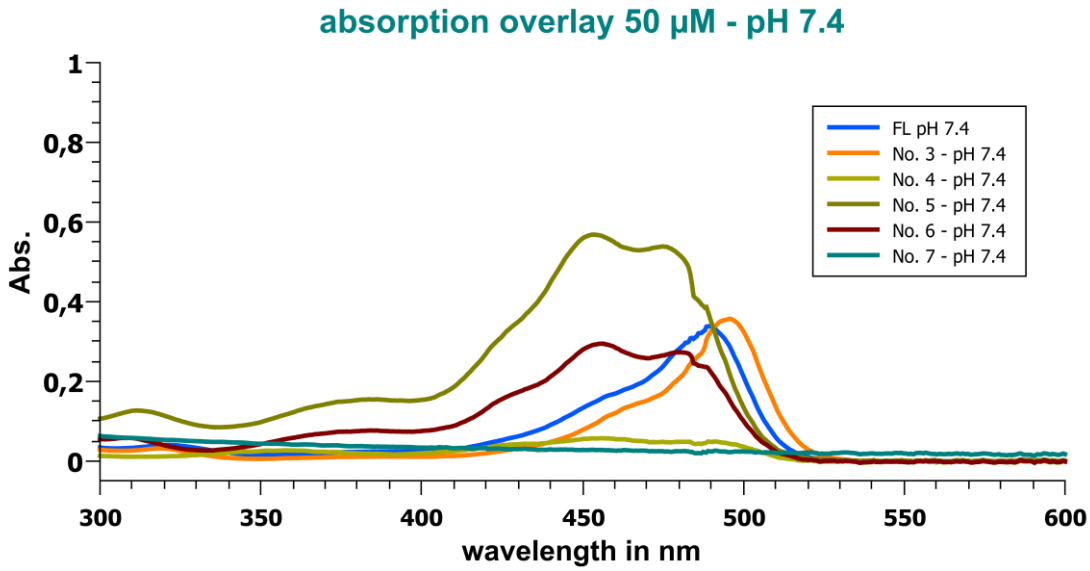
absorption overlay 50 µM - pH 7.4
Abs.
wavelength in nm
FL pH 7.4
No. 3 - pH 7.4
No. 4 - pH 7.4
No. 5 - pH 7.4
No. 6 - pH 7.4
No. 7 - pH 7.4

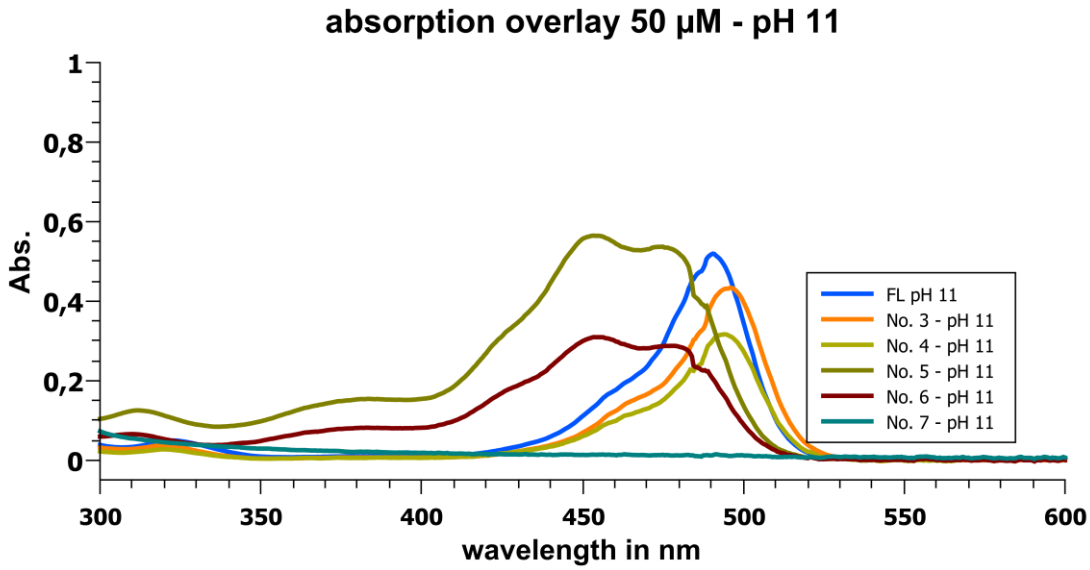
absorption overlay 50 µM - pH 11
Abs.
wavelength in nm
FL pH 11
No. 3 - pH 11
No. 4 - pH 11
No. 5 - pH 11
No. 6 - pH 11
No. 7 - pH 11

Table. S1 Absorption maxima (nm) in pH 3 medium

Comp. No.	$\lambda_{max\ 1}$ (Abs)	$\lambda_{max\ 2}$ (Abs)
FL	443 (0,16)	478 (0,08)
No. 3	443 (0,16)	480 (0,08)
No. 4	358 (0,03)	453 (0,06)
No. 5	323 (0,12)	-
No. 6	442 (0,31)	483 (0,13)
No. 7	nd	-

Table. S2 Absorption maxima (nm) in pH 7.4 buffered medium

Comp. No.	$\lambda_{max\ 1}$ (Abs)	$\lambda_{max\ 2}$ (Abs)	$\lambda_{max\ 3}$ (Abs)	$\lambda_{max\ 4}$ (Abs)	$\lambda_{max\ 5}$ (Abs)
FL	321 (0,04)	458 (0,16)	489 (0,34)	-	-
No. 3	323 (0,05)	457 (0,16)	490 (0,52)	-	-
No. 4	357 (0,03)	458 (0,06)	494 (0,05)	-	-
No. 5	312 (0,13)	379 (0,15)	425 (0,31)	453 (0,57)	477 (0,53)
No. 6	308 (0,06)	384 (0,08)	428 (0,17)	455 (0,29)	481 (0,27)
No. 7	nd	-	-	-	-

Table. S3 Absorption maxima (nm) in pH 11 medium

Comp. No.	$\lambda_{max\ 1}$ (Abs)	$\lambda_{max\ 2}$ (Abs)	$\lambda_{max\ 3}$ (Abs)	$\lambda_{max\ 4}$ (Abs)	$\lambda_{max\ 5}$ (Abs)
FL	323 (0,05)	457 (0,16)	490 (0,52)	-	-
No. 3	321 (0,04)	464 (0,15)	496 (0,43)	-	-
No. 4	320 (0,03)	464 (0,11)	490 (0,32)	-	-
No. 5	312 (0,13)	381 (0,15)	426 (0,32)	454 (0,56)	478 (0,53)
No. 6	310 (0,07)	380 (0,11)	431 (0,19)	455 (0,31)	480 (0,29)
No. 7	nd	-	-	-	-

Table. S4 Calculation of Extinction Coefficients (M^{-1} $cm^{-1)}$ using Lambert-Beer-Law ($E = \varepsilon * c * l$) at corresponding absorption maximum

Comp. No.	E_λ in pH 3 medium	E_λ in pH 7.4 medium	E_λ in pH 11 medium
FL	32000_{443}	68000_{489}	104000_{490}
No. 3	32000_{443}	104000_{490}	86000_{496}
No. 4	12000_{453}	10000_{494}	64000_{490}
No. 5	24000_{323}	114000_{453}	112000_{454}
No. 6	62000_{442}	58000_{455}	62000_{455}
No. 7	No abs.	No abs.	No. Abs

5.3.2 Fluorescence measurements

Fluorescent measurements were performed on Jasco FP-6500 fluorimeter equipped with a Peltier element (Jasco Groß-Umstadt, Germany) for temperature controlling purposes.
50 µM fluorescent probes in pH 3, 7.4 and 11 (see absorption spectra page 80 - 89) were analyzed in Suprasil quartz glass cuvettes with 0.1 cm path length. Excitation and emission scans were performed at 25 °C with the following parameters: 3 nm bandwidth of excitation and emission, data pitch of 1 nm, response time of 0.5 s and scanning speed of 1000 nm per min. The fluorescence outcome is illustrated from page 91 - 98.

The normalized excitation and emission spectra of the xanthene dyes are illustrated in figure 44.

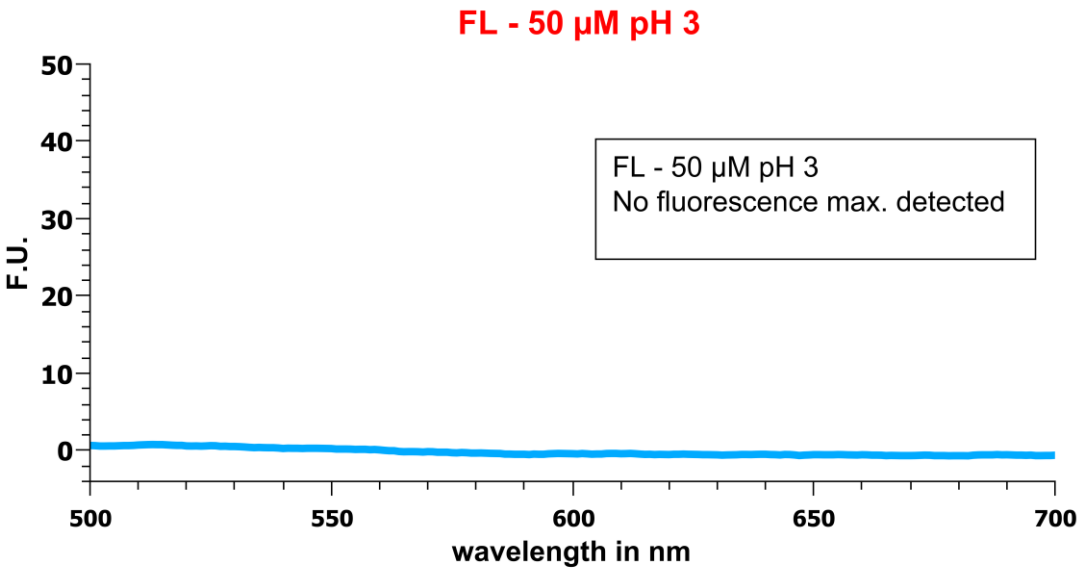
FL - 50 µM pH 3
FL - 50 µM pH 3
No fluorescence max. detected
F.U.
50
40
30
20
10
0
500
550
600
650
700
wavelength in nm

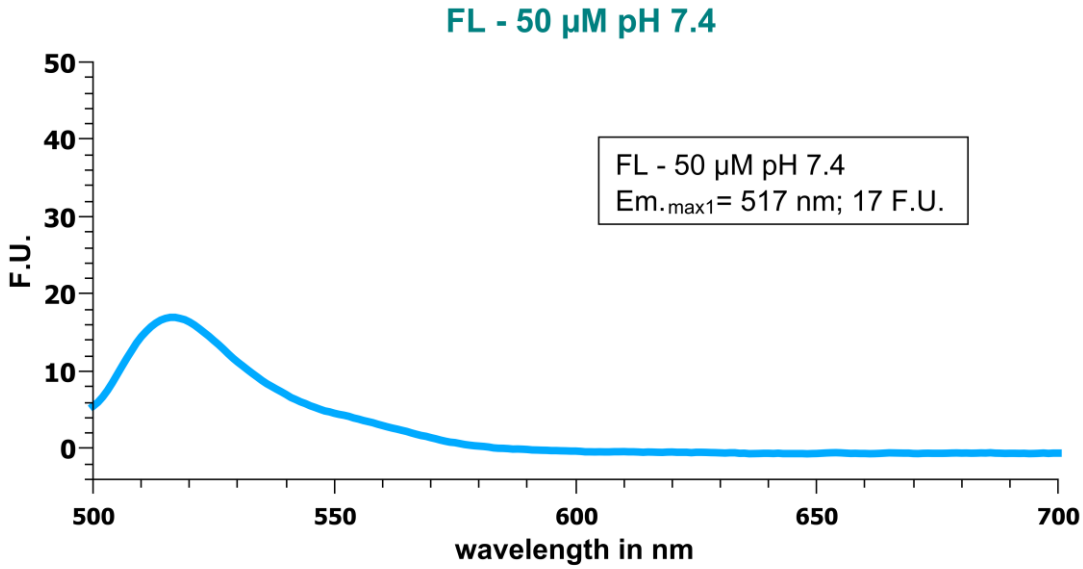
FL - 50 µM pH 7.4
FL - 50 µM pH 7.4
Em.max1= 517 nm; 17 F.U.
F.U.
50
40
30
20
10
0
500
550
600
650
700
wavelength in nm

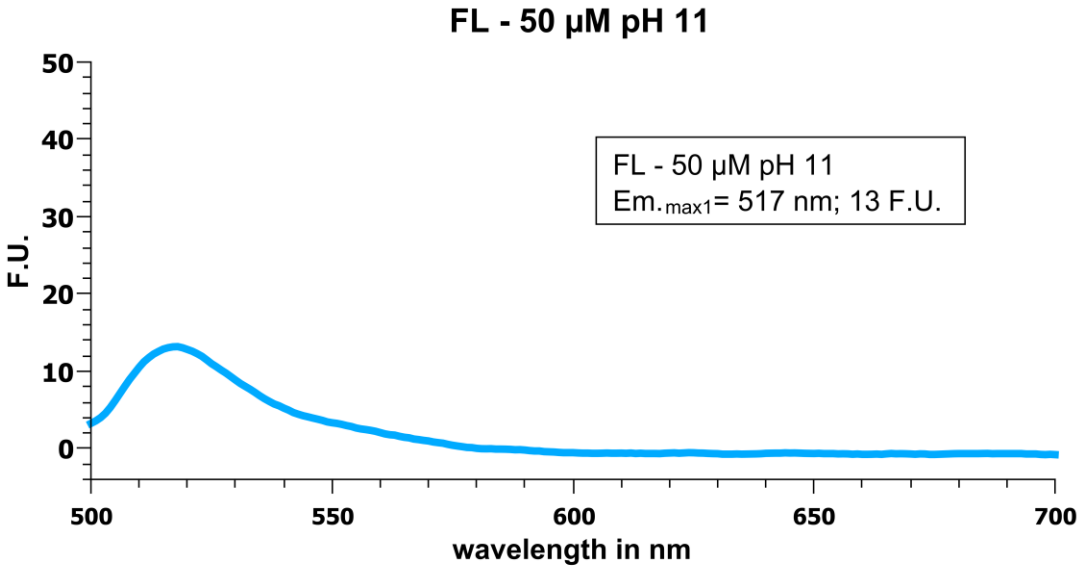
FL - 50 µM pH 11
FL - 50 µM pH 11
Em.max1= 517 nm; 13 F.U.
F.U.
50
40
30
20
10
0
500
550
600
650
700
wavelength in nm

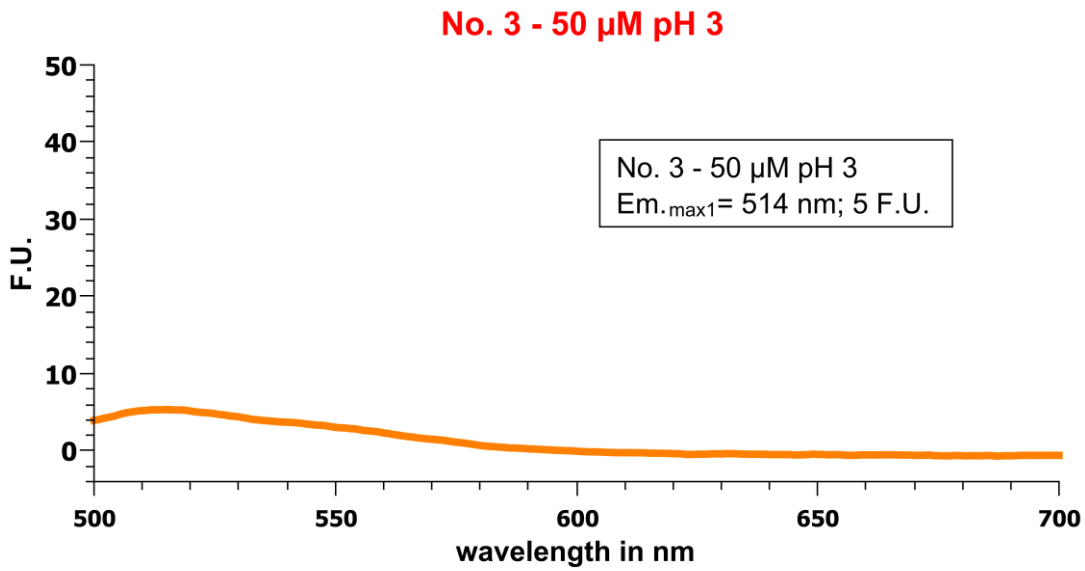
No. 3 - 50 µM pH 3
No. 3 - 50 µM pH 3
Em.max1= 514 nm; 5 F.U.
F.U.
wavelength in nm

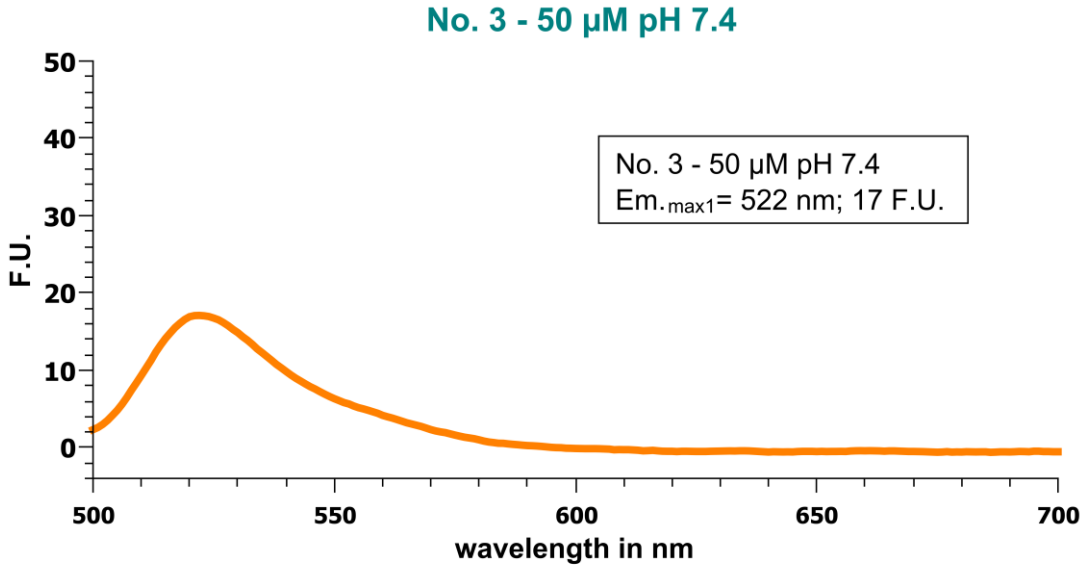
No. 3 - 50 µM pH 7.4
No. 3 - 50 µM pH 7.4
Em.max1= 522 nm; 17 F.U.
F.U.
wavelength in nm

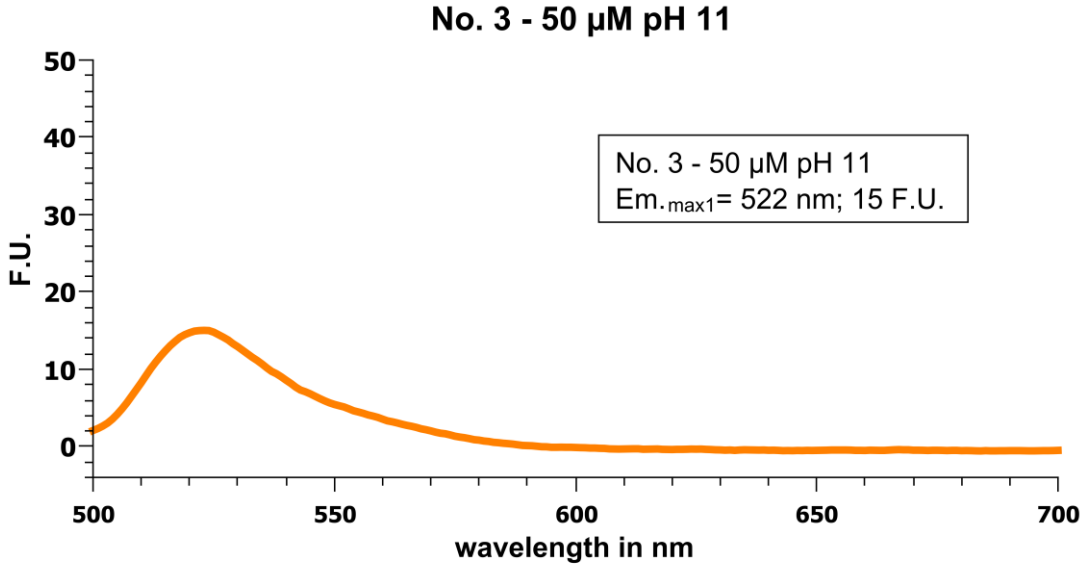
No. 3 - 50 µM pH 11
No. 3 - 50 µM pH 11
Em.max1= 522 nm; 15 F.U.
F.U.
wavelength in nm

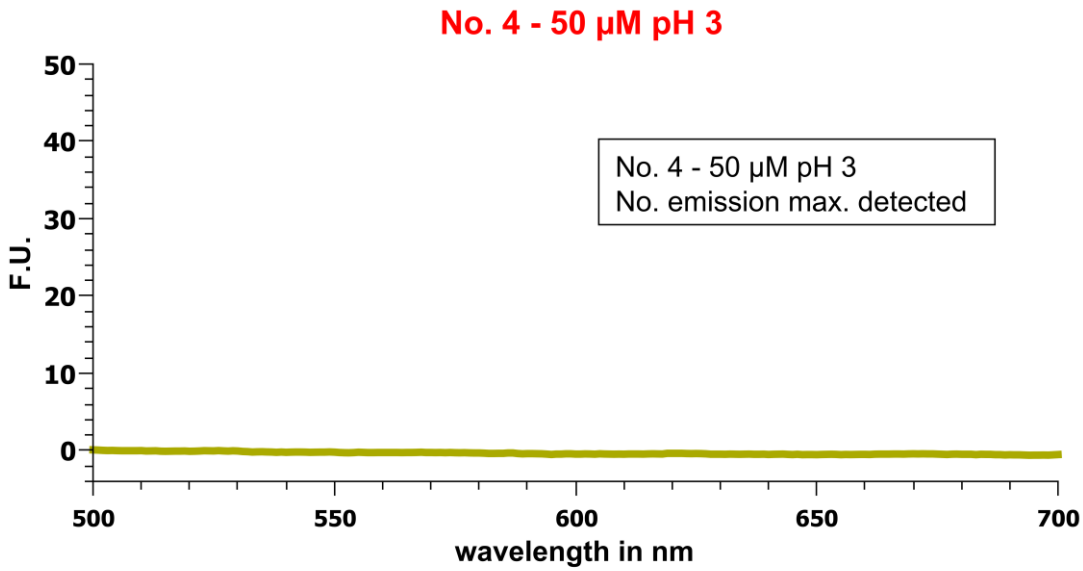
No. 4 - 50 µM pH 3
No. 4 - 50 µM pH 3
No. emission max. detected
F.U.
50
40
30
20
10
0
500
550
600
650
700
wavelength in nm

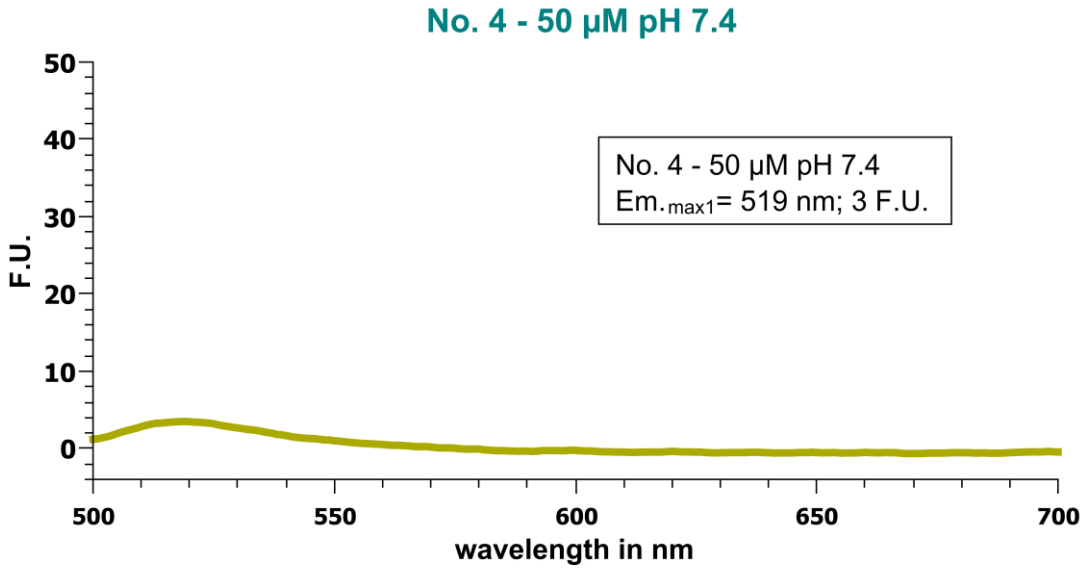
No. 4 - 50 µM pH 7.4
No. 4 - 50 µM pH 7.4
Em.max1= 519 nm; 3 F.U.
F.U.
50
40
30
20
10
0
500
550
600
650
700
wavelength in nm

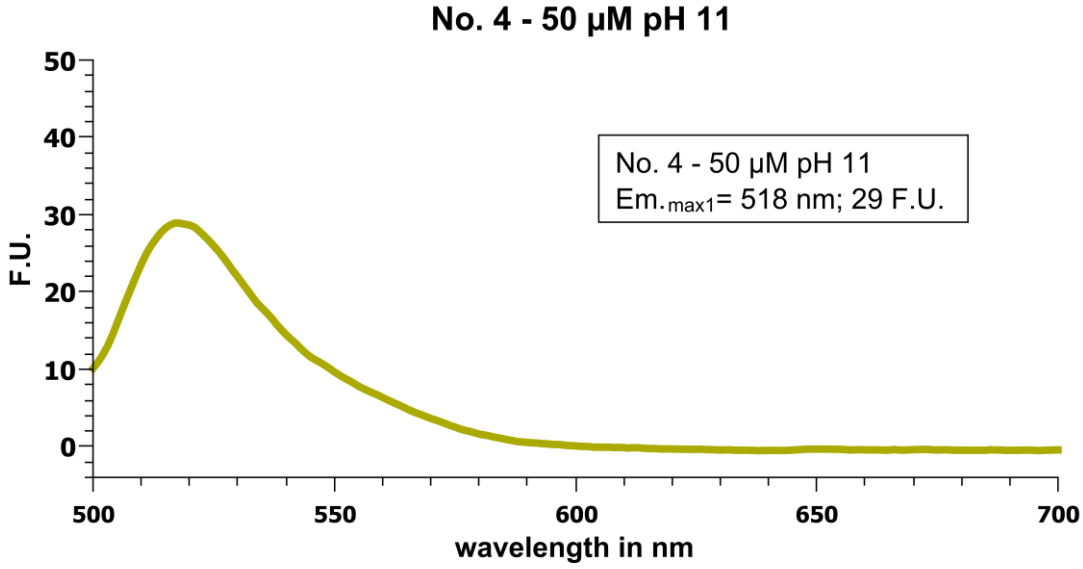
No. 4 - 50 µM pH 11
No. 4 - 50 µM pH 11
Em.max1= 518 nm; 29 F.U.
F.U.
50
40
30
20
10
0
500
550
600
650
700
wavelength in nm

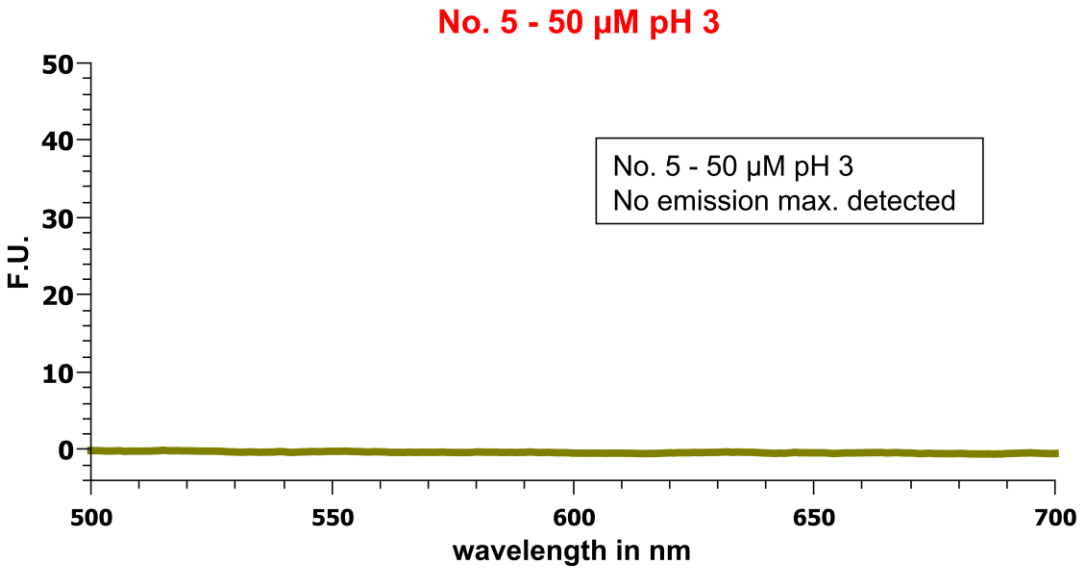
No. 5 - 50 µM pH 3
No. 5 - 50 µM pH 3
No emission max. detected
F.U.
50
40
30
20
10
0
500
550
600
650
700
wavelength in nm

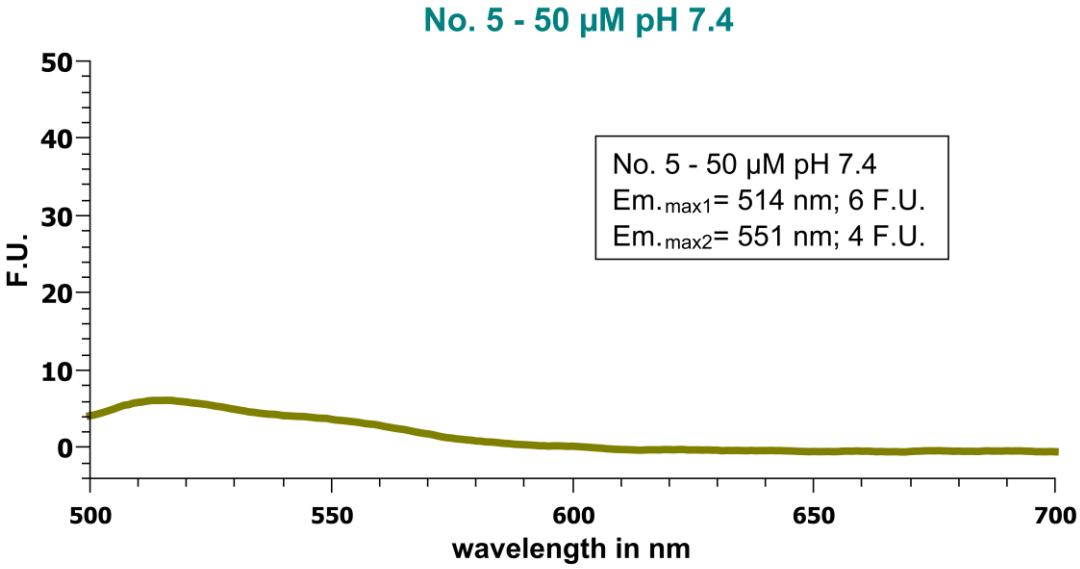
No. 5 - 50 µM pH 7.4
No. 5 - 50 µM pH 7.4
Em.max1= 514 nm; 6 F.U.
Em.max2= 551 nm; 4 F.U.
F.U.
50
40
30
20
10
0
500
550
600
650
700
wavelength in nm

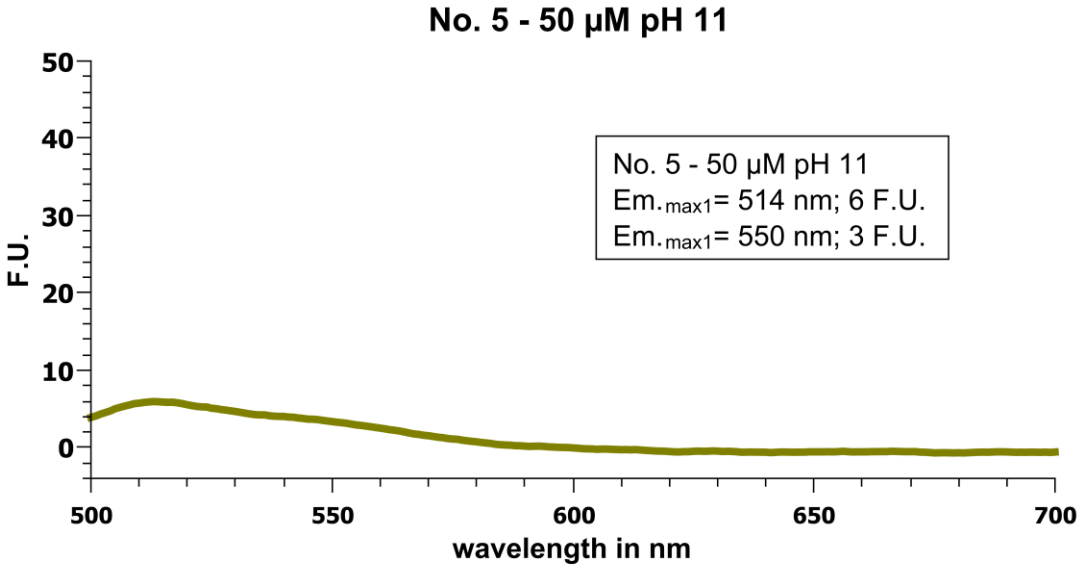
No. 5 - 50 µM pH 11
No. 5 - 50 µM pH 11
Em.max1= 514 nm; 6 F.U.
Em.max1= 550 nm; 3 F.U.
F.U.
50
40
30
20
10
0
500
550
600
650
700
wavelength in nm

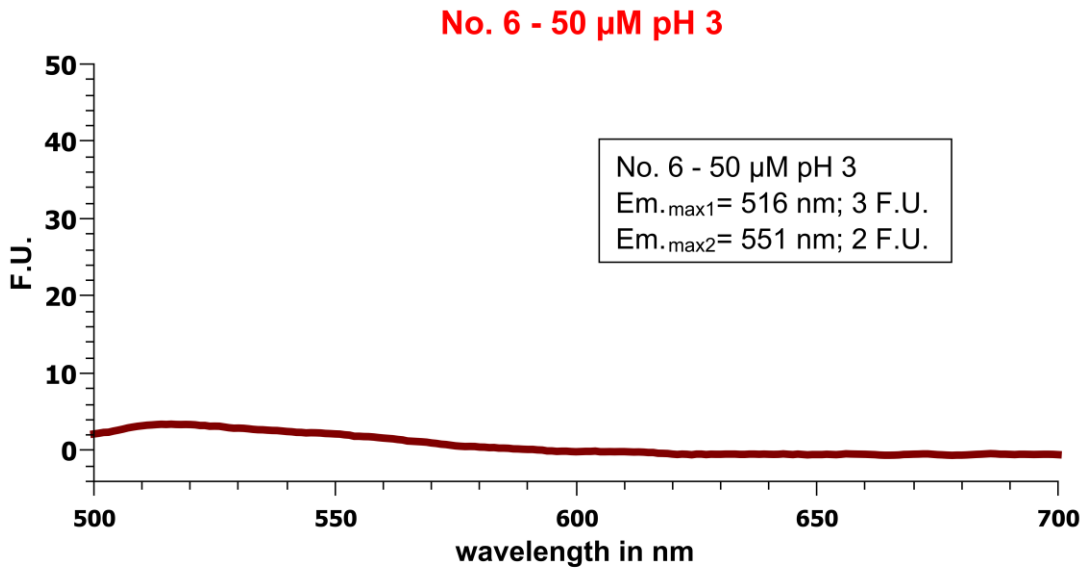
No. 6 - 50 µM pH 3
No. 6 - 50 µM pH 3
Em.max1= 516 nm; 3 F.U.
Em.max2= 551 nm; 2 F.U.
F.U.
wavelength in nm

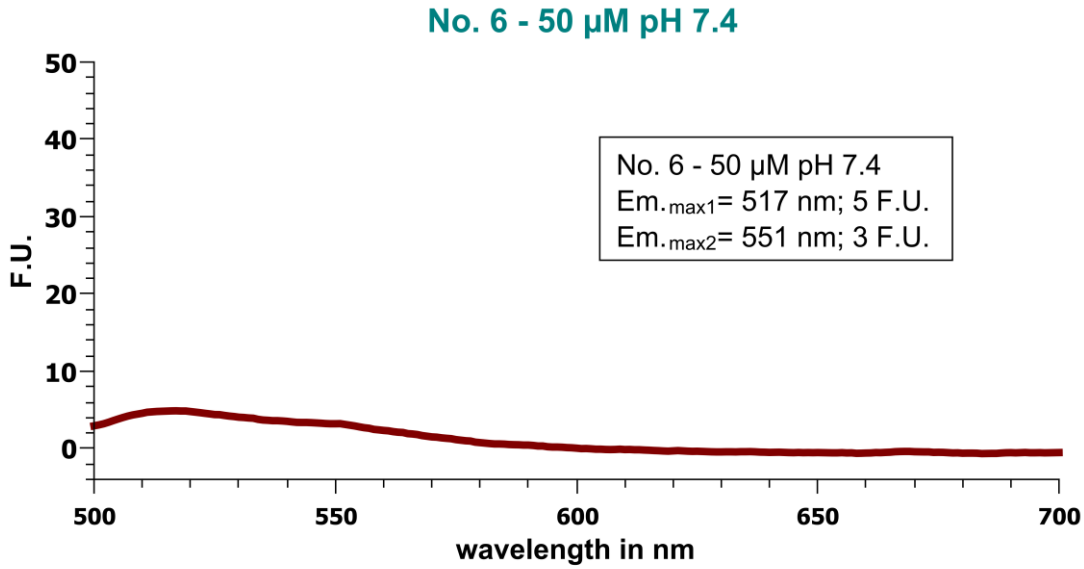
No. 6 - 50 µM pH 7.4
No. 6 - 50 µM pH 7.4
Em.max1= 517 nm; 5 F.U.
Em.max2= 551 nm; 3 F.U.
F.U.
wavelength in nm

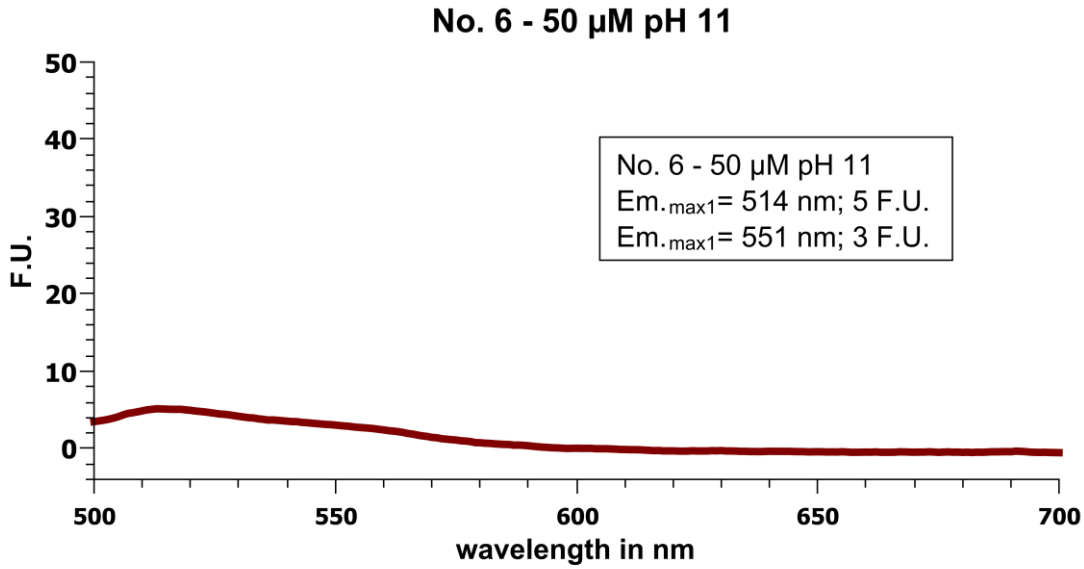
No. 6 - 50 µM pH 11
No. 6 - 50 µM pH 11
Em.max1= 514 nm; 5 F.U.
Em.max1= 551 nm; 3 F.U.
F.U.
wavelength in nm

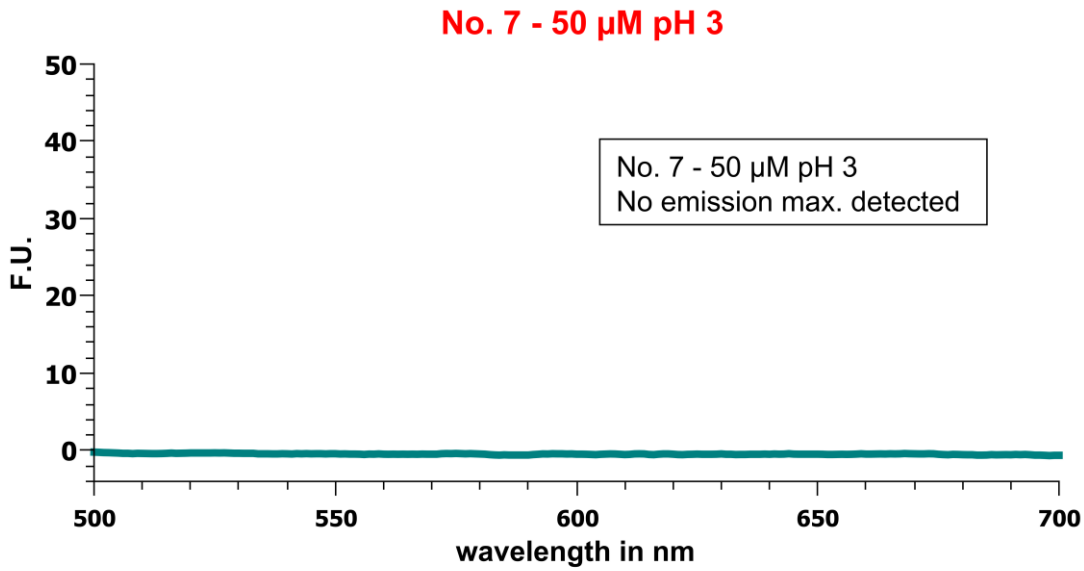
No. 7 - 50 µM pH 3
No. 7 - 50 µM pH 3
No emission max. detected
F.U.
50
40
30
20
10
0
500
550
600
650
700
wavelength in nm

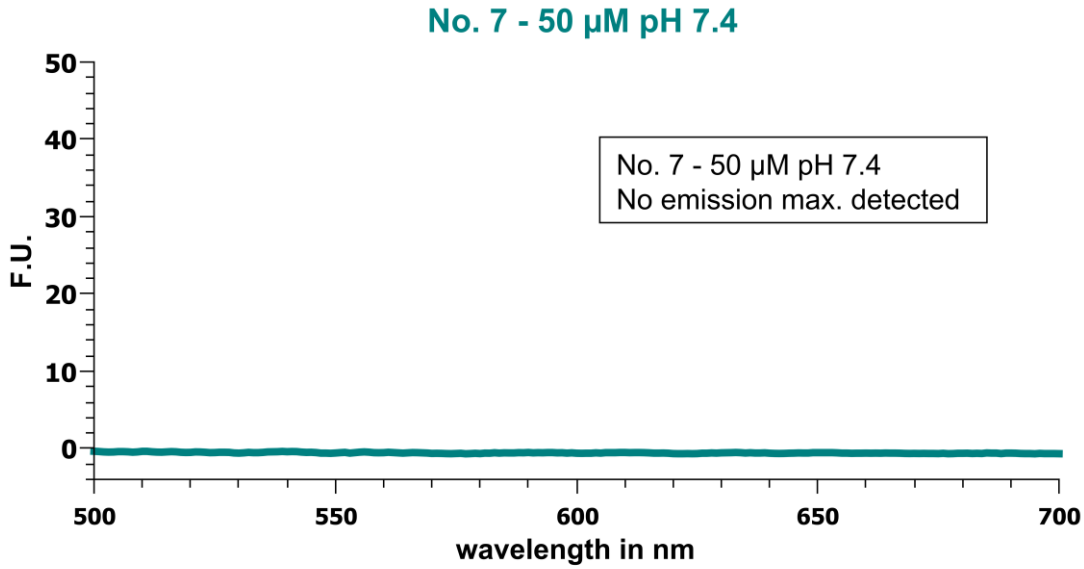
No. 7 - 50 µM pH 7.4
No. 7 - 50 µM pH 7.4
No emission max. detected
F.U.
50
40
30
20
10
0
500
550
600
650
700
wavelength in nm

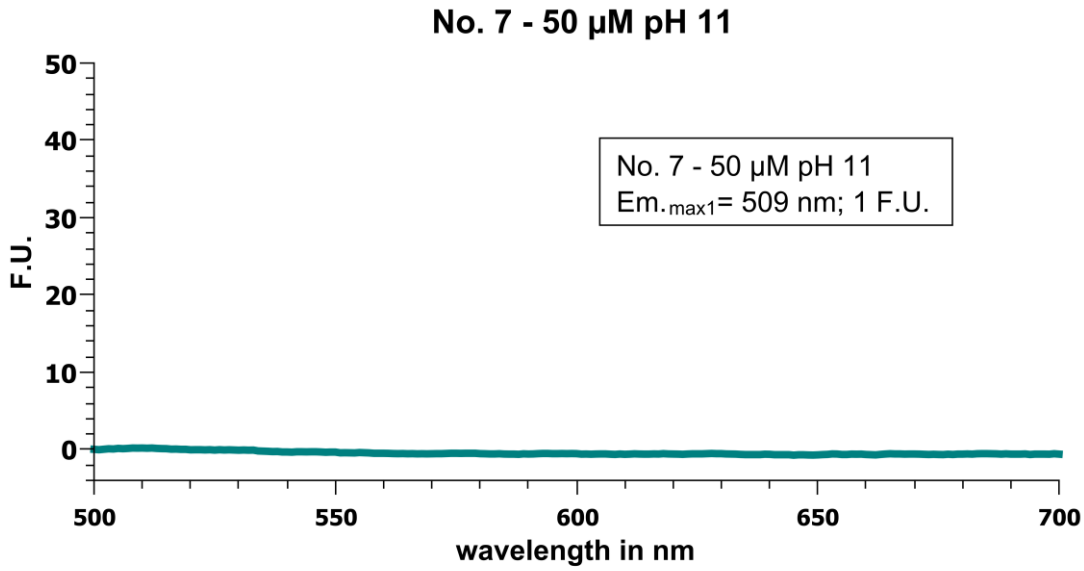
No. 7 - 50 µM pH 11
No. 7 - 50 µM pH 11
Em.max1= 509 nm; 1 F.U.
F.U.
50
40
30
20
10
0
500
550
600
650
700
wavelength in nm

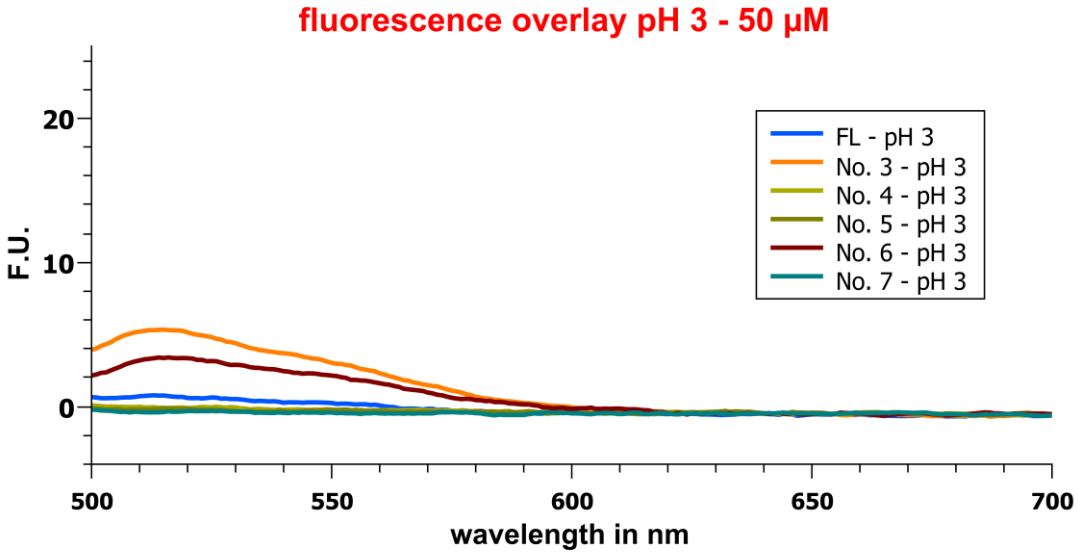
fluorescence overlay pH 3 - 50 µM
F.U.
20
10
0
500
550
600
650
700
wavelength in nm
FL - pH 3
No. 3 - pH 3
No. 4 - pH 3
No. 5 - pH 3
No. 6 - pH 3
No. 7 - pH 3

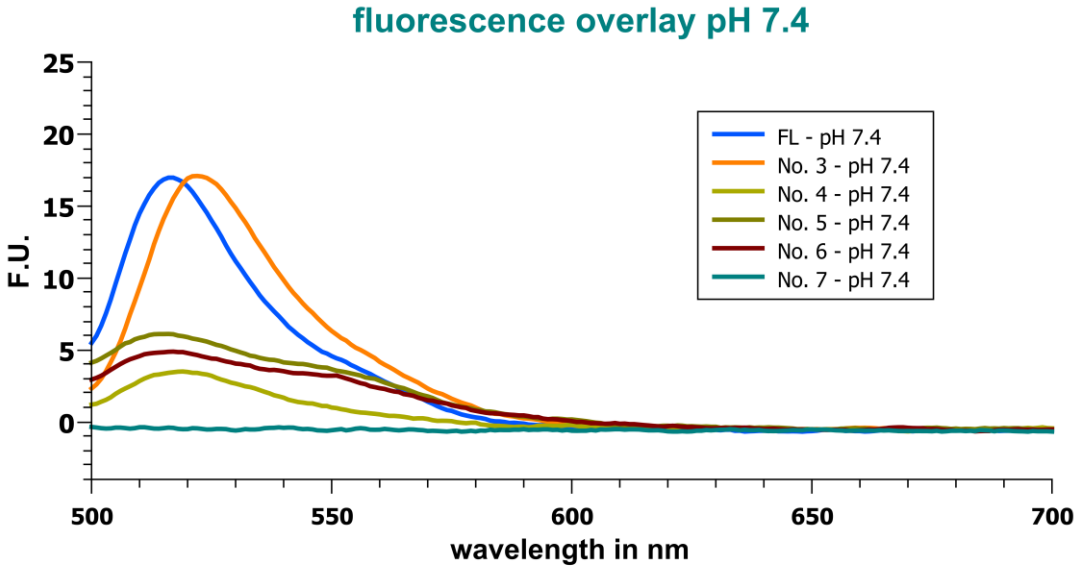
fluorescence overlay pH 7.4
F.U.
25
20
15
10
5
0
500
550
600
650
700
wavelength in nm
FL - pH 7.4
No. 3 - pH 7.4
No. 4 - pH 7.4
No. 5 - pH 7.4
No. 6 - pH 7.4
No. 7 - pH 7.4

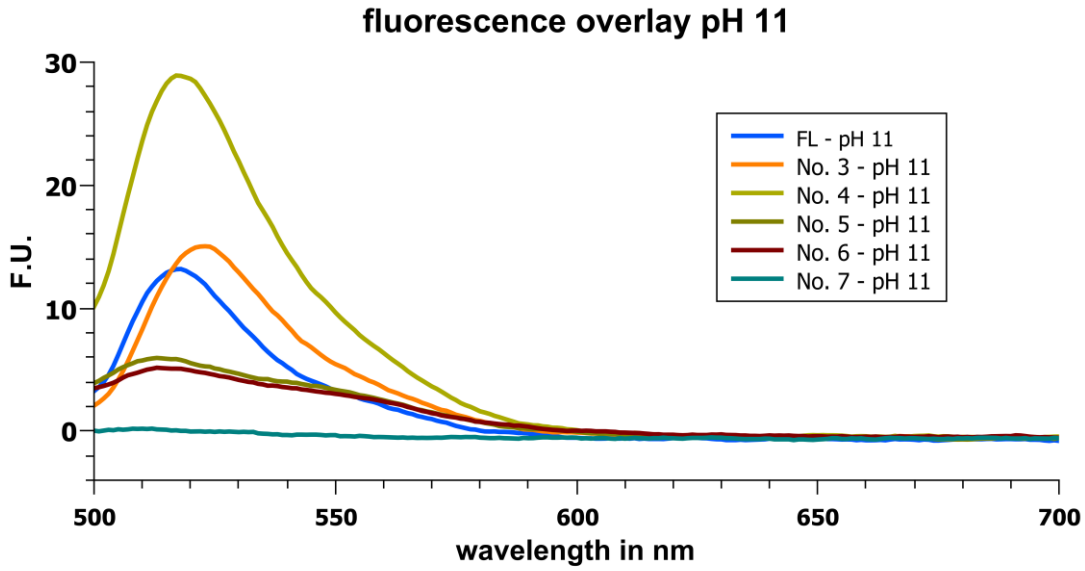
fluorescence overlay pH 11
F.U.
30
20
10
0
500
550
600
650
700
wavelength in nm
FL - pH 11
No. 3 - pH 11
No. 4 - pH 11
No. 5 - pH 11
No. 6 - pH 11
No. 7 - pH 11

Table S5. Emission maxima (nm) after 488 nm excitation in pH 3 medium

Comp. No.	$E_{max\ 1}$ (F.U.)	$E_{max\ 2}$ (F.U.)
FL	nd	-
No. 3	517 (5)	-
No. 4	nd	-
No. 5	nd	-
No. 6	516 (3)	551 (2)
No. 7	nd	-

Table S6. Emission maxima (nm) after 488 nm excitation in pH 7.4 medium

Comp. No.	$E_{max\ 1}$ (F.U.)	$E_{max\ 2}$ (F.U.)
FL	517 (17)	-
No. 3	522 (17)	-
No. 4	519 (3)	-
No. 5	514 (6)	551 (4)
No. 6	517 (5)	551 (3)
No. 7	nd	-

Table S7. Emission maxima (nm) after 488 nm excitation in pH 11 medium

Comp. No.	$E_{max\ 1}$ (F.U.)	$E_{max\ 2}$ (F.U.)
FL	517 (13)	-
No. 3	522 (15)	-
No. 4	518 (29)	-
No. 5	514 (6)	550 (3)
No. 6	514 (5)	551 (3)
No. 7	509 (1)	-

5.3.3 Determination of quantum yields

The quantum yields were determined by using the pH 7.4 PBS buffered 50 µM samples. Emission scans were performed at 25 °C with the following parameters: 3 nm bandwidth of excitation and emission, data pitch of 1 nm, response of 0.5 s, scanning speed of 1000 nm min. Samples were excited at 488 nm and the emission was recorded from at least 500 nm to 700 nm (emission profile). These quantum yields were obtained by comparison of the integrated area of the emission spectra ($\int F_{em,\ sample}$) of the samples with the integrated area of emission spectra of standard sample ($\int F_{em,\ standard}$), fluorescein in PBS buffered solution, which has a quantum efficiency of 0.88.[38,85] The integration using the free math software (QtiPlot) in the section between 500 - 600 nm area delivered the integral values. The quantum yield of a sample was related to that of the standard fluorescein in PBS (pH 7.4), and determined by the equation[115] :

$$\Phi_{sample} = (A_{standard}/A_{sample})\ (\int F_{em,\ sample}/\int F_{em,\ standard})\ (\eta_{sample}/\eta_{standard})^2\ \Phi_{standard}$$

Φ is the fluorescent quantum yield, A is the absorbance at the excitation wavelength, $\int F$ is the area under the emission curve, η is the refractive index of the solvent.

The concentrations and sample conditions were equal in all tested dyes; consequently the refractive index corresponded to 1. By abbreviating the refractive index following equation was used for quantum yield calculation[116] :

$$\Phi_{standard}\ (\int F_{em,\ sample}/\int F_{em,\ standard})\ (A_{standard}/A_{sample})$$

Comp. No.	Φ in pH 7.4 medium
FL	0,88[85,38]
No. 3	0,60
No. 4	No ems.
No. 5	0,51
No. 6	0,77
No. 7	No abs.

Table S8. Quantum yields

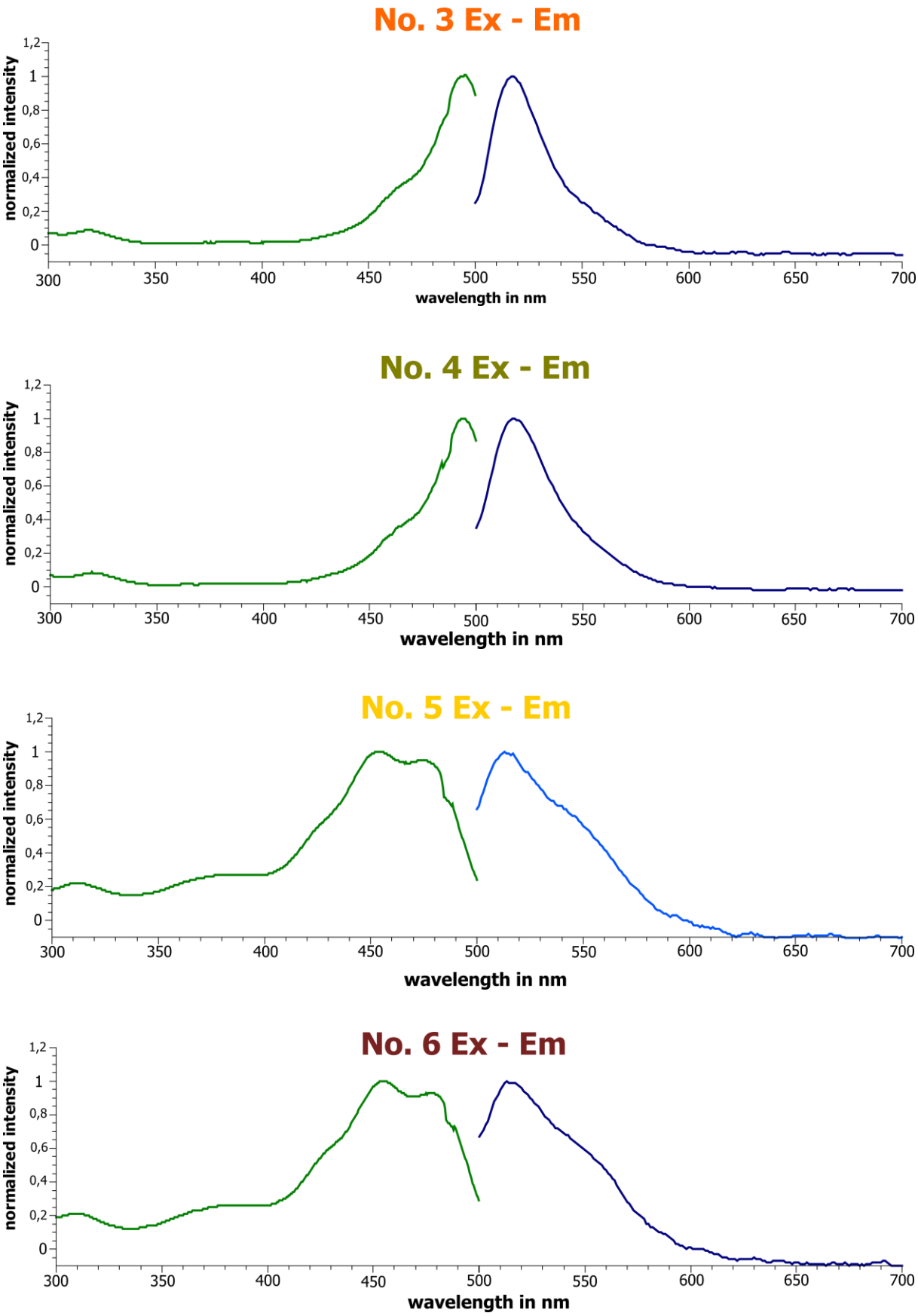

Figure 49. Normalized excitation emission spectra of compound **3 - 6**

Table S9. Spectral data overview for selected asymmetric dyes

Comp. no	λ_{max} [a]	ε at λ_{max} ($M^{-1}cm^{-1}$) [a]	λ_{ex} [b]	λ_{em} [b]	Φ[a]
FL	321, 458, 489	68000_{489}	490	517	0.88[38,85]
No. 3	323, 457, 490	104000_{490}	497	522	0.62
No. 4	357, 458, 494	10000_{494}	478	518	1.02
No. 5	312, 379, 425, 453, 477	114000_{453}	479	514	0.28
No. 6	442, 483	58000_{455}	480	514	0.45
No. 7	nd	-	-	-	-

[a] in pH 7.4 PBS buffered medium, [b] in pH 11 medium

5.4 Click chemistry of applied dyes

The asymmetric azido-functionalized xanthene prodyes (**1** and **2**) were conjugated to deoxy- or ribooligonucleotides. The dyes were "clicked" *via* Cu(I)-catalyzed azide-alkyne cycloaddition (CuAAC)[117] with different commercially available oligonucleotides, bearing a terminal alkyne in alternating positions (Table S13).The Click reaction with each dye took place under light protection in a benchtop thermomixer (500 rpm) for 2 h at 25 °C. The reactions were performed in a mixture of 1:2 water and phosphate saline buffer (pH 6). The Cu(I)-catalyst was generated from $CuSO_4$ pentahydrate, using sodium ascorbate as a reducing agent. THPTA (tris(hydroxypropyl)triazolylmethyl-amine) was applied as stabilizing ligand of the Cu(I)-species. Three different protocols were applied for the Click chemistry (Table S10 – S12).

Table S10. Analytical scale protocol for prodye labeling of oligonucleotides *via* "Click" chemistry

Compound	**c_{stock} (mM)**	**c (mM)**	**V (µL)**
Buffer NaH_2PO_4 (pH 6)	500	100	4
THPTA	50	2.5	1
Na Ascorbate	50	5	2
$CuSO_4 . 5H_2O$	5	0.5	2
Prodye	1	0.05	1
DNA/RNA	0.1	0.01	2
H_2O (MilliQ)	-	-	8
			20

Table S11. Semi-preparative scale protocol for prodye labeling of oligonucleotides *via* "Click" chemistry

Compound	c_{stock} (mM)	c (mM)	V (µL)
Buffer NaH_2PO_4 (pH 6)	500	100	20
THPTA	50	2.5	5
Na Ascorbate	50	5	10
$CuSO_4 . 5H_2O$	5	0.5	10
Prodye	1	0.05	5
DNA/RNA	0.1	0.01	10
H_2O (MilliQ)	-	-	40
			100

Table S12. Preparative scale protocol for prodye labeling of oligonucleotides *via* "Click" chemistry

Compound	c_{stock} (mM)	c (mM)	V (µL)
Buffer NaH_2PO_4 (pH 6)	500	100	200
THPTA	50	2.5	50
Na Ascorbate	50	5	100
$CuSO_4 . 5H_2O$	5	0.5	100
Prodye	1	0.05	50
DNA/RNA	0.1	0.01	100
H_2O (MilliQ)	-	-	400
			1000

The workup was either a $LiClO_4$/acetone- or ethanol precipitation. Further details are given in section 5.6.1 "Precipitation methods".

Table S13. Applied alkynyl DNA and RNA oligonucleotides for Click chemistry

Oligo Nr. (Helm freezer)	Length	Category	Sequence 5'- 3' & modified base (highlighted)	Modification structure	Supplier
MH 476	28	DNA	**C**GC GCG AAG CTT AAT ACG ACT CAC TAT A	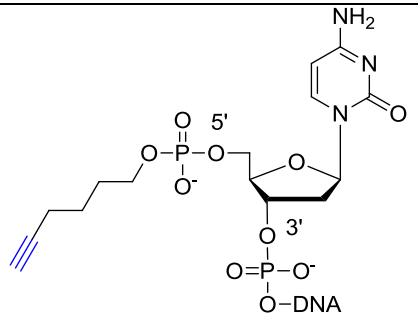	IBA (mod. from Glen Research, USA)
MH 618	28	DNA	**C**GC GCG AAG CTT AAT ACG ACT CAC TAT A	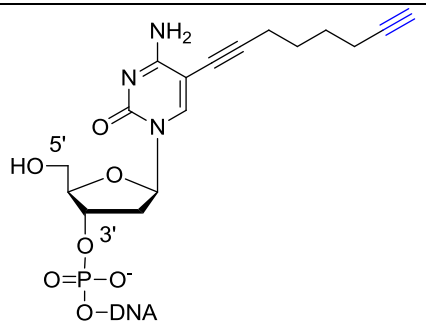	IBA (mod. from Glen Research, USA)
MH 662	22	RNA	GCA AGC UGA CCC UGA AGU UC**C** U	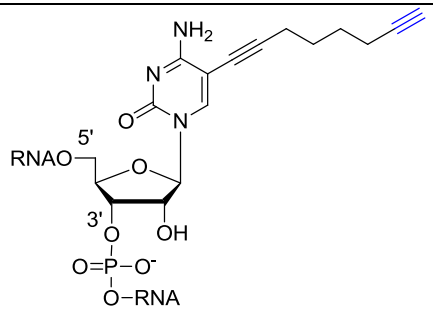	IBA (mod. from Glen Research, USA)

	[Stock] mM	[Final] mM	Volume in µl
TPTA	50	2.5	1
NaAsc	50	5	2
$CuSO_4$ • 5 H_2O	5	0.5	2
Prodye / Atto 647 N-azid	1	0.05	0.5
MH 476 (oligo)	0.1	0.01	2
MilliQ H_2O	-	-	12.5
Sum volume			20

Table S14. First developed Click scheme for prodye conjugation on DNA

	[Stock] mM	[Final] mM	Volume in µl
TPTA	50	2.5	1
NaAsc	50	5	2
$CuSO_4$ • 5 H_2O	5	0.5	2
Prodye / Atto 647 N-azid	1	0.05	0.5
MH 618 (oligo)	0.1	0.01	2
Phosphate buffer pH 6	500	100	4
MilliQ H_2O	-	-	8.5
Sum volume			20

Table S15. Phosphate buffer optimized Click scheme for prodye conjugation on DNA

	[Stock] mM	[Final] mM	Volume in µl
TPTA	50	2.5	1
NaAsc	50	5	2
$CuSO_4$ • 5 H_2O	5	0.5	2
Prodye / Atto 647 N-azid	1	0.05	0.5
MH 662 (oligo)	0.1	0.01	2
Phosphate buffer pH 6	500	100	4
MilliQ H_2O	-	-	8.5
Sum volume			20

Table S16. Phosphate buffer modified Click scheme for prodye conjugation on RNA

5.5 Electrophoretic mobility shift assay by denaturating and native PAGE

PAGE (polyacrylamide gel electrophoresis) has been used for detection and purification of conjugated single strand oligonucleotides with asymmetric prodyes **1** and **2**. The hybridization efficiency and quantification of double stranded oligonucleotides was performed on native polyacrylamide gels. 20 % denaturing and native gels with 2.0 mm thickness were prepared for easier handling purposes. It should be noted that due to the prodye deprotecting conditions of standard PAGE methods with pH 8 - 8.5, a special protocol with pH 7.1 was developed for analyzing the prodye conjugated oligonucleotides. In this gel preparation protocol the 10 x and 1x TBE-buffer was titrated with boric acid until the solutions reached neutral pH, respectively, followed by application of this neutral TBE buffers during gel preparation and run. Samples were loaded as a 1:1 mixture with 60% glycerol in H_2O and as running marker bromophenol blue/xylene cyanol were used to visualize the migration progress during electrophoresis. All gels were run in 1x TBE buffer with 20 W power for 8 - 12 hours.

As staining method of choice, GelRed® (Biotum) was used, in some cases stains all ® (Sigma) or SyberGold ® (Invitrogen) were applied.

Scanning and visualization of PAGE analyses was done by imaging with a Typhoon 9400 (GE Healthcare, Munich). Typhoon 9400 provides 457/488/532/633 nm excitation channels, with the following excitation lasers:

blue 30 mW argon ion laser 488 nm (20 mW) & 547 nm (4 mW)

green 20 mW solid state doubled frequency SYAG laser 532 nm

red 10 mW Helium neon laser 632.8 nm

and corresponding short pass or broad pass emission filters were used during emission scans.

The colored PAGE illustration and preparation was made with the freeware IMAGE J ®.

Table S17. Recipe of 20 % denaturating polyacrylamide gels (20 cm x 20 cm):

	20% PAGE
Sequencing gel concentrate	80 ml
Sequencing gel diluter	10 ml
Sequencing gel buffer concentrate	10 ml
TEMED	80 µl
APS	800 µl

Table S18. Recipe of 20 % native polyacrylamide gels (20 cm x 20 cm):

	20% PAGE
40 % acrylamide	50 ml
10 x TBE (pH 7.1)	10 ml
Aqua purificata	40
TEMED	200 µl
APS	2 ml

5.6 Oligonucleotide conjugate purification

4 methods were applied for purification purposes of prodye conjugated oligonucleotides.

5.6.1 Precipitation methods

a) $LiClO_4$-acetone:

2% m/v solution of $LiClO_4$ in acetone was used for precipitation of oligonucleotides. 10 x times that of the oligonucleotide solution volume was added and centrifuged at 10 000 x g for 0.5 hour at - 4°C. The supernatant was removed and the pellet was rinsed with 50 - 100 µL acetone. After another 15 minutes of centrifugation at 10 000 x g, the acetone was removed and the pellet was allowed to air dry.

b) Ethanol precipitation

5 M Na_4Ac (pH 5.2) was set to 0.5 M final concentration of Na_4Ac by using the probe. 3x volumes –80 °C ethanol were added, the mixture was vortexed and incubated for at least 2 hour at –80 °C. The samples were centrifuged at 12 000 x g for 30 minutes, after which the supernatant was removed. The pellet was carefully rinsed with 50 µl 70% ice cold ethanol and centrifuged again at 12 000 x g for 10 minutes. The supernatant was removed and the pellet was allowed to air dry, before redissolving in 10 µl MilliQ water.

5.6.2 PAGE extraction

The bands of interest were excised, mashed and shaken in 0.5 M NH_4Ac solution overnight. After filtration through a Nanosep® device, ice cold ethanol was added in 2.5 x excess to the filtrate. Samples were stored at - 20 °C for 2 h, followed by centrifugation at
12000 g and - 4 °C for 30 min. After discarding the supernatant, pellets were dried and resuspended in buffer or MilliQ water.

5.6.3 High performance liquid chromatography

15 ml of a 5pMol/µl single strand solution was loaded on a C18 reversed phase Phenomenex column and run at a flow rate of 3 mL/min in acetonitrile/TEAA (0.1 M, pH 7) using the following acetonitrile gradient:
0 min: 5%, 1 min: 10%, 6min: 15%, 8 min: 15%, 11 min: 60%, 17 min: 60%, 21 min: 5%, 25 min: 5%.
The dye conjugated product was collected after 12 minutes, whereas the free unclicked fraction eluted at 15 minutes.

5.6.4 Reversed phase cartridge purification

The easiest, cheapest and fastest way to purify conjugated single strand oligonucleotides went *via* the usage of Sep-Pak® cartridges with a C18 reversed phase based on monofunctional silane surface. The tested loading capacity of the columns was between 0.1 – 10 nMol oligonucleotides. First the column was fixed in a vertical orientation. Then the bonded phase was solvated with 3 ml MeOH (HPLC grade) and let it flow by gravity, no additional pressure was applied with the 10 ml syringe. Followed by equilibrating with 8 ml milliQ water and loading the non-precipitated sample (150 µl). The application of ACN/MilliQ water gradient (see **figure 46**) eluted in the beginning 2 ml of the unclicked oligonucleotide fraction, followed by the elution of clicked oligonucleotides between 3-6 ml. The unclicked dyes arrested because of their lipophilic character on the RP-column and the elution process was finished after 8 ml. As collector device a 96well plate was used, with 300 µl collecting volume of each well. Subsequent green emission scan on a plate reader (Tecan, Austria), PAGE analysis and lyophilisation of prodye conjugated single strand oligonucleotides yielded salt free and pure pellets. Photometric (Nanodrop) concentration analysis of dissolved pellets yielded 92.9 % of clicked DNA/RNA.

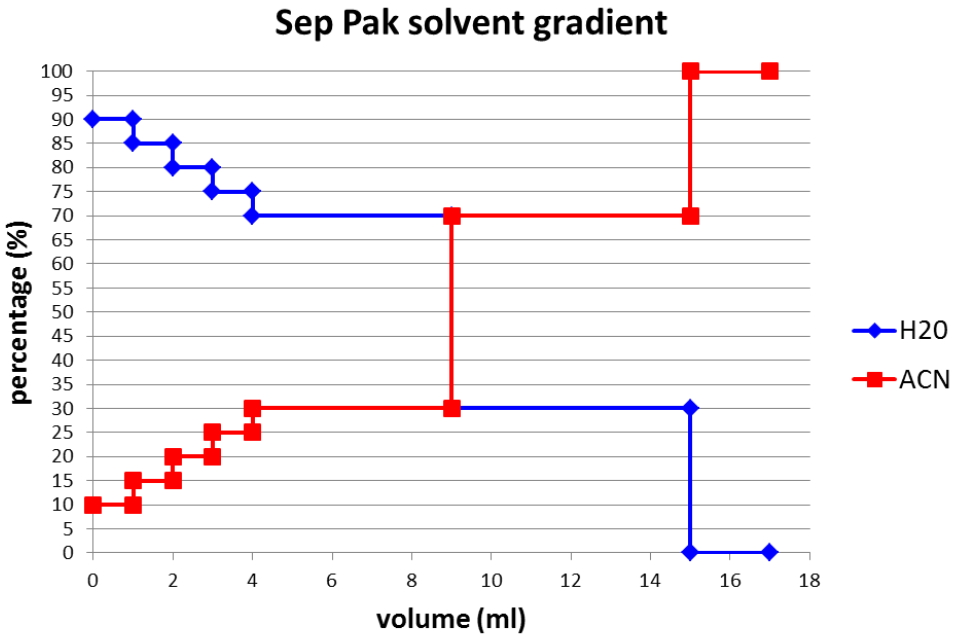

Figure 50. ACN/MilliQ water gradient for Sep-Pak® C18 cartridge elution

5.7 Photometric concentration determination of oligonucleotides

Fluorescent-labeled oligonucleotides concentration were determined by UV measurements on a Nanodrop ND-2000 (PeqLab, Erlangen) using the 260 nm absortionmaximum of nucleosides with less than 0.5 µl sample volume. By measuring the concentrations of labeled oligonucleotides on a Nanodrop ND-2000, the efficiency of the above mentioned precipitations and different purification methods was compared to achieve the best work up procedure.

5.8 Hybridization of oligonucleotides

Double strands were hybridized from 100 µM single strand stock solutions by adding both strands at the desired final concentration in 1x PBS pH 7.4. Samples were thoroughly mixed, incubated for 3 min at 90 °C for complete denaturation followed by 60 min at 37 °C for duplex formation. The hybridization and quantification of double stranded oligonucleotides was performed via native polyacrylamide gel 20%.

5.9 Nanoformulation and cell imaging

RBE4 cells were cultivated under standard conditions in a medium consisting of 45% v/v DMEM, 45% v/v HAM's F-10, 10% v/v serum (e.g. fetal calf or bovine serum), 100 µg/mL penicillin/streptomycin mix and 1 ng/mL basic fibroblast growth factor. For the confocal imaging, the cells were grown on 8-well IBIDI µ-slides. One day before transfection, 10 000 cells per well were seeded in 250 µL growth medium without antibiotics, resulting in about 40% confluency at the day of transfection. An optimized standard protocol for Oligofectamine® was used to transfect RBE4 cells with labeled siRNA duplexes.

1.6 µL of a 5 µM siRNA solution were diluted with 29 µL of OptiMem® (Invitrogen) medium and combined with a mixture of 1.6 µL Oligofectamine and 7 µL OptiMem® and incubated for 20 min. Before adding the half volume of formed lipoplexes drop wise to the cells, the medium was replaced with transfection medium (medium without serum and antibiotics) resulting in a final culture volume of 100 µL. Cells were incubated at 37 °C until fixation. For fixation, cells were washed once with PBS and fixated for 10 min in 4% formaldehyde, diluted in PBS. After two further washing steps with PBS and one with water, cells were mounted by adding three droplets of IBIDI Mounting medium to the well. Samples were stored at 4 °C until imaging. Fixed cell samples were imaged on a Leica inverted confocal microscope TCS SP5, equipped with an oil-immersion objective (63x magnification; NA 1.4) and a 561 nm laser. Images were recorded at 512x512 8-bit-pixel resolution with a pinhole of 130 µm and confocal plane depth of 1.0 µm, resulting in a total image size width and height of 246x246µm. Prodye conjugated constructs were exited at 488 nm with an Argon laser and Atto 590 conjugated oligonucleotides at 561 nm with a DPSS 561 Laser with corresponding emission scans, respectively. The microscopy was performed by Dr. Markus Hirsch at the Insitute of Molecular Biology (IMB) in Mainz. Further reading can be found in Literature[91].

5.10 LC-MS analysis

LC-MS analysis of synthesized compounds were done with an Agilent 1100 HPLC-device coupled to an Agilent MSD 2440 ion trap. Either by using of a liquid chromatography run and subsequent absorption (DAD Detector), emission (MW Detector) and mass (MSD ion trap)

analysis the compounds were characterized or by using the infusion method via an infusion pump (1.5 ml/h) the pure compounds were infunded as 0.01 mg/ml ACN / MeOH-solutions into the ion source of the MSD trap. The measurement was performed on (+) and / or (-) mode with additional MS^n fragmentation pattern.

6 Abbreviations

A, Abs	Absorbance
ACN	Acetonitrile
AMC	7-amino-4-methyl coumarin
AS	Antisense strand
BODIPY	Boron difluoride dipyrromethene
c	Concentration
c	Speed of light
CLSM	Confocal laser scanning microscopy
Cu	Copper
CuAAC	Copper(I)-catalyzed azide-alkyne cycloaddition
$CuSO_4$	Copper sulfate
CyDyes	Cyanine dyes
d	Doublet
dd	Doublet of doublet
DAPI	4’,6’-diamidino-2-phenylindole
DBU	1,8-diazabicycloundec-7-ene
DCM	Dichloromethane
DMF	*N,N’*-Dimethylformamide
DMSO	Dimethyl sulfoxide
DNA	Deoxyribonucleic acid
ds	Double strand
E	Energy
E_{max}	Molar Extinction coefficient at absorption maximum
em	Emission
EMSA	Electrophoretic Mobility Shift Assay
Equiv / eq.	Equivalent
Et	Ethyl
EtOAc	Ethyl acetate
ex	Excitation
FL	Fluorescein

FRET	Fluorescence resonance energy transfer
F.U.	Fluorescence unit
g	Relative centrifuge force
h	Hour(s)
h	Planck’s constant
H	Proton
HCl	Hydrogen chloride
HIV	human immunodeficiency virus
H_2O_2	Hydrogen peroxide
H_2SO_4	Sulfuric acid
HPLC	High pressure liquid chromatography
hν	Energy of photon
$h\nu_{em}$	Energy of the emitted photon
$h\nu_{ex}$	Energy of the excited photon
IBCF	Isobutyl chloro formiate
IR	Infrared spectroscopy
ITC	Intersystem crossing
J	Coupling constant
l	liter
LC-MS	Liquid chromatography – mass spectrometry
LD	Loading dye
$LiClO_4$	Lithium perchlorate
m	Multiplet
M	Molar concentration
MeOH	Methanol
mg	Milligram
min	Minute
µl	Microliter
ml	milliliter
µM	Mikromolar
mM	Millimolar
MOCK	Negative control

MS	Mass spectrometry
Ms / Mesyl	Methanesulfonyl
NaAsc	Sodium ascorbate
NaOH	Sodium hydroxide
N_2	Nitrogen
N3BC	7-azido-4-(bromomethyl)coumarin
nHex	*n*-Hexane
NMR	Nucleic magnetic resonance
NR	Nonradiative
ns	Nano second
ODN	oligodeoxynucleotide
oligo	oligonucleotide
ON	Overnight
PAGE	Polyacrylamide gel electrophoresis
PBS	Phosphate buffered saline
pd	Pseudo doublett
PEG	Polyethylene glycol
PeT	Photoinduced electron transfer
pH	Potential hydrogenii
PLE	Pig liver esterase
pK_a	Acid dissociation constant, negative logarithm
ppm	Parts per million
q	Quadruplet
R_f	Retention factor
RNA	Ribonucleic acid
rpm	Rotation per minute
RP	Reverse phase
RT	Room temperature
rt	Room temperature
s	Singlet
S_1	First electronic single state
S_2	Second electronic single state

SE	Sense strand
siRNA	Small interfering RNA
S_EAr	Electrophilic aromatic substitution
S_NAr	Nucleophilic aromatic substitution
SN_2	Nucleophilic substitution, bimolecular
ss	Single strand
t	Triplet
T_1	Triplet excited state
TBE	Tris/Borate/EDTA
TEAA	Triethylamonium acetate
TEMED	*N*,*N*,*N*',*N*'-Tetramethyl-ethane-1,2-diamine
THPTA / TPTA	Tris(hydroxypropyl)triazolylmethyl-amine
TLC	Thin layer chromatography
TMR	Tetramethylrhodamine
TRIS	tris(hydroxymethyl) aminomethane
TRITC	tetramethylrhodamine isothiocyanate
UV	Ultraviolet
Zn	Zinc
δ	Chemical shift
ε	Molar Extinction coefficient
λ	Wavelength
λ_{em}	Wavelength of maximum emission
λ_{max}	Wavelength of maximum absorption
µl	microliter
ν	Frequency
Φ	Quantum yield

7 Publications and Posters

1) Synthesis of new asymmetric xanthene dyes via catalyst-free S_NAr with sulfur nucleophiles, *Org. Biomol. Chem.***,** 2014, Advance Article
Michaela Kotaskova, Okan Osman Oglou and Mark Helm (shared first authorship)

2) MODOMICS: a database of RNA modification pathways: 2012 update *Nucleic Acids Res* 2013 Jan 1;41(D1): D262-D267
Machnicka MA, Milanowska K, Osman Oglou O, Purta E, Kurkowska M, Olchowik A, Januszewski W, Kalinowski S, Dunin-Horkawicz S, Rother KM, Helm M, Bujnicki JM, Grosjean H

Poster Presentations & Conference Participations

04. – 07. October 2012	7th Meeting of the GBM Study Section RNA-Biochemistry, Bonn Germany, Topic: "First Contact Imaging of nanoparticular siRNA", Okan Osmanoglou & Mark Helm
21. – 23- March 2013	1st International BAU-Drug Design Symposium Participant, Besiktas-Istanbul Turkey
03. – 06. October 2013	Molecular Life Sciences 2013 International Symposium of the German Society for Biochemistry and Molecular Biology (GBM), Frankfurt am Main Germany, "First Contact Imaging of nanoparticular siRNA", Okan Osmanoglou & Mark Helm
09. – 12. October 2014	8th Meeting of the GBM Study Section RNA-Biochemistry, Bonn Germany, Topic: "First Contact Imaging of nanoparticular siRNA", Okan Osmanoglou & Mark Helm

8 References

1. Maxwell, J. C., XVIII.—Experiments on Colour, as perceived by the Eye, with Remarks on Colour-Blindness. *Earth and Environmental Science Transactions of the Royal Society of Edinburgh* **1857,** *21* (02), 275-298.
2. De Broglie, L. Recherches sur la théorie des quanta. Paris, 1924.
3. Valeur, B.; Berberan-Santos, M. N., A Brief History of Fluorescence and Phosphorescence before the Emergence of Quantum Theory. *Journal of Chemical Education* **2011,** *88* (6), 731-738.
4. Stokes, G. G., On the Change of Refrangibility of Light. *Philosophical Transactions of the Royal Society of London* **1852,** *142*, 463-562.
5. Jabłoński, A., Efficiency of anti-Stokes fluorescence in dyes. *Nature* **April 1933,** *131*, 839–840.
6. Ian D. Johnson, M. W. D. http://www.olympusmicro.com/primer/java/jablonski/jabintro/jablonskijavafigure1.jpg.
7. Franck, J.; Dymond, E. G., Elementary processes of photochemical reactions. *Transactions of the Faraday Society* **1926,** *21* (February), 536-542.
8. Condon, E., A Theory of Intensity Distribution in Band Systems. *Physical Review* **1926,** *28* (6), 1182-1201.
9. Condon, E. U., Nuclear Motions Associated with Electron Transitions in Diatomic Molecules. *Physical Review* **1928,** *32* (6), 858-872.
10. de Silva, A. P.; Gunaratne, H. Q. N.; Gunnlaugsson, T.; Huxley, A. J. M.; McCoy, C. P.; Rademacher, J. T.; Rice, T. E., Signaling Recognition Events with Fluorescent Sensors and Switches. *Chemical Reviews* **1997,** *97* (5), 1515-1566.
11. Förster, T., Zwischenmolekulare Energiewanderung und Fluoreszenz. *Annalen der Physik* **1948,** *437* (1-2), 55-75.
12. Sapsford, K. E.; Berti, L.; Medintz, I. L., Materials for Fluorescence Resonance Energy Transfer Analysis: Beyond Traditional Donor–Acceptor Combinations. *Angewandte Chemie International Edition* **2006,** *45* (28), 4562-4589.
13. Lakowitz, J. R., *Principles of fluorescent spectroscopy*. Springer New York: 2006.
14. Lim, D.-S.; Oh, C. S.; Lee, S. J.; Shin, D. H., Auto-fluorescence emitted from the cell residues preserved in human tissues of medieval Korean mummies. *Journal of Anatomy* **2010,** *217* (1), 67-75.
15. Lavis, L. D.; Raines, R. T., Bright Ideas for Chemical Biology. *ACS Chemical Biology* **2008,** *3* (3), 142-155.
16. v. Pechmann, H., Neue Bildungsweise der Cumarine. Synthese des Daphnetins. I. *Berichte der deutschen chemischen Gesellschaft* **1884,** *17* (1), 929-936.
17. Song, C. E.; Jung, D.-u.; Choung, S. Y.; Roh, E. J.; Lee, S.-g., Dramatic Enhancement of Catalytic Activity in an Ionic Liquid: Highly Practical Friedel–Crafts Alkenylation of Arenes with Alkynes Catalyzed by Metal Triflates. *Angewandte Chemie* **2004,** *116* (45), 6309-6311.
18. Rao, H. S. P.; Sivakumar, S., Condensation of α-Aroylketene Dithioacetals and 2-Hydroxyarylaldehydes Results in Facile Synthesis of a Combinatorial Library of 3-Aroylcoumarins#. *The Journal of Organic Chemistry* **2006,** *71* (23), 8715-8723.
19. Sashidhara, K. V.; Palnati, G. R.; Avula, S. R.; Kumar, A., Efficient and General Synthesis of 3-Aryl Coumarins Using Cyanuric Chloride. *Synlett* **2012,** *2012* (04), 611-621.
20. Katerinopoulos, H. E., The Coumarin Moiety as Chromophore of Fluorescent Ion Indicators in Biological Systems. *Current Pharmaceutical Design* **2004**.

21. Cheviron, N.; Rousseau-Plasse, A.; Lenfant, M.; Adeline, M.-T.; Potier, P.; Thierry, J., Coumarin-Ser-Asp-Lys-Pro-OH, A Fluorescent Substrate for Determination of Angiotensin-Converting Enzyme Activity via High-Performance Liquid Chromatography. *Analytical Biochemistry* **2000,** *280* (1), 58-64.
22. Kellner, S.; Seidu-Larry, S.; Burhenne, J.; Motorin, Y.; Helm, M., A multifunctional bioconjugate module for versatile photoaffinity labeling and click chemistry of RNA. *Nucleic Acids Res* **2011,** *39* (16), 7348-7360.
23. Jose, J.; Burgess, K., Benzophenoxazine-based fluorescent dyes for labeling biomolecules. *Tetrahedron* **2006,** *62* (48), 11021-11037.
24. Nakanishi, J.; Nakajima, T.; Sato, M.; Ozawa, T.; Tohda, K.; Umezawa, Y., Imaging of Conformational Changes of Proteins with a New Environment-Sensitive Fluorescent Probe Designed for Site-Specific Labeling of Recombinant Proteins in Live Cells. *Analytical Chemistry* **2001,** *73* (13), 2920-2928.
25. Haugland, R. P. S., M. T. Z.; Johnson, I. D.; Basey, A., *he Handbook: A Guide to Fluorescent Probes and Labeling Technologies*. 10 ed.; 2005.
26. Jung, C.; Müller, B. K.; Lamb, D. C.; Nolde, F.; Müllen, K.; Bräuchle, C., A New Photostable Terrylene Diimide Dye for Applications in Single Molecule Studies and Membrane Labeling. *J Am Chem Soc* **2006,** *128* (15), 5283-5291.
27. Peneva, K.; Mihov, G.; Nolde, F.; Rocha, S.; Hotta, J.-i.; Braeckmans, K.; Hofkens, J.; Uji-i, H.; Herrmann, A.; Müllen, K., Water-Soluble Monofunctional Perylene and Terrylene Dyes: Powerful Labels for Single-Enzyme Tracking. *Angewandte Chemie* **2008,** *120* (18), 3420-3423.
28. Peneva, K.; Gundlach, K.; Herrmann, A.; Paulsen, H.; Mullen, K., Site-specific incorporation of perylene into an N-terminally modified light-harvesting complex II. *Organic & Biomolecular Chemistry* **2010,** *8* (21), 4823-4826.
29. Treibs, A.; Kreuzer, F.-H., Difluorboryl-Komplexe von Di- und Tripyrrylmethenen. *Justus Liebigs Annalen der Chemie* **1968,** *718* (1), 208-223.
30. Loudet, A.; Burgess, K., BODIPY Dyes and Their Derivatives: Syntheses and Spectroscopic Properties. *Chemical Reviews* **2007,** *107* (11), 4891-4932.
31. Liu, C. Y.; Zhang, H.; Christofi, F. L., Adenylyl cyclase co-distribution with the CaBPs, calbindin-D28 and calretinin, varies with cell type: assessment with the fluorescent dye, BODIPY forskolin, in enteric ganglia. *Cell Tissue Res* **1998,** *293* (1), 57-73.
32. Mujumdar, R. B.; Ernst, L. A.; Mujumdar, S. R.; Lewis, C. J.; Waggoner, A. S., Cyanine dye labeling reagents: Sulfoindocyanine succinimidyl esters. *Bioconjugate Chemistry* **1993,** *4* (2), 105-111.
33. Luo, S.; Zhang, E.; Su, Y.; Cheng, T.; Shi, C., A review of NIR dyes in cancer targeting and imaging. *Biomaterials* **2011,** *32* (29), 7127-7138.
34. Osterman, I. A.; Ustinov, A. V.; Evdokimov, D. V.; Korshun, V. A.; Sergiev, P. V.; Serebryakova, M. V.; Demina, I. A.; Galyamina, M. A.; Govorun, V. M.; Dontsova, O. A., A nascent proteome study combining click chemistry with 2DE. *PROTEOMICS* **2013,** *13* (1), 17-21.
35. Choi, C. H. J.; Hao, L.; Narayan, S. P.; Auyeung, E.; Mirkin, C. A., Mechanism for the endocytosis of spherical nucleic acid nanoparticle conjugates. *Proceedings of the National Academy of Sciences* **2013,** *110* (19), 7625-7630.
36. Lavis, L. D.; Raines, R. T., Bright Building Blocks for Chemical Biology. *ACS Chemical Biology* **2014,** *9* (4), 855-866.
37. Baeyer, A., Ueber eine neue Klasse von Farbstoffen. *Berichte der deutschen chemischen Gesellschaft* **1871,** *4* (2), 555-558.
38. Klonis, N.; Sawyer, W., Spectral properties of the prototropic forms of fluorescein in aqueous solution. *J Fluoresc* **1996,** *6* (3), 147-157.

39. Martin, M. M.; Lindqvist, L., The pH dependence of fluorescein fluorescence. *Journal of Luminescence* **1975,** *10* (6), 381-390.
40. Fülöp, L.; Penke, B.; Zarándi, M., Synthesis and fluorescent labeling of beta-amyloid peptides. *Journal of Peptide Science* **2001,** *7* (8), 397-401.
41. Hoffmann, C.; Leroy-Dudal, J.; Patel, S.; Gallet, O.; Pauthe, E., Fluorescein isothiocyanate-labeled human plasma fibronectin in extracellular matrix remodeling. *Analytical Biochemistry* **2008,** *372* (1), 62-71.
42. Fernández-Carneado, J.; Giralt, E., An efficient method for the solid-phase synthesis of fluorescently labelled peptides. *Tetrahedron Letters* **2004,** *45* (31), 6079-6081.
43. Griffin, B. A.; Adams, S. R.; Tsien, R. Y., Specific Covalent Labeling of Recombinant Protein Molecules Inside Live Cells. *Science* **1998,** *281* (5374), 269-272.
44. Mizukami, S.; Watanabe, S.; Akimoto, Y.; Kikuchi, K., No-Wash Protein Labeling with Designed Fluorogenic Probes and Application to Real-Time Pulse-Chase Analysis. *J Am Chem Soc* **2012,** *134* (3), 1623-1629.
45. Ceresole, M. Verfahren zur Darstellung von Farbstoffen aus der Gruppe des Meta-amidophenol-Phtaleiñ s. D.R. Patent No. 44002. 1887.
46. Gonçalves, M. S. T., Fluorescent Labeling of Biomolecules with Organic Probes. *Chemical Reviews* **2009,** *109* (1), 190-212.
47. Khanna, P. L.; Ullman, E. F., 4′ ,5′ -dimethoxy-6-carboxyfluorescein: A novel dipole-dipole coupled fluorescence energy transfer acceptor useful for fluorescence immunoassays. *Analytical Biochemistry* **1980,** *108* (1), 156-161.
48. Horneffer, V.; Forsmann, A.; Strupat, K.; Hillenkamp, F.; Kubitscheck, U., Localization of Analyte Molecules in MALDI Preparations by Confocal Laser Scanning Microscopy. *Analytical Chemistry* **2001,** *73* (5), 1016-1022.
49. Grimm, J. B.; Sung, A. J.; Legant, W. R.; Hulamm, P.; Matlosz, S. M.; Betzig, E.; Lavis, L. D., Carbofluoresceins and Carborhodamines as Scaffolds for High-Contrast Fluorogenic Probes. *ACS Chemical Biology* **2013,** *8* (6), 1303-1310.
50. Li, X.; Gao, X.; Shi, W.; Ma, H., Design Strategies for Water-Soluble Small Molecular Chromogenic and Fluorogenic Probes. *Chemical Reviews* **2014,** *114* (1), 590-659.
51. Zhu, H.; Fan, J.; Xu, Q.; Li, H.; Wang, J.; Gao, P.; Peng, X., Imaging of lysosomal pH changes with a fluorescent sensor containing a novel lysosome-locating group. *Chemical Communications* **2012,** *48* (96), 11766-11768.
52. Beija, M.; Afonso, C. A. M.; Martinho, J. M. G., Synthesis and applications of Rhodamine derivatives as fluorescent probes. *Chemical Society Reviews* **2009,** *38* (8), 2410-2433.
53. Tian, L.; Yang, Y.; Wysocki, L. M.; Arnold, A. C.; Hu, A.; Ravichandran, B.; Sternson, S. M.; Looger, L. L.; Lavis, L. D., Selective esterase–ester pair for targeting small molecules with cellular specificity. *Proceedings of the National Academy of Sciences* **2012,** *109* (13), 4756-4761.
54. Nekongo, E. E.; Popik, V. V., Photoactivatable Fluorescein Derivatives Caged with a (3-Hydroxy-2-naphthalenyl)methyl Group. *The Journal of Organic Chemistry* **2014,** *79* (16), 7665-7671.
55. Miller, E. W.; Bian, S. X.; Chang, C. J., A Fluorescent Sensor for Imaging Reversible Redox Cycles in Living Cells. *J Am Chem Soc* **2007,** *129* (12), 3458-3459.
56. Sletten, E. M.; Bertozzi, C. R., Bioorthogonal Chemistry: Fishing for Selectivity in a Sea of Functionality. *Angewandte Chemie International Edition* **2009,** *48* (38), 6974-6998.
57. Machnicka, M. A.; Milanowska, K.; Osman Oglou, O.; Purta, E.; Kurkowska, M.; Olchowik, A.; Januszewski, W.; Kalinowski, S.; Dunin-Horkawicz, S.; Rother, K. M.; Helm, M.; Bujnicki, J. M.; Grosjean, H., MODOMICS: a database of RNA modification pathways—2013 update. *Nucleic Acids Res* **2013,** *41* (D1), D262-D267.

58. F.H.C., W. J. D. a. C., A Structure for Deoxyribose Nucleic Acid. *Nat Commun* **1953,** *3* (171), 737 - 38.
59. Lee, J. C.; Gutell, R. R., Diversity of Base-pair Conformations and their Occurrence in rRNA Structure and RNA Structural Motifs. *Journal of Molecular Biology* **2004,** *344* (5), 1225-1249.
60. Nakano, S.-i.; Kanzaki, T.; Sugimoto, N., Influences of Ribonucleotide on a Duplex Conformation and Its Thermal Stability: Study with the Chimeric RNA−DNA Strands. *J Am Chem Soc* **2004,** *126* (4), 1088-1095.
61. Breslauer, K. J.; Sturtevant, J. M.; Tinoco, I., Jr., Calorimetric and spectroscopic investigation of the helix-to-coil transition of a ribo-oligonucleotide: rA7U7. *J Mol Biol* **1975,** *99* (4), 549-65.
62. Riley, M.; Maling, B., Physical and chemical characterization of two- and three-stranded adenine-thymine and adenine-uracil homopolymer complexes. *J Mol Biol* **1966,** *20* (2), 359-89.
63. Kricka, L. J., Stains, labels and detection strategies for nucleic acids assays. *Annals of Clinical Biochemistry* **2002,** *39* (2), 114-129.
64. El-Sagheer, A. H.; Brown, T., Click chemistry with DNA. *Chemical Society Reviews* **2010,** *39* (4), 1388-1405.
65. Winz, M.-L.; Samanta, A.; Benzinger, D.; Jäschke, A., Site-specific terminal and internal labeling of RNA by poly(A) polymerase tailing and copper-catalyzed or copper-free strain-promoted click chemistry. *Nucleic Acids Res* **2012,** *40* (10), e78-e78.
66. Paredes, E.; Das, S. R., Click Chemistry for Rapid Labeling and Ligation of RNA. *ChemBioChem* **2011,** *12* (1), 125-131.
67. Shelbourne, M.; Chen, X.; Brown, T.; El-Sagheer, A. H., Fast copper-free click DNA ligation by the ring-strain promoted alkyne-azide cycloaddition reaction. *Chemical Communications* **2011,** *47* (22), 6257-6259.
68. Kotaskova, M.; Osman Oglou, O.; Helm, M., Synthesis of new asymmetric xanthene dyes via catalyst-free SNAr with sulfur nucleophiles. *Organic & Biomolecular Chemistry* **2014,** *12* (23), 3816-3820.
69. Schoch, J.; Jaschke, A., Synthesis and enzymatic incorporation of norbornene-modified nucleoside triphosphates for Diels-Alder bioconjugation. *RSC Advances* **2013,** *3* (13), 4181-4183.
70. Ameta, S.; Becker, J.; Jaschke, A., RNA-peptide conjugate synthesis by inverse-electron demand Diels-Alder reaction. *Organic & Biomolecular Chemistry* **2014,** *12* (26), 4701-4707.
71. Kessler, S. N.; Wegner, H. A., Lewis Acid Catalyzed Inverse Electron-Demand Diels−Alder Reaction of 1,2-Diazines. *Organic Letters* **2010,** *12* (18), 4062-4065.
72. Anderson, E. D.; Boger, D. L., Scope of the Inverse Electron Demand Diels−Alder Reactions of 1,2,3-Triazine. *Organic Letters* **2011,** *13* (9), 2492-2494.
73. Sauer, J.; Heldmann, D. K.; Hetzenegger, J.; Krauthan, J.; Sichert, H.; Schuster, J., 1,2,4,5-Tetrazine: Synthesis and Reactivity in [4+2] Cycloadditions. *European Journal of Organic Chemistry* **1998,** *1998* (12), 2885-2896.
74. Pyka, A. M.; Domnick, C.; Braun, F.; Kath-Schorr, S., Diels–Alder Cycloadditions on Synthetic RNA in Mammalian Cells. *Bioconjugate Chemistry* **2014,** *25* (8), 1438-1443.
75. Kotaskova, M. Synthesis of New Xanthene Derivatives. University of Mainz, 2012.
76. Jung, E. B. u. G., *Organische Chemie, 7. vollst. Überarb. u. erw. Auflage 2012*. 2012.
77. Zona, C.; D'Orazio, G.; La Ferla, B., Controlled-Length Efficient Synthesis of Heterobifunctionalized Oligo Ethylene Glycols. *Synlett* **2013,** *24* (06), 709-712.
78. Shaikh, A.-A. G.; Sivaram, S., Organic Carbonates. *Chemical Reviews* **1996,** *96* (3), 951-976.

79. Vlieghe, P.; Bihel, F.; Clerc, T.; Pannecouque, C.; Witvrouw, M.; De Clercq, E.; Salles, J.-P.; Chermann, J.-C.; Kraus, J.-L., New 3‘-Azido-3‘-deoxythymidin-5‘-yl O-(ω-Hydroxyalkyl) Carbonate Prodrugs: Synthesis and Anti-HIV Evaluation. *Journal of medicinal chemistry* **2001,** *44* (5), 777-786.
80. de Groot, F. M. H.; Busscher, G. F.; Aben, R. W. M.; Scheeren, H. W., Novel 20-Carbonate Linked Prodrugs of Camptothecin and 9-Aminocamptothecin Designed for Activation by Tumour-Associated Plasmin. *Bioorg Med Chem Lett* **2002,** *12* (17), 2371-2376.
81. Hein, C. D.; Liu, X.-M.; Wang, D., Click Chemistry, a Powerful Tool for Pharmaceutical Sciences. *Pharm Res-Dordr* **2008,** *25* (10), 2216-2230.
82. Yang, Y.-h.; Aloysius, H.; Inoyama, D.; Chen, Y.; Hu, L.-q., Enzyme-mediated hydrolytic activation of prodrugs. *Acta Pharmaceutica Sinica B* **2011,** *1* (3), 143-159.
83. N'Da, D. D.; Breytenbach, J. C., Synthesis of methoxypoly(ethylene glycol) carbonate prodrugs of zidovudine and penetration through human skin in vitro. *Journal of Pharmacy and Pharmacology* **2009,** *61* (6), 721-731.
84. Socrates, G., *Infrared and Raman Characteristic Group Frequencies: Tables and Charts*. Wiley: 2004.
85. Sjöback, R.; Nygren, J.; Kubista, M., Absorption and fluorescence properties of fluorescein. *Spectrochimica Acta Part A: Molecular and Biomolecular Spectroscopy* **1995,** *51* (6), L7-L21.
86. Pourceau, G.; Meyer, A.; Vasseur, J. J.; Morvan, F., Synthesis of mannose and galactose oligonucleotide conjugates by bi-click chemistry. *J Org Chem* **2009,** *74* (3), 1218-22.
87. Kellner, S. Functionalization and Detection of RNA and its Modifications. PhD, 2012.
88. Domingo, O. Investigations into the effect of nucleoside modifications on the physicochemical properties and biological function. PhD, 2013.
89. Quigley, J. M.; Jordan, C. G. M.; Timoney, R. F., The synthesis, hydrolysis kinetics and lipophilicity of O-acyl esters of propranolol. *International Journal of Pharmaceutics* **1994,** *101* (1–2), 145-163.
90. BOIKA TSVETKOVA, J. T., PLAMEN PEIKOV, Alkaline, Enzymatic Hydrolysis and Physicochemical Properties of 7-Theophyllineacetic Acid Derivatives. *Journal of Food and Drug Analysis* **2003,** *11* (3), 191 - 194.
91. Hirsch, M. PhD Thesis - Dynamics of small interfering RNA - FRET based integrity measurements of siRNA in the cuvette & inside cells. University Mainz, 2013.
92. Krieg, B. Evaluation of polymeric nanocarriers for RNA delivery. PhD Thesis, 2014.
93. Wu, T.; Ogilvie, K. K.; Pon, R. T., Prevention of chain cleavage in the chemical synthesis of 2'-silylated oligoribonucleotides. *Nucleic Acids Res* **1989,** *17* (9), 3501-3517.
94. Pilz, W.; Johann, I., Spezielle analytische Methoden für die Biochemie und physiologische Chemie. *Z. Anal. Chem.* **1965,** *215* (2), 105-109.
95. Hirsch, M.; Strand, D.; Helm, M., Dye selection for live cell imaging of intact siRNA. 2012; Vol. 393, p 23.
96. Shieh, P.; Hangauer, M. J.; Bertozzi, C. R., Fluorogenic Azidofluoresceins for Biological Imaging. *J Am Chem Soc* **2012,** *134* (42), 17428-17431.
97. Zhang, L.; Duan, D.; Liu, Y.; Ge, C.; Cui, X.; Sun, J.; Fang, J., Highly Selective Off–On Fluorescent Probe for Imaging Thioredoxin Reductase in Living Cells. *J Am Chem Soc* **2014,** *136* (1), 226-233.
98. Hettiarachchi, S. U.; Prasai, B.; McCarley, R. L., Detection and Cellular Imaging of Human Cancer Enzyme Using a Turn-On, Wavelength-Shiftable, Self-Immolative Profluorophore. *J Am Chem Soc* **2014,** *136* (21), 7575-7578.

99. Basak, A.; Das, S.; Bisai, S., Studies on the porcine liver esterase-catalyzed hydrolysis of pentaacetyl catechin and epicatechin: application to the synthesis of novel dimers and trimers. *Bioorg Med Chem Lett* **2008,** *18* (17), 4900-3.
100. Keown, W. A.; Campbell, C. R.; Kucherlapati, R. S., [41] Methods for introducing DNA into mammalian cells. In *Methods in Enzymology*, David, V. G., Ed. Academic Press: 1990; Vol. Volume 185, pp 527-537.
101. Liu, D.; Chiao, E. F.; Tian, H., Chemical methods for DNA delivery: an overview. *Methods in molecular biology* **2004,** *245*, 3-24.
102. Krieg, B.; Hirsch, M.; Scholz, E.; Nuhn, L.; Tabujew, I.; Bauer, H.; Decker, S.; Khobta, A.; Schmidt, M.; Tremel, W.; Zentel, R.; Peneva, K.; Koynov, K.; Mason, A. J.; Helm, M., New Techniques to Assess In Vitro Release of siRNA from Nanoscale Polyplexes. *Pharm Res* **2014**.
103. Davis, M. E., Non-viral gene delivery systems. *Current opinion in biotechnology* **2002,** *13* (2), 128-31.
104. Boussif, O.; Lezoualc'h, F.; Zanta, M. A.; Mergny, M. D.; Scherman, D.; Demeneix, B.; Behr, J. P., A versatile vector for gene and oligonucleotide transfer into cells in culture and in vivo: polyethylenimine. *Proc Natl Acad Sci U S A* **1995,** *92* (16), 7297-301.
105. Tang, M. X.; Redemann, C. T.; Szoka, F. C., Jr., In vitro gene delivery by degraded polyamidoamine dendrimers. *Bioconjug Chem* **1996,** *7* (6), 703-14.
106. Hafez, I. M.; Maurer, N.; Cullis, P. R., On the mechanism whereby cationic lipids promote intracellular delivery of polynucleic acids. *Gene therapy* **2001,** *8* (15), 1188-96.
107. Roux, F.; Durieu-Trautmann, O.; Chaverot, N.; Claire, M.; Mailly, P.; Bourre, J. M.; Strosberg, A. D.; Couraud, P. O., Regulation of gamma-glutamyl transpeptidase and alkaline phosphatase activities in immortalized rat brain microvessel endothelial cells. *Journal of cellular physiology* **1994,** *159* (1), 101-13.
108. Kiernan, J., Formaldehyde, formalin, paraformaldehyde and glutaraldehyde: what they are and what they do. *Microscopy Today* **2000,** *1*, 8-10.
109. Rolls, G. Factors influencing chemical fixation, formaldehyde and glutaraldehyde. http://www.leicabiosystems.com/pathologyleaders/fixation-and-fixatives-2-factors-influencing-chemical-fixation-formaldehyde-and-glutaraldehyde/.
110. Moody, P.; Smith, M. E.; Ryan, C. P.; Chudasama, V.; Baker, J. R.; Molloy, J.; Caddick, S., Bromomaleimide-linked bioconjugates are cleavable in mammalian cells. *ChemBioChem* **2012,** *13* (1), 39-41.
111. Nathani, R. I.; Chudasama, V.; Ryan, C. P.; Moody, P. R.; Morgan, R. E.; Fitzmaurice, R. J.; Smith, M. E. B.; Baker, J. R.; Caddick, S., Reversible protein affinity-labelling using bromomaleimide-based reagents. *Organic & Biomolecular Chemistry* **2013,** *11* (15), 2408-2411.
112. Rodriguez-Perez, T.; Fernandez, S.; Sanghvi, Y. S.; Gotor, V.; Ferrero, M., Preparation of nucleoside-carbohydrate phosphodiester prodrug analogues by chemoenzymatic procedure. *Nucleic acids symposium series* **2008,** (52), 101-2.
113. Bruni, C. B.; Sica, V.; Auricchio, F.; Covelli, I., Further kinetic and structural characterization of the lysosomal α-d-glucoside glucohydrolase from cattle liver. *Biochimica et Biophysica Acta (BBA) - Enzymology* **1970,** *212* (3), 470-477.
114. Banwell, M. G.; Jones, M. T.; Loong, D. T. J.; Lupton, D. W.; Pinkerton, D. M.; Ray, J. K.; Willis, A. C., A Pd[0]-catalyzed Ullmann cross-coupling/reductive cyclization approach to C-3 mono-alkylated oxindoles and related compounds. *Tetrahedron* **2010,** *66* (47), 9252-9262.
115. Peng, T.; Yang, D., Construction of a library of rhodol fluorophores for developing new fluorescent probes. *Org Lett* **2010,** *12* (3), 496-9.

116. Lavis, L. D.; Rutkoski, T. J.; Raines, R. T., Tuning the pK(a) of fluorescein to optimize binding assays. *Anal Chem* **2007,** *79* (17), 6775-82.
117. Rostovtsev, V. V.; Green, L. G.; Fokin, V. V.; Sharpless, K. B., A stepwise huisgen cycloaddition process: copper(I)-catalyzed regioselective "ligation" of azides and terminal alkynes. *Angew Chem Int Ed Engl* **2002,** *41* (14), 2596-9.

9 Appendix

No. **(1)** H-NMR in $CDCl_3$

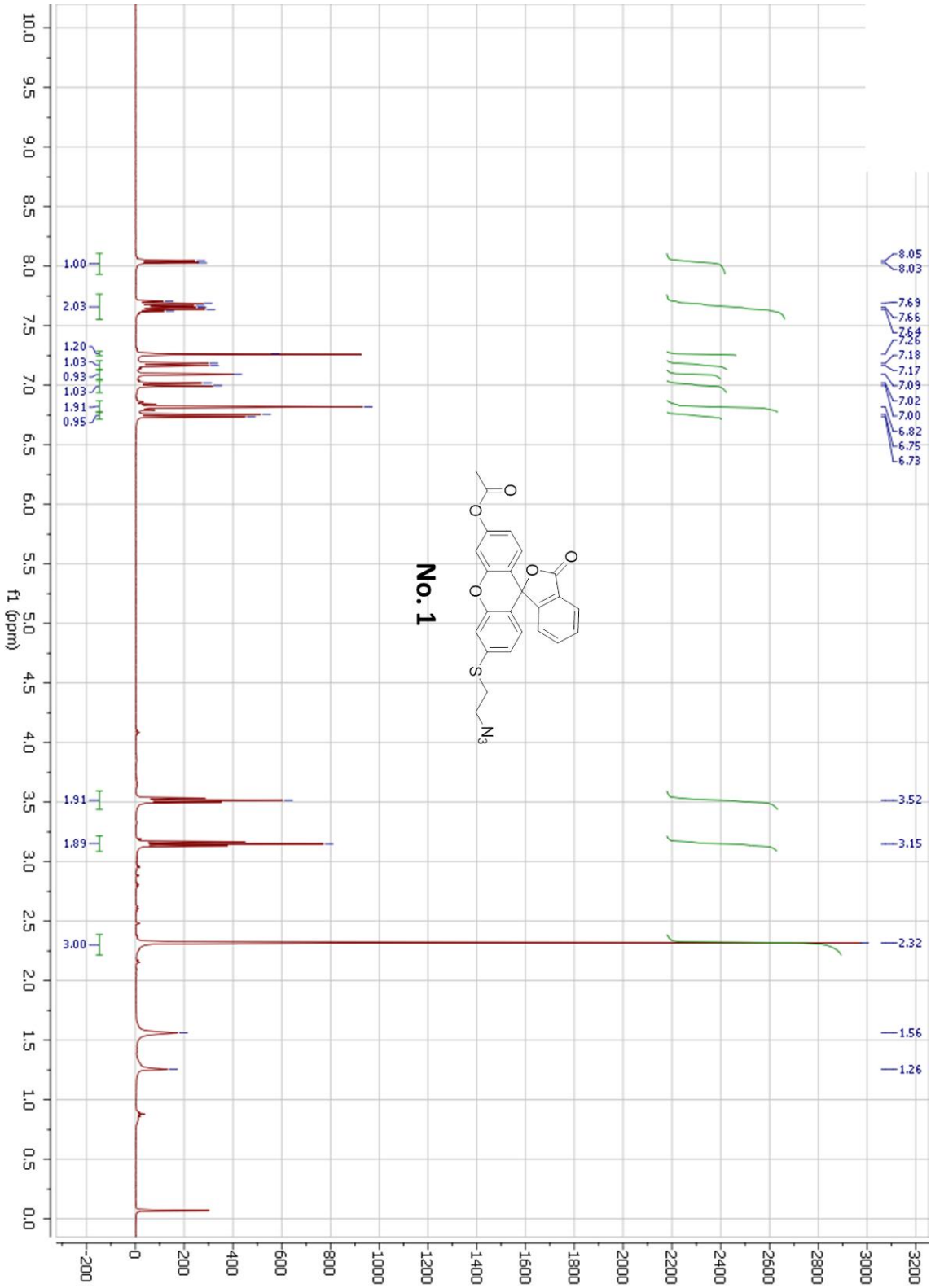

No. (**1**) FT-IR

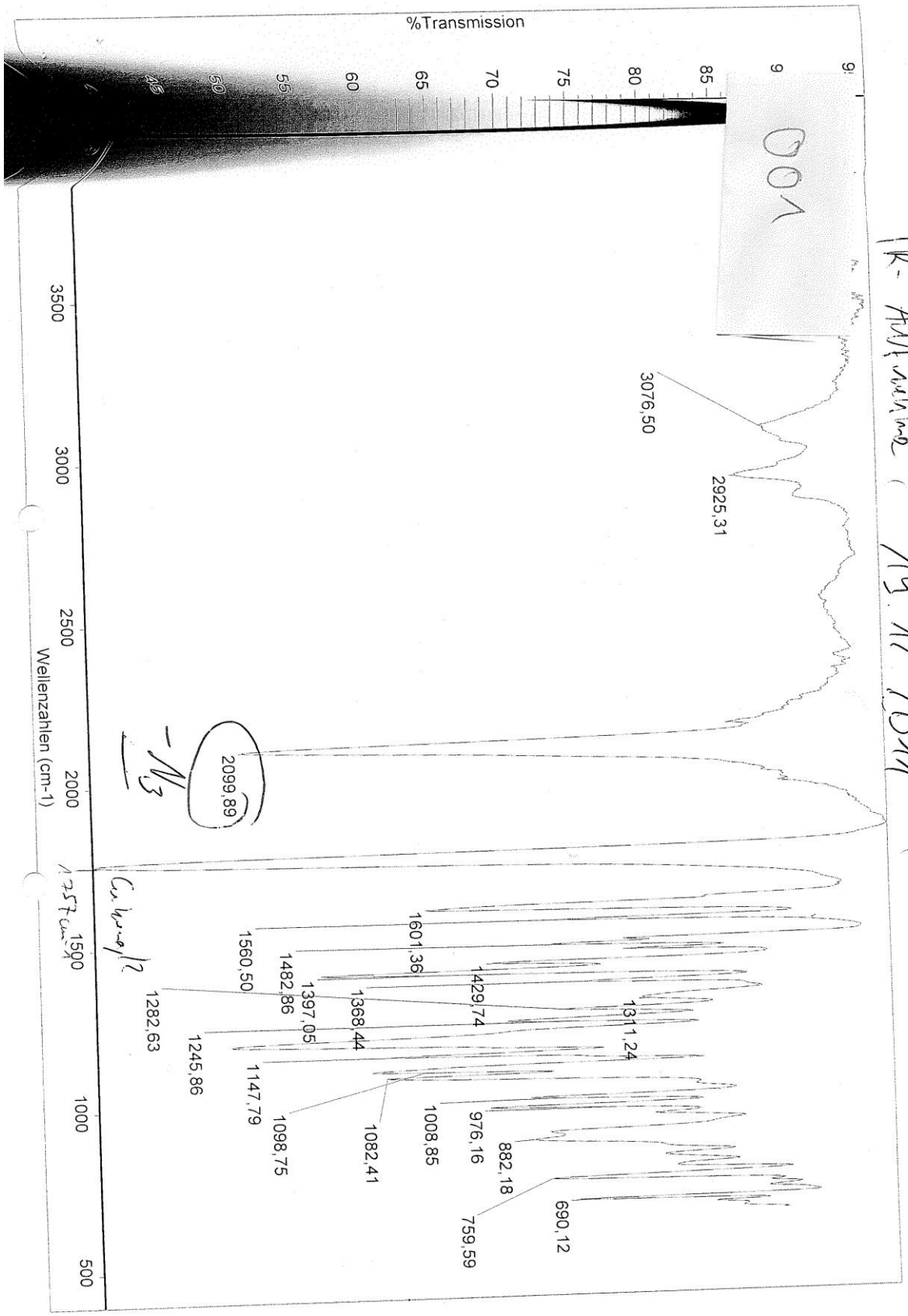
%Transmission
Wellenzahlen (cm-1)
3076,50
2925,31
2099,89
1601,36
1560,50
1482,86
1429,74
1397,05
1368,44
1311,24
1282,63
1245,86
1147,79
1098,75
1082,41
1008,85
976,16
882,18
759,59
690,12

No. **(2)** H-NMR in CDCl

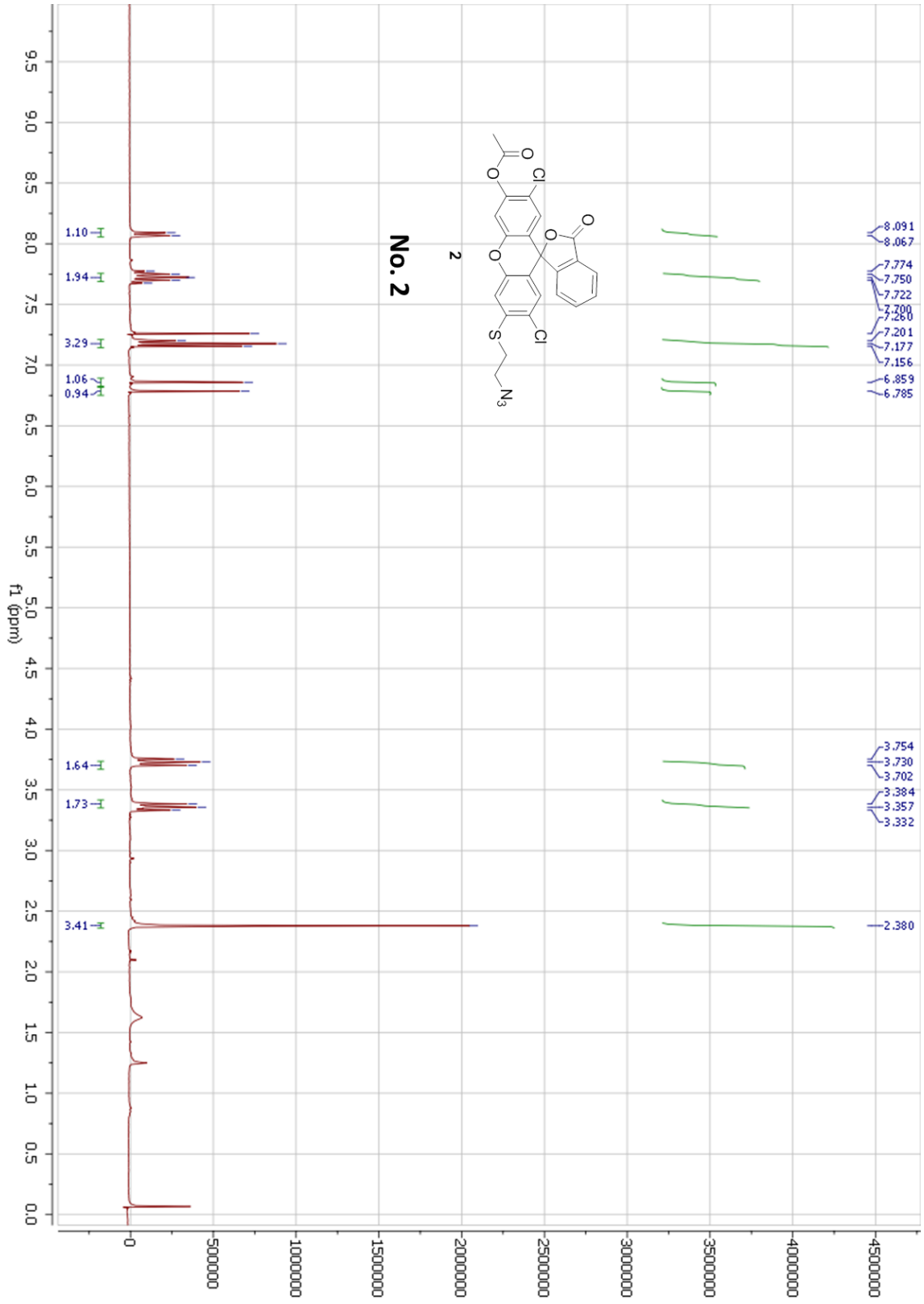

No. **(2)** C-NMR in $CDCl_3$

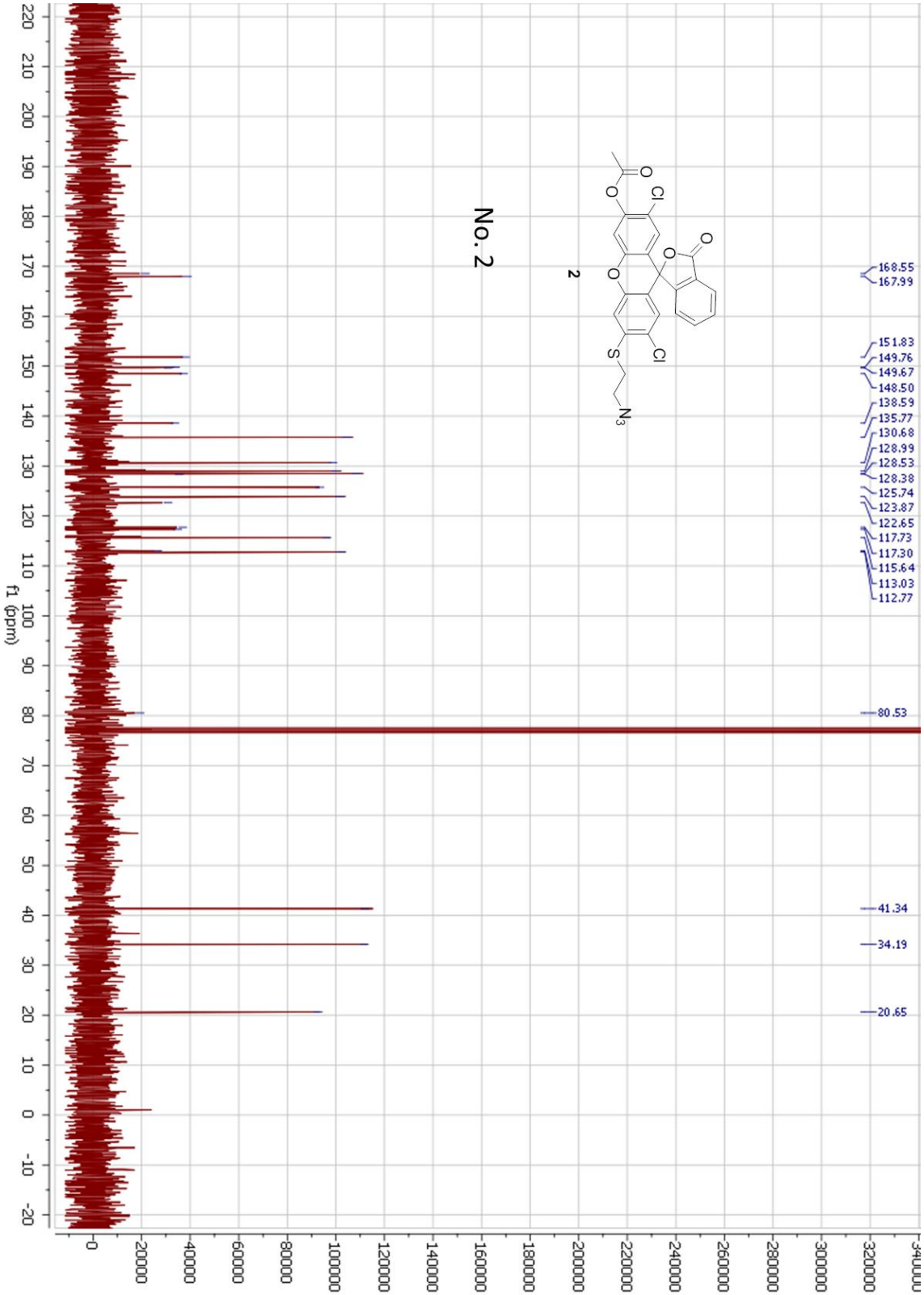

No. (**2**) FT-IR

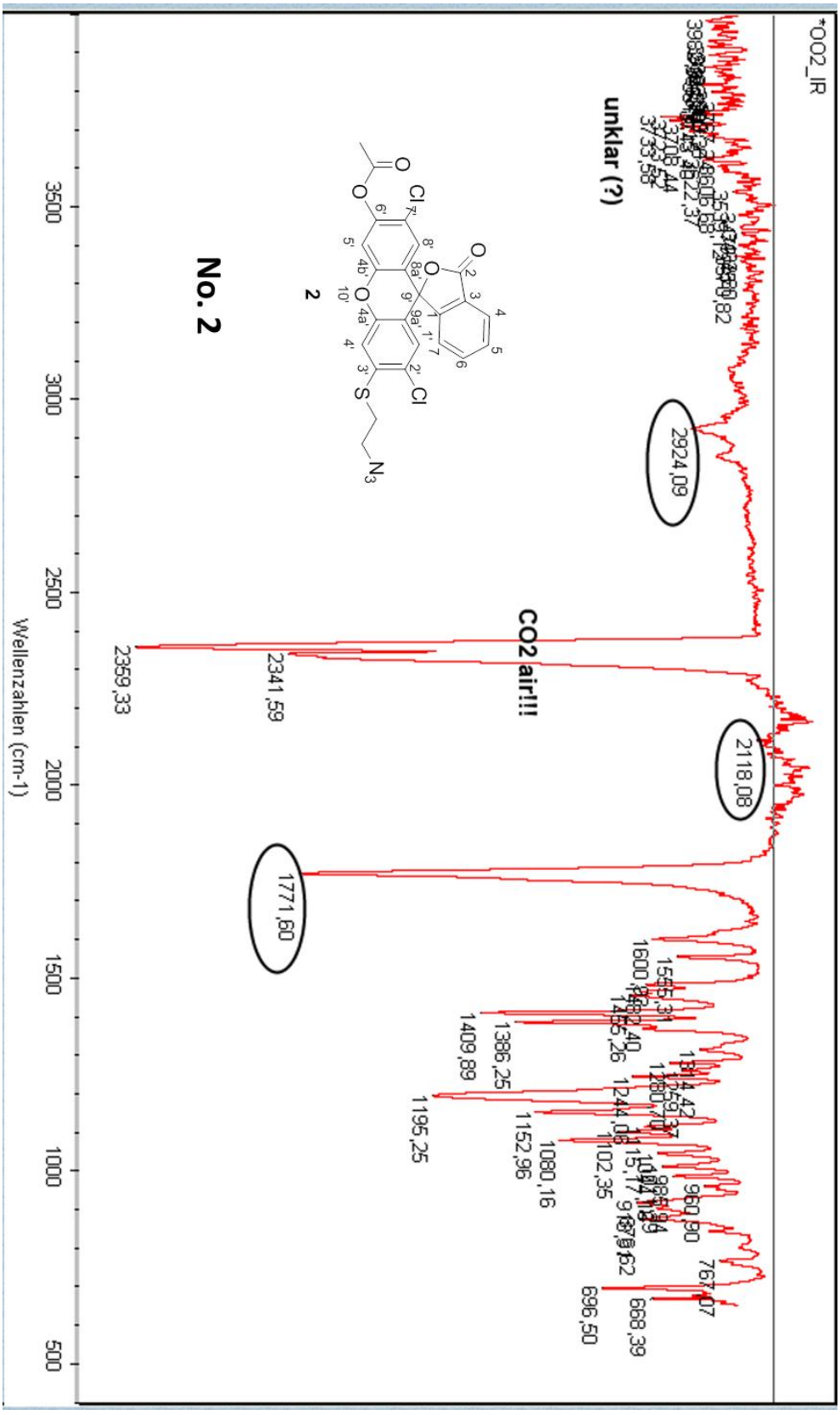
*002_IR
unklar (?)
No. 2
CO2 air!!!
2924,09
2118,08
1771,60
2359,33
2341,59
1600,78
1565,31
1409,89
1386,25
1195,25
1152,96
1080,16
960,90
767,07
696,50
668,39
Wellenzahlen (cm-1)
3500
3000
2500
2000
1500
1000
500

No. (**3**) H-NMR in DMSO-d6

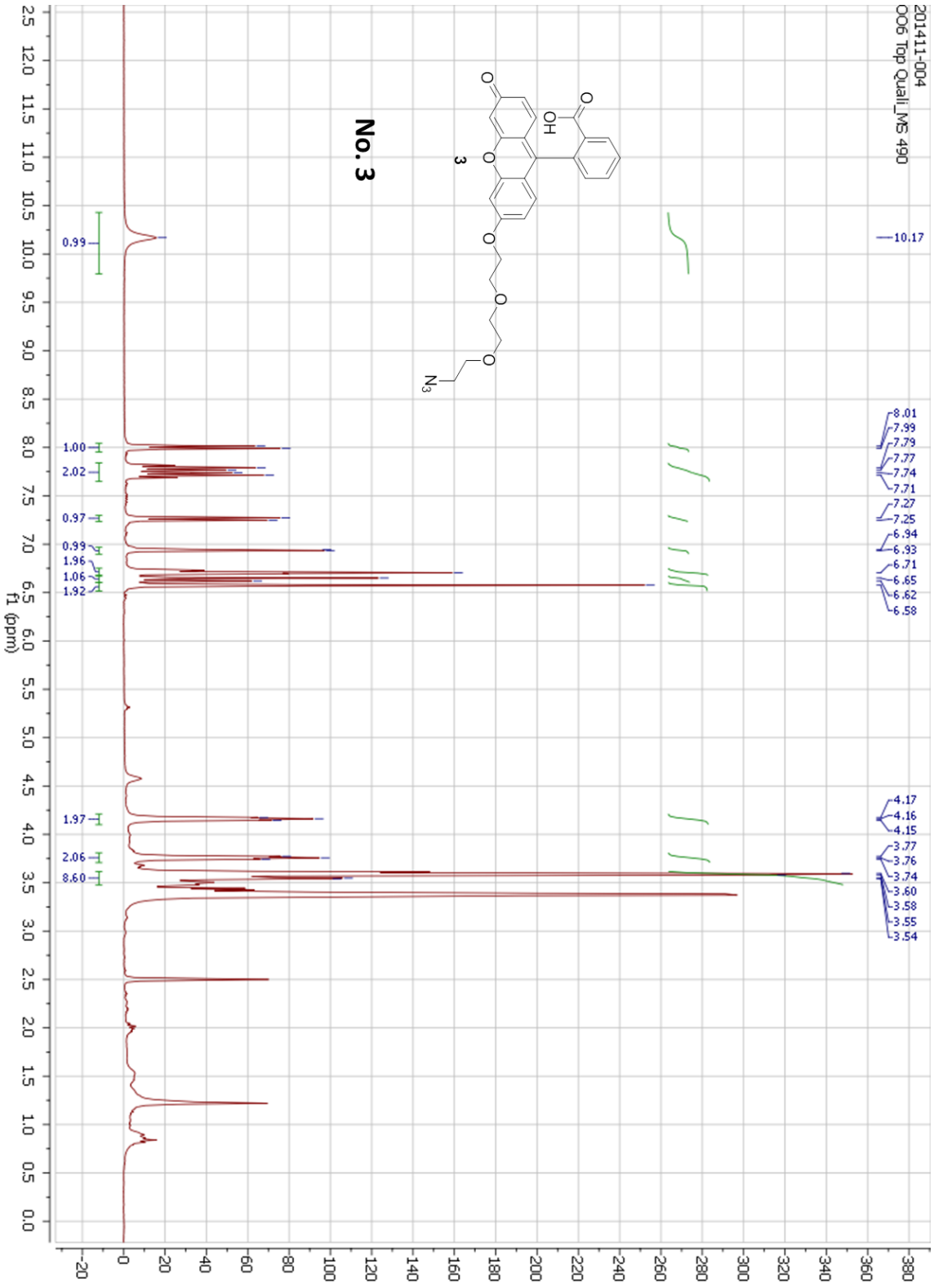

No. (**3**) C-NMR in DMSO-d6

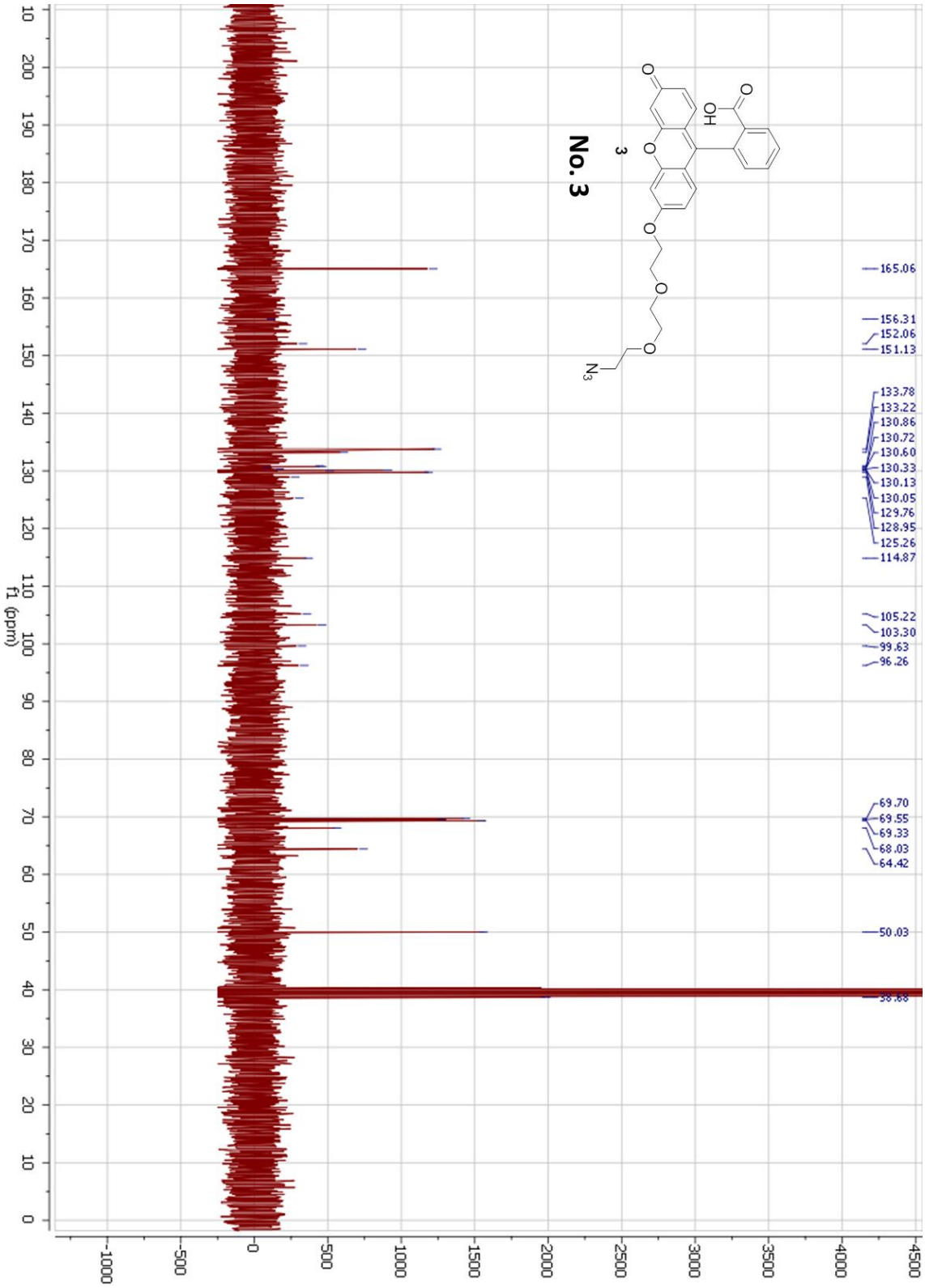

No. (**3**) ESI-MS in ACN (positive scan mode)

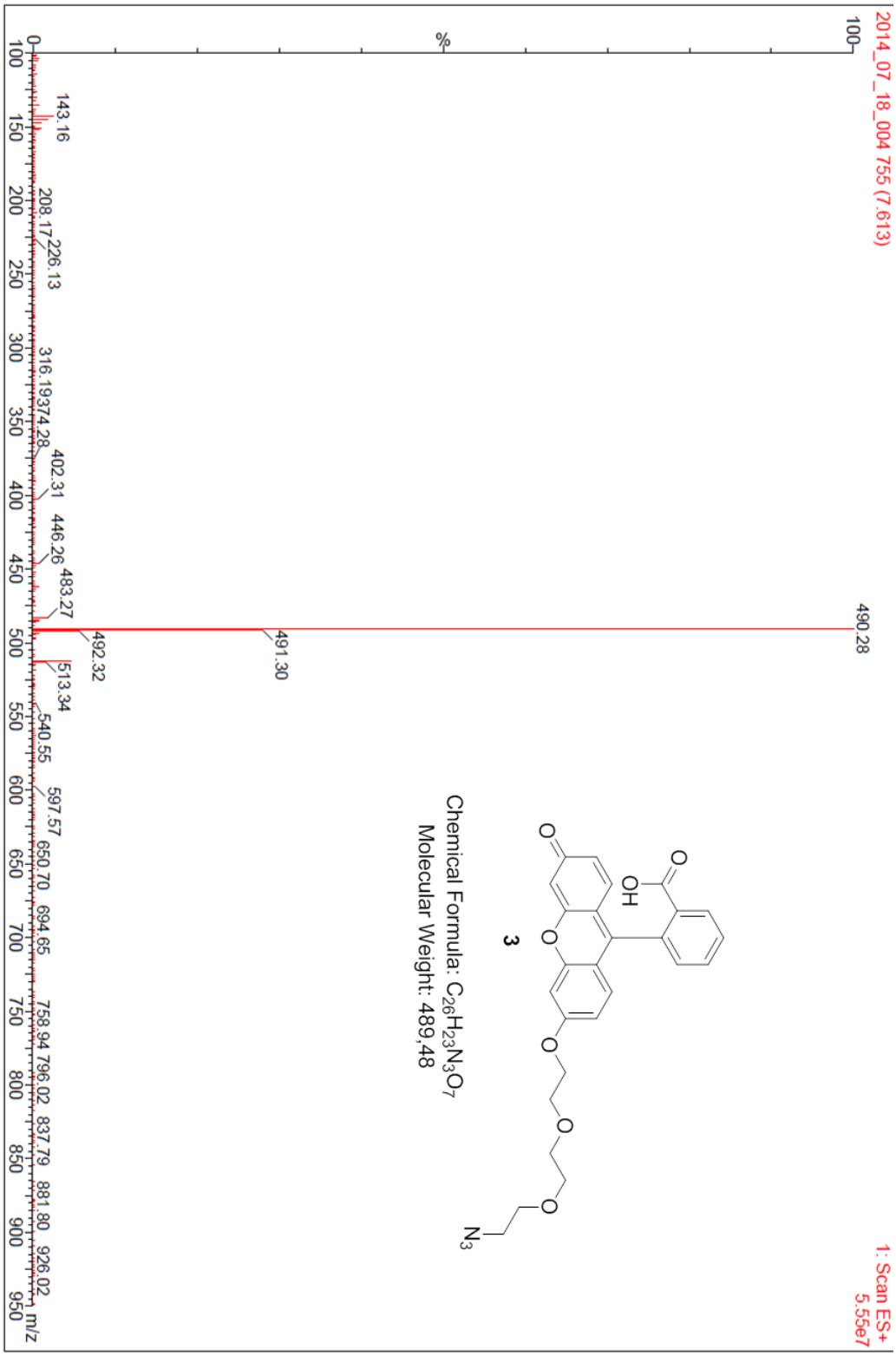

No. (**3**) ESI-MS in ACN (negative scan mode)

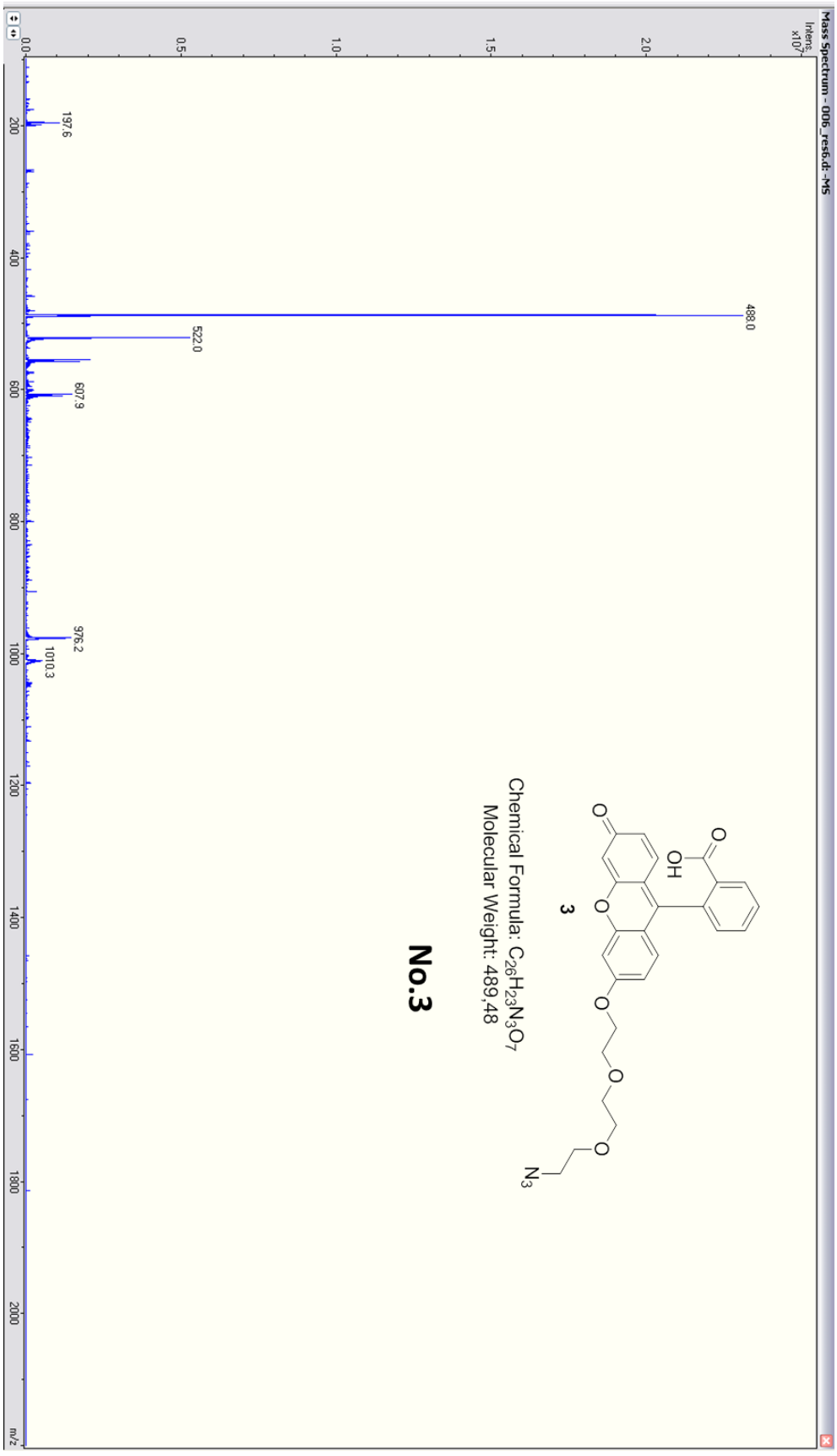

No. (**3**) FT-IR

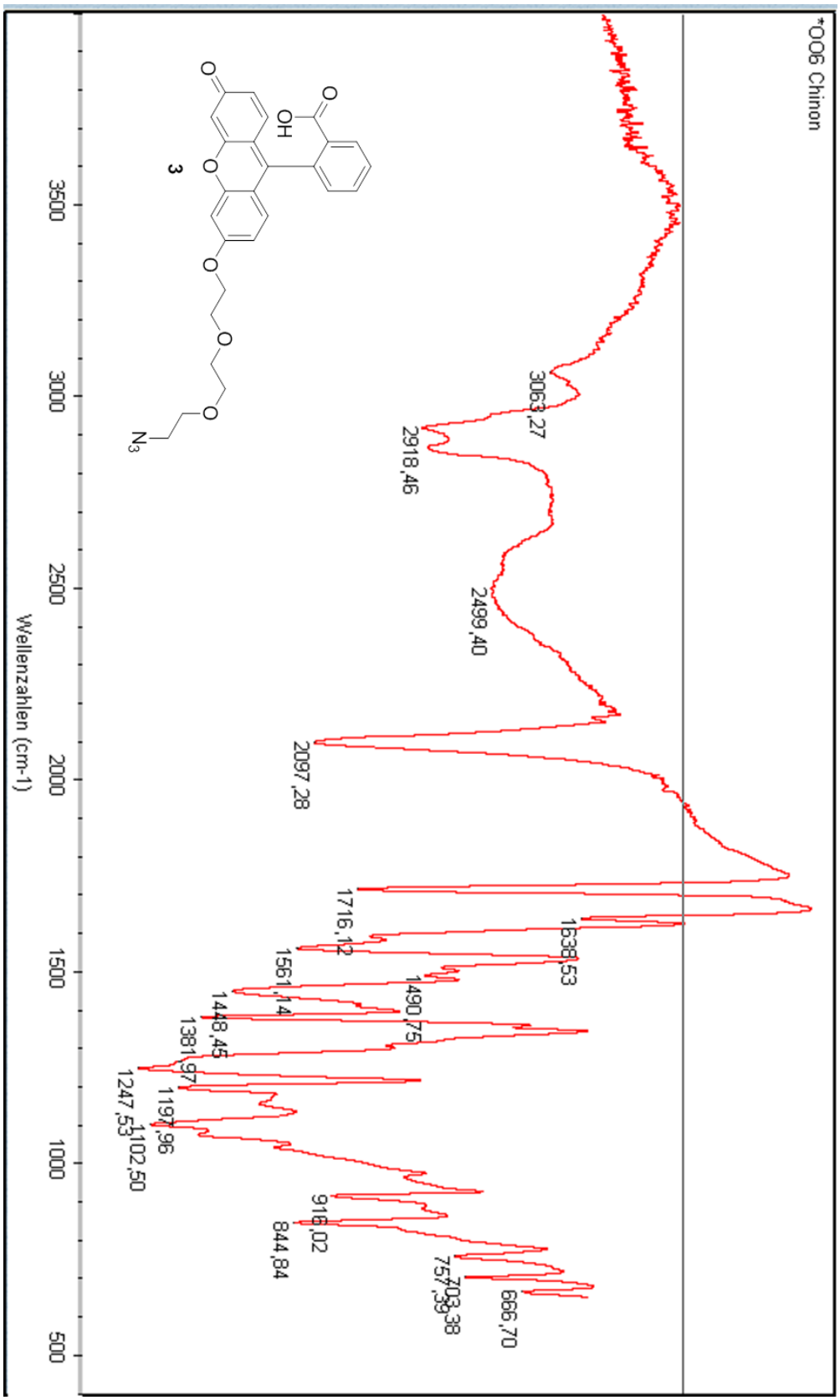
*006 Chinon
3063,27
2918,46
2499,40
2097,28
1716,12
1638,53
1561,74
1490,75
1448,45
1381,97
1247,53
1197,96
1102,50
916,02
844,84
757,39
703,38
666,70
Wellenzahlen (cm-1)
3500
3000
2500
2000
1500
1000
500
OH
O
O
O
O
O
O
O
N3
3

No. (**4**) H-NMR in DMSO-d6

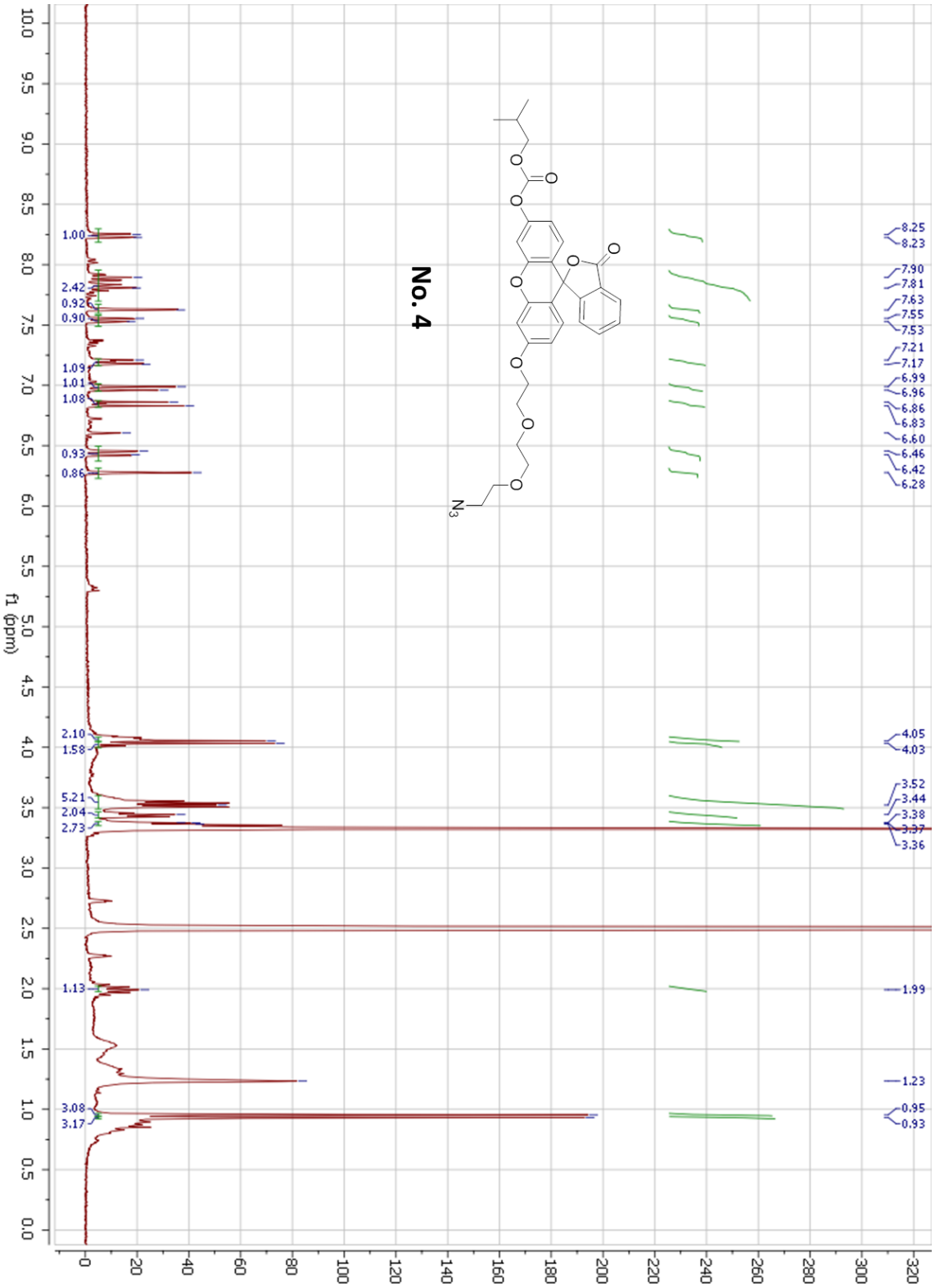

No. (**4**) C-NMR in DMSO-d6

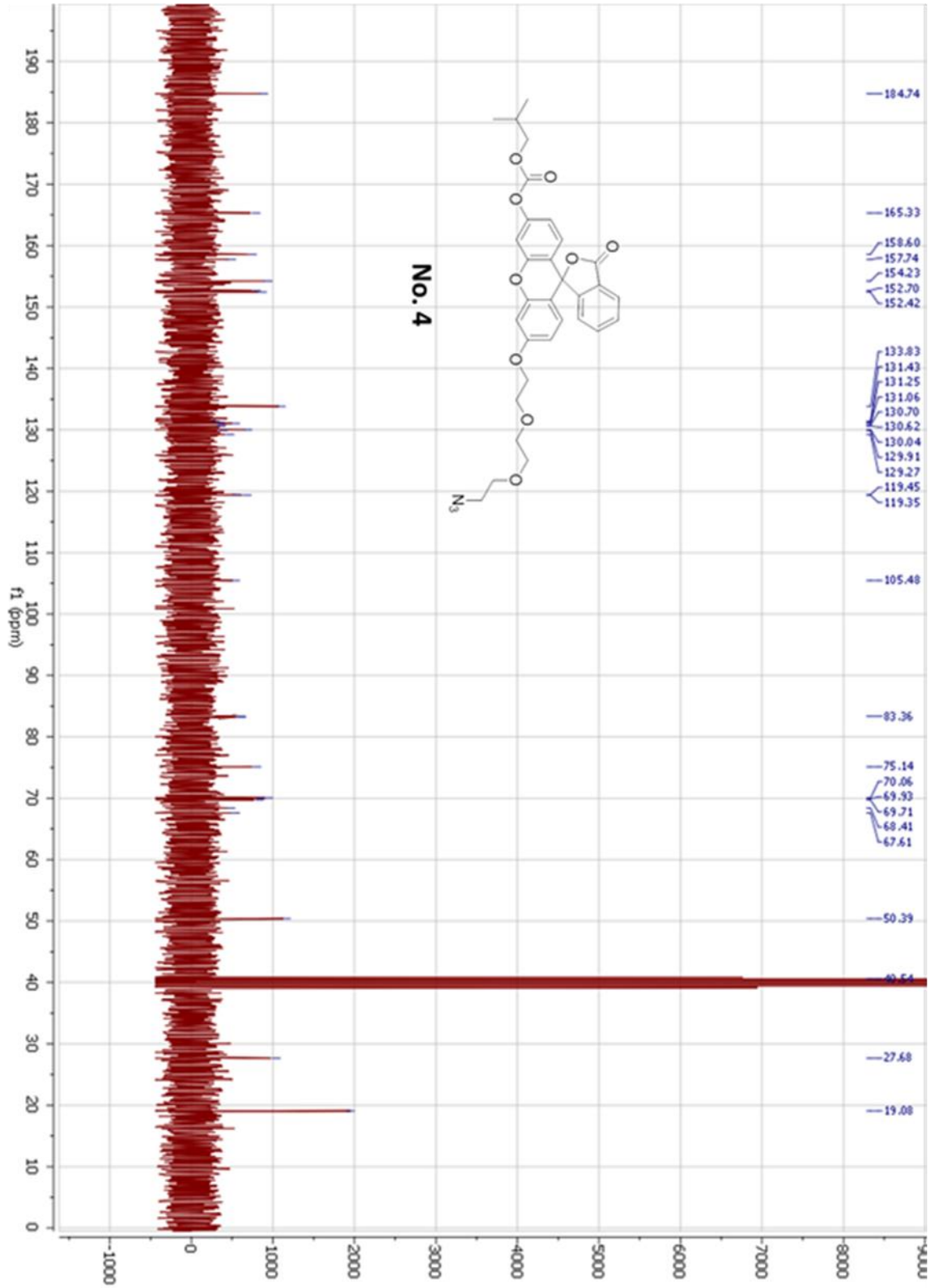

No. (**4**) ESI in MeOH (pos. scan mode)

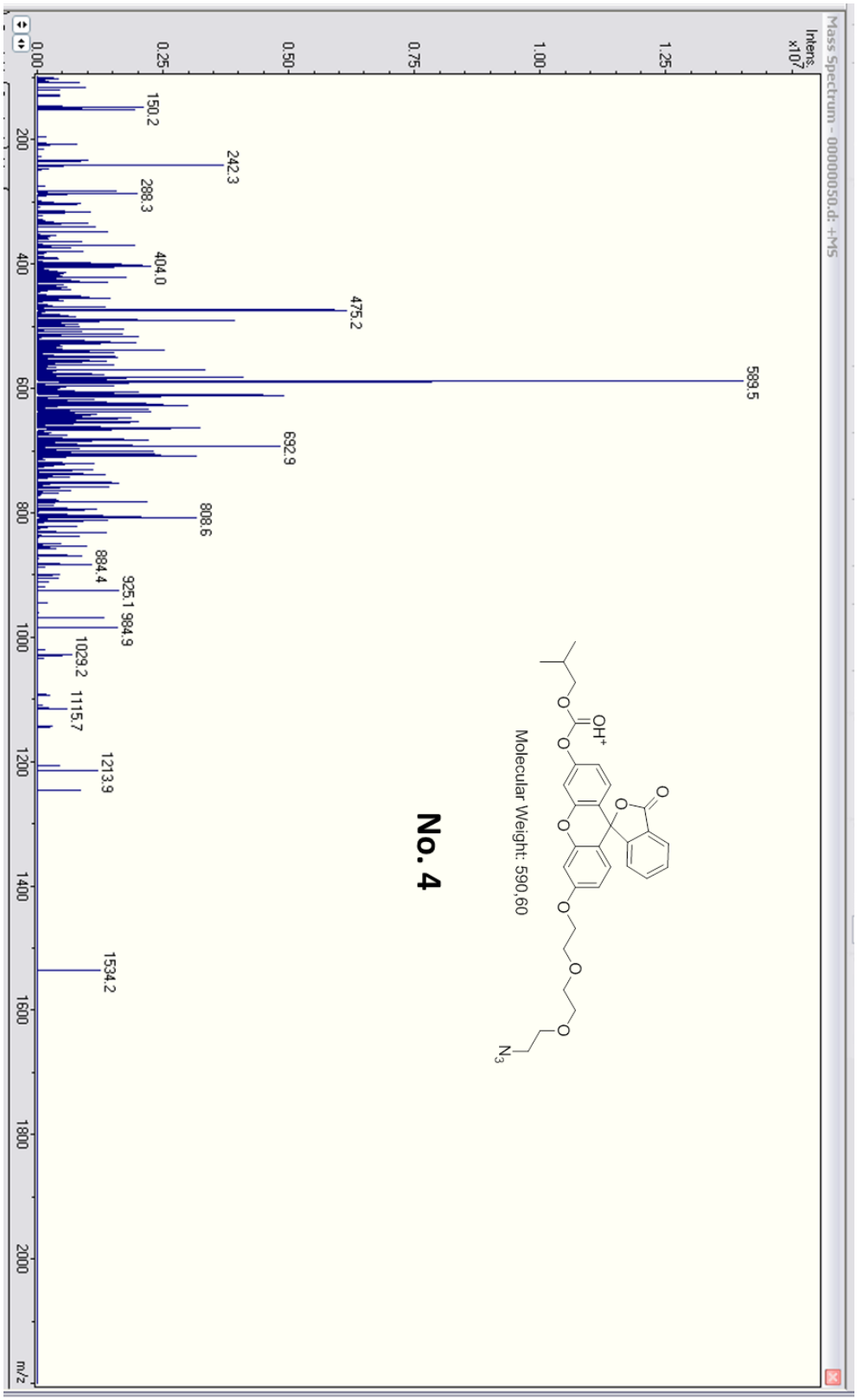

No. (**4**) ESI in ACN: fragmentation pattern of motherion (positive scan mode)

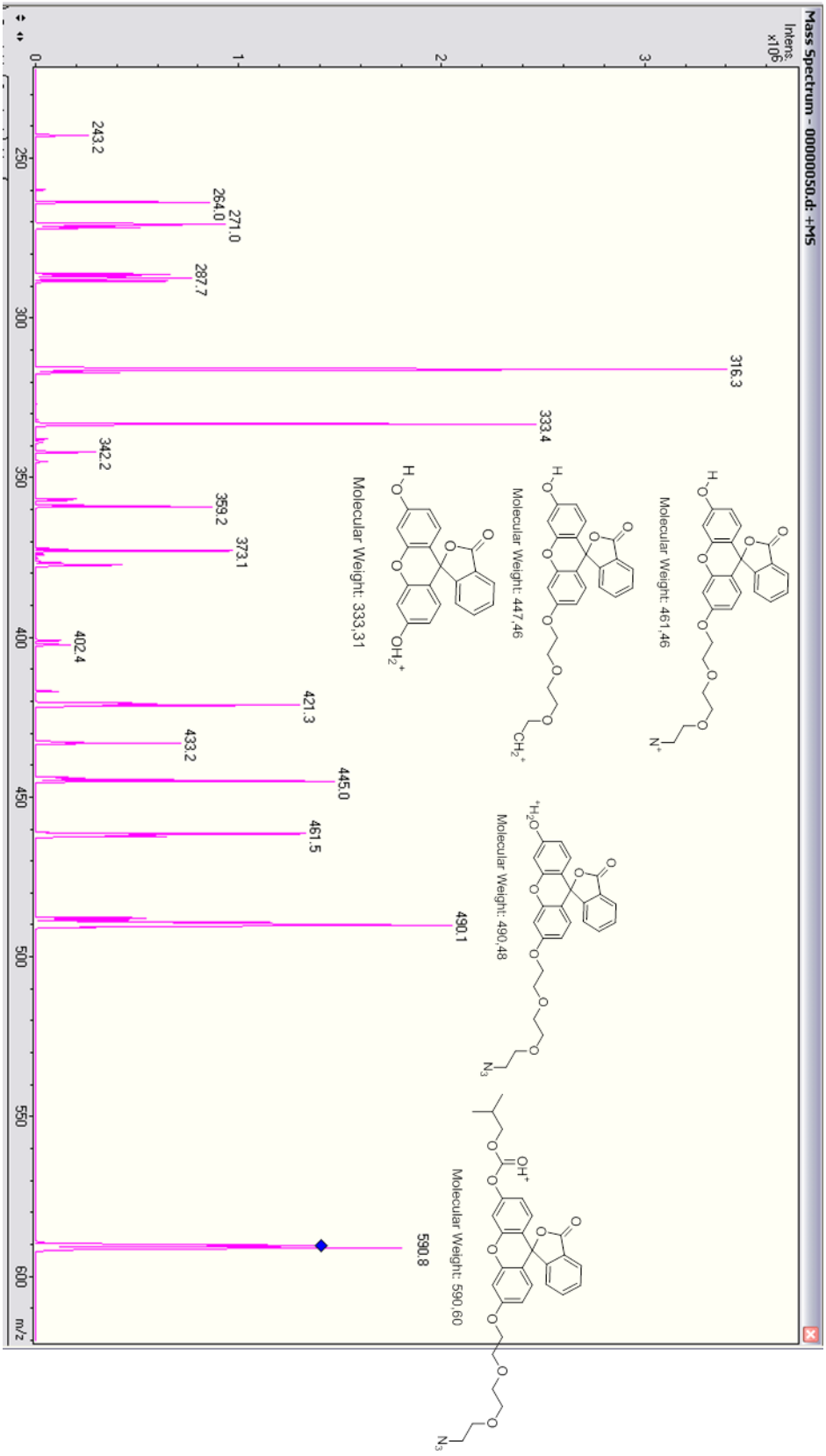

No. (**4**) FT-IR

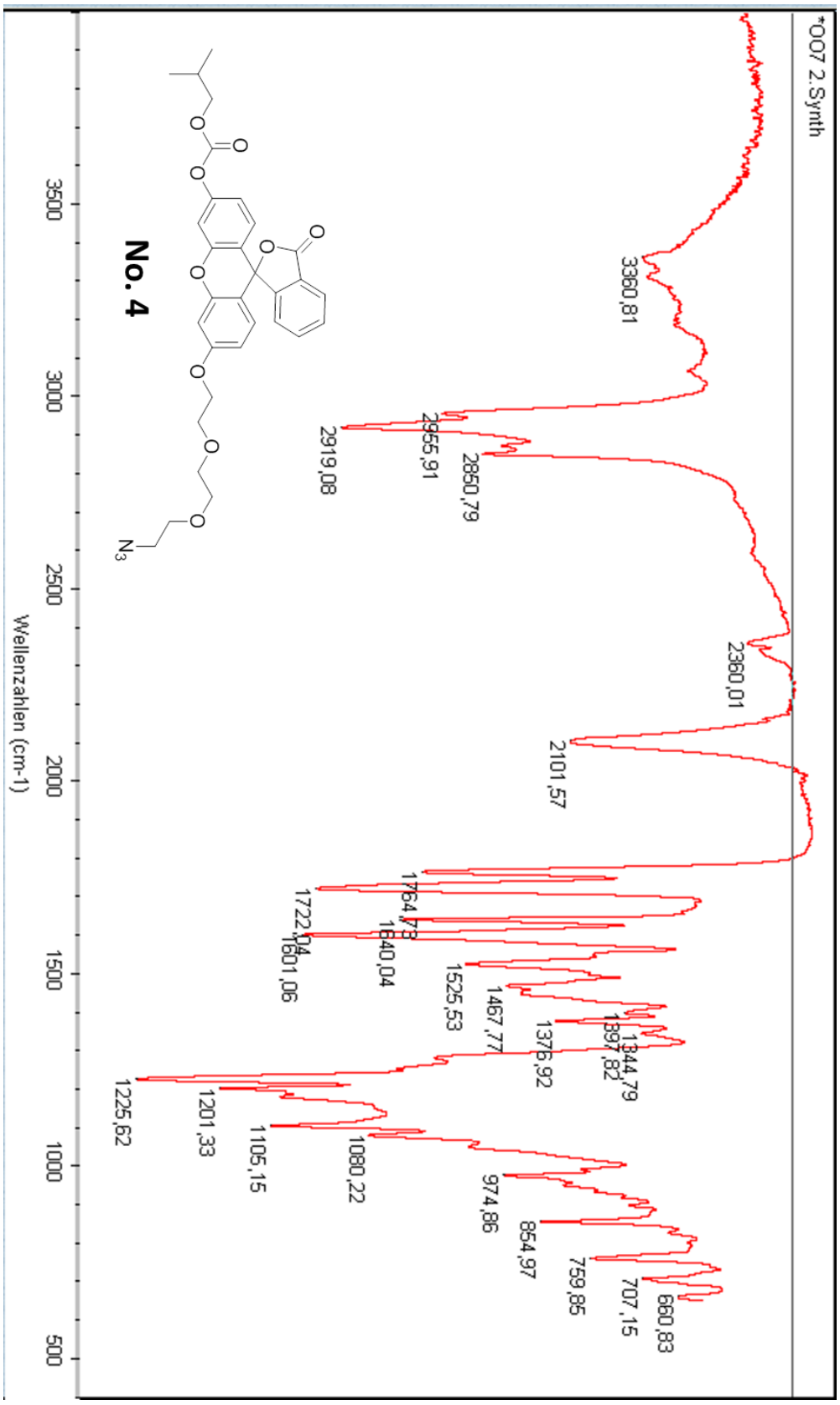
*007 2.Synth
No. 4
3360,81
2919,08
2955,91
2850,79
2360,01
2101,57
1764,73
1722,04
1801,06
1640,04
1525,53
1467,77
1397,82
1344,79
1376,92
1225,62
1201,33
1105,15
1080,22
974,86
854,97
759,85
707,15
660,83
3500
3000
2500
2000
1500
1000
500
Wellenzahlen (cm-1)

No. (**5**) H-NMR in DMSO-d6

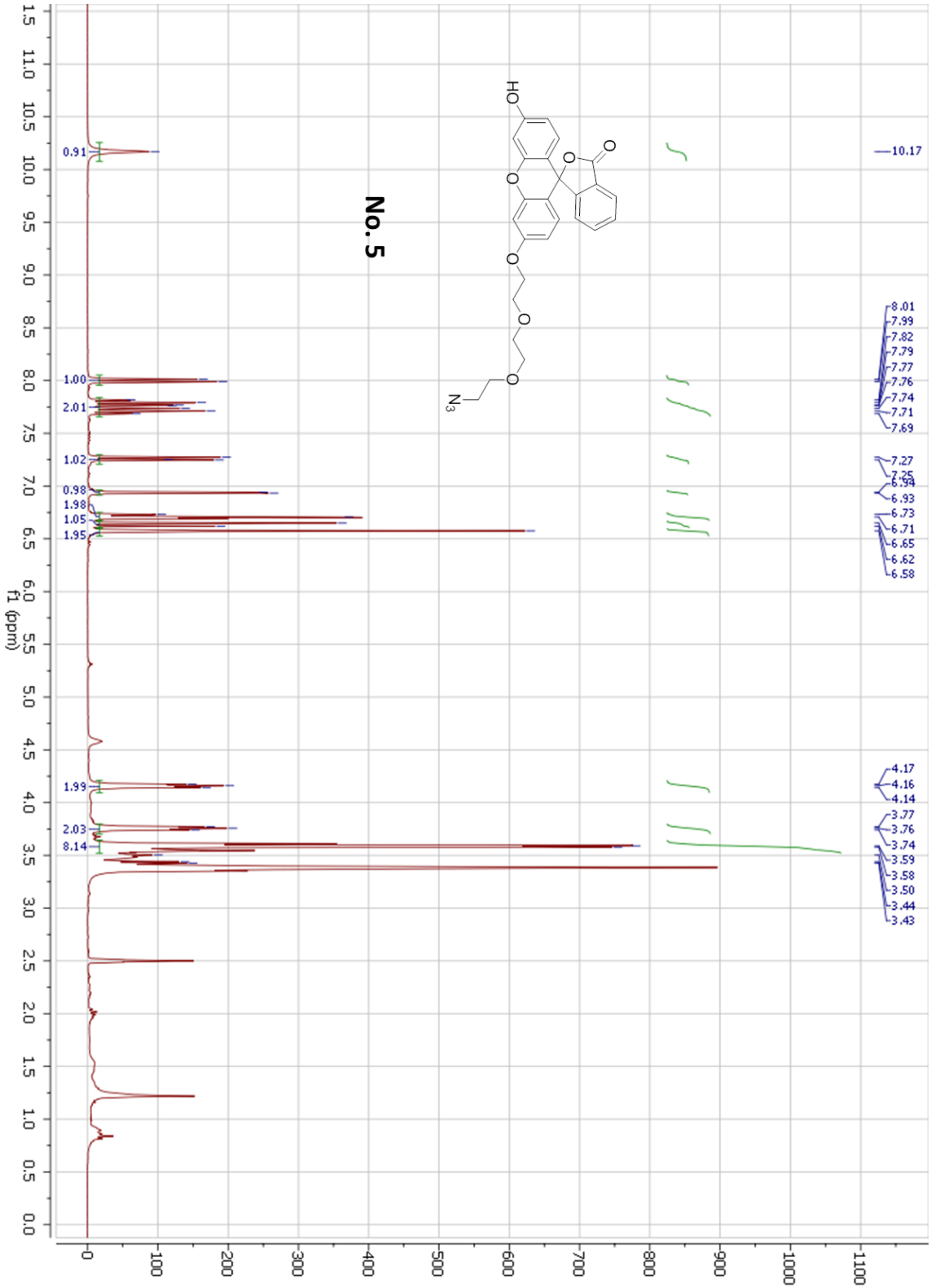

No. (**5**) C-NMR in DMSO-d6

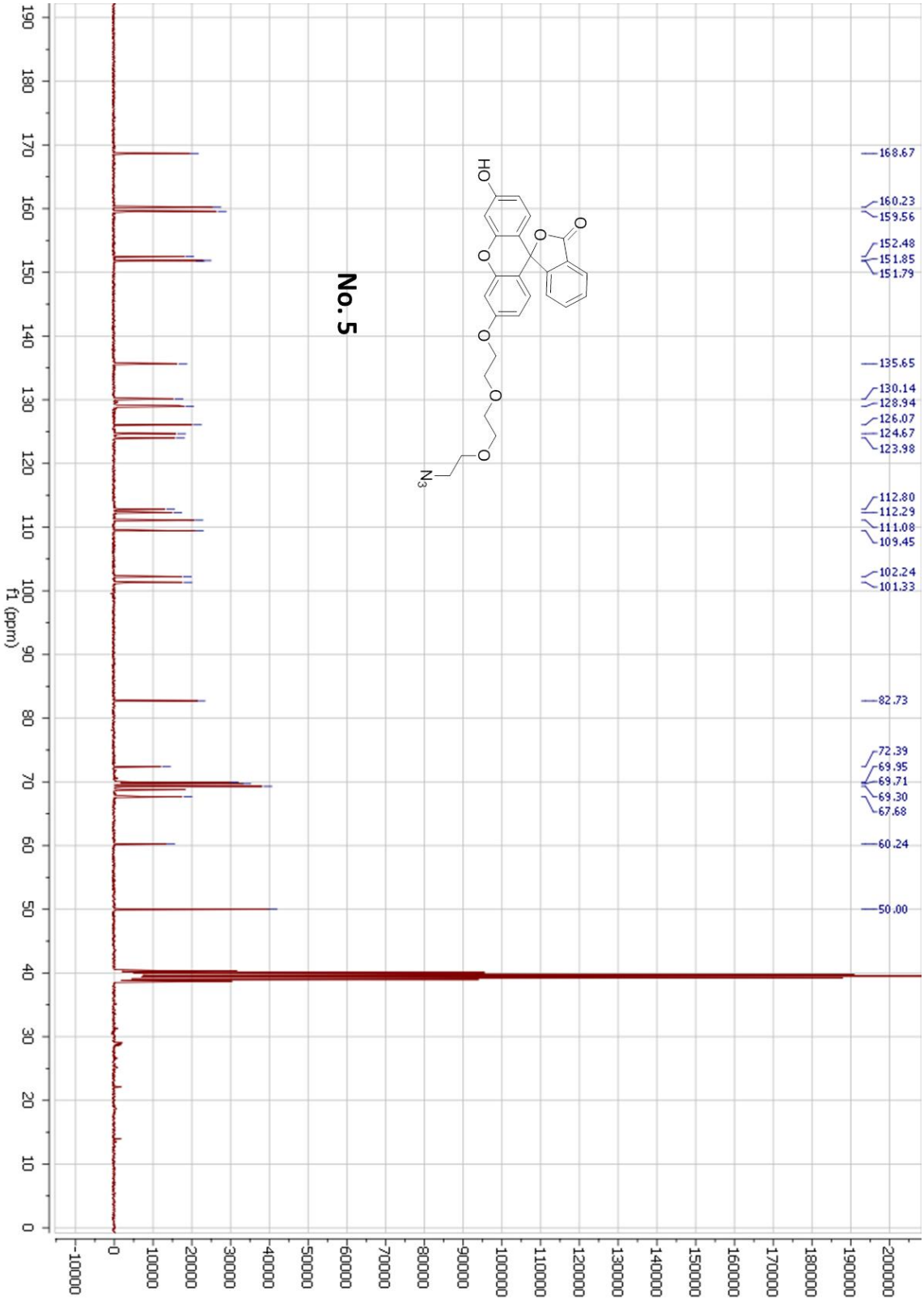

No. (**5**) ESI in ACN (pos. scan mode)

No. (**5**) ESI in ACN (pos. scan mode)

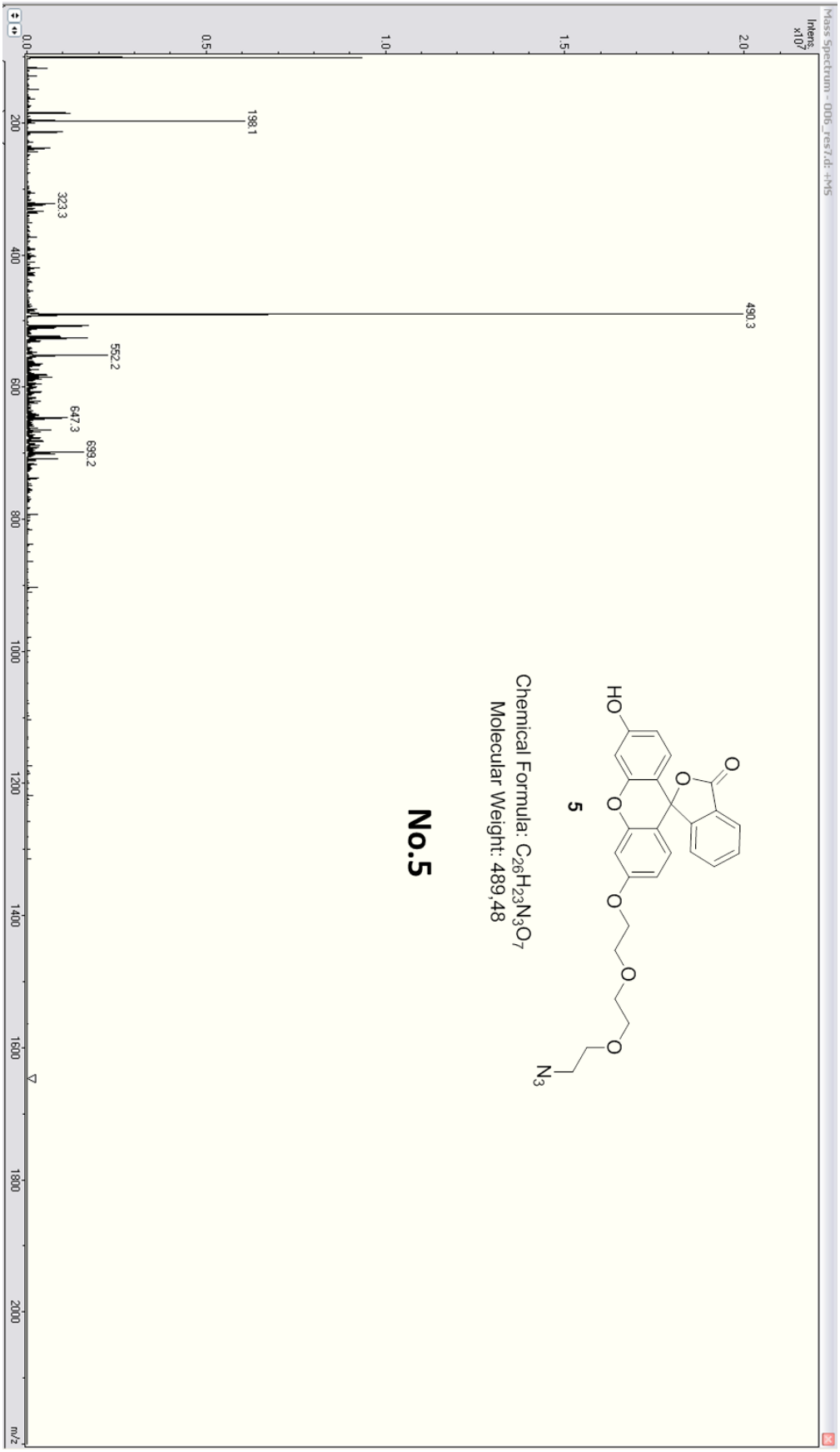

No. (**5**) FT-IR

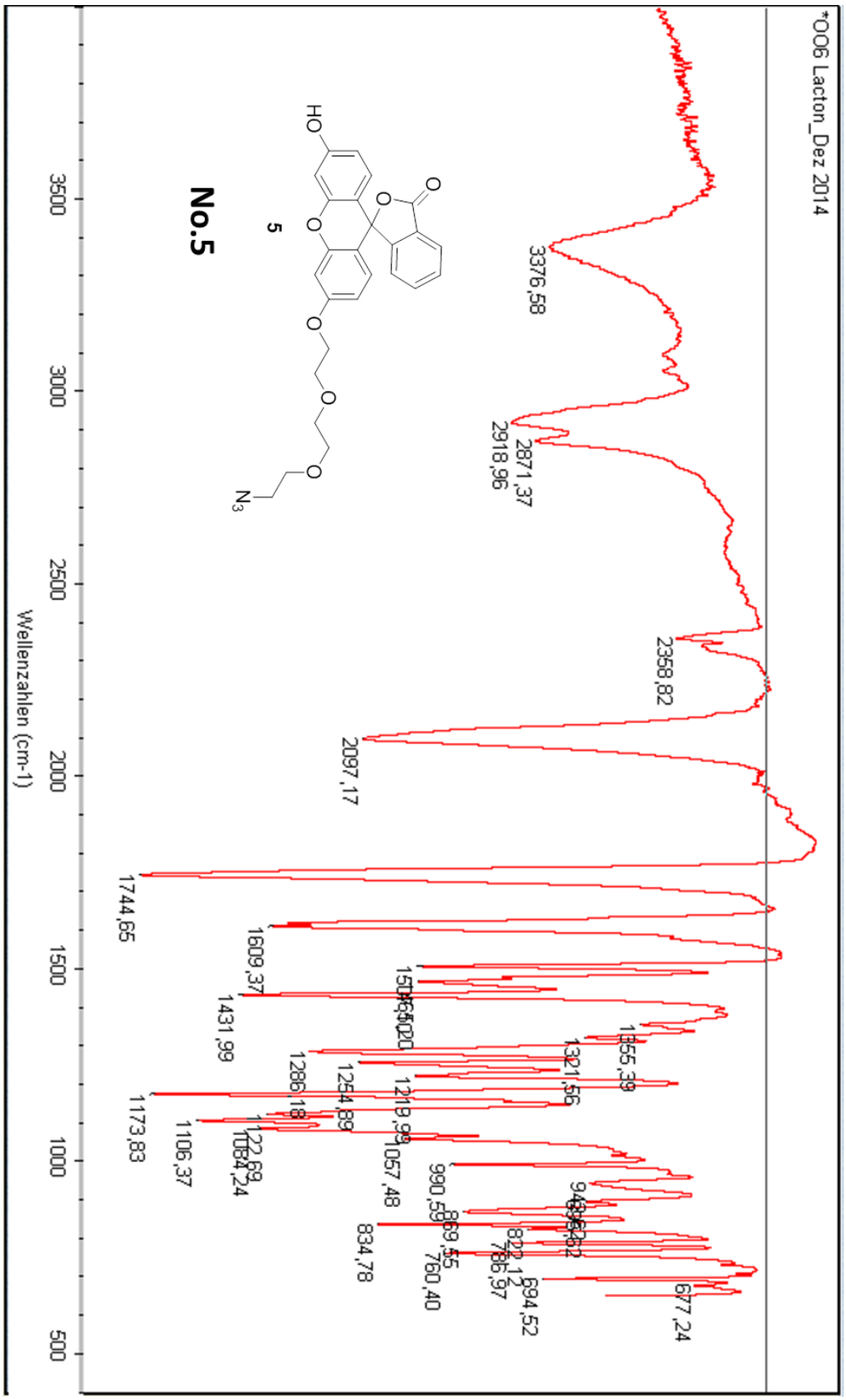
*006 Lacton_Dez 2014
No.5
5
HO
O
O
O
O
O
O
O
N3
3376,58
2918,96
2871,37
2358,82
2097,17
1744,65
1609,37
1431,99
1321,56
1254,89
1219,99
1173,83
1106,37
1084,24
1057,48
990,59
834,78
760,40
694,52
677,24
3500
3000
2500
2000
1500
1000
500
Wellenzahlen (cm-1)

No. (**6**) H-NMR in DMSO-d6

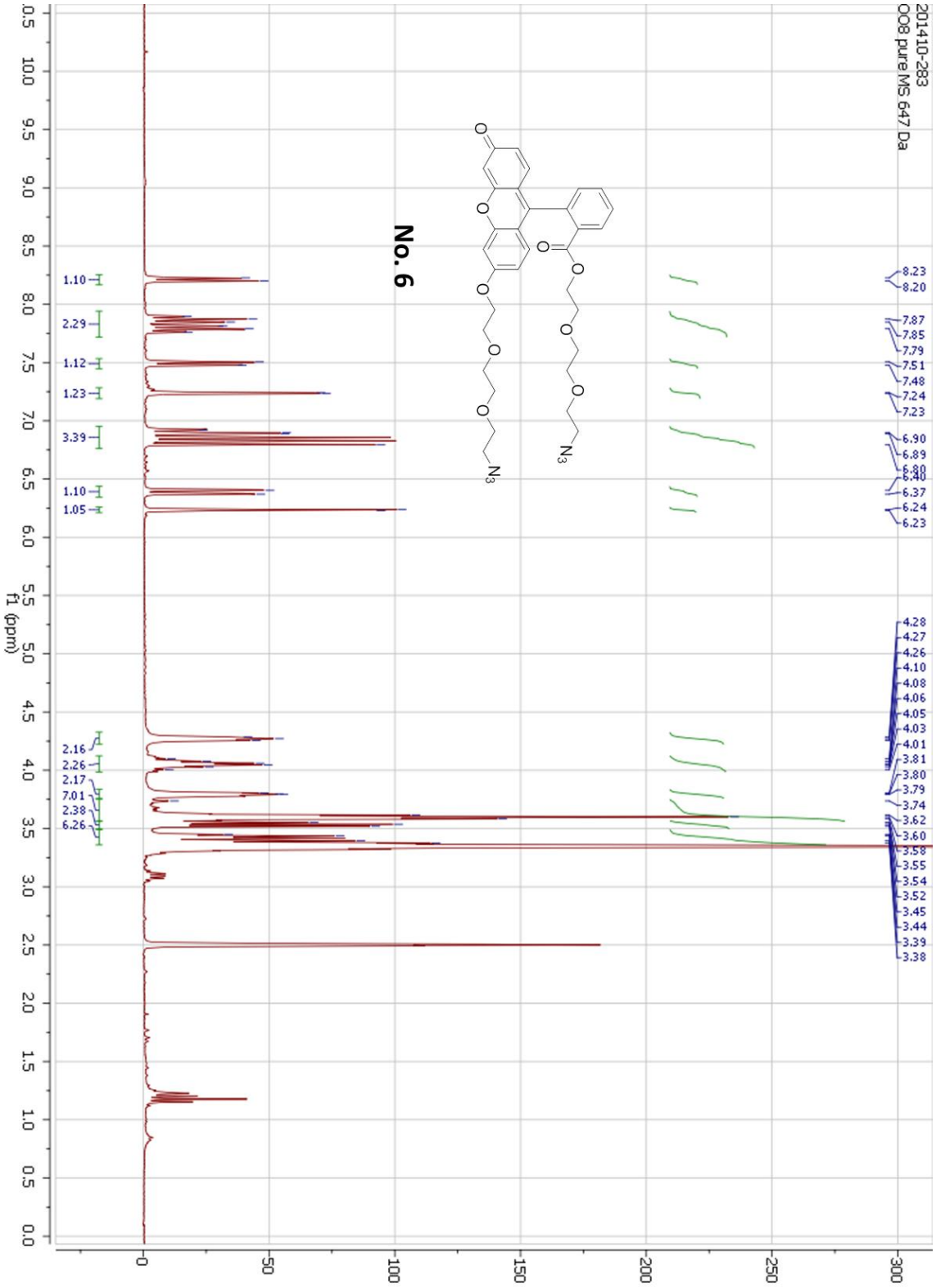

No. (**6**) C-NMR in DMSO-d6

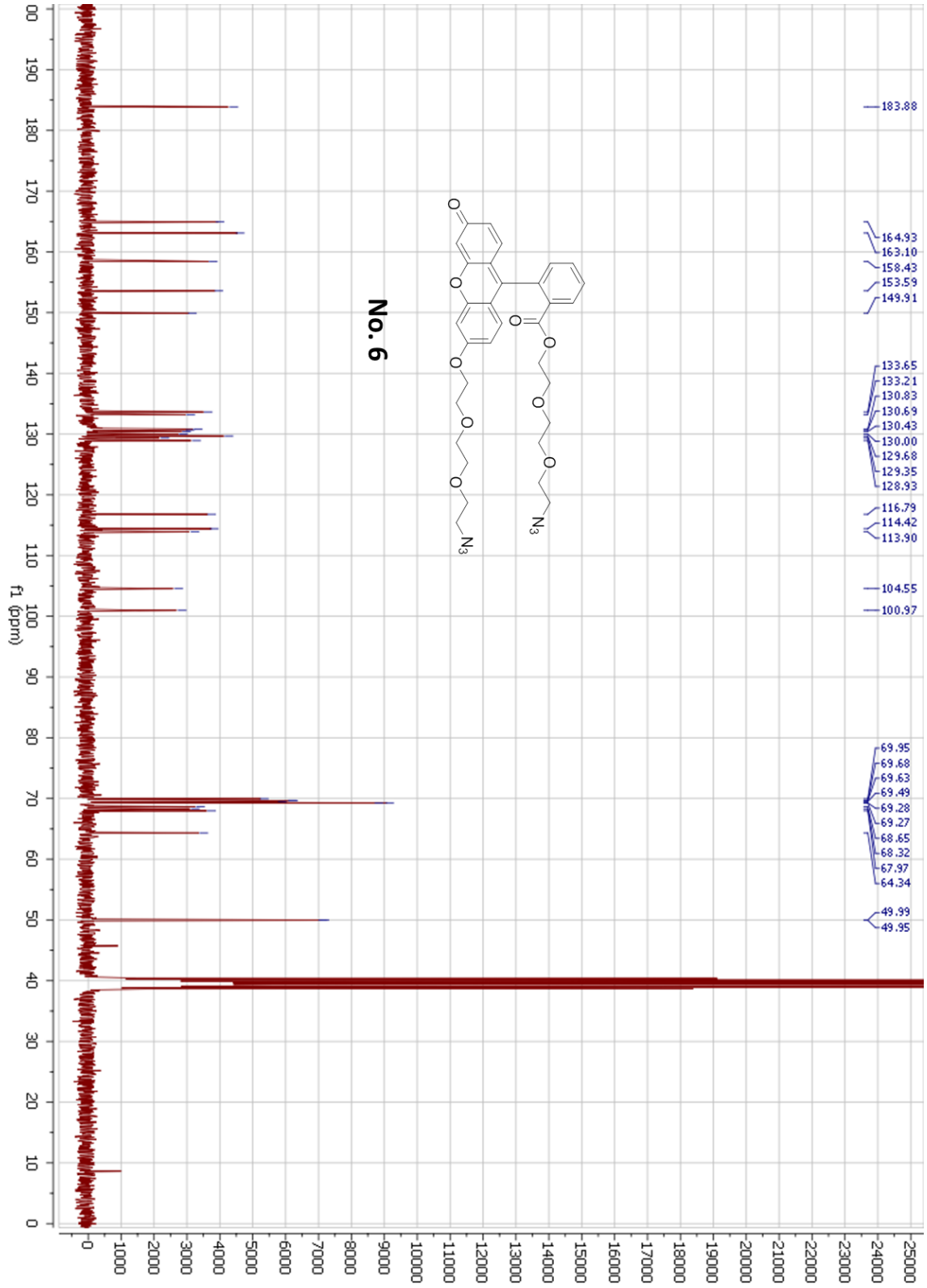

No. (**6**) ESI in ACN (pos. scan mode)

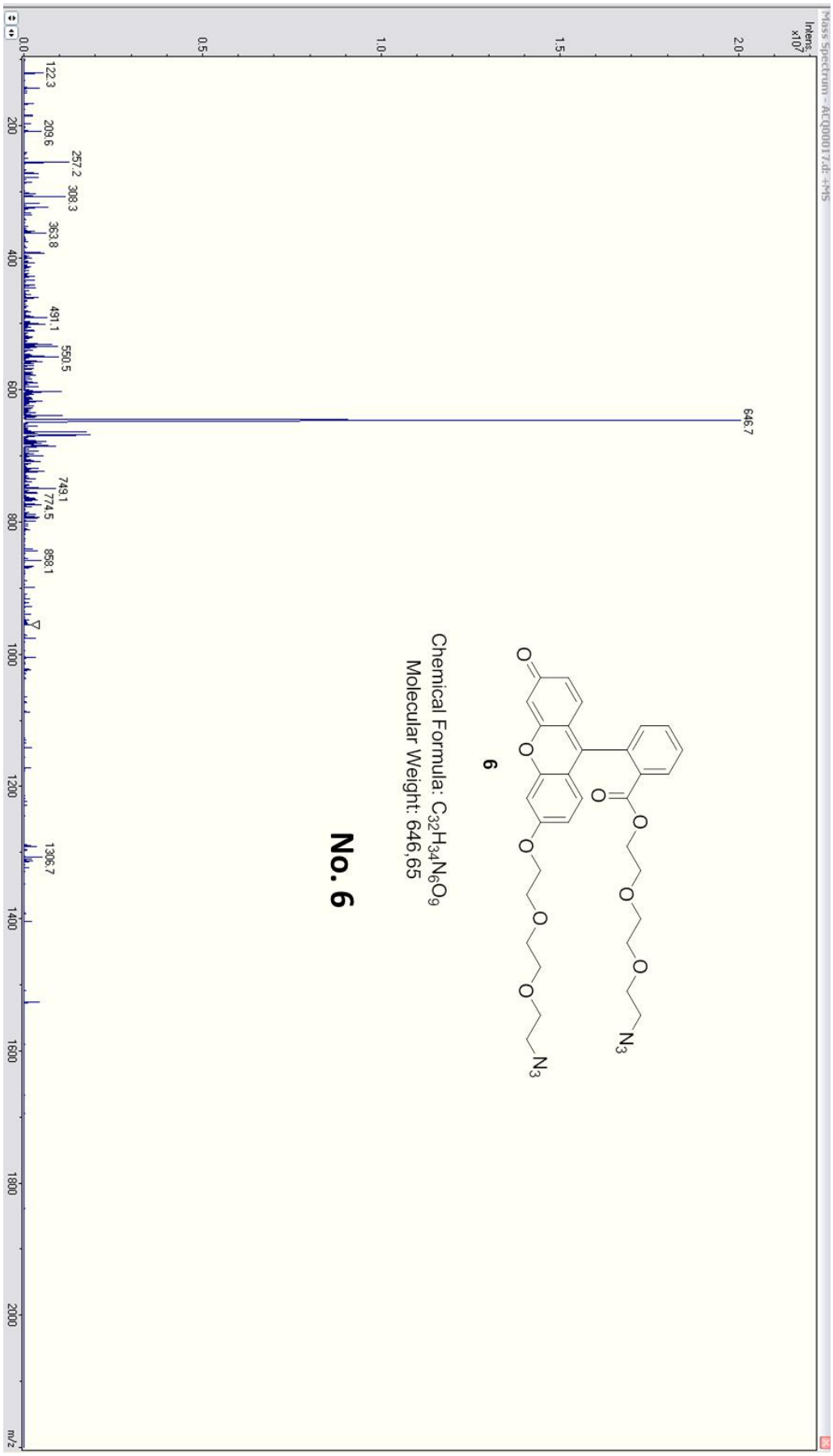

No. (**6**) FT-IR

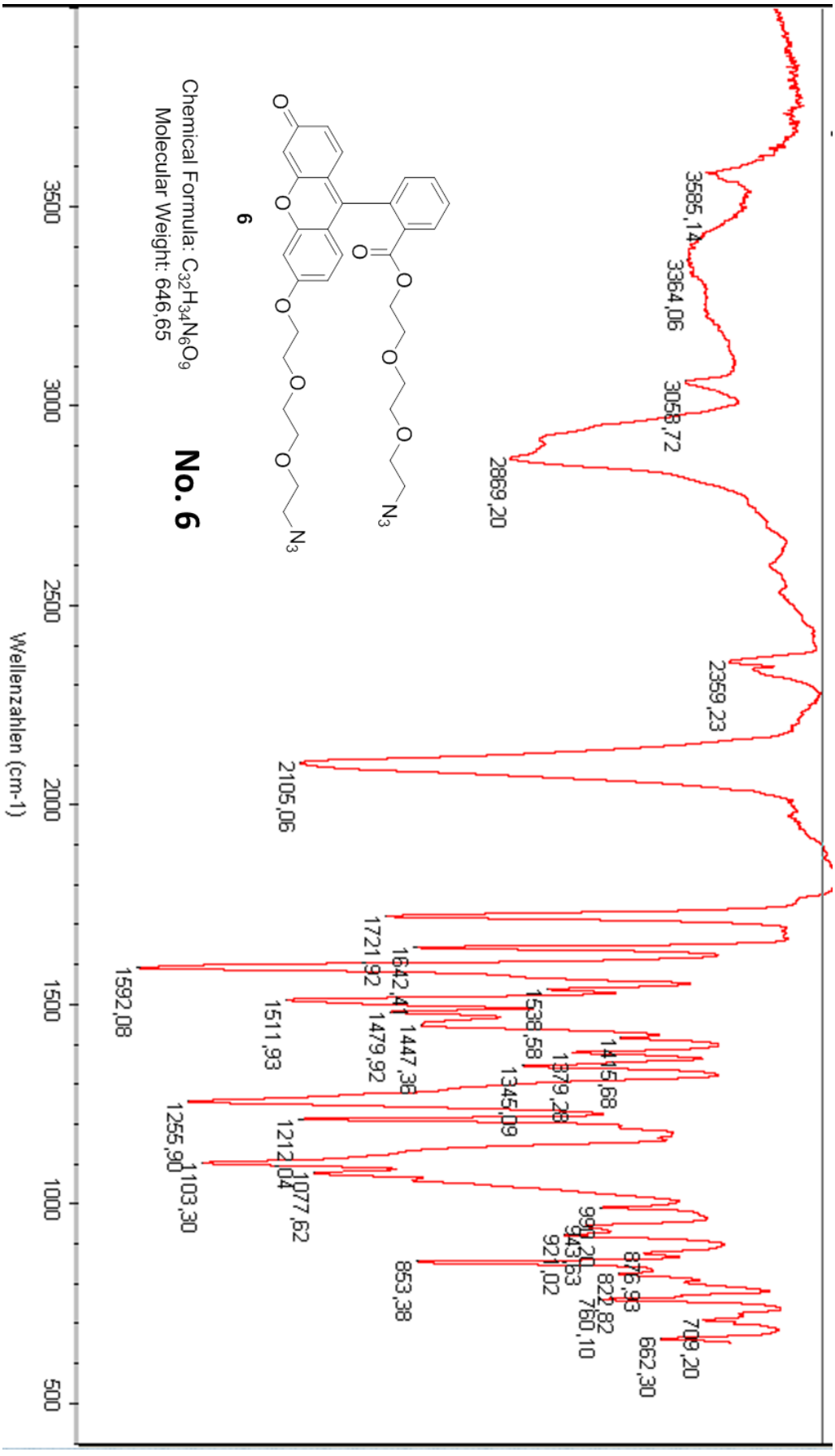
No. 6
Chemical Formula: C32H34N6O9
Molecular Weight: 646,65
6
Wellenzahlen (cm-1)
3500
3000
2500
2000
1500
1000
500
3585,14
3364,06
3058,72
2869,20
2359,23
2105,06
1721,92
1642,41
1592,08
1538,58
1511,93
1479,92
1447,36
1415,68
1379,28
1345,09
1255,90
1212,04
1103,30
1077,62
999,20
945,63
921,02
876,93
853,38
822,82
760,10
709,20
662,30

No. (**7**) H-NMR in $CDCl_3$

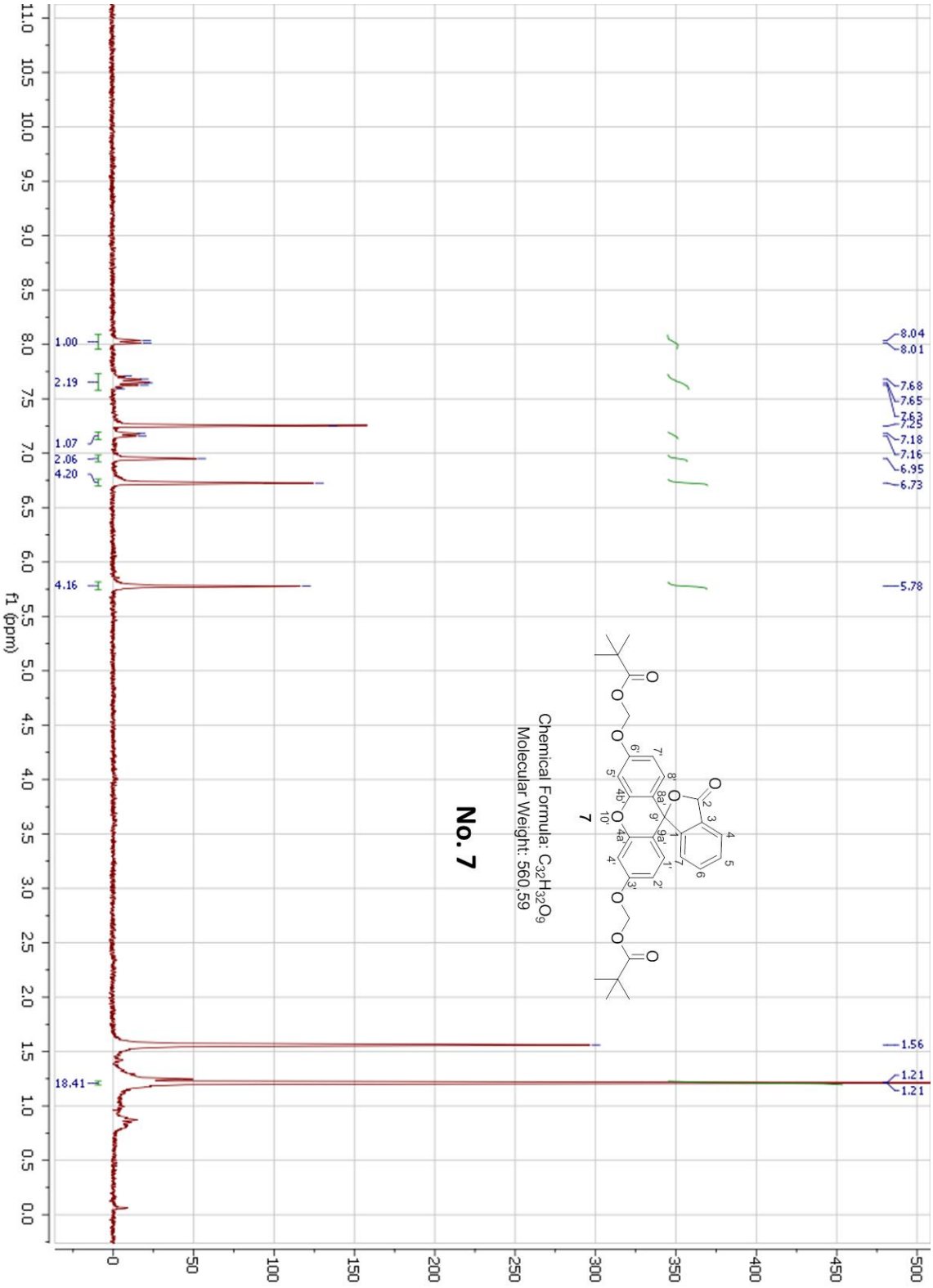

No. (**7**) C-NMR in $CDCl_3$

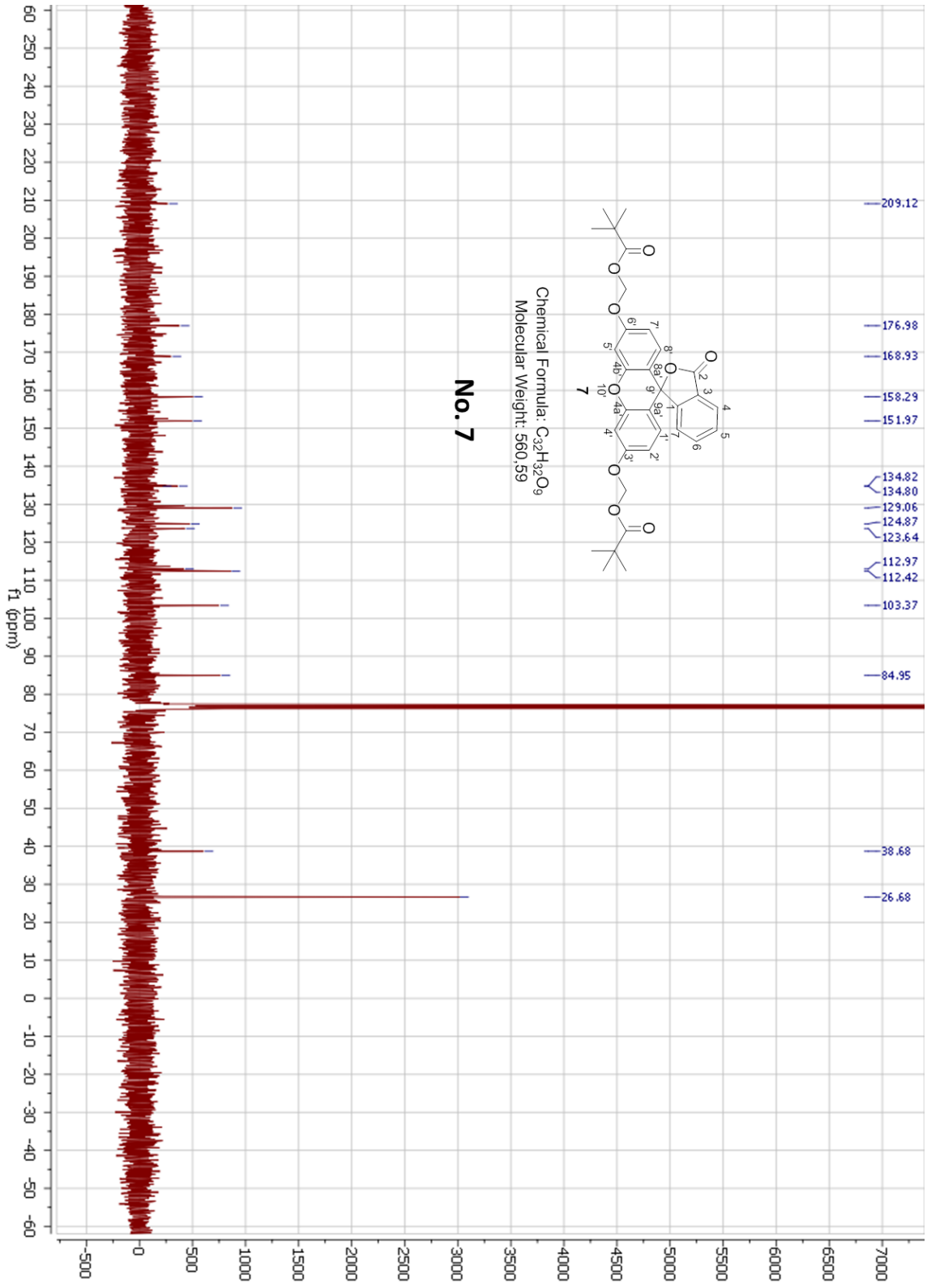

No. (**7**) ESI in ACN (pos. scan mode)

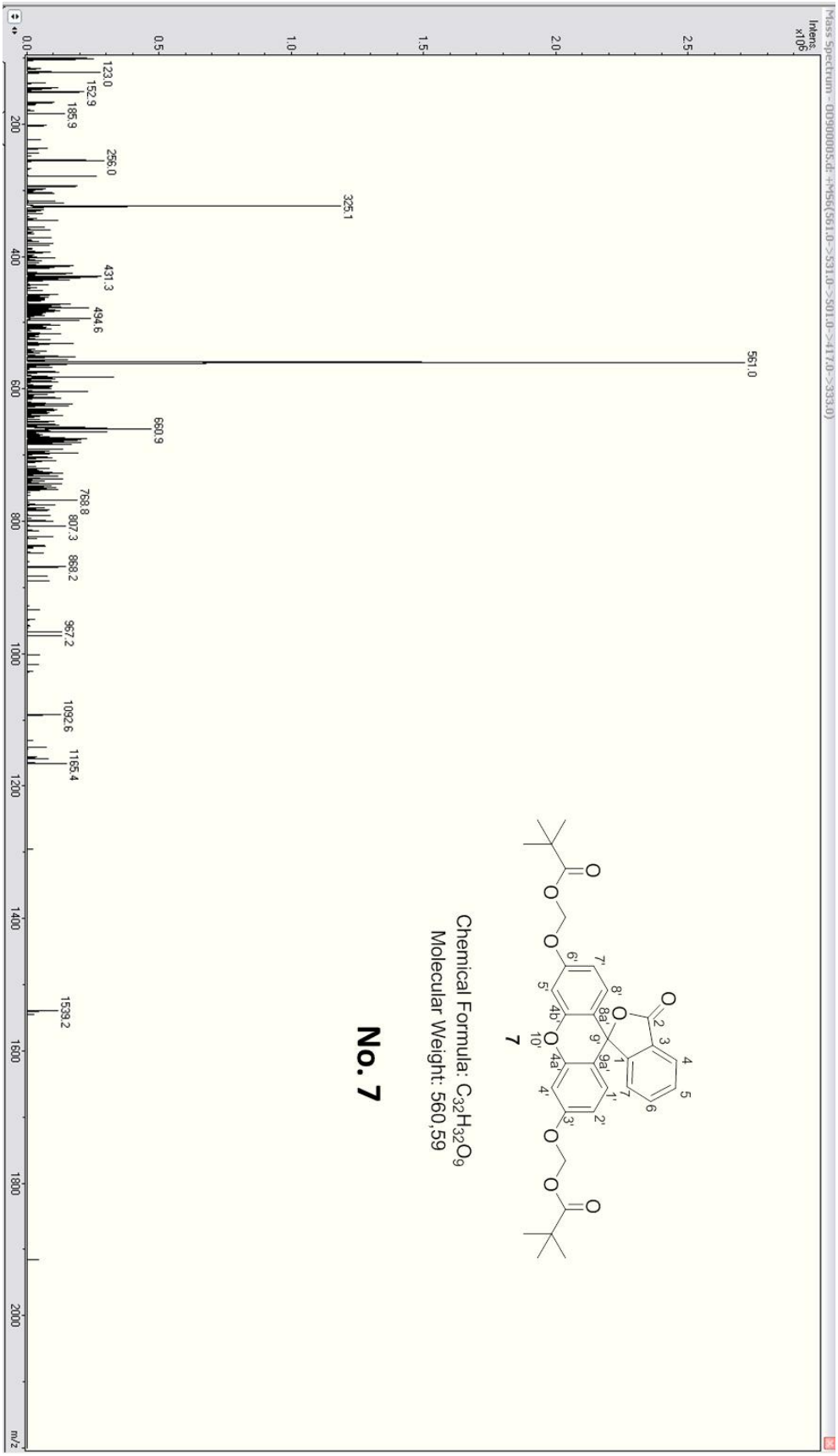

No. (**7**) FT-IR

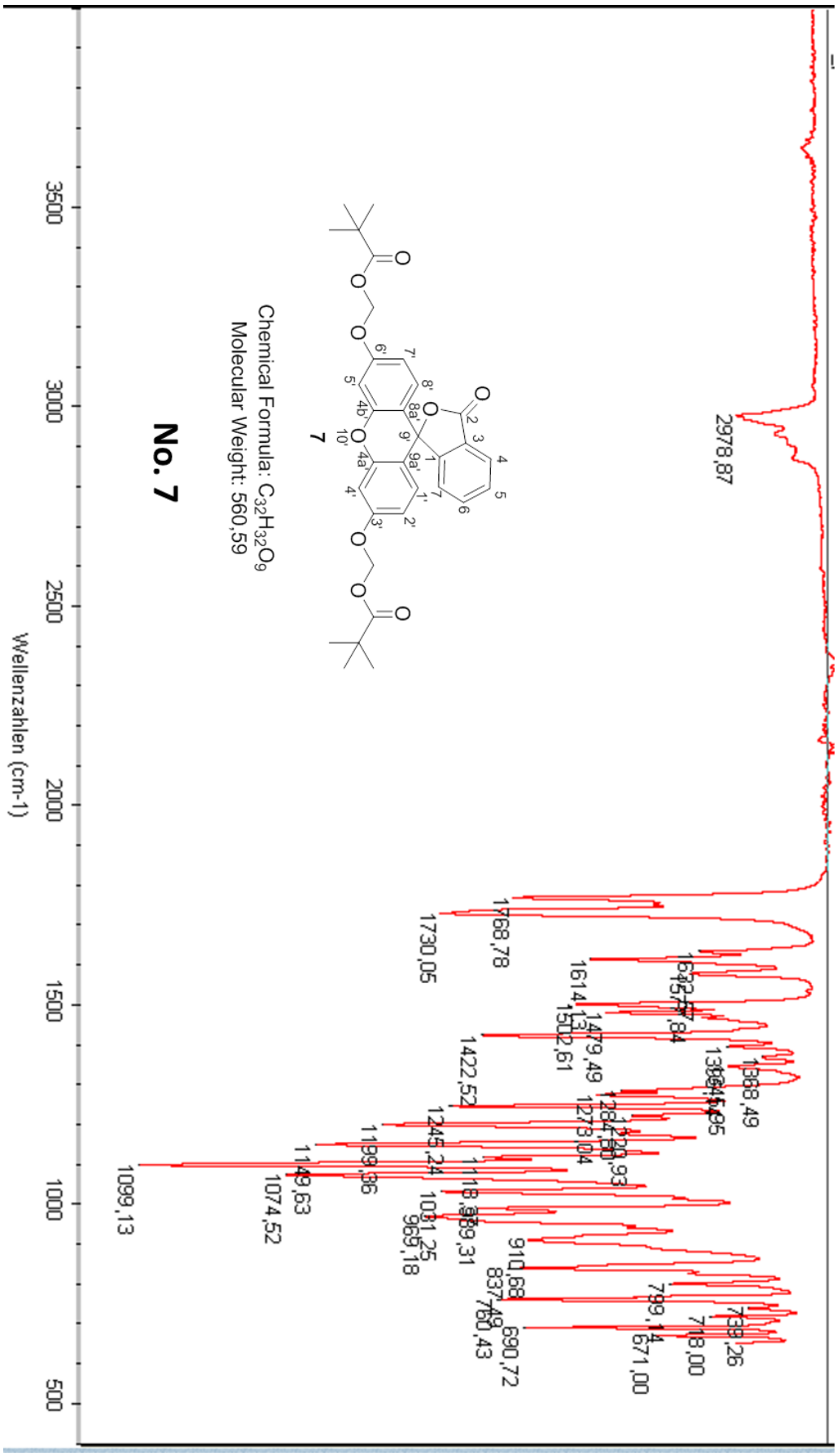
No. 7
Chemical Formula: C32H32O9
Molecular Weight: 560,59
7
Wellenzahlen (cm-1)
3500
3000
2500
2000
1500
1000
500
2978,87
1768,78
1730,05
1614,13
1502,61
1479,49
1422,52
1368,49
1273,04
1245,24
1149,63
1099,13
1074,52
969,18
910,68
837,49
799,14
760,43
738,26
718,00
690,72
671,00

No. (**8**) ESI in MeOH (pos. scan mode)

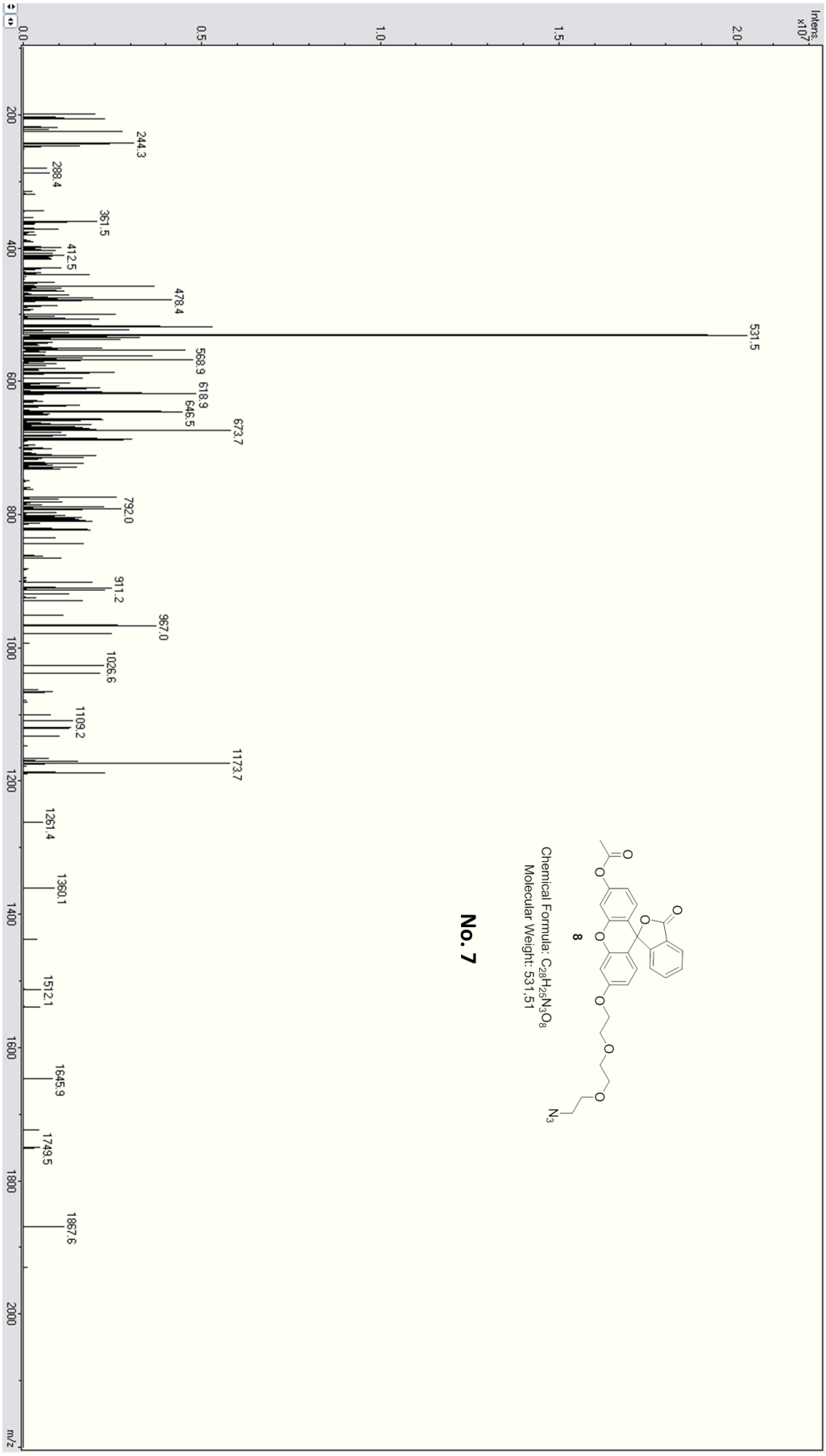

No. (**8**) FT-IR

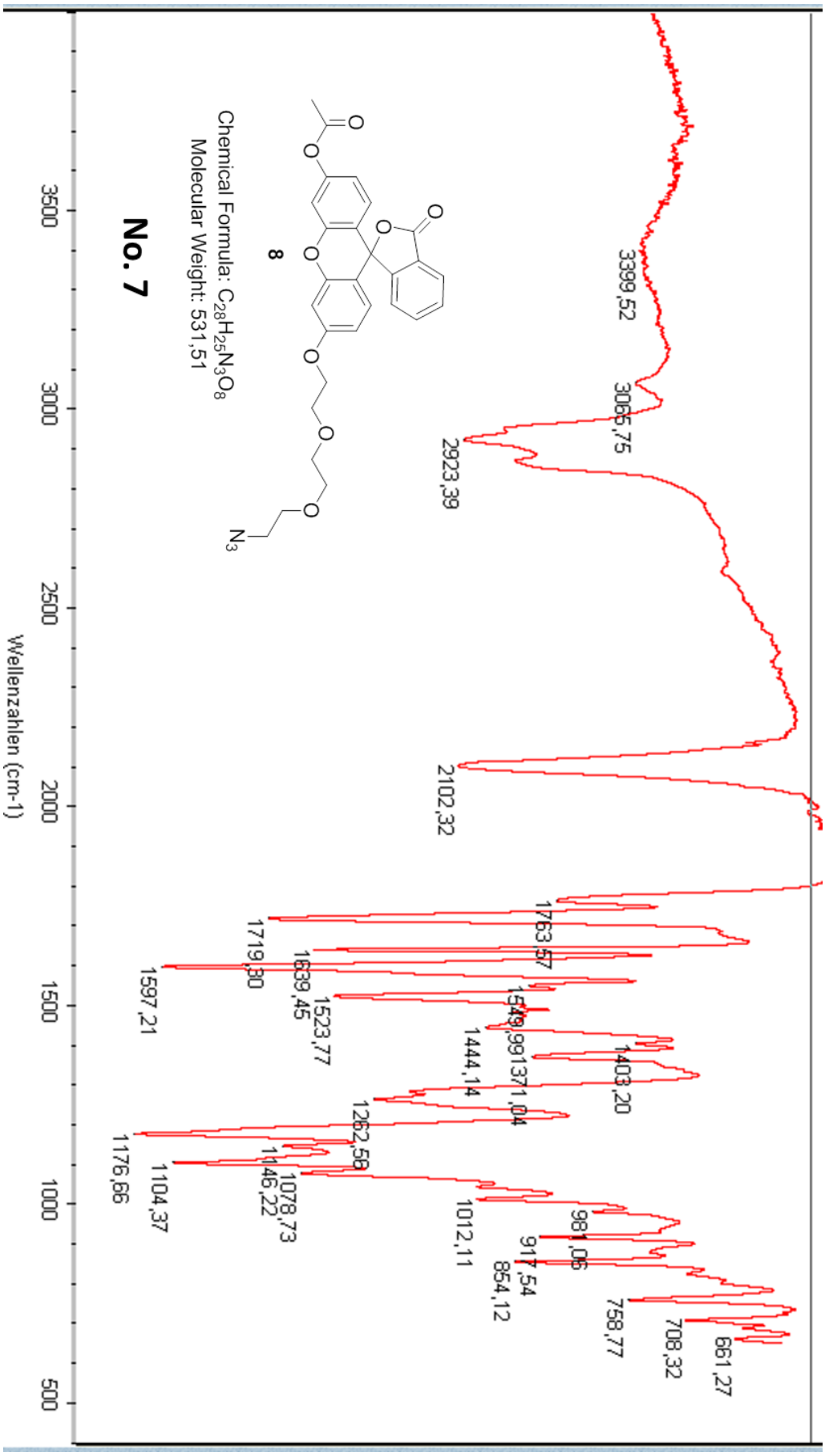
No. 7
Chemical Formula: $C_{28}H_{25}N_3O_8$
Molecular Weight: 531,51
8
Wellenzahlen (cm-1)
3500
3000
2500
2000
1500
1000
500
3399,52
3065,75
2923,39
2102,32
1763,57
1719,30
1639,45
1597,21
1523,77
1444,14
1403,20
1371,04
1262,59
1176,66
1104,37
1078,73
1046,22
1012,11
981,06
917,54
854,12
758,77
708,32
661,27

No. (**9**) H-NMR in $CDCl_3$

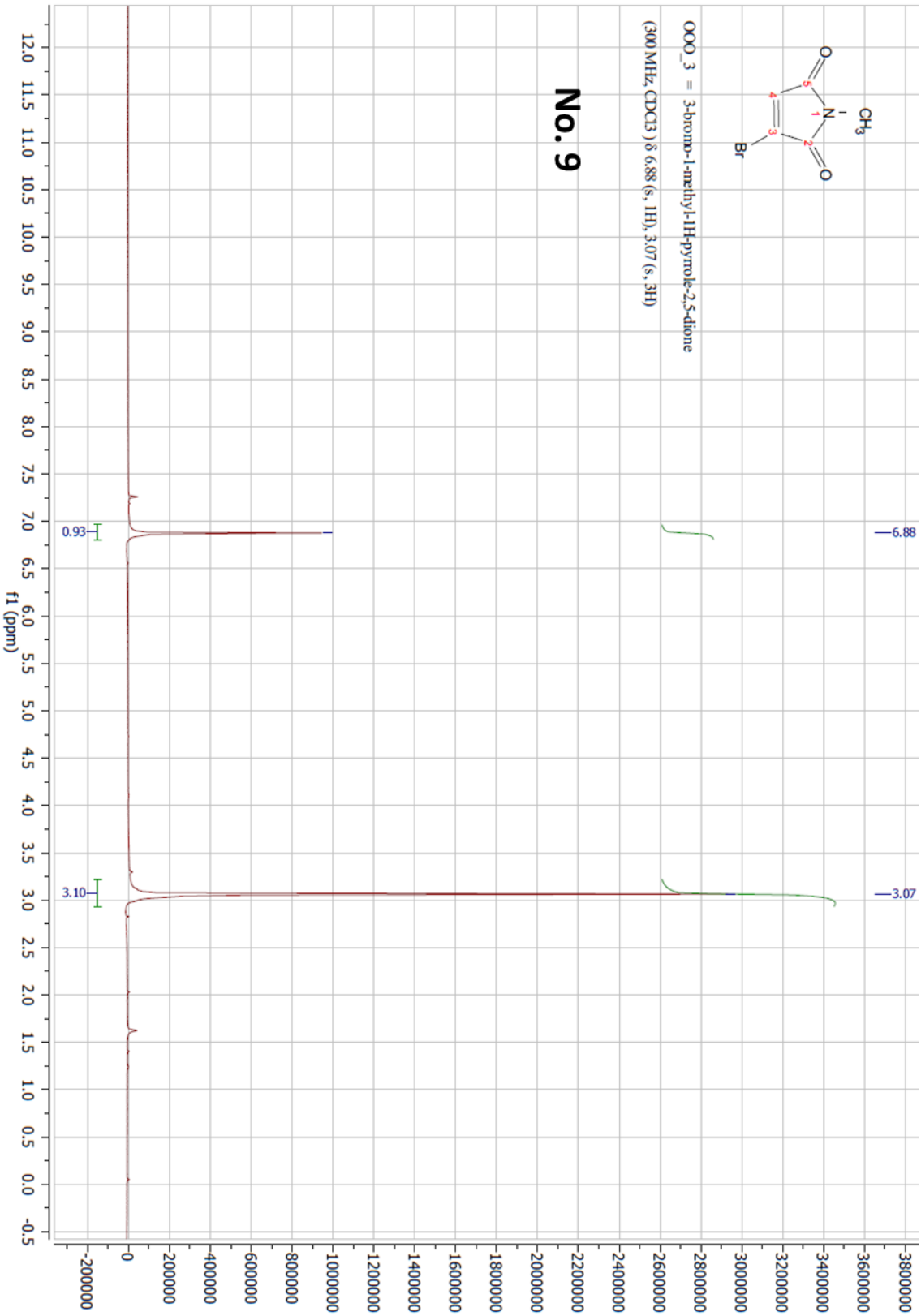

No. (**9**) C-NMR in $CDCl_3$

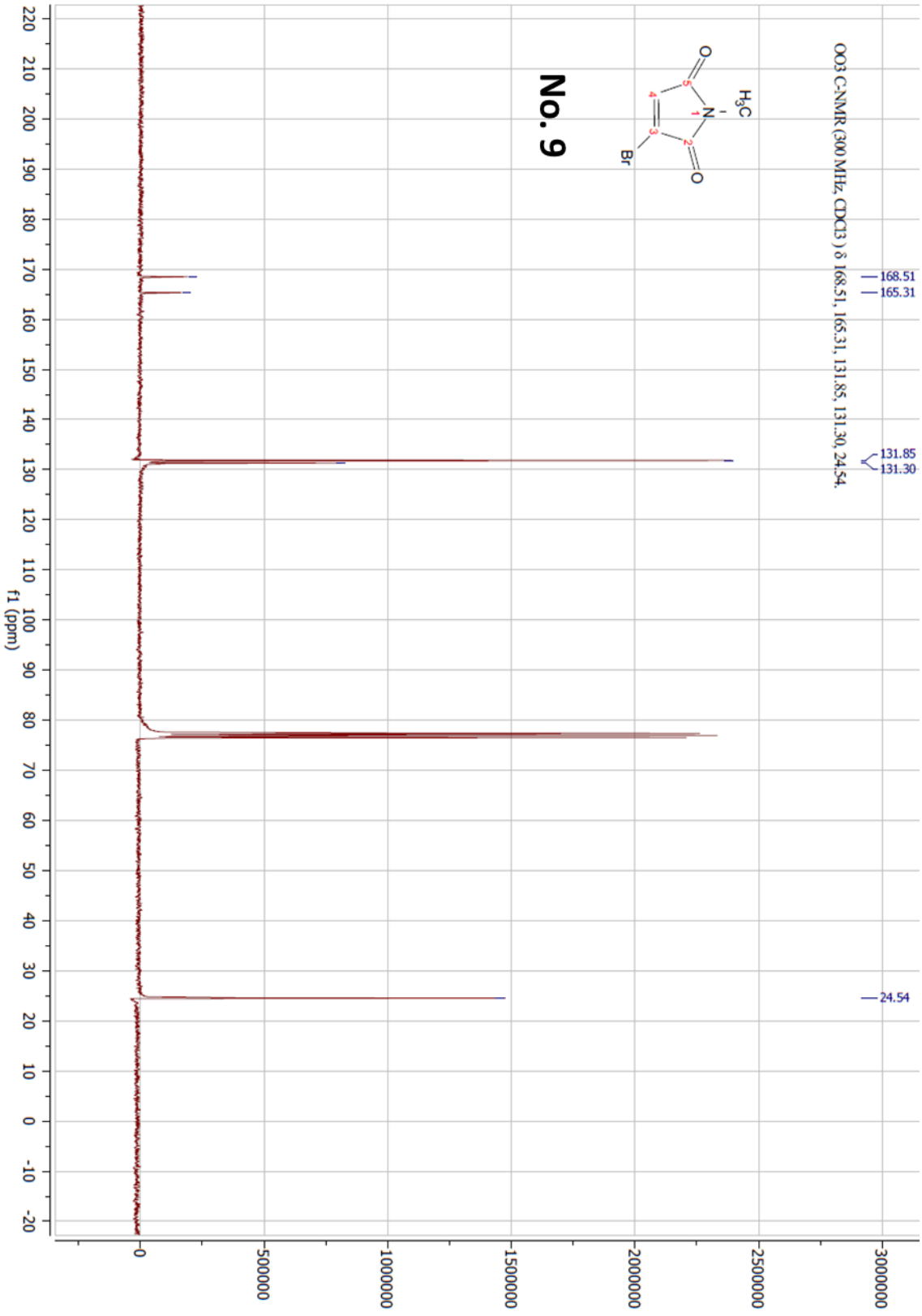

No. (**9**) FT-IR

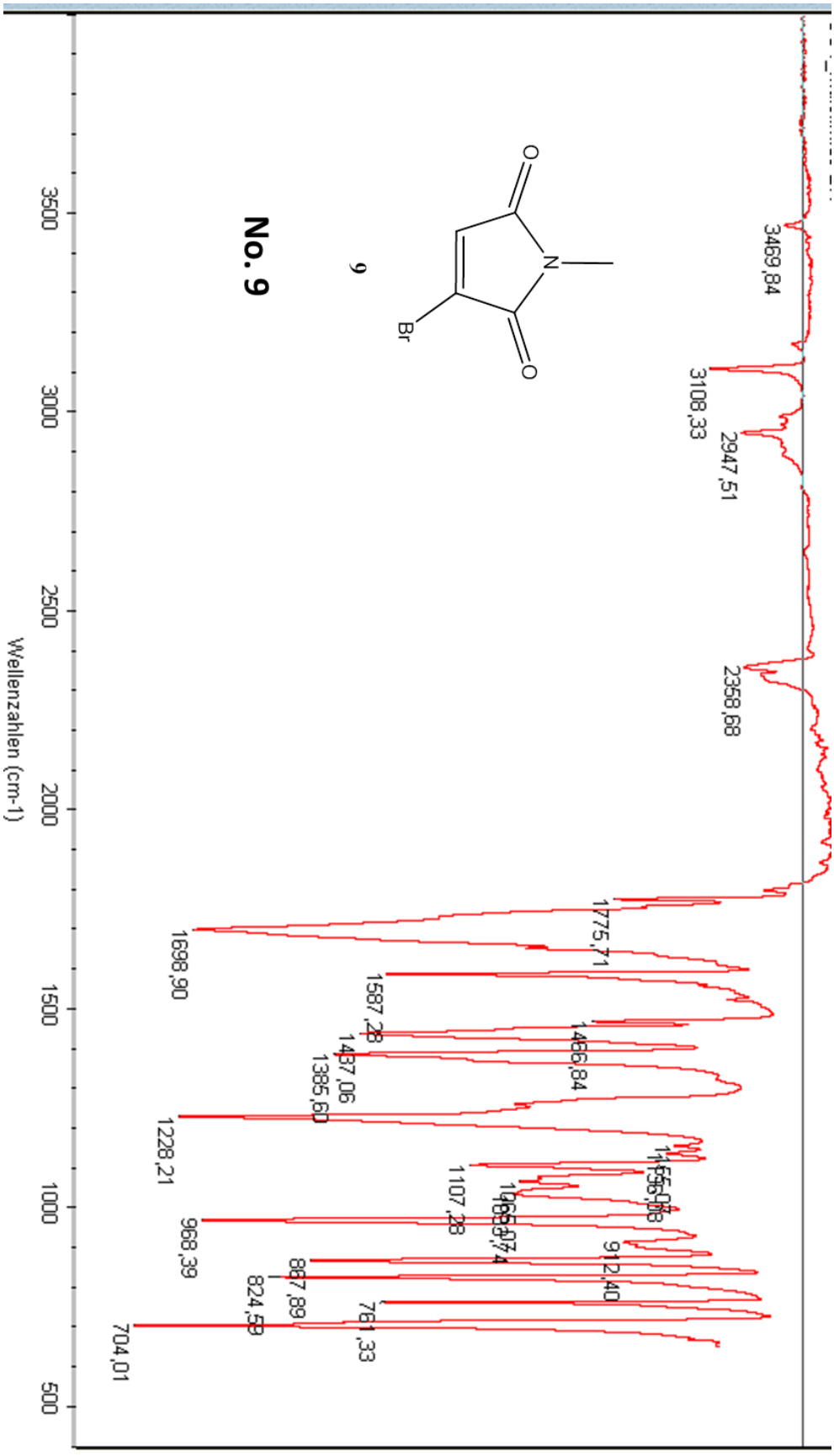
No. 9
9
Br
O
N
O
3469,84
3108,33
2947,51
2358,68
1775,71
1698,90
1587,28
1466,84
1437,06
1385,60
1228,21
1107,28
968,39
912,40
887,89
824,59
761,33
704,01
3500
3000
2500
2000
1500
1000
500
Wellenzahlen (cm-1)

No. (**10**) H-NMR in DMSO-d6

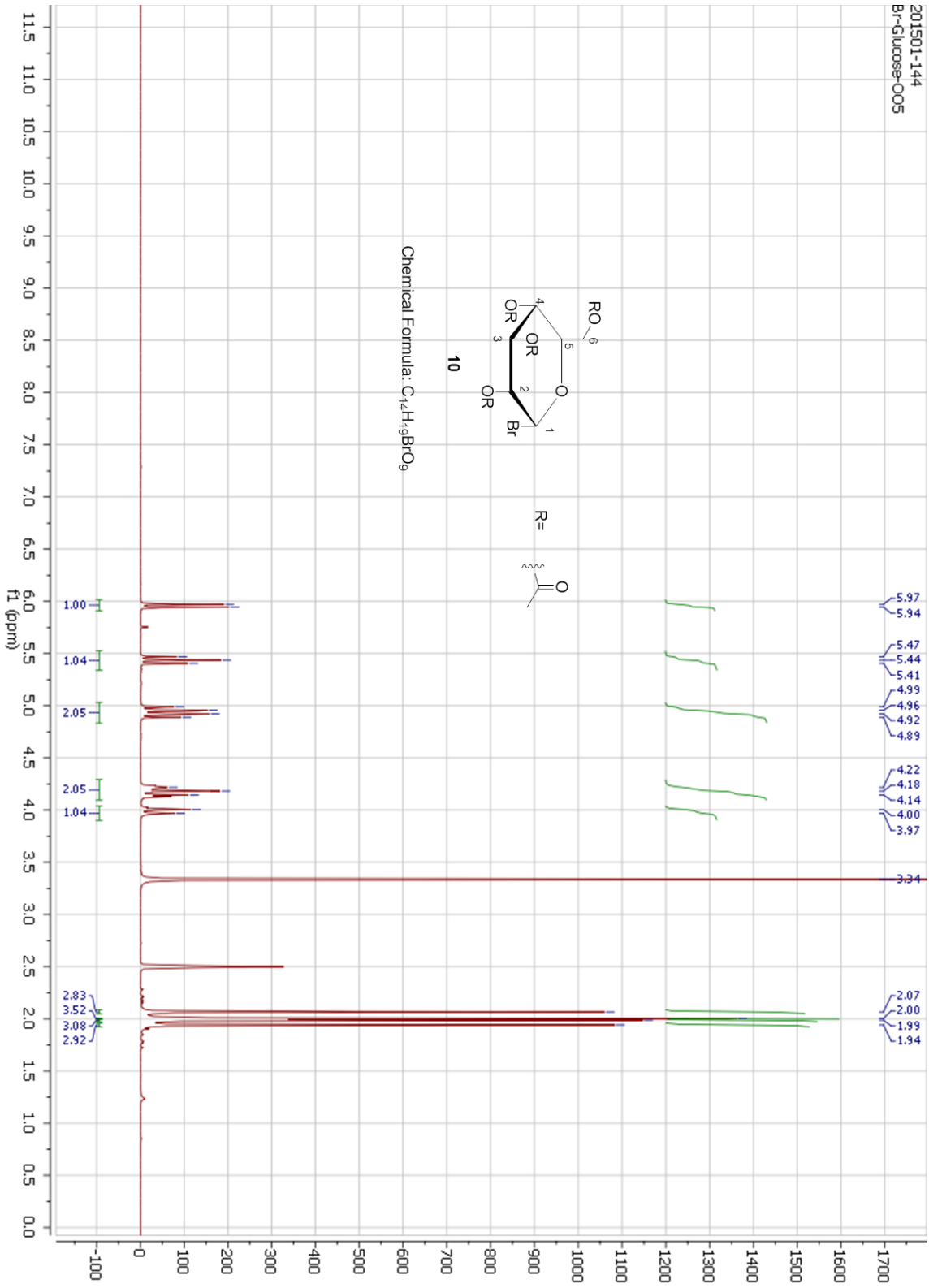

No. (**10**) C-NMR in DMSO-d6

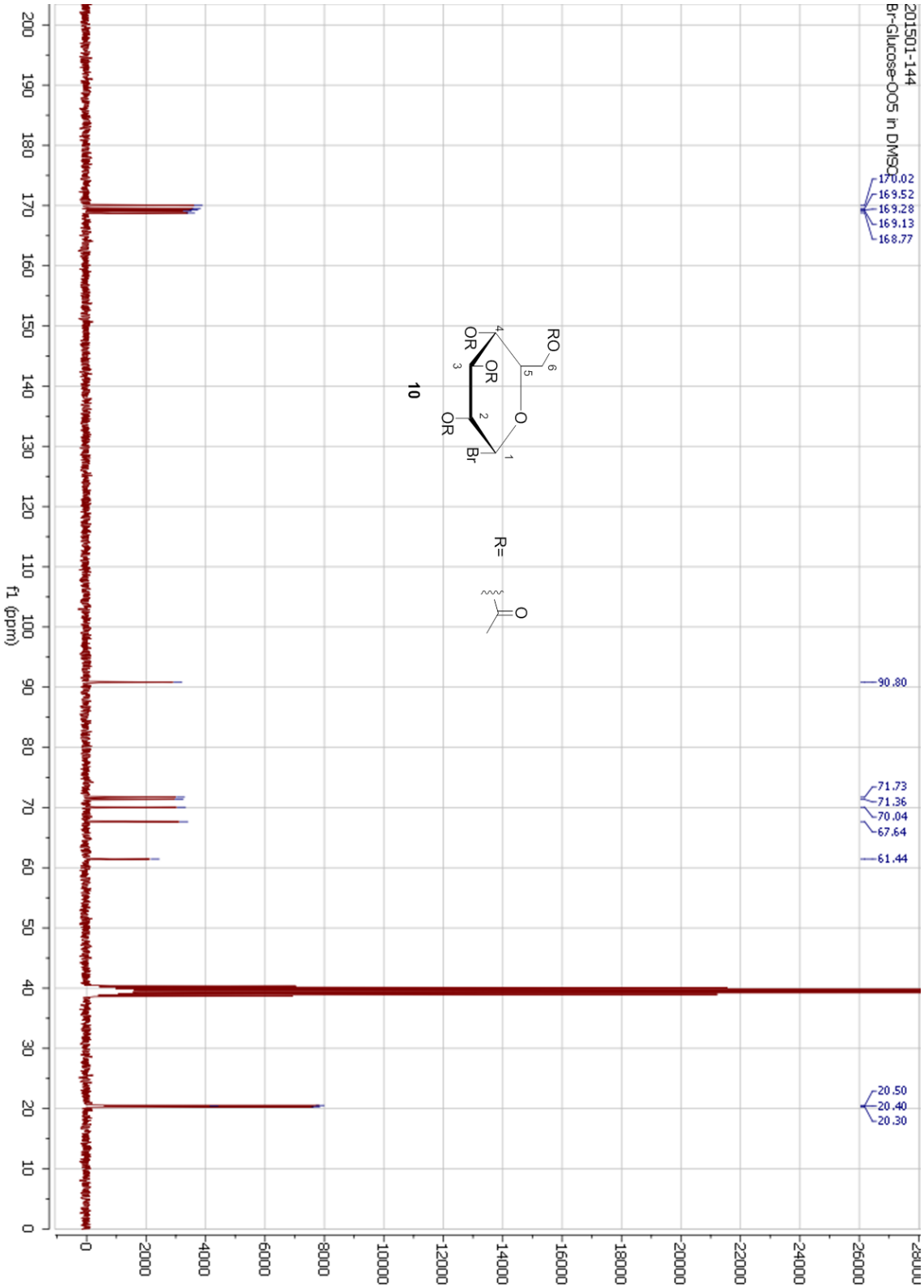

No. (**10**) ESI in ACN (pos. scan mode)

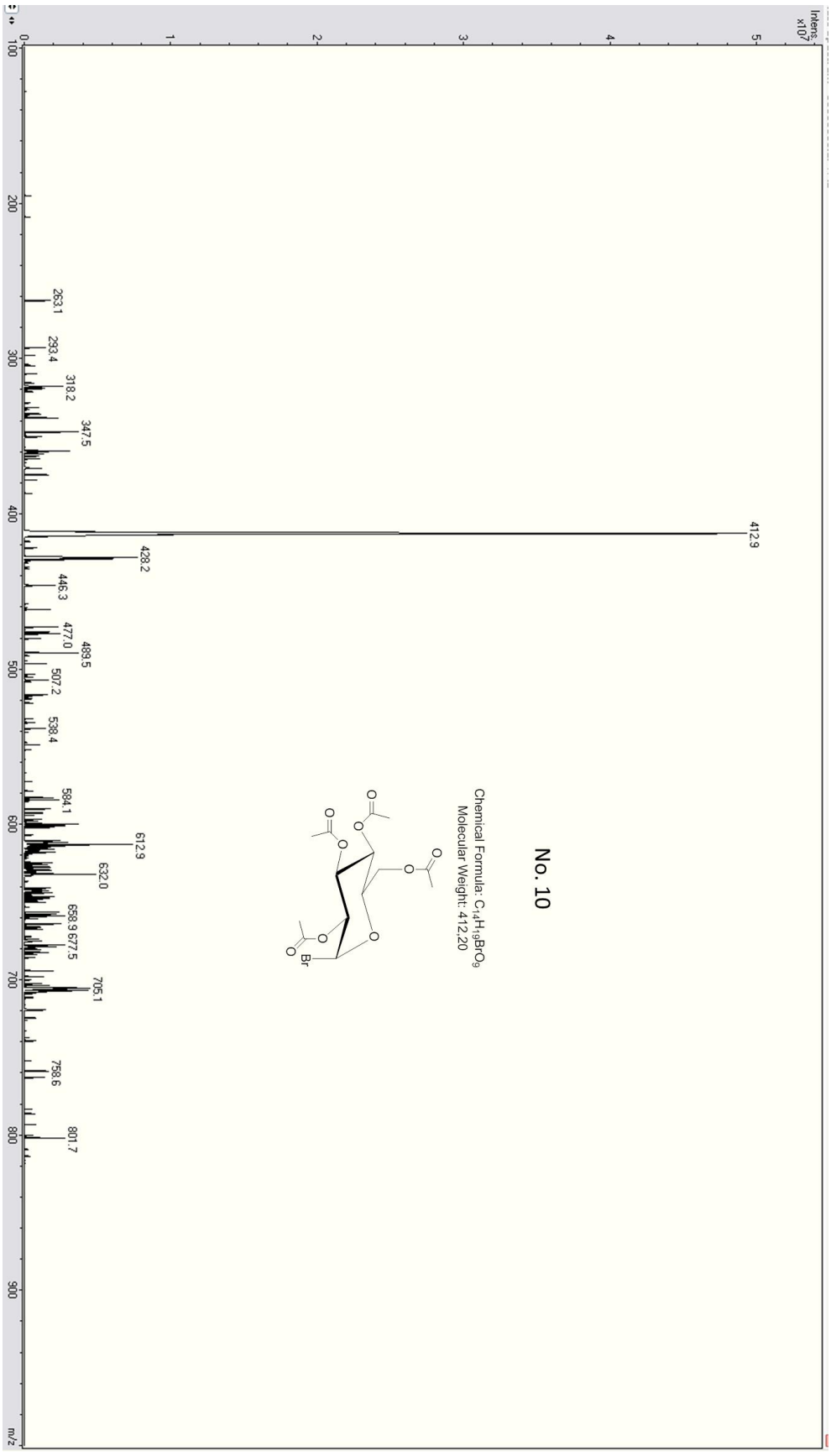

No. (**10**) FT-IR

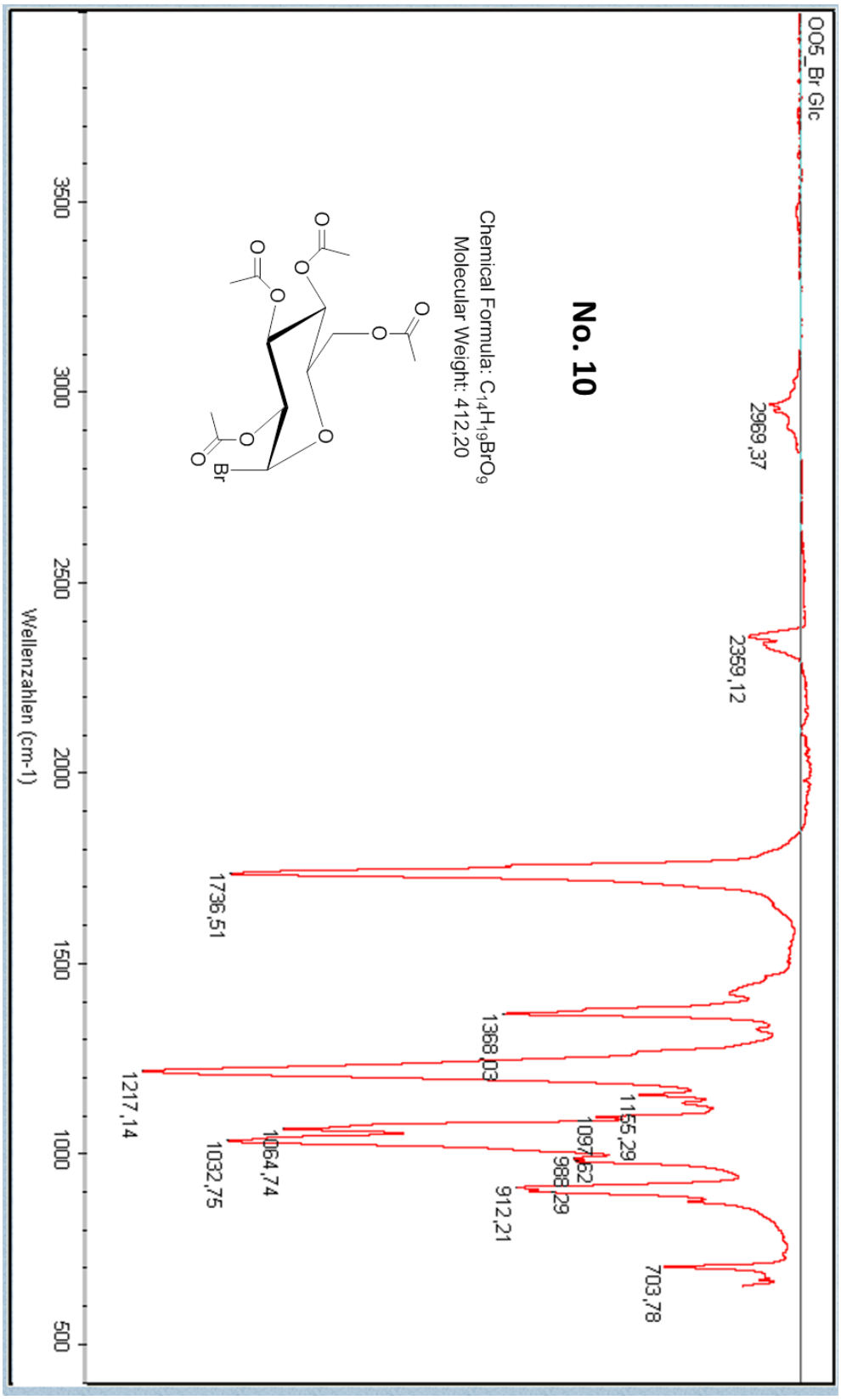
005_Br Glc
No. 10
Chemical Formula: C14H19BrO9
Molecular Weight: 412,20
Br
2969,37
2359,12
1736,51
1368,03
1217,14
1155,29
1097,62
1064,74
1032,75
988,29
912,21
703,78
3500
3000
2500
2000
1500
1000
500
Wellenzahlen (cm-1)

10 CURRICULUM VITAE

Personal Data

Name: Okan Osman Oglou